“Improving Leukaemia diagnosis and management with Selected Ion Flow Tube Mass Spectrometry and vibrational spectroscopy techniques”

Thesis submitted for the degree of

Doctor of Philosophy

Muhammad Rashid Siddique

Lead Supervisor: Professor Josep Sulé – Suso

Keele University and

Oncology Department, Royal Stoke University Hospital

June 2017

Keele University

SUBMISSION OF THESIS FOR A RESEARCH DEGREE

Part I. DECLARATION by the candidate for a research degree. To be bound in the thesis

Degree for which thesis being submitted Doctor in Philosophy

Title of thesis Improving leukaemia diagnosis and management with SIFT-MS and vibrational Spectroscopy techniques

This thesis contains confidential information and is subject to the protocol set down for the submission and examination of such a thesis.

~~YES/~~ No [please delete as appropriate; if YES the box in Part II should be completed]

Date of submission 03/03/2017 Original registration date 02/04/2012
(Date of submission must comply with Regulation 20)

Name of candidate Muhammad Rashid Siddique

Research Institute ISTM Name of Lead Supervisor Dr Josep Sulé-Suso

I certify that:

(a) The thesis being submitted for examination is my own account of my own research
(b) My research has been conducted ethically. Where relevant a letter from the approving body confirming that ethical approval has been given has been bound in the thesis as an Annex
(c) The data and results presented are the genuine data and results actually obtained by me during the conduct of the research
(d) Where I have drawn on the work, ideas and results of others this has been appropriately acknowledged in the thesis
(e) Where any collaboration has taken place with one or more other researchers, I have included within an 'Acknowledgments' section in the thesis a clear statement of their contributions, in line with the relevant statement in the Code of Practice (see Note overleaf).
(f) The greater portion of the work described in the thesis has been undertaken subsequent to my registration for the higher degree for which I am submitting for examination
(g) Where part of the work described in the thesis has previously been incorporated in another thesis submitted by me for a higher degree (if any), this has been identified and acknowledged in the thesis
(h) The thesis submitted is within the required word limit as specified in the Regulations

Total words in submitted thesis (including text and footnotes, but excluding references and appendices) 40473

Signature of candidate Muhammad Rashid Siddique Date 03/03/2017

Note

Extract from Code of Practice: If the research degree is set within a broader programme of work involving a group of investigators – particularly if this programme of work predates the candidate's registration – the candidate should provide an explicit statement (in an 'Acknowledgments' section) of the respective roles of the candidate and these other individuals in relevant aspects of the work reported in the thesis. For example, it should make clear, where relevant, the candidate's role in designing the study, developing data collection instruments, collecting primary data, analysing such data, and formulating conclusions from the analysis. Others involved in these aspects of the research should be named, and their contributions relative to that of the candidate should be specified (*this does not apply to the ordinary supervision, only if the supervisor or supervisory team has had greater than usual involvement*).

Abstract

Leukaemia is 11th most common cancer worldwide, associated with poor prognosis. The 10 years' survival for leukaemia is between 44% - 47%. One of the main reasons for this is the disease being diagnosed in late stages. Most of leukaemia screening techniques are invasive or give radiation. It is therefore obvious to improve prognosis and refine diagnostic techniques for early detection, and better management of its therapeutic response. Spectroscopic and spectrometric techniques are widely used by a huge group of scientists; as biochemical analysis of the disease, may provide biochemical signatures to be used in diagnostics and management of the disease. In this work, the feasibility of measuring both qualitatively and quantitatively VOCs released by PBMC, leukaemia cells and BM cells *in vitro* has been shown. There are clear differences in the VOCs profile even among different leukaemia cells lines as well as from leukaemia cells exposed to drugs, PBMCs and bone marrow. These differences in the VOCs release could be exploited towards a clinical application of SIFT-MS in the diagnosis and therapeutic response of the disease. Direct sampling is the most convenient method of sampling, which could avoid loss of the many important VOCs by diffusion and/or absorption. Since it is not very easy to obtain direct breath, appropriate storage of exhaled breath and transportation are very important issues to be considered. My study proved that stability over time might vary for different VOCs, especially those present in smaller concentrations. The addition of Imatinib or Nilotinib to K562 cell clones induces changes in cell biology and cellular structure which translates into changes in the S-FTIR spectra and Raman Spectra of the cells. There are remarkable differences in the biochemical composition of cells incubated at different drug concentrations and at different levels of oxygen. Further studies are needed to confirm these changes in the spectra.

Table of Contents

List of Figures

List of Tables

List of Abbreviations

AA: Acetaldehyde

ADH: Alcohol dehydrogenase

ALDH: Acetaldehyde dehydrogenase

BCC: Basal cell carcinoma

CML: Chronic myeloid Leukaemia

CM: Complete Medium

CT: Computed tomography

DFSP: Dermatofibrosarcoma protuberans

DMEM: Dulbecco's Modified Eagle Medium

DMSO: Dimethyl Sulphoxide

DSF: Disulfiram

EGF: Epidermal growth factor

EGFR: Epidermal growth factor receptor

EMSC: Extended multiplicative signal correction

FBS: Foetal bovine serum

FSM: Full Scan Mode

FTIR: Fourier Transform Infrared

GISTs Gastro-intestinal stromal tumors

GC-MS: Gas Chromatography – Mass Spectrometry

MIM: Multi-ion monitoring mode

MRI: Magnetic Resonance Imaging

NAD^+: Nicotinamide adenine dinucleotide

PBMC: Peripheral blood mononuclear cells

PCs: Principle components

PCA: Principle component analysis

PBS: Phosphate buffered saline

PDGFR: Platelet derived growth actor (PDGFR)

PET: Positron emission tomography

PFA: Paraformaldehyde

Ph Philadelphia chromosome

Ph+ALL Philadelphia Chromosome positive

PPBV: Part-per-billion-by-volume

PPM: Parts-per-million

RH: Relative humidity

RPMI Roswell Park Memorial Institute medium

SD: Standard deviation

S-FTIR Synchrotron Fourier Transform Infrared

SIFT-MS: Selected Ion Flow Tube – Mass Spectrometry

SNV: Standard normal variate

VOCs: Volatile organic compounds

ACKNOWLEDGEMENTS

In the name of Allah, the Most Gracious and the Most Merciful

Alhamdulillah, all praises to Allah for the strengths and blessings He bestowed upon me during the completion of this study. I wish to extent my gratitude to my academic supervisor Prof. Josep Sulé – Suso for without whom, this thesis would not be possible. In early 2012, Josep was gracious enough to accept me into his research group as a PhD student. His wisdom and sharp wit have helped me resolve many issues during the course of this research and made the process very enjoyable; to him I am forever indebted. I would like to thank him for being a wonderful supervisor and also a wonderful friend.

Gratitude is extended to those that have helped me with SIFT-MS studies, Professor D. Smith, Professor Patrik Španěl and Dr Thomas Chippendale, the majority of the research presented herein was undertaken under their great support. All of them who I have encountered in the previous four years have had some part to play in this thesis and for that I am very thankful.

I wish to acknowledge the researchers, involved at the Diamond Light Source MIRIAM B22 beamline; Dr Gianfelice Cinque, Dr Mark Frogley, Dr Katia Wehbe and Dr Jacob Filik for their collaboration and support. I would also like to thank the beamline staff at Soleil Synchrotron, Dr Paul Dumas and Dr Christophe Sandt (who regularly goes above and beyond to share knowledge and the joys of France with us.) for their unconditional and continuous support during our time in their beamline.

I would like to extend my gratitude to the person who helped me, support me, guided me, motivated me, directed me throughout my PhD. I will have to state that without her this work was distant for me. Dr Abigail Victoria Rutter thank you very much for your tireless encouragement, support, and help. Thank you very much for all unforgettable laughter and time we spent during beamtime and all the conferences and summer schools.

Finally, and most importantly, I wish to express tremendous gratitude to my family and friends. Dad, Mum, Ch Faisal Siddique, Ch Kashif Siddique, and Ch Atif Siddique have provided me with the tools I need to not just complete a Ph.D. thesis, but to get through life. Your support, both moral and financial, has helped me to get to where I am now and I hope I have made you proud. And Dad, I'm sorry I didn't end up as a medical doctor, I hope you can cope with me being a biologist! You are an inspiration.

I also wish to thank staff and students at the Institute of Science and Technology in Medicine, Keele University, Stoke on Trent. I also wish to thank Mohammed Nasim Abed Abo Donia, Humza Owida, Marwan Ibrahim Abdullah, Marwan Mohammed Merkhan, for being excellent friends and colleagues. I would also like to extent thanks to the remainder of ISTM colleagues for their patients of bearing me with them all the time.

I would also like to give big thanks to my friends, who always stood side me and helped me during tough times. Mr Ateeq Ur Rehman, Mr Zeeshan Munir, and Waqas Hayat Warraich thank you very much.

Last of all I want to express my hearty gratitude to My lovely wife Zunaira Siddique, and my angels Dua Siddique, Zoya Siddique and My Champion Abdulrehman Siddique for being by my side over the last 6 years. Zunaira is the most important person in my life and her support and love means everything to me. So to Zunaira, I love you and thank you for being support when I needed the most, for holding me tight when I was falling down, for motivating me all the time whenever I was losing hope. Thank you.

List of Outputs

Publications

1. **Siddique M. R.**, Rutter A. V., Cinque G., Wehbe K., and Sulé-Suso J.. Study of drug effects on leukaemia cells by cell cloning and vibrational spectroscopy. Analyst, 2016, DOI: 10.1039/C6AN01914E.

2. **Siddique M. R.**, Rutter A. V., and Sulé-Suso J. Release of volatile organic compounds by leukaemia cells *in vitro* measured with the Selected Ion Flow Tube Mass Spectrometry (SIFT-MS) (in preparation).

3. Rutter A. V., **Siddique. M. R**., Filik. J., Sandt. C., Dumas. P., Sockalingum. G. D., Yang. Y. and Sulé-Suso. J. (2014) Study of Gemcitabine Sensitive/Resistant Cancer Cells by Cell Cloning and Synchrotron FTIR Microspectroscopy. Cytometry, Part A, 85(8), 688-697.

Oral Presentations

1. Study of Volatile Compounds released by Leukaemia. 14-16 September, International Association of Breath Research (IABR) Summit, Breath 2015, Vienna, Austria; September, 2015.

Posters

1. Rutter A. V., **Siddique M. R.**, Yang Y., Španěl P., Smith D. and Sulé-Suso J. Detecting volatiles from lung cancer with selected the ion flow tube mass spectrometry. Midlands Academy of Medical Sciences Research Festival. Birmingham, UK, April, 2016.

2. **Siddique M. R.**, Abigail V. Rutter A. V., Cinque G., Katia Wehbe, Sandt C., Dumas P., Bellisola G. and Sulé-Suso J. Effects Of Imatinib On Leukaemia Cells By Cell Cloning And Synchrotron IR Microspectroscopy. CLIRSPEC Summer School, Windermere, UK; July, 2015.

3. Rutter A. V., **Siddique M. R.**, Yang Y., Forsyth N., Španěl P., Smith D., and Sulé-Suso J.. The role of culture conditions on the release of volatile organic compounds by lung cells measured with the Selected Ion Flow Tube Mass Spectrometry technique. IABR Summit, Breath 2015, Vienna, Austria; September, 2015.

4. Sulé-Suso J., Rutter A. V., **Siddique M. R.**, Gilani S., Watson N, Jegannathen A., Brunt A. M., Belcher J., Yang Y., Španěl P., and Smith D. Volatile Organic Compounds in breath of lung cancer patients measured with the Selected Ion

Flow Tube Mass Spectrometry technique. IABR Summit, Breath 2015, Vienna, Austria; September, 2015.

5. Alhaidari S., Rutter A. V., **Siddique M. R.**, de Amarante M. R. and Sulé-Suso J. Levels of acetaldehyde released from cancerous, fibroblast and epithelial lung cells (oral presentation 766). 6th Annual Forum for medical research. King Abdullah International Medical Centre, Riyadh, Saudi Arabia. December, 2015.

6. **Siddique M. R.**, Rutter A. V., Cinque G., Yang Y., Bellisola G., and Sulé-Suso J. Synchrotron based IR microspectroscopy of leukemia cells in 2D and 3D models. Spec2014, Krakow, Poland; August, 2014.

7. Rutter A. V., **Siddique M. R.**, Filik J., Sandt C., Dumas P., Cinque G., Sockalingum G. D., Yang Y., and Sulé-Suso J. Synchrotron Based FTIR Spectroscopy as a Tool to Detect Sensitive/Resistant Cloned Populations of Cancer Cells. Diamond Light Source Scientific Away Day, Diamond Light Source, Oxford; June, 2013.

8. Li W. W., Rosa J. O., **Siddique M. R.**, Bajana B., Sulé-Suso J., and Richardson A. Anti-cancer thymoquinone from *Nigella sativa.* 61st International Congress and Annual Meeting of the Society for Medicinal Plant and Natural Product Research. Münster, Germany.September 2013.

Chapter 1

Introduction

1.1: Leukaemia (Bone Marrow Cancer)

Medical science has advanced a great deal in last few decades, especially in the diagnosis and management of cancer. However, in spite of these developments, cancer is still the leading cause of death worldwide. The latest statistics available are from 2012, when about 14.1 million new cases of cancer were reported worldwide, with 8.2 million cancer-related deaths accounting for 22,000 deaths each day. In the same year, around 163,300 cancer cases were diagnosed among children aged 0-14 years worldwide with around 80,000 cancer-related deaths. It is expected that by 2030, the global burden of cancer will grow to 21.7 million with expected deaths of 13×10^6 [Cancer Research UK]. Mortality trends over the last decades have decreased for 12 out of 20 cancer types in males and 11 out of 20 cancer types in females. Examples are lung, bowel, breast, and prostate cancer, and leukaemia, for which the decrease in mortality over the last decades in the UK is due to the advances in cancer screening programmes and awareness for cancer as disease, coupled with higher standards of cancer care [Cancer Research UK]. Early detection of the disease is one of the main aspects in increasing cancer survival rates. However, many of the cancer screening techniques (imaging, blood tests, …) are invasive or give radiation. Thus, these screening processes are important but might be associated to risks. On the other hand, some of these screening techniques might not always be able to identify cancer in early stages, i.e. before patients present with symptoms. It is therefore obvious that further developments are needed.

The human body produces blood cells inside the bone marrow, the soft inner portion of the bones. The bone is made up of compact bone, spongy bone, and bone marrow (soft fatty/spongy tissue inside bone cavity). Compact bone makes up the outer layer of the bone. Spongy bone is found mostly at the ends of bones and contains red marrow. Bone marrow is found in the center of most bones containing many blood vessels. There are two types of bone marrow: red and yellow. Red marrow contains blood stem cells that can become red blood cells, white blood cells, or platelets [Queensburry 2001]. Yellow marrow consists of mostly fat cells and few primitive blood cells. The human body needs these blood cells to perform different functions such as oxygen transport (e.g. red blood cells), fight infections and immune response (e.g. white blood cells) and stop bleeding (e.g. platelets) amongst other. The human body is producing new blood cells constantly. Every day, billions of the red blood cells, white blood cells, and platelets are produced in the bone marrow, which replace the dead cells (dead due to illness or normal processes). The process of new blood cells production is called haematopoiesis. A group of master cells (stem cells) inside the bone marrow is responsible for the production of the blood cells, having the ability to produce all sorts of blood cells. These stem cells divide into one of three major types of mature blood cells, red blood cells (erythrocytes), white blood cells (leukocytes) and platelets. These white blood cells are further divided into three major types of white blood cells e.g. granulocytes, lymphocytes, and monocytes (Figure 1).

Granulocytes and monocytes are collectively called myeloid cells. These myeloid cells play a vital role in innate immunity, as upon pathogen attack these cells are rapidly recruited into local tissues via various receptors and become activated for

phagocytosis as well as secreting inflammatory cytokines. Any genetic alteration or mutations in these cells may cause an abnormal increase in mature/immature myeloid or blast cells that could result in chronic or acute myelogenous leukaemia [Kawamoto 2004].

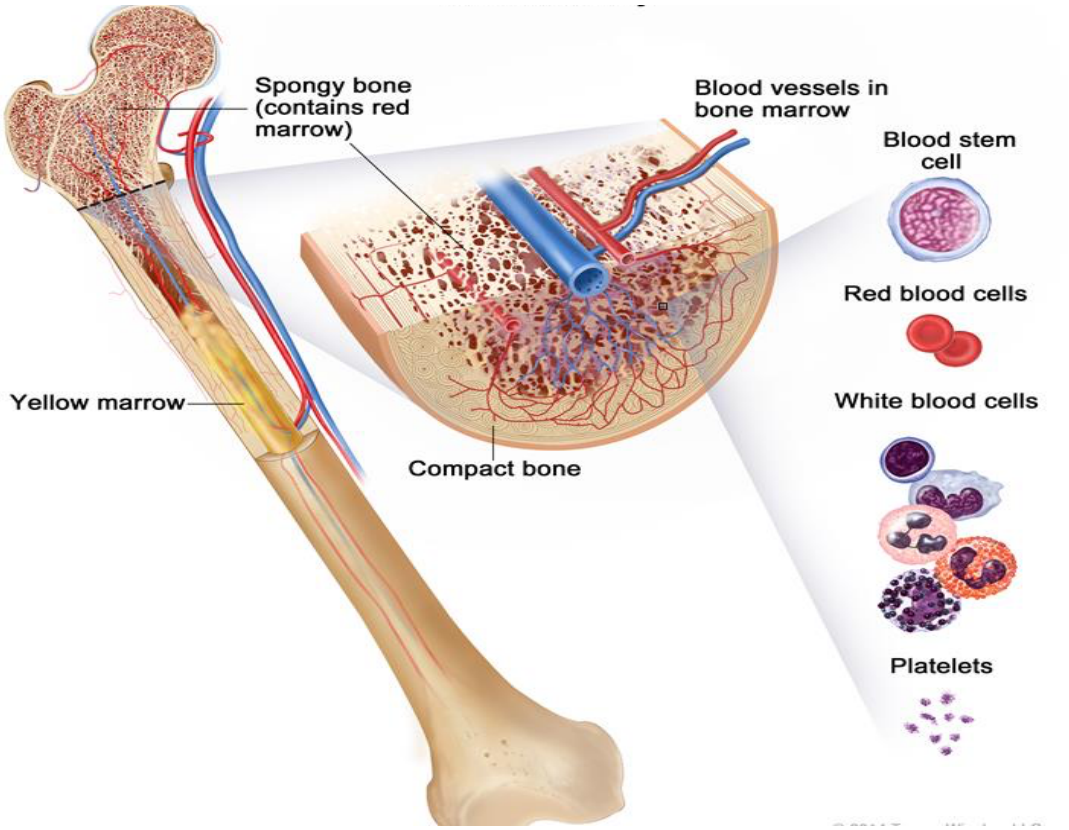

Figure 1: Normal production of blood cells: [www.ghr.nlm.nih.gov (online)].

These blood cells are not just produced in the blood stream but in their specific blood producing organs, specifically marrow of certain bones. In a human body, all of the red blood cells, most of the white blood cells and all the platelets are produced by bone marrow. However other lymphatic tissues as well as thymus, spleen, and the lymph nodes produce lymphocytes. Two types of these lymphocytes, T and B cells, are produced in lymph nodes and spleen. B type cells are responsible for the production of antibodies and attacking invading bacteria, viruses or any toxin, while

T type of cells destroys infected cells or cancerous cells. Any abnormality in these cells may cause abnormal production of these B and T type of cells and cause acute or chronic leukaemia.

Leukaemia is an abnormal proliferation of haematopoietic stem cells in the bone marrow, which leads to a high number of immature white cells in blood [Cancer Research UK]. White blood cells are the most important part of our immune system, which help our body to fight infections. During abnormal production of white blood cells, it becomes harder for the body to get rid of infections. Furthermore, these abnormal or immature cells may also build up in different parts of our lymphatic system and in the spleen[1] and overcrowd the bone marrow, making it harder to produce normal cells. This also translates into a lower normal blood cell count. Low number of normal blood cells or higher number of abnormal white blood cells is the one of the first signs of leukaemia.

There are several types of leukaemia. When leukaemia is diagnosed by doctors, it is very important to know exactly what type of leukaemia doctors are dealing with, as the treatment will vary for each type of leukaemia. There are four major types of leukaemia.

1.1.1: Acute Lymphoblastic Leukaemia

Acute lymphoblastic leukaemia (ALL) is a disorder of lymphoid progenitor cells occurring in children as well as in adults. It arises from T type or B type lymphocytes,

[1] The spleen is a vital abdominal organ responsible for the storage and getting rid of non-healthy blood cells.

also called lymphoblasts. Genetic abnormality or abnormalities in a single lymphocyte or lymphoblast may trigger disordered cell proliferation, abnormal survival and lethal accumulation of immature cells. Acute (sudden onset) lymphoblastic leukaemia is a rapid progression form of leukaemia with high number of white blood cells (lymphocytes, lymphoblast) unable to properly fight infection [Pui 2008; Quensenberr 1995]. It is the most commonly occurring type of leukaemia with almost 25% of all cases, and is more common in males than in females [Quensenberry 1995].

1.1.2: Acute Myelogenous Leukaemia

Acute myelogenous or myeloid leukaemia (AML) is a rapidly progressing heterogeneous clonal disorder of progenitor cells leading to an abundance of immature blood forming cells in the blood stream and bone marrow, which decreases the production of normal blood cells. These cells become immune cells at differentiation. These immature cells are named blast cells, which fill the bone marrow and spill into the main blood stream [Newson 2011]. AML may occur in adult and children, but more commonly in adults. It is also abbreviated as ANLL (Acute nonlymphocytic leukaemia)

1.1.3: Chronic Lymphocytic Leukaemia

Chronic lymphocytic leukaemia (CLL) is a monoclonal disorder characterized by functionally incompetent lymphocytes and is the most common form of adult leukaemia in the western world [Dohne 2000]. It causes the slow increase of white blood cells called B cells. These abnormal cells crowd other type of cells in bone

marrow, which thwarts the production of red blood cells, normal white blood cells and platelets. These cancerous cells spread in the blood stream, infiltrating lymph nodes or other organs such as the liver or spleen [Newson 2011]. Chronic lymphocytic leukaemia is the second most common type of leukaemia occurring in adults and rarely occurring in children.

1.1.4: Chronic Myelogenous Leukaemia

Chronic myelogenous or myeloid leukaemia (CML) is a very slow developing disease. It is a white blood cell disorder in which abnormal proliferation of granulocytic cells increases but they remain immature. With time, these granulocytes accumulate in the spleen causing its enlargement. These granulocytes also overcrowd the bone marrow preventing the production of normal white blood cells, red blood cells, and platelets [Quintas-Cardama 2006]. CML typically affects middle-aged individuals. This disease is very uncommon in youngsters. CML is among those few cancers known to be caused by a single specific genetic mutation [Newson 2011]. This mutation takes place on Philadelphia chromosome (chromosome 22). A reciprocal swap of the location between the pieces of chromosome 9 and 22 happens. Chromosome 9 contains gene c-ABL and 22 contain BCR. So, the newly formed gene as a result of this translocation is called the BCR-ABL (appendix 3) gene that starts producing mutated protein, which in turn converts the marrow stem cells from normal to leukemic [Kimball 1999].

1.2: Leukaemia Incidence

The incidence of leukaemia in the world is about 1 per 100,000 of all cancers diagnosed per year [Cartwright 1992; Bhayat 2009]. According to the latest statistics

available from 2012, about 352,000 cases were diagnosed with leukaemia worldwide [Cancer Research UK]. It is the 11th most common cancer in the world accounting for 2.5% of all cancers [Cancer Stats Incidence 2009-UK] and accounts for more than 8,000 new cases diagnosed every year [Cancer Research UK], with a higher incidence in the older population. However, 4.5 % of cases are diagnosed in children aged 10 or younger [Davies 2014]. As childhood malignancy, it accounts for around 31% of all cancer diagnosed in children under the age of 15 [Cancer Stats childhood cancer Great Britain & UK 2010]. While the 5-year survival for all types of leukaemia is greater than 65%, the survival is worse with increased age at diagnosis [Davies 2014]. The incidence of leukaemia is higher in men than in women with a ratio of 7:5.

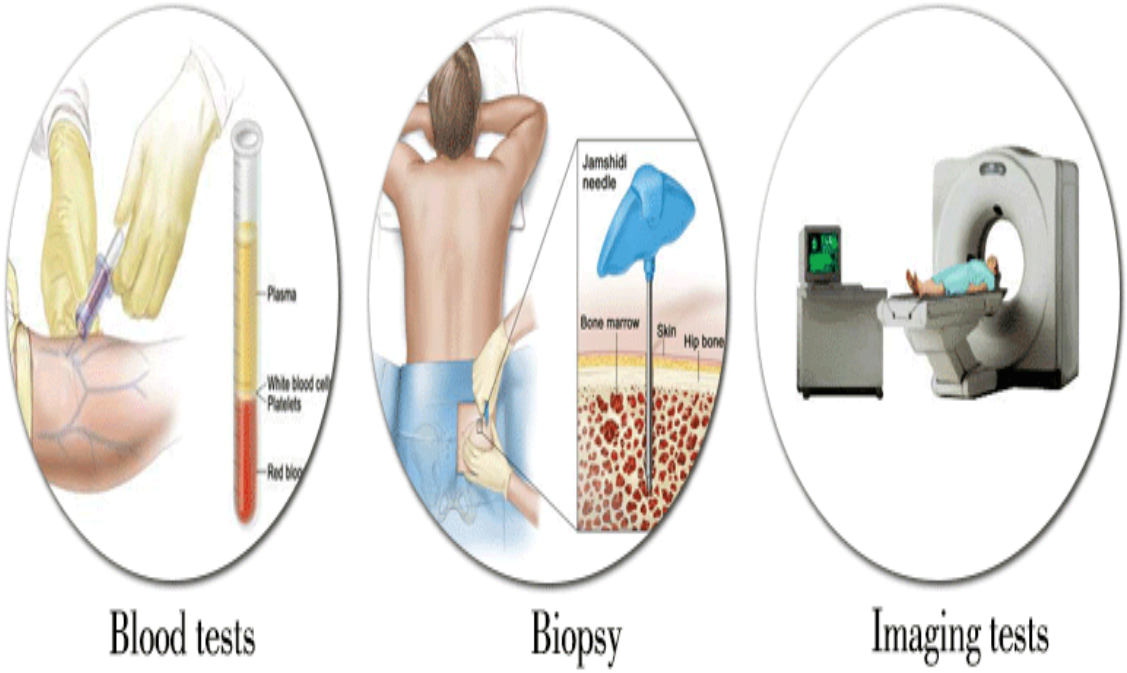

Figure 2: Schematic image of the main steps in the diagnosis of leukaemia. [www.nlm.nih.gov (online)].

1.3: Diagnosis of Leukaemia

The symptoms for leukaemia such as fever, nausea, sleeplessness, and flu can easily go unnoticed for years. They are also likely to be associated with other diseases. Figure 2 shows the main steps involved in the diagnosis of leukaemia.

1.3.1: Anamnesis

First, doctors have to obtain the patient's complete medical history in order to have a detailed medical review of his/her general health, family's medical conditions and of any symptoms and signs [2]that could be associated with leukaemia [Fayed 2006].

1.3.2: Physical Examination

During the physical examination, doctors may examine the body looking for lumps, bleeding areas, and sources of infection amongst other [Fayed 2006].

1.3.3: Blood Test

A full blood count (FBC) which includes number of red, and white cells and platelets amongst other, and blood smears can help to detect leukaemia. When blood samples are observed under microscope, changes in cells' morphology and numbers can be identified [Fayed 2006].

[2] A symptom is any subjective evidence of disease, while a sign is any objective evidence of disease.

1.3.4: Biopsy

Bone marrow biopsy and aspiration are done at the same time. Biopsy entails the removal of soft tissues present inside the bone marrow and aspiration is the sampling of just liquid present inside the bone marrow [Fayed 2006]. In the case of bone marrow biopsy, a large bore needle is inserted in the hipbone or occasionally the breastbone or any other large bone, and samples of the bone marrow are obtained (Figure 3). Aspiration is carried out using a smaller needle to take the sample. A pathologist then examines the sample to assess the presence of leukaemia cells. Lymph node biopsy can also be performed when there is nodal infiltration [Fayed 2006; Cancer Health Centre (Online); Bain 2001].

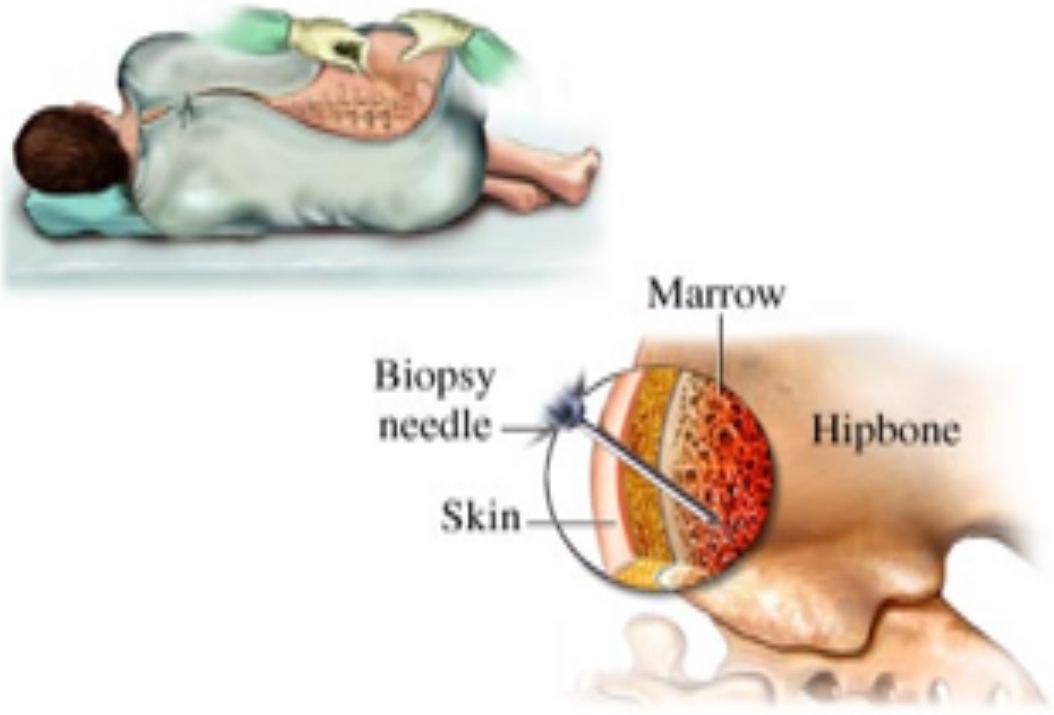

Figure 3: Schematic image of Bone Marrow Biopsy. [www.nlm.nih.gov (online)].

1.3.5: Lumbar puncture

Lumbar Puncture (LP), known also as spinal tap, is carried out in order to assess central nervous system involvement [Robert 2008; Pearson 2012]. A needle is inserted into the subarachnoid space in the lower back (lumbar area) into the spine. The subarachnoid space is the canal within the spinal column that contains cerebrospinal fluid (CSF). CSF is a transparent fluid acting as a protecting cover of the brain and the spinal cord. This fluid is constantly produced in the choroid plexus of the brain. CSF is spun down and analysed for the presence of malignant/abnormal cells in the sample [Pearson 2012].

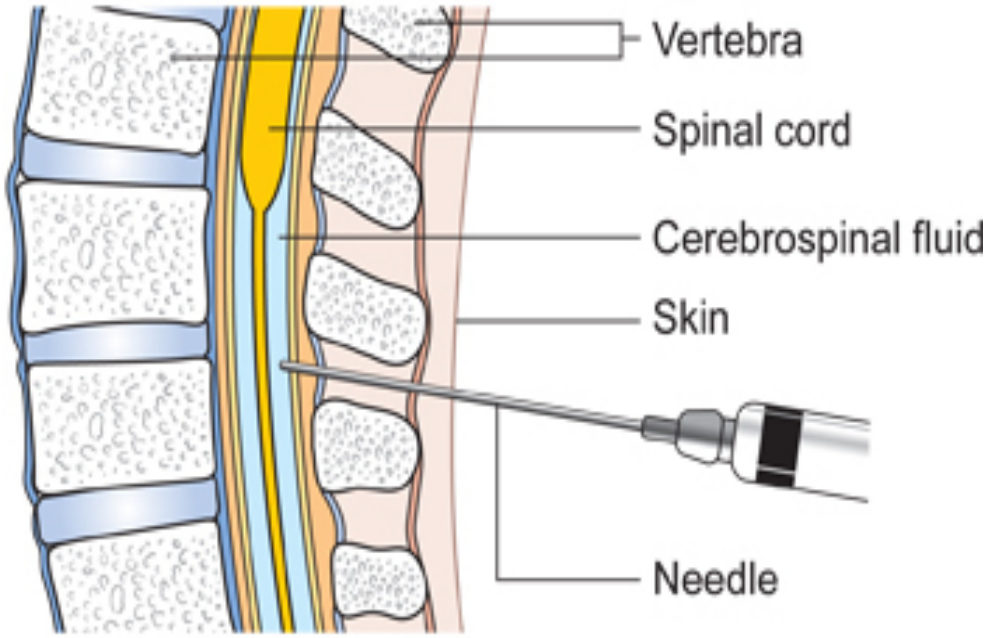

Figure 4: Schematic image of Lumbar Puncture [Cancer Research UK (online)]

1.3.6: Immunophenotyping

Immunophenotyping refers to the technique of characterizing and identifying different molecules and biomarkers present in the inner or outer side of the cell

surface [Maeda 1993; Campana 2000]. Specifically, this technique refers to the labelling of white blood cells (WBC) with antibodies linked to surface antigens[3]. Leukaemia has got characteristic groupings, which allow immunophenotyping to help in the diagnosis and characterization of cancerous cells in the blood or from biopsies. This technique also gives indication of the aggressiveness of the disease and can help in choosing the right treatment [Maeda 1993; Campana 2000].

1.3.7: Cytogenetic or Chromosome Analysis

Cytogenetic analysis involves the study of chromosome/genes at cell level. In the case of leukaemia, studies of chromosomes have significant impact in the diagnosis. Most of the time, chromosomal abnormalities are involved in the pathogenesis of leukaemia. In many cases, molecular studies of chromosomal aberrations have identified specific genes implicated in the progression of leukaemia [Cross 1986; Dohner 2000; Mrozek. 2004]. Cytogenic analysis is the most important diagnostic technique in determining prognosis in some types of leukaemia especially AML, as the majority of patients with this type of leukaemia have shown to have chromosomal aberrations. This technique has also helped to clone many genes, opening a new era of disease diagnosis and treatment [Mrozek 2004]. Along with conventional techniques to perform cytogenetic tests, reverse transcriptase polymerase chain reaction (RT-PCR) [Slack 1998; Coco 1999], fluorescence in situ hybridization (FISH), and immunostaining with particular antibodies are more recently developed

[3] An antigen is any substance that causes an immune system to produce antibodies against it.

techniques used for genetic analysis. These techniques have changed the diagnostic approach, making diagnosis more reliable and precise [Maeda 1993; Fayed 2006].

1.4: Imaging Techniques Used to Diagnose Leukaemia

1.4.1: X-Ray, Ultrasound, Computed Tomography (CT) Scan, Magnetic Resonance Imaging (MRI)

Chest X Rays (CXR) are used in the diagnosis of leukaemia to assess the lungs and, to less extent, lymph nodes in the chest. However, the sensitivity is very limited. In a study of leukaemia patients having chest symptoms, CXR were inadequate in establishing an etiological diagnosis [Godet 2012]. Ultrasound can be used to look for masses or abnormally large lymph nodes. It can detect leukaemia cell masses inside the body in liver, kidneys or spleen amongst other. CT scan is a specialized type of diagnostic imaging technique producing cross sectional detailed images of the body. It is used in leukaemia for diagnostic purposes and to assess tumour response to treatment. Magnetic Resonance Imaging (MRI) uses radio waves along with strong magnets to acquire the image of targets inside the body. MRI is able to characterize soft tissues better than CT Scan aiding to the diagnosis of leukaemia [Dimopoulos 2009].

1.5: Treatment of Leukaemia

Recently, significant developments have taken place in the treatment of leukaemia, which have led to increased survival rates for this disease. Leukaemia has many

treatment options including watchful waiting, targeted therapy[4], biological therapy,[5] radiation therapy and stem cell transplantation, but the main treatment at present is chemotherapy. Combinations of these treatments are also used depending upon the case and age of the patient. There are few factors that play a vital role in deciding the treatment choice such as type of leukaemia, age of the patient, and stage of the disease (Appendix 2). Cytotoxic drugs used in the treatment of leukemia include doxorubicin, methotrexate, cytarabine, etoposide and cisplatin amongst other [Friesen 1999].

Imatinib Nilotinib

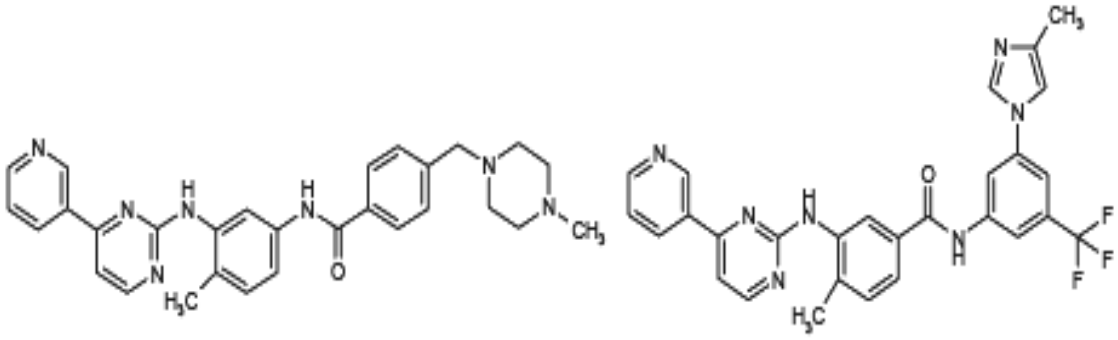

Figure 5: Chemical structure of Imatinib and Nilotinib.

Imatinib (figure 5) is an anti-leukemic selective tyrosine kinase inhibitor with specific activity for ABL, Platelet derived growth factor receptor, c-kit, and Albeson-related gene [Druker 2003]. It was first used clinically in 1998 for the treatment of CML. It is

[4] Targeted therapy is cancer treatment that uses drugs to more precisely identify and attack cancer cells.

[5] Biological therapy is treatment that acts on processes in cells i.e. stopping cancer cells from dividing, encourage immune system to attack cancer cells

an orally bioavailability mesylate salt, a multi-target inhibitor of v-Abl, c-Kit and PDGFR with IC50 of 0.6 μM, 0.1 μM and 0.1 μM in cell-free or cell-based assays, respectively.

Imatinib (Glivec®) is a frequently used drug for some types of Leukemia i.e. CML, Philadelphia Chromosome positive (Ph+ALL), chronic eosinophilic Leukemia, and blood disorders myelodysplastic and myeloproliferative conditions, and as hallmark of target therapies for many malignant diseases i.e. gastro-intestinal stromal tumors (GISTs), and dermatofibrosarcoma protuberans (DFSP). However, one of the main problems is the development of resistance which often cannot be overcome even with higher doses of Imatinib.

Nilotinib (figure 5) is a second-generation inhibitor of BCR-ABL tyrosine kinase used as an alternative to Imatinib when cells become resistant. The drug is a derivative of Imatinib, with similar structure to Imatinib but is more potent, and therefore, able to overcome mutations that can cause Imatinib resistance. Nilotinib inhibits the autophosphorylation, at IC50 values as indicated, 20-60 nM for Bcr-Abl, 69 nM for PDGFR and 210 nM for c-Kit. Cells that did not express the BCR-ABL were resistant to Nilotinib below 2 μM. Nilotinib was active against many mutant forms of BCR-ABL that proved resistant against Imatinib and few mutants were less sensitive to Nilotinib with IC50 values of 150 - 390 nM, while T351I was resistant up to below 10,000 nM. Using the same cell lines Nilotinib inhibited viability and proliferation with IC50 values ranging from 8 to 24 nM [Scientific discussion. Online at http://www.ema.europa.eu]. Since IC 50 values for this drug vary vastly within each cell line, preliminary experiments showed that most cells were alive when incubated

for five days with 10 μM Imatinib and no cells survive in the presence of 500 μM Nilotinib.

Nilotinib and Imatinib (figure 5) (drugs used in this work) are kinase inhibitors mainly used for leukaemia treatment. These are selective inhibitors of BCR-ABL tyrosine kinase giving a high response rate. These inhibit other kinases as well as c-kit, ARG, and platelet-derived growth factor [Quintas-Cardama 2006] by hindering their interaction with ATP thereby inhibiting their ability to phosphorylate and activate downstream proteins. These are mainly used for chronic myeloid leukaemia [Peggs 2003]. It is estimated that 10-40% of patients using Imatinib for leukaemia get resistance to this drug, so there is an immediate need of alternative treatments.

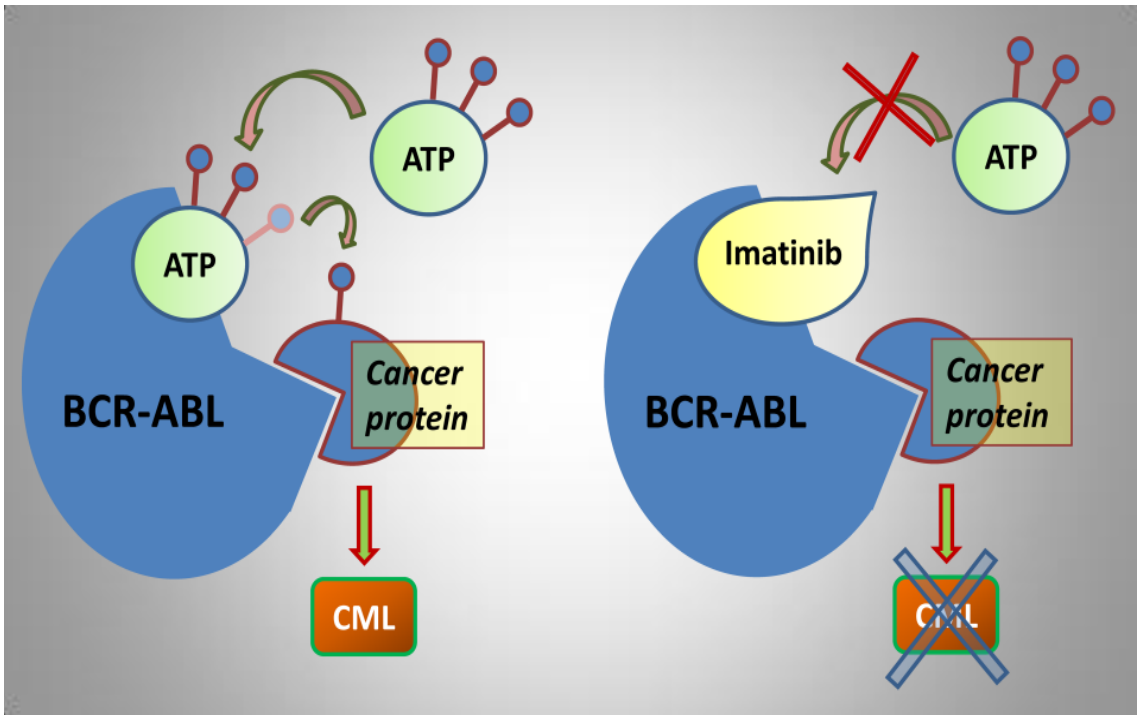

Figure 6: Schematic representation of the mechanism of action of Imatinib [Zaharieva 2013]

The mechanism of action of Imatinib is depicted in Figure 6. It attaches to the ATP binding site of BCR-ABL tyrosine kinase, thus stopping the transfer of phosphate groups to other proteins, which blocks downstream signalling resulting in cell death [Zaharieva 2013].

It is well known that cancer cells can become resistant to cytotoxic drugs through a process called multi drug resistance [Krishna 2006]. Leukemia cells become resistant to Imatinib. Therefore, researchers at Novartis Pharmaceuticals designed novel inhibitors with effective results against Imatinib resistant mutants of BCR-ABL, which was based upon the crystal structure of the Imatinib-ABL complex [Schindler 2000]. Their hypothesis about alternative binding groups led them to the development of AMN107 Nilotinib. It is a high affinity amino pyrimidine-based ATP competitive inhibitor, which decreases the proliferation and viability of wild type BCR-ABL and Imatinib resistant BCR_ABL mutant expressing cells by inhibiting BCR_ABL auto phosphorylation. Nilotinib has proven superior potency to Imatinib in a wide range of CML derived cells lines in-vitro [Golemovic 2005].

1.5.1: Limitations with Diagnosis and Treatment

The use of chemotherapy or combination chemotherapy at high doses for leukaemia patients before transplantation kills the leukemic cells and stem cells as well, placing patients at high risk of infection. Transplanted stem cells need time (24 hours) to reach to the bone marrow and then start dividing and multiply in order to develop new immune cells, which can fight infectious diseases. Infection may develop due to the time delay in the renewal of the immune system with white blood cells.

One of the problems in the management of leukaemia and solid tumours is assessing whether the disease will be sensitive or not to a chemotherapy drug or combination of drugs. FACS (Fluorescence-activated cell sorting analysis) or PCR determines minimal residual disease to check the patient's response to the treatment. Due to discomfort, high costs, need of skilled manpower, and risk involving bone marrow sampling, these measurements cannot be done on a daily basis throughout the treatment period. Thus, a method to assess tumour cell sensitivity to chemotherapy is still needed. Similarly, new drug development requires different tests to assess tumour cell sensitivity to new drugs. There are several chemotherapy sensitivity/resistance assays such as gene expression profiling, *in vitro* clonogenic and proliferation assays, molecular assays, and *in vivo* tumour growth and survival assays amongst other [Chang 2003; Robert 2004; Blumenthal 2007; Cree 2009]. It is not clear yet whether these assays can improve the outcome of patients with cancer [Samson 2004; Schrag 2004] and, so far, the clinical application has proved difficult [Cree 2009]. Therefore, further techniques are needed to improve the management of leukaemia.

1.5.2: Companion Diagnostics

Companion diagnostics are assays intended to help physicians to select or monitor therapy, and facilitate precision medicine by selecting the correct drug for the right patient at the precise dose. Companion diagnostic tests are needed to assess whether a new drug will work against a specific genetic or biological target, but not for all patients with a certain cancer or disease. These tests are used to categorise who would benefit from certain treatment or combination of treatments and sometimes to

establish whether a patient would not benefit, or could be harmed by the use of a certain treatment. Companion diagnostics are a key part of personalized medicine and will likely continue to rapidly increase in number and application to disease areas [Agarwal 2015, Olsen 2013]. Despite of the promising results of companion diagnostics, there are also complications i.e. developing a successful companion diagnostic with its complementary drug is complex, disintegrated and with several challenges. The components involved in companion diagnosis development require specific expertise which are not really found within a single organization, puts several challenges ahead in their development. The key challenges can be categorised in four broad categories [Moore 2012]. Strategic business challenges, Regulatory challenges, Financial challenges, Logistical challenges.

1.5.2.1: Currently used companion diagnostic techniques, their advantages and disadvantages.

1.5.2.1.1: IHC (immunohistochemistry)

This process is easy and routinely performed, very suitable for small tumours. It is quick, cost effective and does not require a highly-qualified person to perform [Gremel 2013]. It is easy to preserve the information gained through this technique. However, IHC is semi-quantitative and requires skilled staff for the interpretation of results. Since it requires sample preparation, it could vary in fixation procedure, staining protocol, and antibody selection [Gremel 2013].

1.5.2.1.2: Quantitative real-time PCR (qRT-PCR)

Quantitative real time PCR is very important technique used for companion diagnostics and has got large dynamic range. Qrt-PCR is also associated with some disadvantages as there is no histological information retained during the procedure [Gremel 2013]. Contamination of test results by stromal/normal tissue is possible. It has got increased time, cost and technological requirements. qRT-PCR results may also vary depending on tissue quality and RNA extraction/processing [Gremel 2013].

1.6: New Techniques to Be Explored

There is still a vacuum for the development of new techniques to improve the treatment and management of all cancers so further work is needed to establish new approaches. During my PhD, I have worked on several techniques to improve the diagnosis and management of leukaemia i.e. Synchrotron based Fourier Transform Infrared (FTIR) Spectroscopy, Raman Spectroscopy and the Selected Ion Flow Tube Mass Spectroscopy (SIFT-MS). These are discussed below.

1.6.1: Vibrational Spectroscopy

In recent years, an immense field of studies has shed light (using spectroscopic technique) on the medical and biomedical fields. The first application of vibrational spectroscopy took place in 1850 [Paul 2006]. Thanks to the developments in technology, vibrational spectroscopy has become very important in the field of biomedical science in recent years.

When light interacts with matter, it may be absorbed or scattered or may not interact with the matter at all. Stretching and bending are the two main oscillations of the atoms, which correspond to vibrational modes. Stretching involves asymmetric and symmetric motion while bending motions are scissoring, wagging, rocking, and twisting (Figure 7).

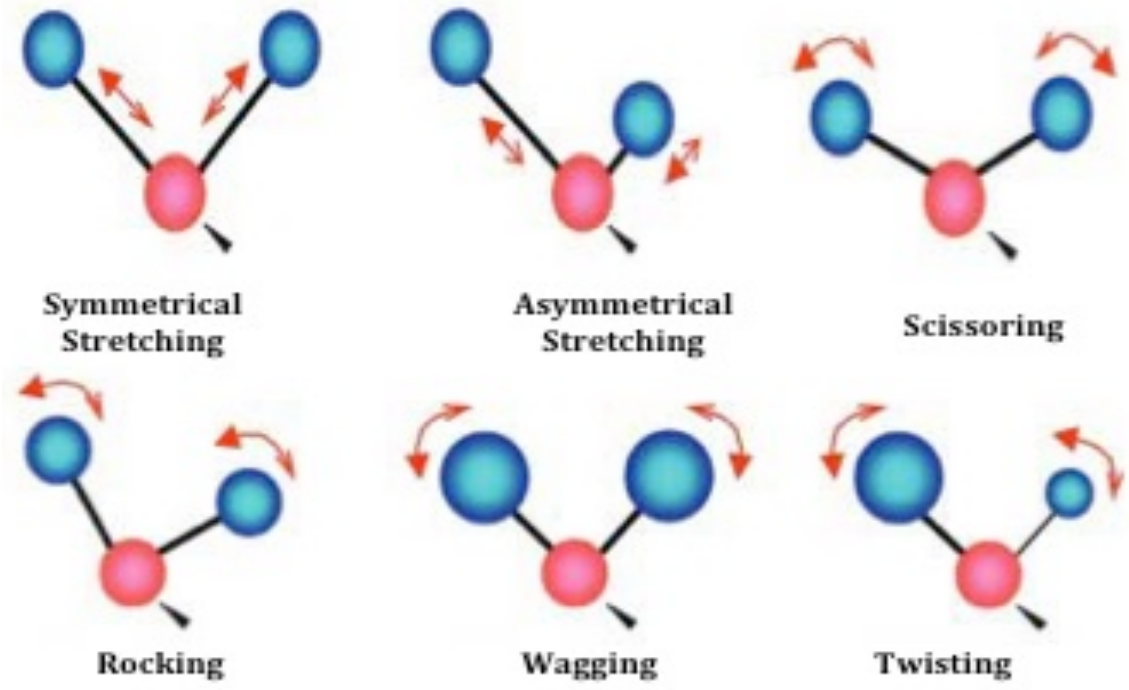

Figure 7: Different vibrational modes of a molecule.

Spectroscopic techniques are used to detect the loss or gain of energy through vibrational motion in molecules, which could be of infrared absorption or Raman scattering. The detection of loss of energy of radiation is called absorption spectroscopy. Vibrational spectroscopy uses an infrared (FTIR spectroscopy) or a laser (Raman spectroscopy) beam to study the biochemical composition and physical structures of cells and tissues amongst other, with the help of their spectral patterns (fingerprinting). When an infrared or a laser beam passes through the sample, some

of the radiation is absorbed by the sample while some will go through. This difference in light emitting from the sample can be recorded by specialised detectors that produce a spectrum based on the biochemical composition of the sample [Miller 1992; Jagannatha 2002]. Infrared and Raman spectroscopy are techniques presently used to detect and recognise disease and improve its management. In fact, vibrational spectroscopy can detect changes in structural composition of a molecule from normal to cancerous state, [Jackson 1998] which could be applied in early diagnosis of malignancy. This technique does open new horizons in the field of biomedical sciences because of its non-invasive nature

1.6.2: Infrared Spectroscopy

Infrared radiation is one part of the electromagnetic spectrum. Infrared Spectroscopy is a well-known, non-destructive technique, which can identify vibrational motions of molecules describing its structure. Chemical functional groups of a sample can be detected when it is placed in the path of an infrared beam in a non-destructive manner.

In the case of infrared spectroscopy, a range of frequencies is directed towards the sample and absorption occurs. The loss of this frequency of radiation from the beam due to the absorption is detected and measured. Infrared spectroscopy can be used to analyse gases, liquids, and solids. Perkin Elmer in 1944 offered the first ever-infrared spectrometer at commercial level. It produced a computer controlled IR spectrometer in 1976 [Miller 1992].

1.6.3: Fourier Transform Infrared Spectroscopy

Fourier transform infrared spectroscopy has become a powerful tool to fingerprint the chemical composition at molecular level because of its ability to provide detailed biochemical information. The development of the Michelson Interferometer (Figure 8) in 1880 allowed the study of samples with FTIR spectroscopy using several wavelengths simultaneously (figure 8).

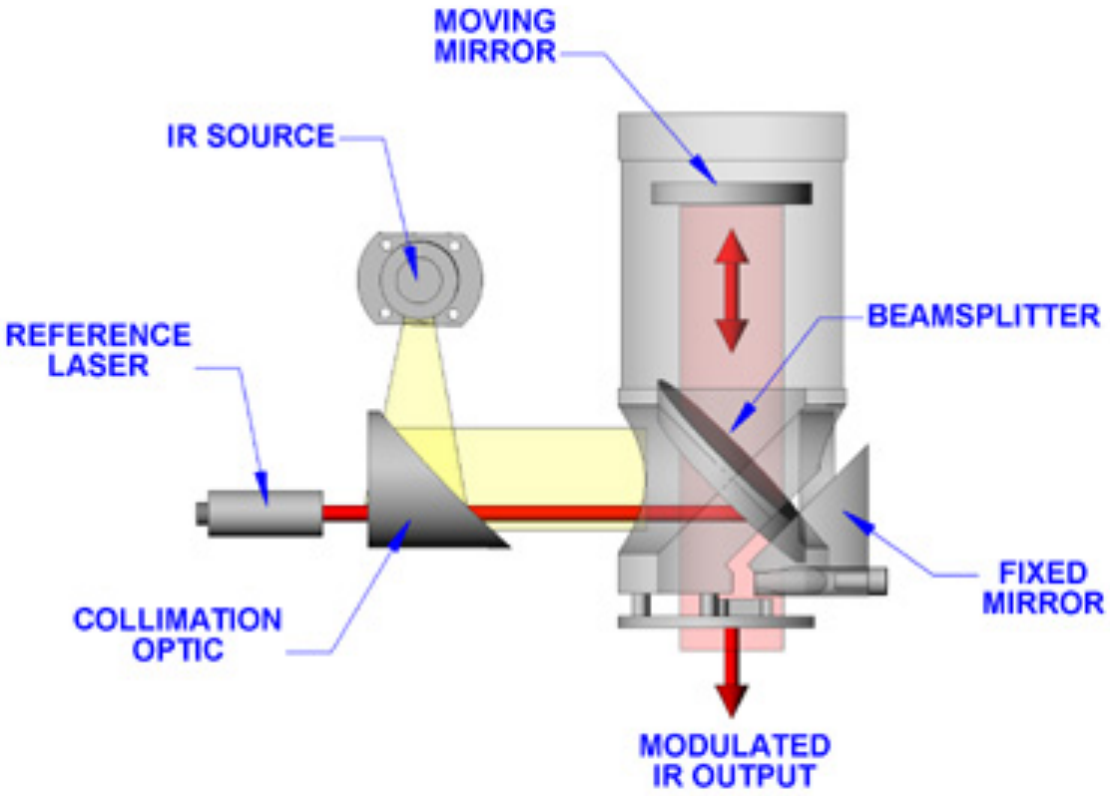

Figure 8: Michelson Interferometer.

The basic set up of FTIR Spectroscopy consists of a broadband radiation source, interferometer, a sample chamber/microscope and a detector. FTIR Spectroscopy has been used in cancer diagnosis with encouraging results [Bhargava 2007; Kendall 2009; Bellisola 2012; Petibois 2010] and to study the effects of chemotherapy agents

on cancer cells [Liu 2001; Zhou 2001; Gasparri 2003; Sulé-Suso 2005; Draux 2009; Bellisola 2010]. The development of mathematical and statistical methods has helped in the analysis and management of large amounts of spectral data.

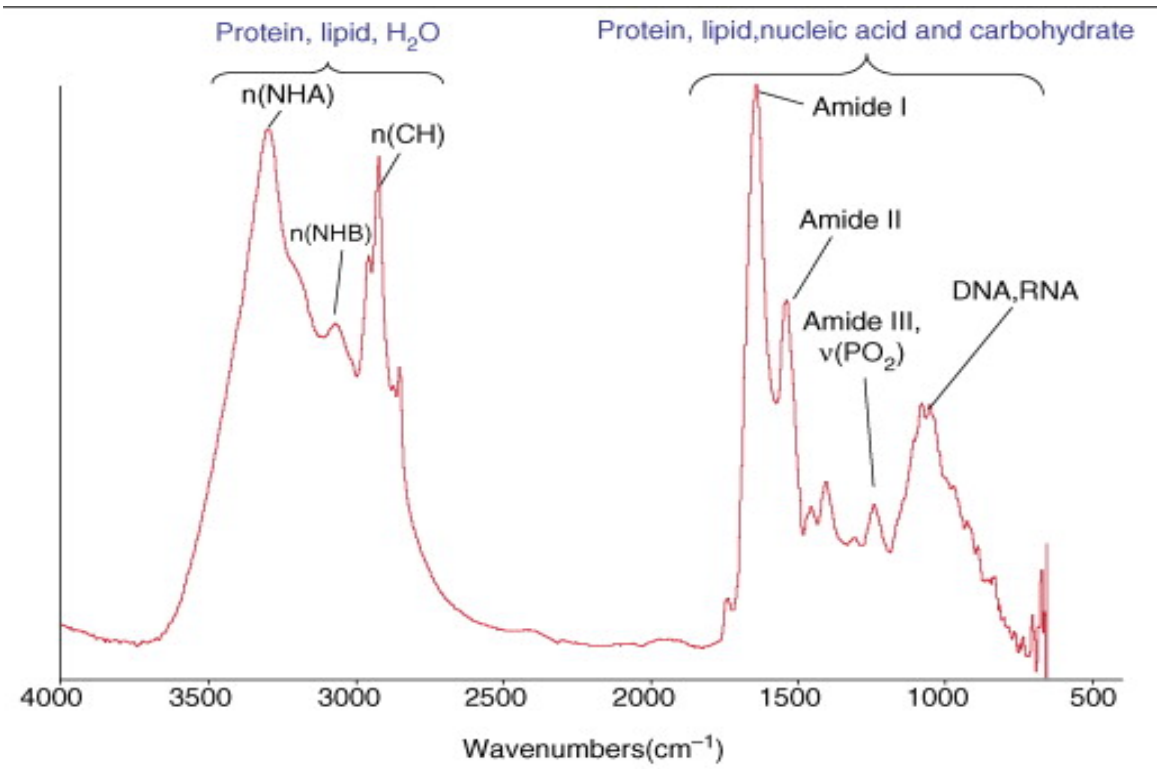

Figure 9: A typical IR spectrum of a cell.

A typical infrared spectrum of a biological sample can be divided into two main portions, one includes protein, lipid, and H_2O and the second one contains information about protein, lipid, nucleic acid and carbohydrate (Figure 9). This technique can provide very valuable composite information about the lipids. The vibrations in lipids are due to the CH_2 stretching which appears in the region of 3100 to 2800 cm^{-1} (Figure 9), CH_2 asymmetric mode at 2920 cm^{-1} (Figure 9) and symmetric at 2851 cm^{-1}. Methylene and methyl groups appear in the region of 1500-1350 cm^{-1} (Figure 9) and CH_2 bending occurs at 1470 cm^{-1} (Figure 9). Proteins are a basic functional unit of the cell, with each cell having its distinct functional protein. Infrared

spectra of proteins show their characteristic amide I group (C=O stretching) in the 1600-1700 cm^{-1} region. The amide II band is due to N-H bending and C-N stretching which occurs in infrared spectra at the region around 1150 cm^{-1} to 1450 cm^{-1} (Figure 9). The amide III band arises from coupling of C-N stretching and N-H bending giving rise to bands in the 1230-1300 cm^{-1} region. One of the most important infrared bands of proteins is the amide I, very useful for the analysis of secondary structures of proteins (Figure 9).

1.6.4: Synchrotron FTIR Spectroscopy

There is increasing interest in infrared microscopy with the development of Synchrotron radiation sources, a source of infrared radiation produced by electrons travelling at high speed in vacuum whose path is controlled by magnets (Figure 10) [Yarwood. 1984, Elleaume. 2002].

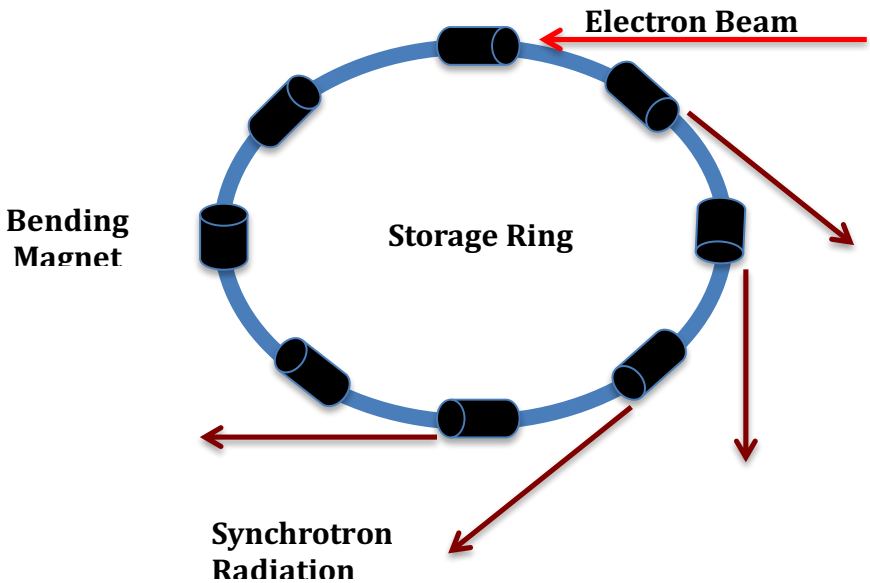

Figure 10: Schematic presentation of a Synchrotron. Magnetic field accelerates electrons by curving its path, as a result synchrotron radiation is produced.

It has very high brilliance and much smaller spot size when compared to conventional sources, allowing the study of biological samples at both cellular and subcellular levels extending from x-ray to infrared frequency [reviewed in: Dumas 2007]. It provides an intense light source of up to 1000x brighter than a globar source improving the detection of molecular information at the subcellular level with excellent spectral quality.

1.6.5: Raman Spectroscopy

When light interacts with matter, it is possible for the photons that make up the light to interact with the molecules and scatter as a resulting light. These scattering photons can be observed with the help of detectors at particular angle to the incident light. Scattering is a widely-used technique.

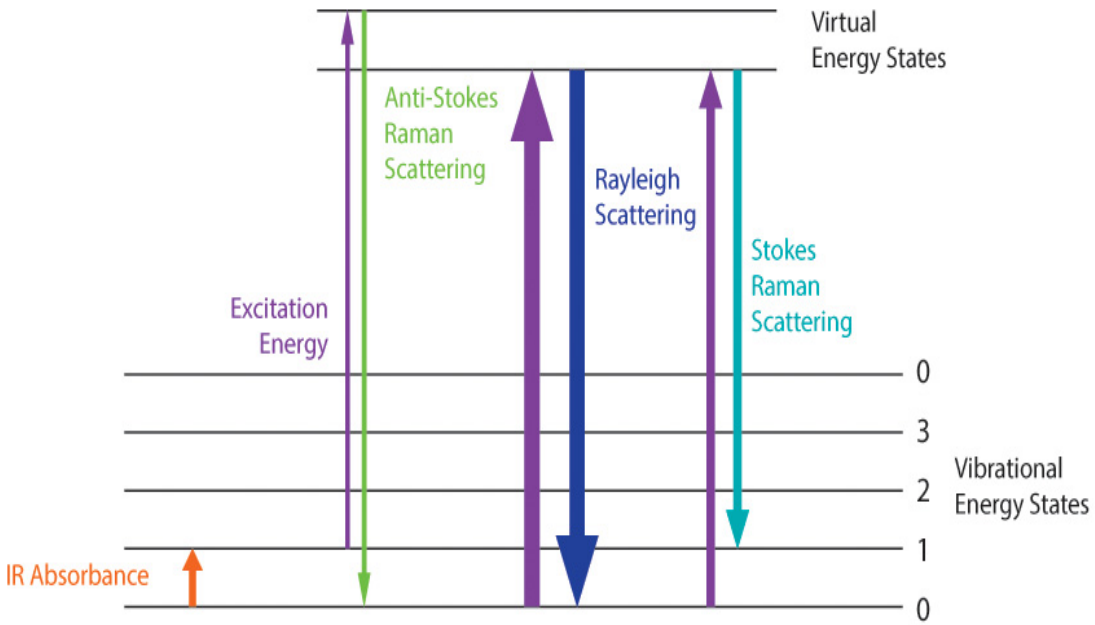

Figure 11: Energy-level diagram showing the states involved in Raman signal.

One every day illustration of scattering is the blue colour of the sky due to the higher energy blue light scattering from molecules in the atmosphere than lower energy red light. Raman spectroscopy is the main technique used to measure scattering to identify molecules. Figure 11 is a simple illustration of the different energy levels involved in Raman signal. Raman spectroscopy uses a single frequency of radiation directed to the sample and the radiation scattered from the molecules is recorded and measured. Raman spectroscopy can be used to detect changes at molecular level both *in vivo* and *in vitro* and compare diseased versus normal tissues (figure 12). There are three main components in Raman spectrometer, the laser, the spectrometer and the sampling interface.

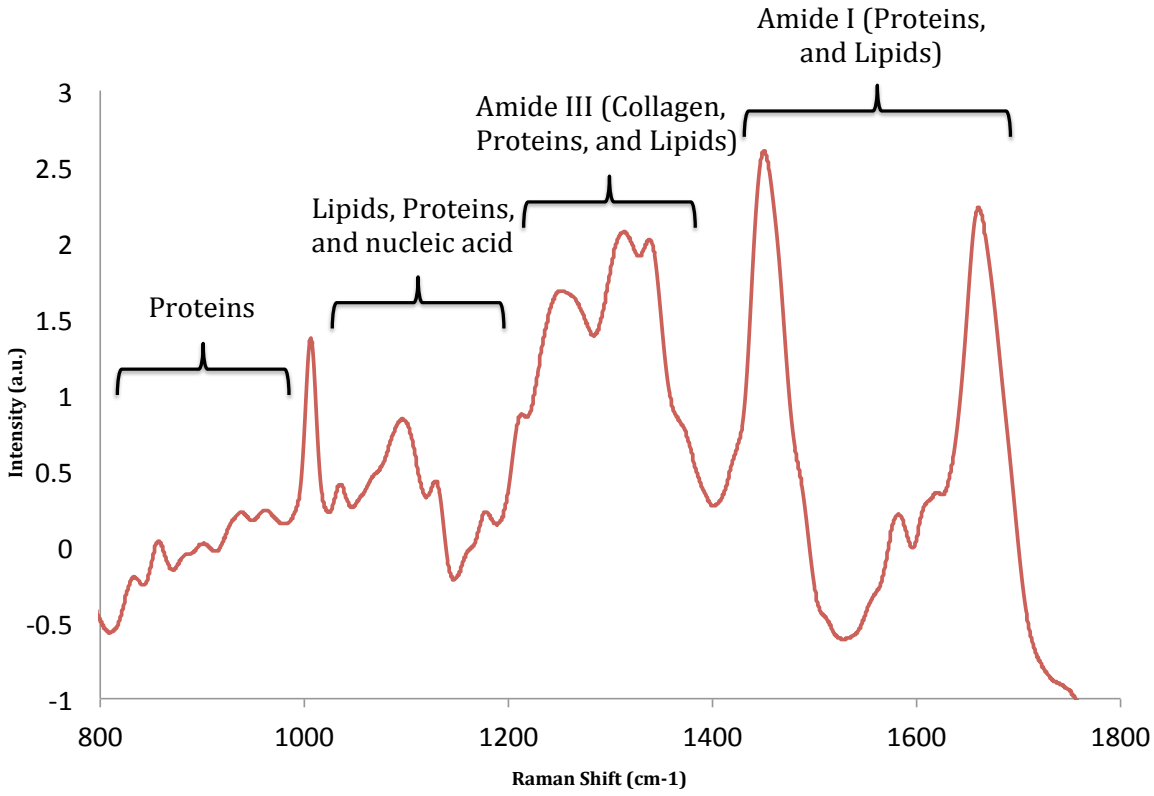

Figure 12: Representative Raman spectrum of a cell [Downes 2010].

The advantage of both FTIR and Raman spectroscopies is providing chemical information both at cellular and sub-cellular level without the need of stains and labels or external agents. The differing underlying mechanisms give rise to a complementarity of the two techniques, such that vibrations of asymmetric, polar bonds tend to be strong in IR spectra, whereas Raman is particularly suitable as a probe of symmetric, nonpolar groups. A further implication of the differing physical origins of the techniques is that, whereas IR monitors the absorption of IR radiation, Raman scattering can be employed in the UV, visible or near-IR regions of the spectrum. Raman scattering thus offers intrinsically higher spatial resolution for mapping or profiling, the limit of resolution being (classically) determined by the wavelength (<1 μm for Raman, ~5-10 μm for IR) (Byrne 2014).

All the diseases present with chemical and/or structural changes that can be identified with vibrational spectroscopy and compared to normal conditions. These changes in spectra can be used as spectral markers of a specific disease. These techniques have been used in a variety of different fields of biology, i.e. single human normal and leukemic cell analysis [Benedetti 1988], biomedical application in diagnosis [Krafft 2006], chemical imaging using Synchrotron IR [Miller 2006], clinical diagnostics [Dubois 2004], metabolic fingerprinting [Ellis 2006] and biochemical analysis of cells [Swain 2007]

In this thesis, I have worked with both Synchrotron-FTIR and Raman Spectroscopy for the treatment and management of leukaemia using two different leukaemia cell lines, Jurkat and K562. The resistance to the drug is a challenging issue in cancer treatment and management. One of the aims of this work was to establish whether

FTIR and Raman spectroscopies could be used to identify the resistance and/or sensitivity of leukaemia cells prior to treatment.

1.7: Release of Volatile Compounds from Leukaemia

Phillips *et al.* (1994) stated there are 3,481 different compounds in human exhaled breath which have been observed at different concentrations ranging from parts per billion by volume (ppbv) to parts per trillion by volume (pptv), which vary from person to person. Among this number of volatile organic compounds (VOCs), only a small number of VOCs are common among all people. These include isoprene, acetone, ethanol, and methanol amongst other. Along with these, exhaled breath also contains NO, H_2 NH_3, and CO_2. Some of these compounds show negative alveolar gradient[6], as they are in higher concentrations in inhaled air rather than exhaled breath. About 1,753 compounds were observed showing positive alveolar gradient (higher concentration exhaled breath than inhaled air) [Phillips 1994; Phillips 1999]. Over the last few years, there has been an increased interest in the study of VOCs released by cancer cells. Several techniques such as Gas Chromatography Mass Spectrometry (GC-MS), Proton Transfer Reaction Mass Spectrometry (PTR-MS), ion mobility spectrometry (IMS), and Selected Ion Flow Tube Mass Spectrometry (SIFT-MS) have been used in the study of VOCs released by cancer cells [Amann 2005]. All above-mentioned techniques have their own advantages and shortcomings.

[6] The Alveolar arterial gradient (A-a gradient) is a measure of the difference between the alveolar concentration (A) of oxygen and the arterial (a) concentration of oxygen.

Alveolar gradient SIFT-MS, used in this work, detects accurately and in real time several compounds simultaneously down to concentrations of parts-per-billion by volume (ppbv). More importantly, it obviates sample preparation that could not only alter the sample but take up valuable time [Smith 2005; Španěl 2011]. Several groups have applied the SIFT-MS technique to study the release of volatiles by cancer cells [Sulé-Suso 2009] aimed mainly at developing applications of this sensitive technique for cancer diagnosis.

Table I: Current Breath Analysis Techniques.

Analytical Technique	Mode of operation	Detection Limit	Sensitivity	Specificity
SIFT-MS	Direct/Real-time [Smith 2005]	ppbv	High	High
PTR-MS	Direct/Real Time [Lindinger 1998; Kushch 2008]	pptv	High	Medium/High
IMS	Real time [Ulanowska 2008]	ppbv	Medium	Medium
GCMS	Pre-Concentration [Ligor 2008; Fuchs 2010]	pptv-ppbv	Very high	Very high

In breath analysis, lung pathophysiology and lung diseases have been widely studied to achieve an early diagnosis of lung cancer [Di Natale 2003; Mazzone 2008; Bajtarevic 2009; Sponring 2009]. However, this methodology could be extended to other medical applications such as the study of blood diseases thanks to the exchange of volatiles through the blood-gas interface in lung alveoli [Sapoval 2002]. It has been estimated that the mean number of alveoli in a healthy lung is around 480 x 10^6 [Ochs 2004] providing a surface area of around 70 m^2 [Notter 2000]. Thus, it could be hypothesised that the presence of a high number of leukaemia cells in patients' blood and/or in the bone marrow could lead VOCs profiles in breath different from those of healthy people. To better characterise the VOCs released by leukaemia cells, I have carried out the present study comparing VOCs released by 2 leukaemia cell lines to healthy peripheral blood mononuclear-cells.

1.7.1: Selected Ion Flow Tube Mass Spectrometry (SIFT-MS)

SIFT-MS is an innovative investigative method. The history of this technique starts with the development of Selected Ion Flow Tube in 1976 by Dr David Smith, [Španēl 2001] the concept of which was to study the ion molecule reactions in the gas phase at thermal energies. This instrument has made great progress in the field of gas analysis with the help of a quantitative Mass Spectrometer. SIFT-MS is based upon the principle of chemical ionization (CI), which uses specifically chosen reagent ions H_3O^+, NO^+, and O_2^+ (which do not react readily with major molecules present in the air but most of the trace gases and vapors of medical interest) along with flow tube technology and quantitative mass spectrometry. It works on real-time quantification of several trace gases simultaneously in air and breath. Absolute concentrations of

trace gases in single breath exhalation/headspace can be determined by SIFT-MS down to ppb levels, obviating sample modification. SIFT-MS utilizes the reaction of mass selected precursor ions with sample ions that are introduced into a flow tube via a helium gas carrier. The subsequent product ions are then studied by a downstream mass spectrometer (Figure 13). Mass selected precursor ions are created using a microwave resonator; commonly selected ions are H_3O^+, NO^+ and O_2^+ ions, for the simple reason that they do not react readily with the common constituents of air [Španěl 2011; Michalčíková 2014].

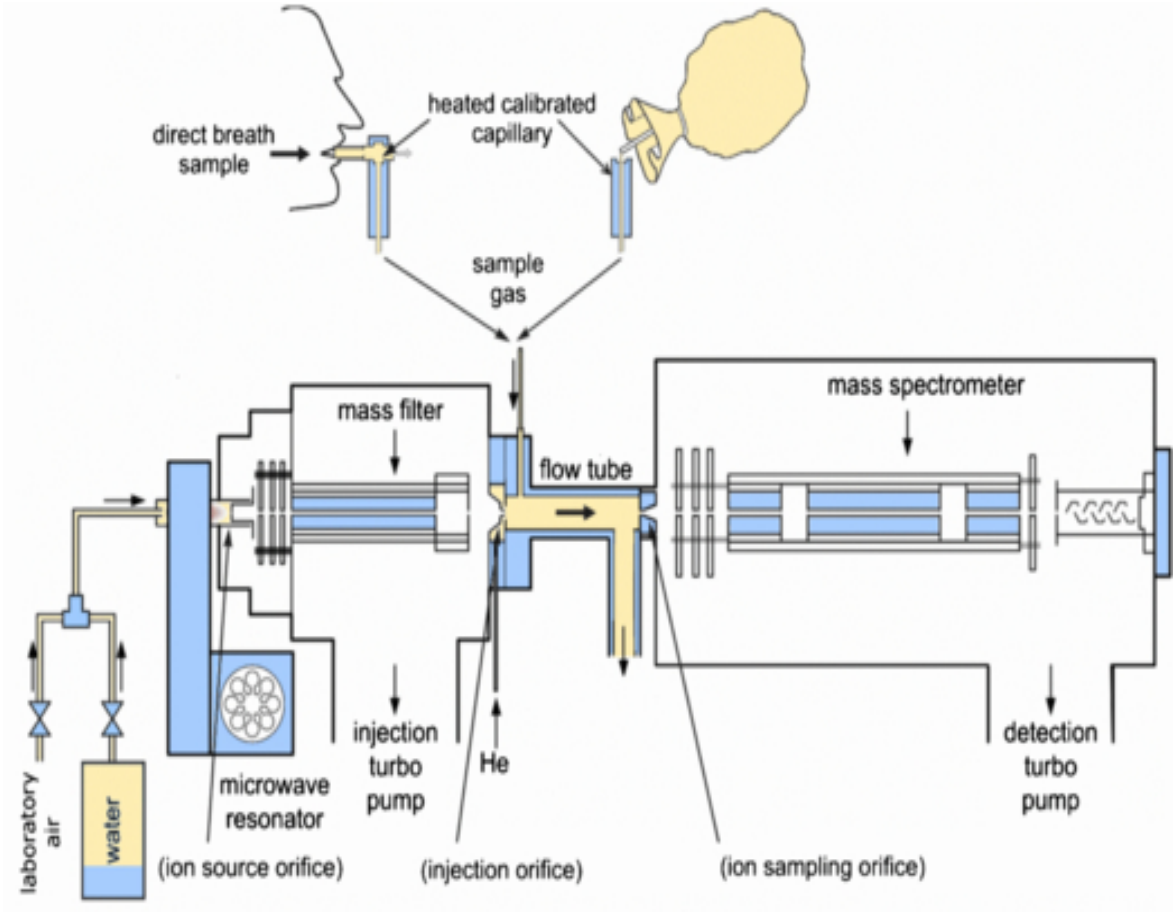

Figure 13: Typical Schematic diagram of a SIFT-MS machine being used in this study [Smith 2011].

A downstream mass spectrometer is then used to select the correct ions generated by the microwave generator. A series of pumps and sampling orifices are used to maintain the correct pressure and to focus the ions along the SIFT-MS. The downstream mass spectrometer operates at around 5-10 Torr, the proceeding flow tube operates at 0.5 Torr in order to achieve articulate gas reactions. Venturi inlets are used to sustain such changes in pressure but maintain a focussed flow of ions. Once a stream of defined precursor ions has been established the sample of interest is then injected into the flow tube through a helium carrier gas; the gas again being specific for this purpose, due to its inert nature at a pressure of around 1 Torr. The introduced ion species from the sample of interest then reacts with the precursor ions (preselected by the upstream quadrupole) as they travel across the flow tube at high speed (Španěl 2011). Product ions and precursor ions travel through a final sampling orifice where they are met by the downstream quadrupole. An electron multiplier then amplifies the signal given from the final quadrupole. An on-line computer is then able to calculate the relative concentration of trace compounds from the reaction of product ions and sample gas (Smith 2005; Španěl 2011). These data are analyzed in real time with the help of chemical information recorded in SIFT's extensive compound library giving instant, accurate quantification of all compounds in the samples.

The primary advantage of SIFT-MS, in contrast with GC-MS, is that the compounds' concentrations in the sample can be measured in real time (seconds) while in case of GC-MS the speed of measurement is limited by the retention time.

In this thesis, I have also worked on the analysis of VOCs released from both Leukemia cell lines, the difference in the VOCs' profile of different clones from the same cell line, differences in the VOCs' profile after drug administration and difference in the release of VOCs in hypoxic and normoxic conditions.

1.8: AIMS of the Study

In order to improve the early diagnosis and management of leukaemia, further work is needed to develop and apply in the clinical practice techniques that provide fast and robust results. While I acknowledge that further work is needed to take these techniques into a hospital set up, the work carried out here shows promise for both techniques as helping aids to clinicians managing patients with leukaemia.

1. To assess whether vibrational spectroscopy and SIFT-MS could have the potential, that could be used in clinical practice.
2. To characterize the best methodology for these techniques to translate their best use into clinics.

Chapter: 2

General Material and Methods

2.1: Cell Culture

The cells used in this study were:

Jurkat (kind gift of Dr Bellisola, University of Verona), an Acute T Cell Leukaemia cell line, established from the peripheral blood of a 14-year-old male by Schneider et al. (1977).

K562 (kind gift of Dr Bellisola) is a Chronic Myelogenous Leukaemia cell line. This cell line is derived from a 53-year-old female with chronic myelogenous leukaemia (CML). K562 is used widely as a highly sensitive *in vitro* target for many different drug assays [Pietarinen 2015].

Fresh Human Peripheral Blood Mononuclear cells (PBMC) bought from ZenBio, Inc. (UK). A blood cell with one nucleus is called a peripheral blood mononuclear cell (PBMC). PBMC are very important part of the blood system containing cells of the immune system, a natural defence system against infections. PBMC contain all types of leukocytes including T type, B Type, natural killer cells, monocytes, basophils, neutrophils, and eosinophil cells. These cells were extracted from whole blood of a healthy person. I used these cells as control against leukaemia cell lines.

Human bone marrow aspirates (BMA) from the iliac crest of 3 different healthy donors were purchased from Lonza, USA.

Both leukaemia cell lines (Jurkat, K562) were maintained in RPMI 1640 supplemented with 10% Foetal Bovine Serum (FBS), 1% L-Glutamine, 1% Hepes Buffer, and 1% Antibiotic/antimycotic. Growth conditions were maintained within culture flasks (Sarstedt, UK) at 37°C and 5% CO_2. Media was changed every 3-4 days. Cells were passaged before reaching confluence. These cells grow in suspension.

Fresh PBMC were thawed and cultured in RPMI 1640 supplemented with 30% FBS 1% L-Glutamine, 1% Hepes Buffer, and 1% Antibiotic/antimycotic. Growth conditions were maintained within culture flasks (Sarstedt, UK) at 37°C and 5% CO_2. These cells grow in suspension.

Whole bone marrow samples were seeded at a density of 7.5 x 10^6 cells in 20 mL of Dulbecco's Modified Eagle's Medium (DMEM) supplemented with 5 ml Hepes buffer, 5% FBS, 1% L-glutamine and 1% NEAA on 10 ng/ml fibronectine-coated T-75 tissue culture flasks (Sigma, UK). Samples were incubated at 37 °C and 5% CO_2.

2.1.1: Cell Viability

Cell viability was determined with the Trypan Blue exclusion method. 20 µL of 0.4% Trypan Blue solution (Sigma Aldrich, UK) were added to 20 µL of cell suspension and mixed gently. A haemocytometer was then loaded with the stained suspension. Live and dead cells were counted under the microscope (non-stained cells were

considered as live cells, those cells that take up the Trypan blue stain, are considered as non-viable).

2.1.2: Cell Cloning

K562 cell line was used to obtain leukaemia cell clones [Chu 2009; Rutter 2014]. For this purpose, cells were collected from the culture flasks and centrifuged at 950 rpm for 3 minutes. Supernatant was then discarded and the cell pellet was dislodged and resuspended in fresh complete medium. After adding the medium, the cells were counted using the trypan blue exclusion assay. Cells then were seeded in flat-bottomed 96 well plates at a concentration of 0.5 cells/well in 200 µL/well complete media (for example and for simplicity, for 100 wells, 50 cells were placed in 20 mL of medium and distributed evenly in these 100 wells. Diluted such that the probability is 0.5 cells/well).

The plates were wrapped in foil to avoid dehydration, incubated at 37°C and 5% CO_2. Media was changed after one-week culture by spinning the plates at 1200 rpm for 7 minutes. Following this, 100 µL of media were removed and 100µL of fresh complete media were added. Plates were further incubated at 37°C and 5% CO_2 for one week to allow the clones to develop. Clones were inspected regularly so those wells with more than 1 clone could be discarded. Figure 14 is a representative example of four different clones 1, 2, 3 and 4 used during the experiment, while, figure 15 is the example of clones, which were discarded. The number of clones obtained with this experimental set up was more than 15 clones per each 96 well plate (Figure 14).

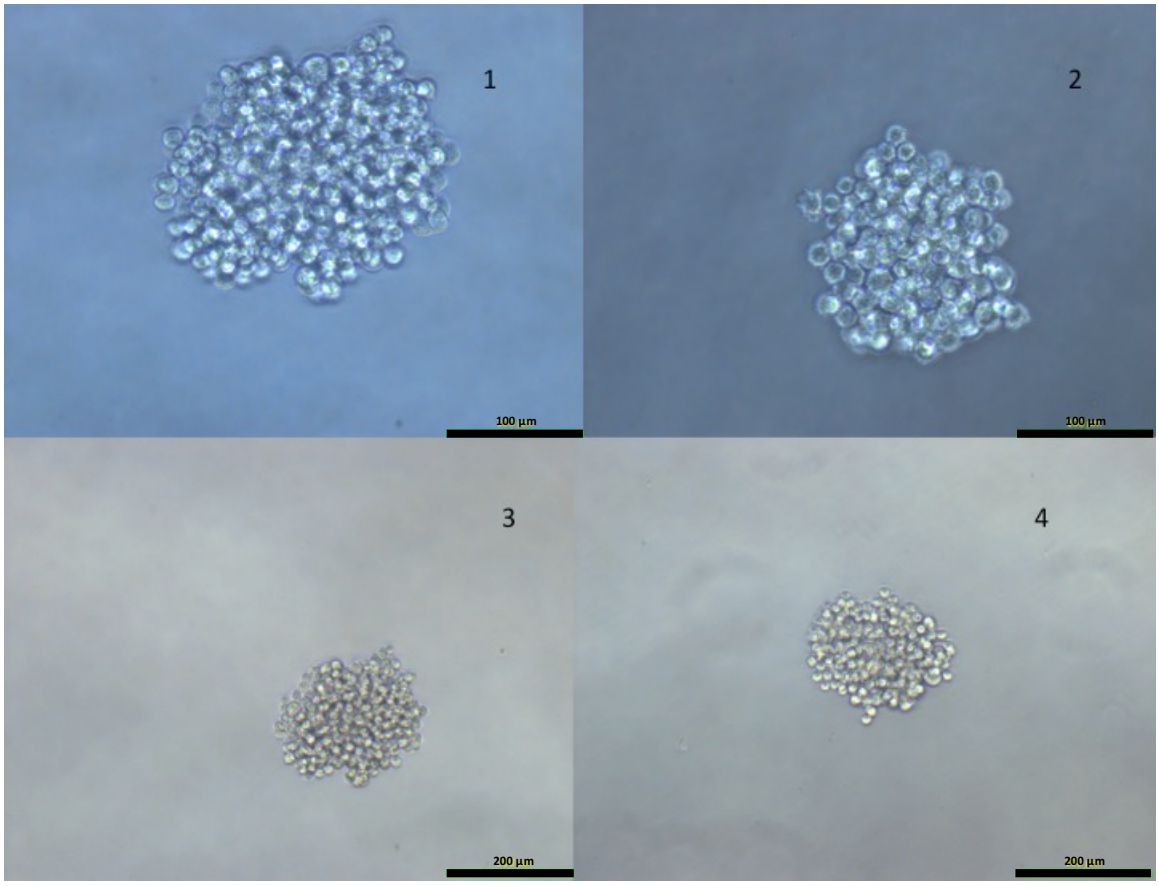

Figure 14: Representative examples of four K562 Clones (clone 1, clone 2, clone 3, and cone 4) (Pictures taken at 7th day of Seeding).

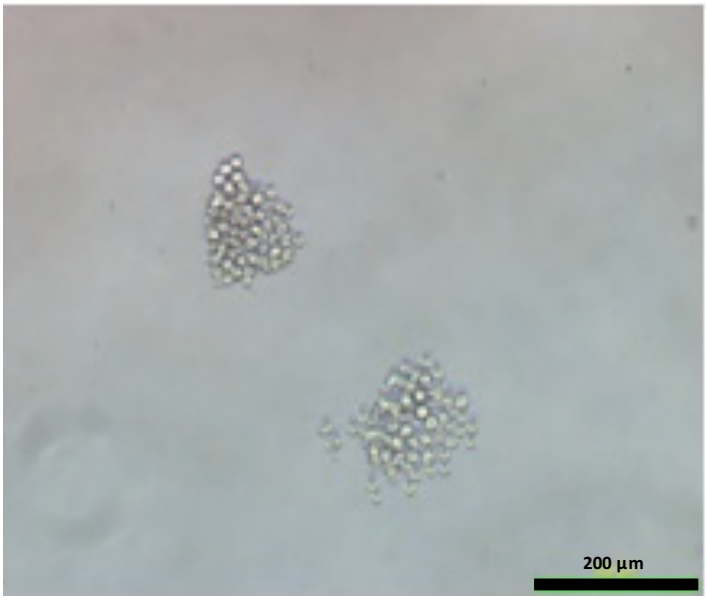

Figure 15: Representative example of K562 clones in single well, those clones were discarded.

2.2: Imatinib

The doses of Imatinib used in the present work were 50 μM and 100 μM. Since IC 50 values for this drug varies vastly with in each cell line, preliminary experiments showed that most cells were alive when incubated for five days with 10 μM Imatinib and no cells survive in the presence of 500 μM Imatinib.

Imatinib mesylate was a kind gift of Novartis (Switzerland). The drug was provided in powder form (58 mg). The powder was reconstituted with distilled water to a final concentration of 10 mM according to the provider's instructions and stored at -20 °C.

2.3: Nilotinib

The doses of Nilotinib used in the present work were 50 μM and 100 μM. Since IC 50 values for this drug varies vastly with in each type of cell line same as Imatinib, preliminary work proved that ratio of live over dead cells was high when incubated for five days with 10 μM Nilotinib and low in the presence of 500 μM Nilotinib.

Nilotinib was also a kind gift of Novartis (Switzerland). The drug was provided in powder form (100 gm). The powder was reconstituted with DMSO to a final concentration of 10 mM according to the provider's instructions and stored at -20 °C.

2.4: Disulfiram Inhibition

Disulfiram (tetraethylthioperoxydicarbonic diamide) (DSF), known as Antabuse, has been used in the treatment of alcoholism since 1948, as an alcohol aversion agent [Bell 1949]. DSF given to patients with alcohol consumption results in acetaldehyde

accumulation [Bell 1949], due to disulfiram ethanol reaction [Maracto 2011]. It is an Acetaldehyde dehydrogenase (ALDH) inhibitor, which primarily inhibits ALDH by covalently modifying sulfhydryl group, leading to high blood levels of Acetaldehyde. DSF also inhibits other copper-dependent enzymes, such as carboxyl esterase and cholinesterase [Zemaitis 1976], due to which DSF is thought to induce proteasome inhibition and subsequently cancer cell apoptosis [Wang 2011]. Lin et al. (2011) observed also inhibition by disulfiram of prostate cancer cell growth along with DNA-DE-methylation [Lin 2011]. Currently, clinical trials are on-going to testify DSF's ability to inhibit cancer growth [Lin 2011].

It has been suggested that acetaldehyde produced by microorganisms present in the mouth and throat may affect analysis of acetaldehyde [Jones 1995]. *In vitro* inhibition of ALDH by DSF was studied during this work to confirm the release or consumption of Acetaldehyde by Leukaemia cells.

DSF (SIGMA-ALDRICH) was provided in powder form (300 mg). It was dissolved in DMSO to a final concentration of 20 mM, and was stored at -20 °C. DMSO was selected to be the common solvent for the inhibition experiment, as it has relatively low vapour pressure so it was not expected to interfere significantly with headspace analyses [Chippendale 2012]. Disulfiram inhibits ALDH-II at IC50 = 10 nM more potently than ALDH-I's IC 50 >20 μM [Keung 1993]. Kim 2013, reported an inverse correlation between the percentage of cells expressing ALDH and IC values for disulfiram. Notably, the IC of disulfiram for hTERT-HPNE cells by far exceeded those of Mia PaCa-2 and CFPAC-1 cells, indicating that a sufficiently wide therapeutic window can be secured

[Kim 2013]. As DSF was already reported being used by Thomas, W. E. C. 2012, at 20 μM, I used two concentrations, 20 μM and 40 μM.

2.5: Selected Ion Flow Tube Mass Spectrometry

Volatile organic compounds (VOCs) from the headspace of cell cultures were measured using an analytical technique, Selected Ion Flow Tube Mass Spectrometry Profile 3 instrument, from Instrument Science, UK (Figure 16). Selected reagent ions are produced by water and air by a microwave discharge ion source and categorized with the help of a mass quadrupole. During my study, I used H_3O^+ and NO^+ as precursor ions. The humid headspace of the cell cultures was acquired through a heated sampling line, a hypodermic needle puncturing the septum of the culture bottles connecting the headspace directly into the inlet port of the Profile 3 instrument. During headspace sampling, the cell culture bottles were maintained within a water bath at 37°C.

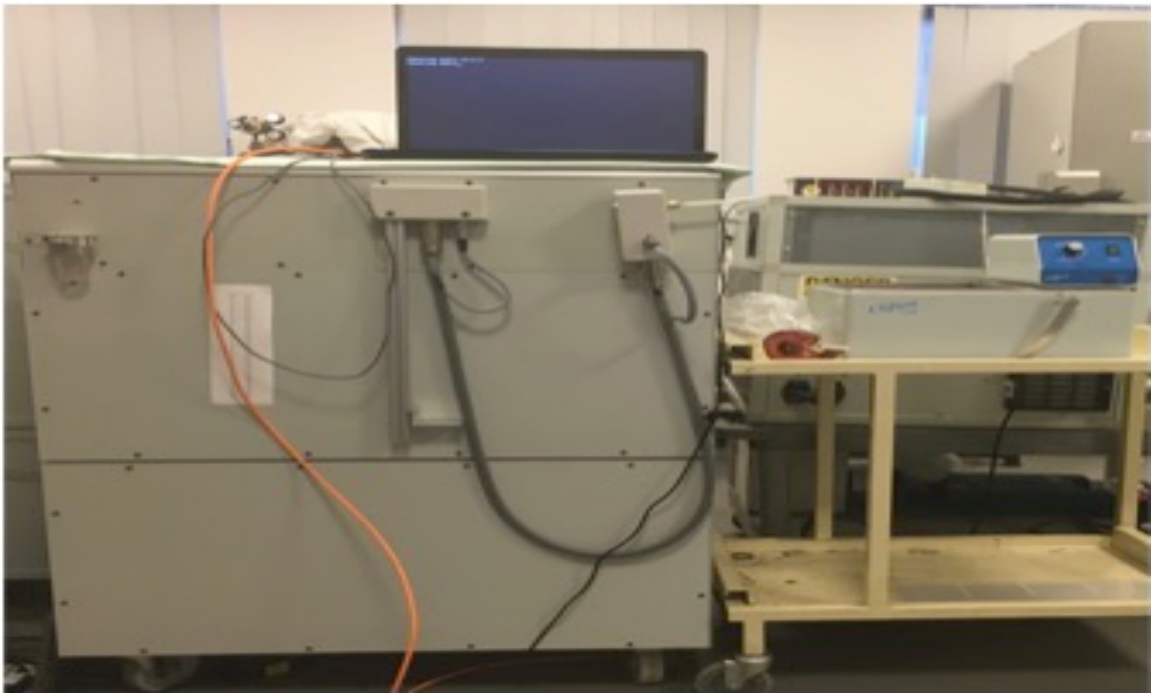

Figure 16: Profile 3 SIFT-MS instrument at ISTM, Keele University, UK.

SIFT-MS kinetic library provides a list of the compounds present in the sample. The instrument was used either in multi-ion monitoring mode (MIM), to study chosen VOCs, or on Full Scan mode (FSM), to study possible species in the range between 10 - 180 m/z.

2.5.1: Sample Preparation for SIFT-MS

The SIFT-MS studies of parental cells were carried out as follows. Cells were cultured in culture flasks (Sarstedt, UK) at 37°C and 5% CO_2 for 5 days. Media was changed on the 3rd day, and cells were incubated further 2 days. After this incubation period, cells were collected and counted using the trypan blue exclusion method after centrifuging at 950 rpm for 3 minutes. The cells were then seeded at 10, 20 or 40 x 10^6 cells/bottle in 150 ml glass bottles. These bottles were incubated under standard conditions described above for 2 hours with the lids slightly loose. After this incubation period, the bottles were air purged with dry air for 1 minute, the lids were then closed tightly and further sealed using parafilm. The bottles were then incubated at 37°C for a further 16 hours.

In order to compare the VOCs released by clonal populations to the parental cell line, I acquired the clones as previously described. The selected clones after two weeks' incubation were then transferred to 24 well plates. After one-week incubation in 24 well plates at 37°C and 5% CO_2, cells were transferred to T25 flasks (Sarstedt, UK). These flasks were further incubated for one week; media was changed on the 3rd day. Following one-week incubation, the clonal cells were collected and counted using the trypan blue exclusion assay. Cells were seeded at 10 x 10^6 cells/bottle in 150 mL glass bottles. This cell concentration was used in order to keep to a minimum the

number of passages needed to get a number of cells high enough to run these experiments. It is widely accepted that the higher the number of passages the more different the cells are from the original one [Masters 2007]. The bottles were incubated at 37°C and 5% CO_2 for two hours with the lids loosely closed. Following this incubation time, the bottles were air purged with dry air, lids tightly closed and further sealed with parafilm, and incubated overnight for 16 hours. SIFT-MS experiments were carried out following this incubation period.

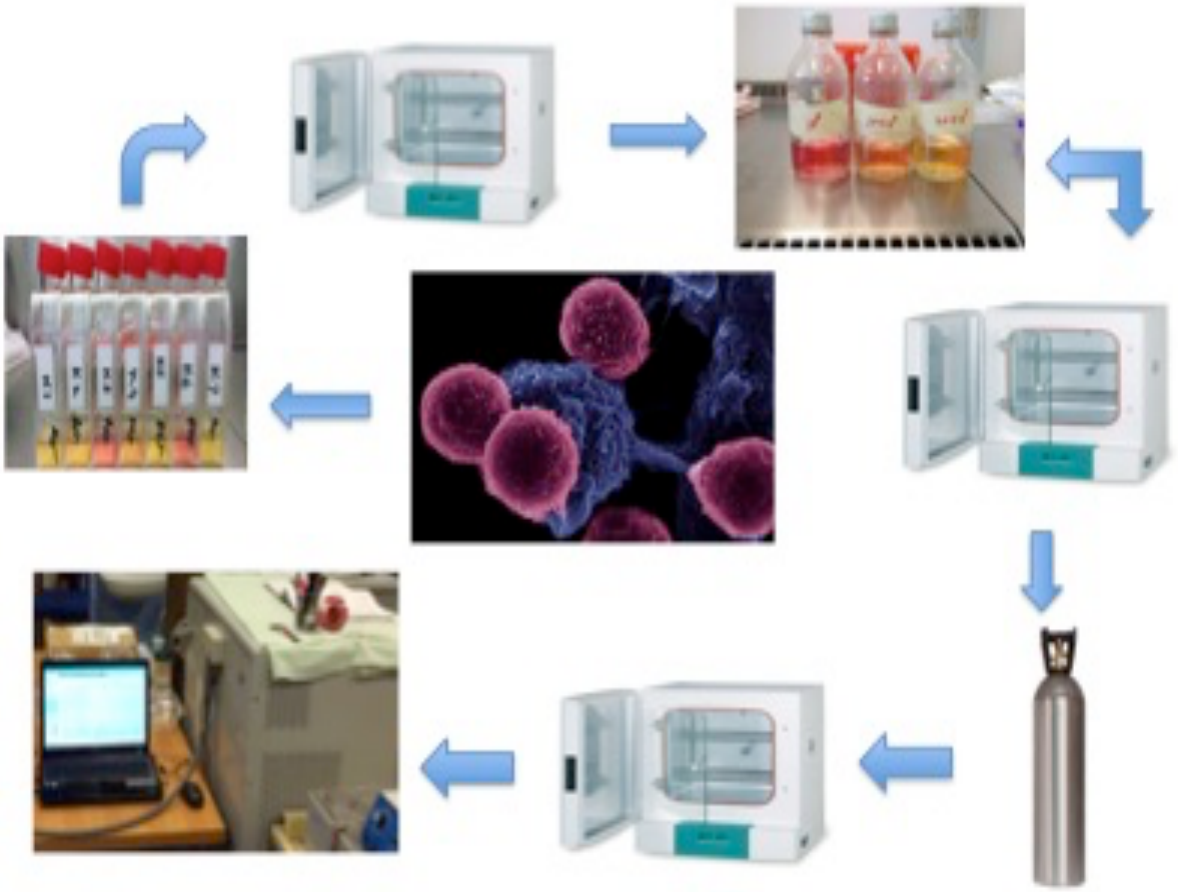

Figure 17: Schematic stepwise presentation of SIFT-MS set up and sampling.

In order to assess the possible differences in the VOCs released by cells following the incubation with drugs, the following experiments were carried out: cells were

collected and counted using the trypan blue exclusion assay after centrifuging at 950 rpm for 3 minutes. Following counting, cells were seeded in 150 mL glass bottles at a concentration of 10 x 10^6 cells/bottle. These bottles were then incubated for 2 hours with their lids loosely closed. Following this incubation period, Imatinib or Nilotinib was added at a concentration of 50 μM, or 100μM. The bottles were air purged with dry air for 1 minute; lids tightly closed and further sealed with parafilm, and incubated overnight for 16 hours. SIFT-MS experiments were carried out following this incubation period.

To determine that acetaldehyde release is not coming from the metabolic activity of the ethanol, the ALDH inhibition test was performed as follows: cells were collected and counted using the trypan blue exclusion assay after centrifuging at 950 rpm for 3 minutes. Following this, cells were seeded in 150 mL glass bottles at the desired concentrations. These bottles were then incubated for 2 hours with their lids loosely closed. Following this incubation period, DSF was added at the concentration of 20 μM, or 40 μM. The bottles were air purged with dry air for 1 minute; lids were tightly closed and further sealed with parafilm, and cells were incubated overnight for 16 hours. SIFT-MS experiments were carried out following this incubation period. Cells were recounted after the SIFT-MS experiment to confirm cell survival.

In order to translate SIFT-MS into clinics, the breath sampling method needs to be well characterised. At present, three main sampling techniques are used by different groups, i.e., direct breath, bottles, and Nalophan bags. In order to obtain breath samples, healthy controls were asked not to eat or drink anything apart from water in the morning prior to giving a breath sample. They were not allowed to brush their

teeth as some VOCs from the toothpaste could interfere with VOCs' measurement. Patients were allowed to take their medication if indicated. Samples were taken before 9.00 AM.

Exhaling directly into the machine allowed to obtain direct breath.

For bag samples, Nalophan tube sheeting was cut into 30 cm length and a 3 cm poly-tubing length was inserted into one end, fixing it into place with a cable tie and sealed with parafilm. The other end of the sheet was sealed using a cable tie and parafilm. Individuals were asked to exhale 3 times into the bag. A syringe was used to seal the end tube of the sampling bag after the breath was collected. Parafilm was used to further seal it.

Bottle sampling was done by asking the individuals to fill the glass bottles of 150 ml volume with the help of 10cm straw, inserted 8 cm into the bottles. These bottles were sealed after the breath was exhaled into them with a tightly closed cap and parafilm. The caps contain a septum through which SIFT-MS sampling with a needle is carried out.

Bag and Bottles were sampled at different incubation time points, 1, 3, 6, and 24 hours. Incubation was carried out at room temperature to assess how delays in breath sampling could affect the VOCs profile.

As described in first chapter in 1.7.1, SIFT-MS can run in 2 different modes using three different precursors. Direct breath was sampled just in MIM mode; as full scan

mode requires longer duration to acquire the data making it impossible for a patient to exhale enough breath in one go. On the other hand, bags and bottles samples were run in both modes, MIM mode using both H_3O^+ and NO^+ precursors, and Full Scan mode.

2.5.2: Data Processing

Humidity in each sample might vary due to environmental reasons and/or physiological characteristics of the individual giving a breath sample. The humidity can affect the quantification of VOCs, especially when using H_3O^+. To compensate for changes in humidity, a 6% water correction method (already being used by different groups in the field) was used. Each individual VOC measured was corrected to 6% water level using the flow rate adjustment built in the SIFT-MS software. The kinetic library then quantifies VOCs on this percentage of water [Smith 2011].

2.5.3: Data Analysis

The data obtained using the SIFT-MS is presented in ASCII. Using SIFT-MS software, it was transferred into Excel. Principal Component Analysis was carried out using. Unscrambler software (Camo, Oslo, Norway) and visualised using Graph Pad Prism 6.

2.6: Aldefluor Assay

Aldefluor™ kit was purchased from STEMCELL Technologies™ Cambridge, UK. Flow cytometry (CYTOMICS FC 500 Beckman Coulter) was used to carry out the Aldefluor assay to assess ALDH activity in cells.

Aldefluor assay has been used for the identification, evaluation and isolation of stem and progenitor cells expressing high levels of ALDH [Zhang 2014]. Aldefluor™ is a reagent kit used in the identification of cells that express high levels of ALDH Activated Aldefluor™ reagent, BODIPY-aminoacetaldehyde (BAAA) is a fluorescent substrate for ALDH that easily penetrates cells. If ALDH enzyme is present, BAAA is converted into BODIPY-aminoacetate (BAA) that is retained by the cell. This ALDH activity is measured by flow cytometry (figure 18). The amount of fluorescent reaction produced is directly proportional to the ALDH activity in the cell. Aldefluor™ kit reagents were prepared and stored according to the provider's instructions. Aldefluor assay was conducted by following the instructions from the kit providers using in-house flow cytometry (Figure 18).

Figure 18: Image of the flow cytometer (CYTOMICS FC 500 Beckman Coulter).

2.7: Synchrotron Based FTIR Spectroscopy

2.7.1: Application of Drugs to Cells

As described in the cloning section (2.1.2), cells were cloned and following 2 weeks culture, clones were removed from the 96 well plates, by mixing the media in each individual well containing a clone and collecting both the total media (200 µL) and cells. Collected cells were then seeded proportionally in 3 wells in 96 flat-bottomed plates. They were allowed to grow for 24 hours at 37 °C and 5% CO_2. Following this incubation period, Imatinib and Nilotinib were added as follows. Plates were spun at 1200 rpm for 7 minutes. Following this, 100 µL of medium were removed and 100 µL of fresh medium with different concentrations of Imatinib or Nilotinib were added (0 µM, 50 µM or 100 µM). Cells were allowed to grow for 5 days at 37 °C and 5% CO_2 in order to assess clone survival. Five days were decided in order to establish if the cell population was sensitive or resistant to the drug. It was observed that keeping cells growing for more than 5 days translated into cells overgrowing in control wells (in the absence of Imatinib or Nilotinib).

2.7.2: Clone Selection

Synchrotron beam time at Diamond Light Source, Oxford, UK and Synchrotron Soleil, France, are limited in their time allocation, so I was able to use only few clones. Table II shows a representative example of clones obtained from one 96 well plate. Clones in which cells in control wells were completely confluent were discarded as this could modify their metabolical and proliferative properties. The clones were selected by visually observing the wells under the microscope and classed as sensitive where no

cells were seen or very low number of cells in the well were identified, resistant clones were those with semi-confluent wells even at high concentration of the drugs and semi-resistant/semi-sensitive clones were those where the wells were half full. When possible, these 3 types of clones were selected for further studies.

2.7.3: Sample Preparation

The selected clones in the presence and absence of Imatinib and Nilotinib were collected from 96 well plates by mixing the medium within the well and collecting the cell suspension. Cells were then spun in eppendorf at 950 rpm for 3 minutes. Supernatant was removed and cells were re-suspended in 0.9% NaCl, to wash off the remaining medium.

Cells were then cytospun (cytospin is a technique widely used within the clinical environment for cytology [Kocjan 2009]) onto CaF_2 slides for 1 minute at 550 rpm, through a cytofunnel and filter card (Shandon, UK). Once cells had been deposited on CaF_2 slides as a single monolayer, samples were placed in a Petri dish and fixed using 4% Paraformaldehyde (PFA) in 0.9% NaCl for 20 minutes, as previously described [Pijanka 2009]. This was followed by 3 washes with 0.9% NaCl and 3 washes with distilled water. Samples were air-dried at room temperature. UV grade CaF_2 slides (26 x 22 x 0.5 mm) suitable for both FTIR and Raman spectroscopy (Crystan Ltd, UK) were used.

Table II: Representative example of identification of K562 Clones following 5 days' incubation with Imatinib or Nilotinib at different doses. 2 plus signs indicate semi-confluent wells; one plus sign indicates wells with cells occupying roughly half the surface of the well; plus and minus sign indicates the presence of very few cells; minus sign indicates absence of cells.

Clones	Control	50 µM	100 µM
1	++	+/-	+/-
2	++	+	++
3	++	+	+/-
4	++	+	+
5	++	+	+
6	++	+	+
7	++	+	+
8	++	+	+
9	++	+	+
10	++	+	+
11	++	+	+/-
12	++	+	+
13	+-	+/-	+/-
14	++	+/-	+/-
15	++	+	+
16	++	+/-	-
17	++	+/-	+/-
18	++	+/-	-

2.7.4: S-FTIR Spectroscopy Measurement

Two different synchrotron sources were used to obtain the FTIR data, Diamond Light Source, Oxford, UK, and Soleil Synchrotron, Paris, France.

Figure 19: Diamond Light Source, Oxford, UK (top) and Synchrotron Soleil, Paris, France (bottom)

The SMIS beamline at Synchrotron Soleil, has a Nicolet continuum XL IR microscope and a Nicolet 5700 Nexus FTIR spectrometer (Thermo) with a MCT/A detector. Omnic software (Thermo, Omnic version 8.2) was used to register the spectra and images via a 32x infinity corrected Schwarzchild objective.

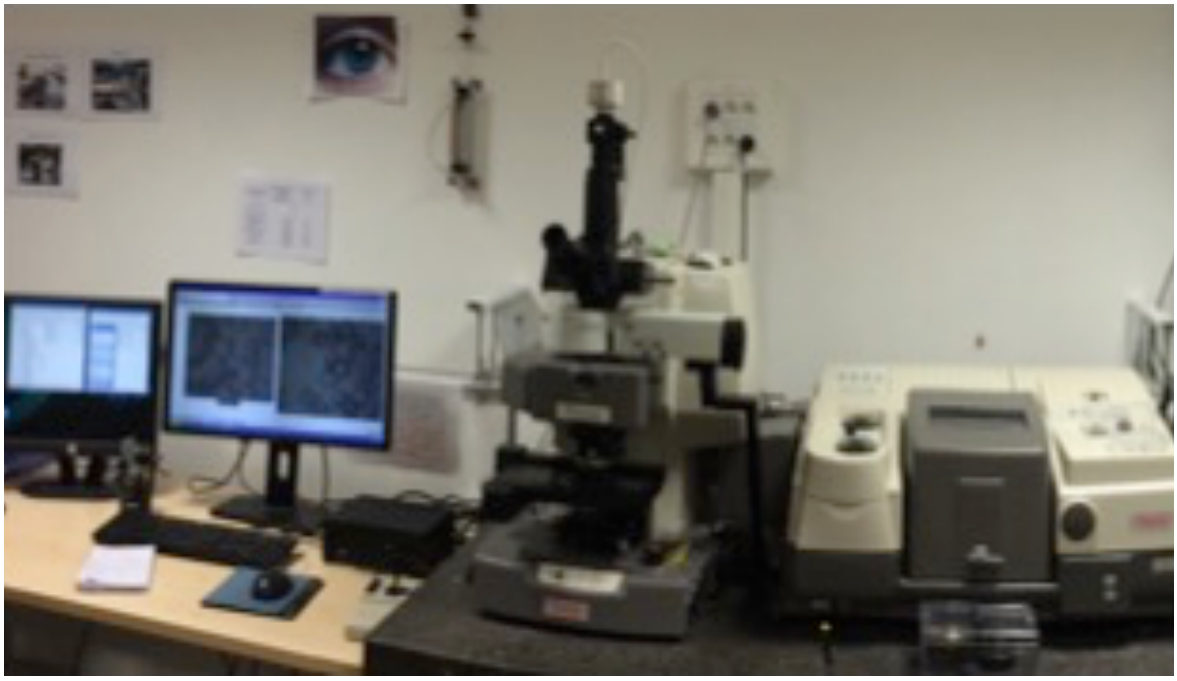

Figure 20: End station at SMIS beamline, Synchrotron Soleil, France.

At the MIRIAM (Multimode Infrared Imaging and Micro-spectroscopy) or B22 beamline at Diamond Light Source, Oxford UK, the end station has a Hyperion 3000 microscope (Bruker) with a liquid nitrogen cooled Bruker 80V FTIR spectrometer and a 100 x 100 μm^2 MCT/A detector. Opus (Bruker) software was used to record the spectra and images of the samples using a 36x Schwarzchild objective.

Spectra were collected at 4 cm^{-1} resolution with 128 co-added spectra. Measurements were taken in transmission mode, using 15×15 μm aperture via a 36x objective. The measurements were taken by centring the aperture at the nucleus of the cells. Background spectra of the substrate were taken after every 15th cell measurement. Images of the studied cells were taken so they could be identified when further studied with Raman spectroscopy. About 50 or more cells, where possible, were collected from each sample.

Figure 21: End station at Diamond Light Source, UK.

2.7.5: S-FTIR Spectra Pre-processing and Analysis

All S-FTIR spectra were imported into Matlab 7.5 (Mathworks, Natick, USA) to apply Extended Multiplicative Signal Correction (EMSC) in order to correct for Mie scattering effects using an algorithm created by Dr Achim Kohler [Kohler 2008]. I used this method for the corrections, as the work I already have done, and the people in diamond working on the same line used the same corrections method. Resonant Mie scattering correction was not used as this is not a widely-used method to correct spectral data. S-FTIR Spectra were processed using The Unscrambler Software (Version X, Camo, Oslo, Norway) normalised (Standard Normal Variate (SNV)) and smoothed (Savitzky-Golay). Following the baseline correction and EMSC application, spectra were imported into Unscrambler (VERSION X, Camo, Oslo, Norway), then cropped to the area to be analysed (2700 cm^{-1} to 3100 cm^{-1} for the lipid region and 1000 cm^{-1} to 1800 cm^{-1} for the fingerprint area) and normalized using standard

normal variate (SNV). This removes the effect of sample thickness and any baseline offset that may have occurred.

Principle Component Analysis (PCA) was used in the study as an important technique which helps by reducing the number of parameters needed to represent the variance in the acquired spectral dataset. It is an unsupervised analysis that allows reducing big numbers of variables into a few principle components. PCA is a very important technique which can sort a complex dataset into a few key spectral components thus identifying and isolating important trends within the dataset. The application and interpretation of PCA could be a first step to assess the presence or absence of differences between samples. However, other data analysis techniques such as pairwise PCA (Bonnier 2012) might be more useful to either identify bigger differences between samples when compared to PCA or to identify differences that might be difficult to see when using PCA. This way, I was able to understand and grasp where differences in my data sets lie. So, PCA was performed using the Unscrambler Software (VERSION X, Camo, Oslo, Norway). Loading plots were also produced using the same software.

2.8: Raman Spectroscopy

A Senterra Micro Raman laser class 1 (Bruker) spectroscope at Diamond Light Source, equipped with 532 nm Laser and CCD thermoelectrically cooled was used. Opus (Bruker) software was used to obtain the spectra and images via a 100X objective. The spectra were recorded using a Raman shift between 40-4450. Spectra were collected at 9-18 cm^{-1} resolutions with 2 co-added spectra with integration time of 10 seconds with 50 μm pinhole type aperture. The measurements were taken by

pointing the laser at the nucleus of the cell. Five spectra of each individual cell were recorded. Background spectra of the substrate were taken at the start of measurement. Spectra of 50 or more cells, when possible, were collected from each sample.

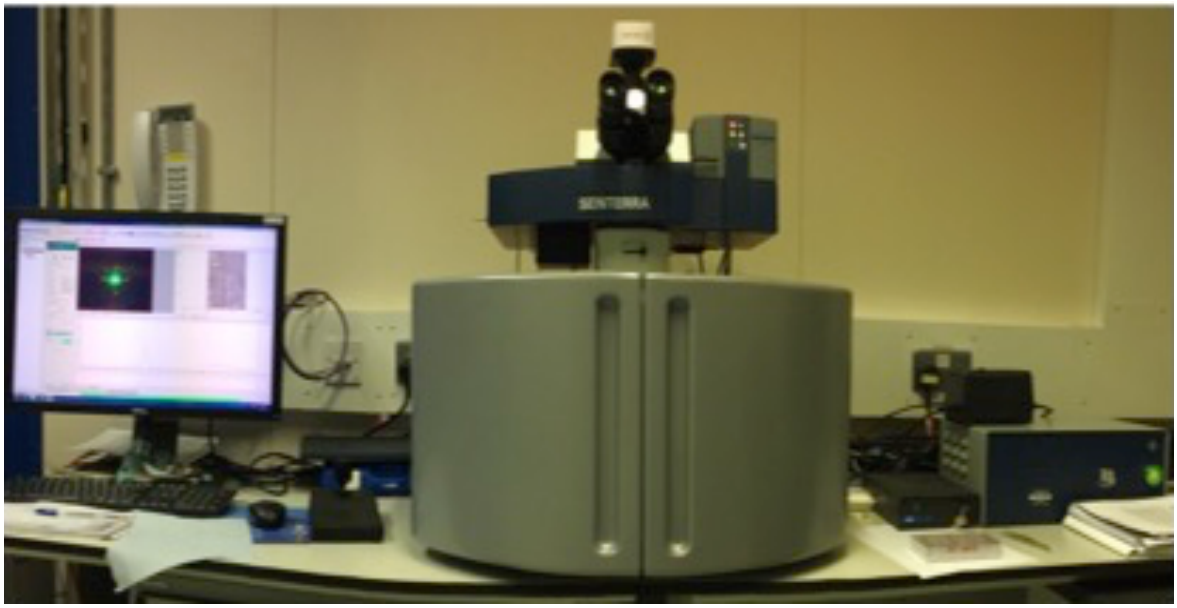

Figure 22: Senterra Micro (Bruker) Raman Spectroscopy at Diamond Light Source, UK

2.8.1: Data Processing

Since manual interpretation of several Raman spectra is difficult and time consuming, to fully understand the biochemical information present in the data obtained by Raman, numerous techniques can be applied. In the present work, I used Principal component analysis (PCA) to do data analysis.

The spectrum was processed using Unscrambler (VERSION X, Camo, Oslo, Norway), only baseline correction was done on the data and then PCA was performed to assess spectral differences.

Chapter 3

Analysis of Volatiles Organic Compounds Released by Leukaemia Cells.
Another Step-in Leukaemia Management?

3.1: Introduction

Leukaemia is an abnormal proliferation of haematopoietic stem cells in the bone marrow, which leads to a high number of immature white cells in blood [Davies 2014]. The initial diagnostic procedures include, amongst others, the examination of blood samples and bone marrow biopsies. These invasive techniques are also used to assess the therapeutic response of leukaemia. It is therefore imperative to develop new non-invasive techniques for early diagnosis of leukaemia, treatment response and/or follow-up. Both physicians and patients, especially the younger population and their relatives, would welcome this. Furthermore, a robust technique able to quickly assess tumour response to treatment could also reduce the number of blood samples and or/biopsies helping to reduce hospital costs worldwide.

Over the last few years, there has been an increased interest in the study of Volatile Organic Compounds (VOCs) released by cancer cells [Smith 2005; Smith 2011; Spanel 2011]. Several techniques such as Gas Chromatography Mass Spectrometry, Proton Transfer Reaction Mass Spectrometry, ion mobility spectrometry (IMS), and Selected Ion Flow Tube Mass Spectrometry (SIFT-MS) have been used in the study of VOCs released by cancer cells [Aman 2005].

SIFT-MS, used in this work, detects accurately and in real time several compounds simultaneously down to concentrations of parts-per-billion by volume (ppbv). More importantly, it obviates sample preparation that could not only alter the sample but also take up valuable time [Smith 2005; Smith 2011; Spanel 2011]. Several groups have applied the SIFT-MS technique to study the release of volatiles by cancer cells [Sulé-Suso 2009; Rutter 2013; Kumar 2013; Navaneethan 2015] aimed mainly at developing applications of this sensitive technique for cancer diagnosis.

In breath analysis, lung pathophysiology and lung diseases have been widely studied, specially aimed at achieving an early diagnosis of lung cancer [Chen 2007; Wehinger 2007; Filipiak 2008; Bajtarevic 2009; Sponring 2009; Filipiak 2010; Fuchs 2010; Corradi 2015,]. However, this methodology could be extended to other medical applications such as the study of blood diseases thanks to the exchange of volatiles through the blood-gas interface in lung alveoli [Sapoval 2002]. On this basis, I carried out the present study in order to better understand the metabolism behind some VOCs released by 2 leukaemia cell lines and compared them to VOCs released by healthy peripheral blood mononuclear cells (PBMC) and bone marrow cells.

3.2: Aims

1. To find out possible biomarkers (VOCs) for leukaemia diagnosis and management with the help of SIFT-MS.
2. To assess whether there are any differences in the VOCs profile of PBMC when compared to leukaemia cells.

3.3: Materials and Methods

3.3.1: Leukaemia Cell lines

The cell lines used in this study were the K562 cell line, and the Jurkat cell line. Both cell lines were cultured in suspension in 75 cm^2 cell culture flasks (Sarstedt, UK) and expanded in complete medium (CM) made up of RPMI 1640 with 10% Foetal Bovine Serum (FBS), 2 mM L-glutamine, Hepes buffer, and antibiotic/antimycotic at 37°C and 5% CO_2. Every 3-4 days, dead cells and debris were removed by spinning cells at 950 rpm for 3 minutes. After the supernatant was removed, the cell pellet was gently dislodged and cells were re-suspended in fresh media. Viable cells were counted using the trypan blue exclusion method.

3.3.2: Peripheral Blood Mononuclear Cells

PBMC[7] were purchased from ZenBio, Inc (UK). PBMC are an important part of the blood components as they play a major role in the immune system. PBMC include all mononuclear blood cells such as T[8] type and B[9] Type leukocytes, natural killer cells, monocytes, basophils, neutrophils, eosinophil cells. These cells were obtained from whole blood of a healthy donor. I used these cells as control cells against leukaemia cell lines. PBMC were thawed and cultured in RPMI 1640 supplemented with 30% Foetal Bovine Serum (FBS), 1% L-Glutamine, 1% Hepes Buffer, and 1%

[8] T type cells are lymphocytes, is a main part of cell mediated immune system, which does not depend on the presence of circulating antibodies.

[9] B type cells are lymphocytes, characterised by the presence of immunoglobulins on their surface, and upon stimulation with antigen. Plays a part in humoral immunity.

Antibiotic/antimycotic. Growth conditions were maintained within culture flasks (Sarstedt, UK) at 37°C and 5% CO_2. These cells also grow in suspension.

3.3.3: Bone marrow aspirates

Human bone marrow aspirates (BMA) from the iliac crest of 3 different healthy donors were purchased from Lonza, USA. Whole bone marrow samples were seeded at a density of 7.5 x 10^6 cells in 20 mL of Dulbecco's Modified Eagle's Medium (DMEM) supplemented with 5 ml Hepes buffer, 5% FBS, 1% L-glutamine and 1% NEAA on 10 ng/ml fibronectine-coated T-75 tissue culture flasks (Sigma, UK). Samples were incubated at 37 °C and 5% CO_2.

3.3.4: Sample Preparation

Following 6 hours' incubation, PBMC cells were collected and centrifuged at 400 g for 10 minutes. Supernatant was discarded and the cell pellet was gently resuspended into fresh RPMI 1640 CM. Cells were counted using the trypan blue exclusion method.

Leukaemia cells were removed from the culture flasks as described above. After the supernatant was removed, the cell pellet was gently dislodged and cells were re-suspended in fresh media. Viable cells were counted using the trypan blue exclusion method.

For Bone Marrow, following 7 days of culture, half the volume of media was removed and fresh DMEM culture medium added. On the second week, whole medium was

replaced with complete fresh DMEM medium. After further 24 hours incubation, cells were trypsinized, collected and seeded in 50 mL of medium in 150 mL glass bottles.

All cells were seeded in 150 ml glass bottles sealed with lids and septa in a final volume of 50 mL of CM prior to carry out he SIFT-MS experiments. Cells were incubated for 8 hours with the lid of each bottle slightly open to allow the air to exchange with the incubator environment (37 °C in 5% CO_2 atmosphere) to ensure they remained suitably oxygenated during this initial period. Following this stage, the air space in each bottle was purged with dry cylinder air and the lids were tightly closed and sealed with parafilm. Cells were then incubated for a further 16 hours at 37 °C in order to allow the headspace to develop and equilibrate, as it has been previously described [Sulé-Suso 2009]. For the duration of the SIFT-MS measurement, bottles were placed within a 37°C heated water bath, to mimic in vivo conditions.

3.4: Selected ion Flow Tube Mass Spectrometry

Both the principle of the SIFT-MS technique [Smith 2005; Smith 2011; Španėl 2011], and the measurements of volatile biomarkers in the headspace of the cell cultures using a Profile 3 SIFT-MS instrument (Trans Spectra Limited, UK) [Rutter 2013] have been previously described in the introduction chapter.

3.4.1: Data Processing (Water Correction)

Data processing for SIFT-MS has been previously described in chapter 2. For each acquired sample, a 6% water correction was applied during MIM mode of SIFT-MS for

the H_3O^+ precursor only. Each measurement was first brought up to 6% water level using the flow rate adjustment built in the SIFT-MS software.

3.4.2: Data Analysis

SIFT-MS data was transferred from SIFT-MS software to Microsoft Excel. Principal Component Analysis was carried out using. Unscrambler software (Camo, Oslo, Norway) and visualised using Graph Pad Prism 6. The data presented here established the basis for further studies with a higher number of experiments whose data analysis will include also p-values.

3.5: ALDEFLUOR™ test

The ALDEFLUOR™ kit test (Stem Cell Technologies Inc) was used to identify the expression of the enzyme aldehyde dehydrogenase (ALDH) in cells according to the manufacturer's instructions. Following the conversion of the Aldefluor substrate into a fluorescent product retained in cells, the amount of intracellular fluorescence was measured using flow cytometry. The Beckman Coulter Cytomics FC500 model was used to gather both forward scatter and side scatter information; 10^5 events/sample being collected on FL1. Cyflogic 1.2.1 software was then used to interpret and analyse the data by gating the population.

3.6: Results and Discussion

The system allows a rapid switch between both methods, without loss of sensitivity. I first looked at acetaldehyde (AA), an aldehyde known to interfere with DNA synthesis and repair [Seitz 2007], and to have mutagenic and carcinogenic effects

[Lanchenmeier 2009]. I also studied and expected that the addition of disulfiram, an inhibitor of the enzyme acetaldehyde dehydrogenase (ALDH) (Figure 23), would increase the amount of acetaldehyde present in the headspace of cultured cells. ALDH is the enzyme responsible for the transformation of acetaldehyde into acetate.

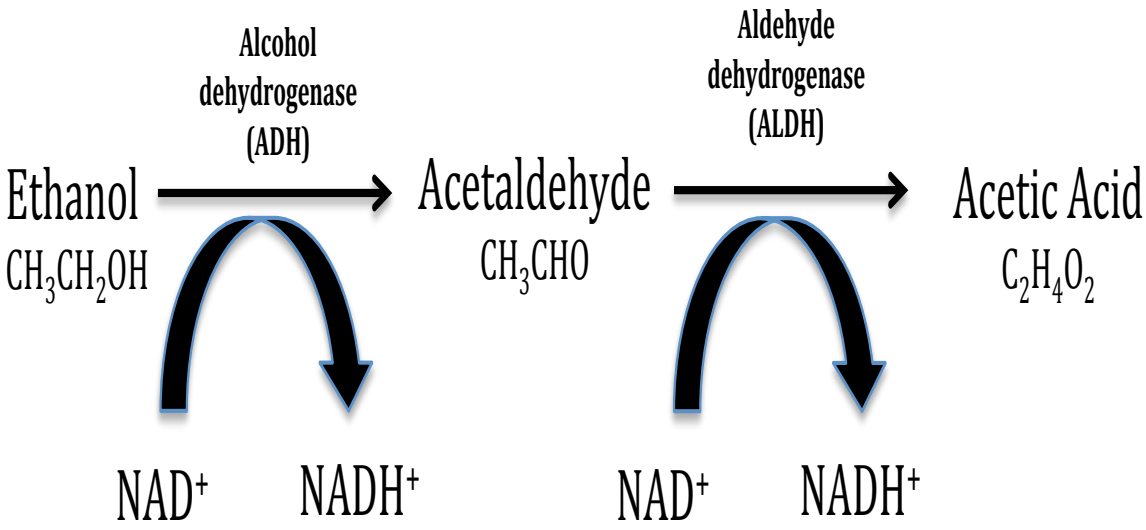

Figure 23: Schematic representation of the metabolical pathway of ethanol and acetaldehyde.

It has been reported that high expression of ALDH is related to leukaemia stem cell features [Ran 2009], poor prognosis [Ran 2009] and relapses from leukaemia [Gerber 2012]. It has also been reported that high expression of ALDH has significant effects on cell proliferation and drug resistance [Marcato 2011; Moreb 2012]. It has been reported that disulfiram has anticancer effects and that might even increase survival in lung cancer patients, as recently shown in a clinical trial [Nechushtan 2015].

Table III: Cell survival following 16 hours incubation in 150 mL glass bottles. All data are the mean of 3 independent experiments.

	RPMI medium		DMEM medium	
Number of cells	**% Survival**	**SD (±)**	**% Survival**	**SD (±)**
PBMC				
10 x10^6	88.95	4.77	-	-
K562				
10 x10^6	84.14	3.36	92.52	3.94
20 x 10^6	90.00	3.97	94.13	0.59
40 x 10^6	94.33	2.48	89.39	1.47
Jurkat				
10 x10^6	93.37	3.02	92.41	4.25
20 x 10^6	93.87	1.25	93.24	1.93
40 x 10^6	94.64	1.86	91.68	0.99

Further work is required to better understand the toxic effects of disulfiram in cells and more importantly, whether this cytotoxic effect could translate into a full clinical application. Disulfiram was used in this work to assess the level of inhibition of ALDH in cells and the release of acetaldehyde by cells following the inhibition with

disulfiram. Disulfiram is dissolved in dimethyl sulphoxide (DMSO), which has a relatively low vapour pressure (1.8 mbar at 37 °C), thus it was not expected to interfere significantly with headspace analyses [Chippendale 2012].

Preliminary work was carried out to assess cell survival in the experimental conditions. As can be seen in Table III, cell survival remained high for all cell lines. Leukaemia cell survival in DMEM will be discussed later.

It was also important to assess whether the addition of disulfiram to culture medium could affect cell survival. As can be seen in Table IV, the addition of disulfiram to a final concentration of 40 μM did not affect PBMC survival.

However, a significant decrease in cell survival for both leukaemia cell lines K562 and Jurkat even at the lower dose of 20 μM was seen. In order to confirm that DMSO, used to dissolve disulfiram, did not cause this decreased survival in K562 and Jurkat, both cell lines were also incubated with DMSO alone as controls, with the same volumes of DMSO used to prepare 20 μM (50 μL DMSO) and 40 μM (100 μL DMSO) of disulfiram. Table IV shows that DMSO alone did not markedly affect cell survival.

The next step was to compare the levels of acetaldehyde released by PBMC and both leukaemia cell lines in the absence and presence of disulfiram. As can be seen in Figure 24, the release of acetaldehyde in the headspace of PBMC, did not show any significant changes when compared to the acetaldehyde level to of the control media without cells. Furthermore, the exposure of PBMC to 40 μM of disulfiram, did not cause major changes either. On the other hand, while the levels of acetaldehyde

released did not significantly differ between the control media and the leukaemia cells incubated in the absence of disulfiram, the addition of disulfiram to both leukaemia cell lines translated into an increase in the levels of acetaldehyde released. Interestingly, the increase of this ratio was smaller for Jurkat cells (table V).

Table IV: Cell survival following the addition of disulfiram reconstituted with DMSO, and DMSO alone. All data are the mean of 3 independent experiments.

Number of cells 10 x 10^6	**% Survival**	**SD (±)**
PBMC + 40 µM disulfiram	91.77	3.07
K562 + 20 µM disulfiram	68.21	6.77
K562 + 40 µM disulfiram	68.15	5.78
K562 + 50 µL DMSO	89.37	9.11
K562 + 100 µL DMSO	84.49	9.41
Jurkat + 20 µM disulfiram	68.56	2.10
Jurkat + 40 µM disulfiram	64.56	9.34
Jurkat + 50 µL DMSO	88.77	2.74
Jurkat + 100 µL DMSO	89.89	3.86

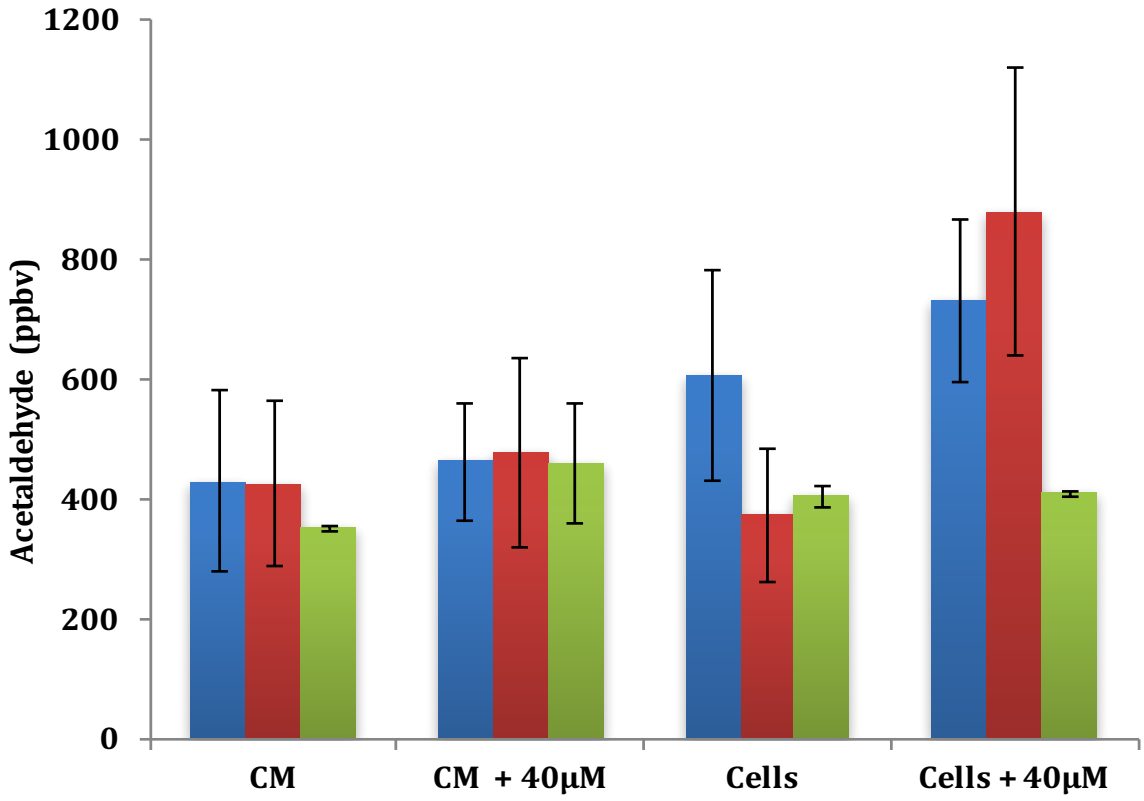

Figure 24: Means of acetaldehyde released by 10 x 10^6 cells in the headspace of culture medium in the absence or presence of disulfiram. Jurkat (Blue), K562 (Red), and PBMC (Green) (mean of 3 independent experiments).

It has been previously described that SIFT-MS identifies acetaldehyde in the headspace of culture medium alone, coming from the foetal calf serum present in the media. [Sulé-Suso 2009]. It could be argued that the increased ratios following the addition of disulfiram could be partially due to a decrease in the number of cells due to the cytotoxic effects of disulfiram, and, therefore, to a reduction in ALDH activity which could translate into increased acetaldehyde levels. However, the levels of acetaldehyde in control medium were similar to those present in the headspace of cells incubated in the absence of disulfiram. This would not be the case for PBMC as there was no increase in the levels of acetaldehyde and, furthermore, the survival of PBMC was not affected by the addition of disulfiram.

Table V: Mean ratios of acetaldehyde released by 10 x 10^6 cells over acetaldehyde present in the headspace of culture media (mean of 3 independent experiments).

Cell Lines	Mean	SD (±)
K562	0.22	0.11
10 x 10^6 + 20 µM disulfiram	1.60	0.83
10 x 10^6 + 40 µM disulfiram	1.55	0.56
Jurkat	1.21	0.20
10 x 10^6 + 20 µM disulfiram	1.82	0.58
10 x 10^6 + 40 µM disulfiram	1.51	0.11

Hence, to verify this, I studied the expression of ALDH in both K562 and Jurkat cell lines and PBMC. Figure 25 shows a representative example of ALDH expression in PBMC (Figure 25A and 25B), K562 (Figure 25C and 25D), and Jurkat (Figure 25E and 25F) cell lines using the Aldefluor™ test. Using this test, the expression of ALDH was present in 3.47% (SD ±2.56), 48.1 % (SD ±6.0) and 12.2 % (SD ± 1.2) in PBMC, K562 and Jurkat cells, respectively (mean of 3 independent experiments). These results indicate that the increased presence of acetaldehyde in the headspace of K562 cells and following the addition of disulfiram is definitely due to inhibition of the ALDH enzyme. However, in the case of Jurkat cells, the lower expression of ALDH enzyme would explain the lesser increase in the release of acetaldehyde following the addition of disulfiram.

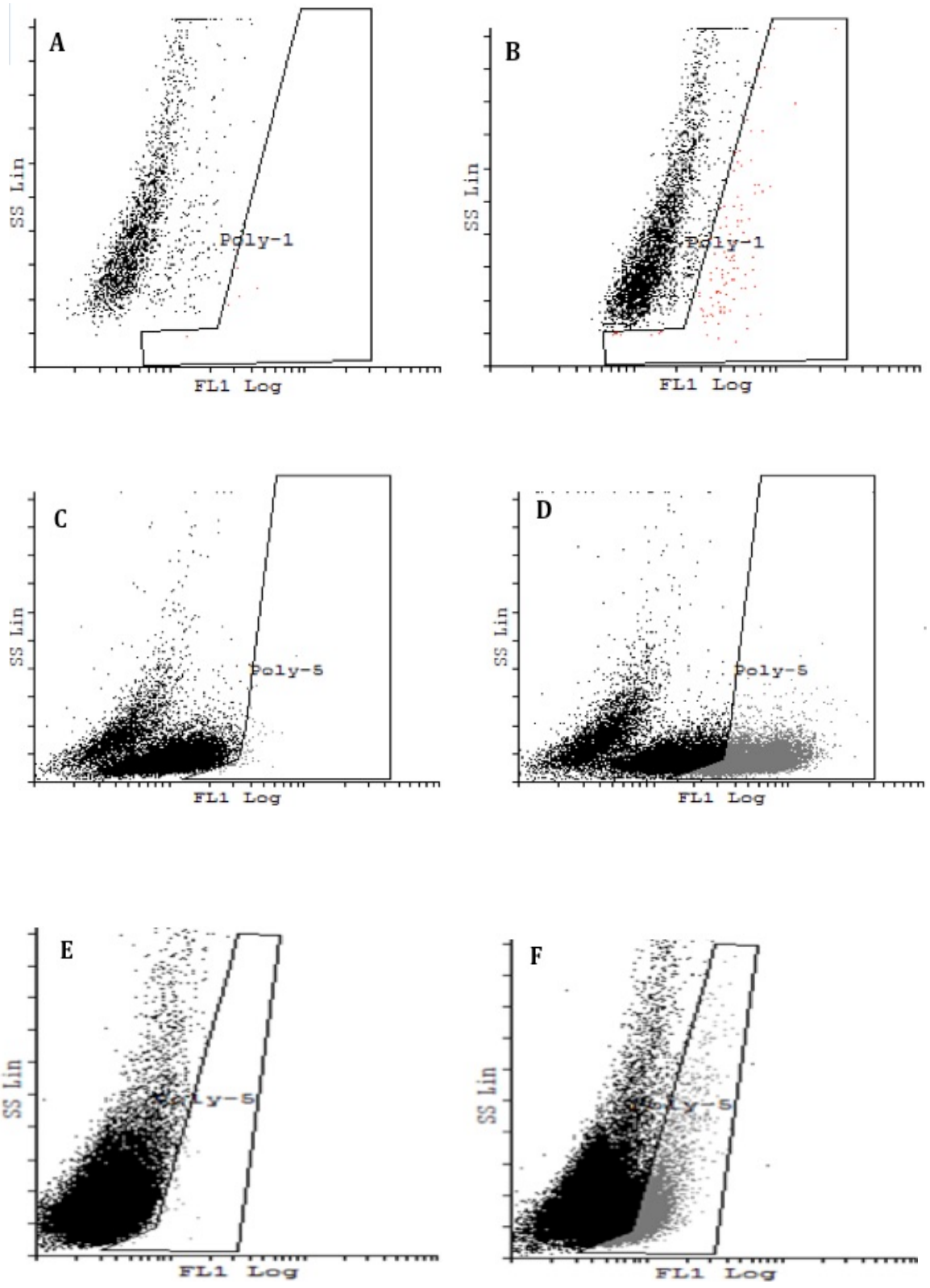

Figure 25: Representative examples of ALDH expression in PBMC (25 A and B), and K562 (25 C and D) and Jurkat (25 E and F) cell lines using the Aldefluor™ test. Cells were labelled with aldefluor (BAAA) (Figures 25 A, 25 C, and 25 E) and without (Figures 25 B, 25 D, and 25 F) the ALDH inhibitor DEAB.

It has been previously reported that K562 cells express ALDH [Moreb 2012]. In fact, K562 is one of the cells lines suggested to be used as a positive control in the Aldefluor™ test by the manufacturers. Taken together, the data would indicate that leukaemia cell lines release acetaldehyde but that it is metabolised quickly, thus it cannot be detected in the headspace of these cells in culture. The inhibition of ALDH translates into an increase of acetaldehyde in the headspace of these cells. Furthermore, PBMC might not be producing acetaldehyde as the inhibition of the enzyme does not translate into increased levels of acetaldehyde in the headspace of these cells in culture. Further work is needed to confirm this and, more importantly, to assess whether the production of acetaldehyde by leukaemia cells could have value both in a diagnostic set up and to assess tumour response to treatment. In fact, correlation between levels of acetaldehyde released and cell number has been described before in lung cancer cell lines [Sulé-Suso 2009; Rutter 2013].

Another compound for which a differential was found between its release by cells and its presence in the headspace of control medium was ethanol. I have carried out previous work showing that the presence of ethanol in the headspace of control medium is due, like in the case of acetaldehyde, to the presence of foetal calf serum [Sulé-Suso 2009].

It is widely known that ethanol is involved in the development of different types of cancer, including leukaemia in mice [Garaycoechea 2012]. As can be seen in Table VI, the ratio of ethanol production by leukaemia cells and ethanol present in the headspace of control media increases with the number of cells in culture. This differential is greater for K562 cells when compared to Jurkat cells. This was not the

case for PBMC (data not shown). Further work is needed to assess whether and how ethanol could be a biomarker related to leukaemia cell numbers in blood.

Table VI: Mean levels of ethanol released by leukaemia cells and in the headspace of culture media, and mean ratios of ethanol released by leukaemia cells over ethanol in the headspace of culture media. All data are the mean of 3 independent experiments.

	Ethanol release (ppbv)		**Ratio of ethanol released by cells over ethanol from culture medium**	
Cell Lines	**Means**	**SD (±)**	**Mean**	**SD (±)**
K562				
CM	1215	305		
10 x10^6	1680	574	1.37	0.16
20 x 10^6	1968	466	1.63	0.10
40 x 10^6	2268	1003	2.17	0.45
Jurkat				
CM	1664	358		
10 x10^6	1831	301	1.11	0.06
20 x 10^6	2063	421	1.24	0.08
40 x 10^6	2343	664	1.40	0.24

When large dataset is to be analysed, reduction in the dimensionality of the dataset while retaining most of the variable in the data, is desired, PCA is the best algorithmic technique to attain this. To confirm whether different leukaemia cell lines can be differentiated using SIFT-MS on the basis of VOCs released by these cell lines I performed PCA of full scan data of each cell line at different concentrations along with PBMC (Figure 26A). Figure 26A is the representative graph showing PCA of ratios of analytes from cells over media headspaces measured with SIFT-MS from K562 cell line, Jurkat cell line and PBMC. Each data point is the mean of 3 independent experiments. It is clear from the PCA (Figure 26A) that there is clear separation between the VOCs released by the leukaemia cell lines versus VOCs released from PBMC.

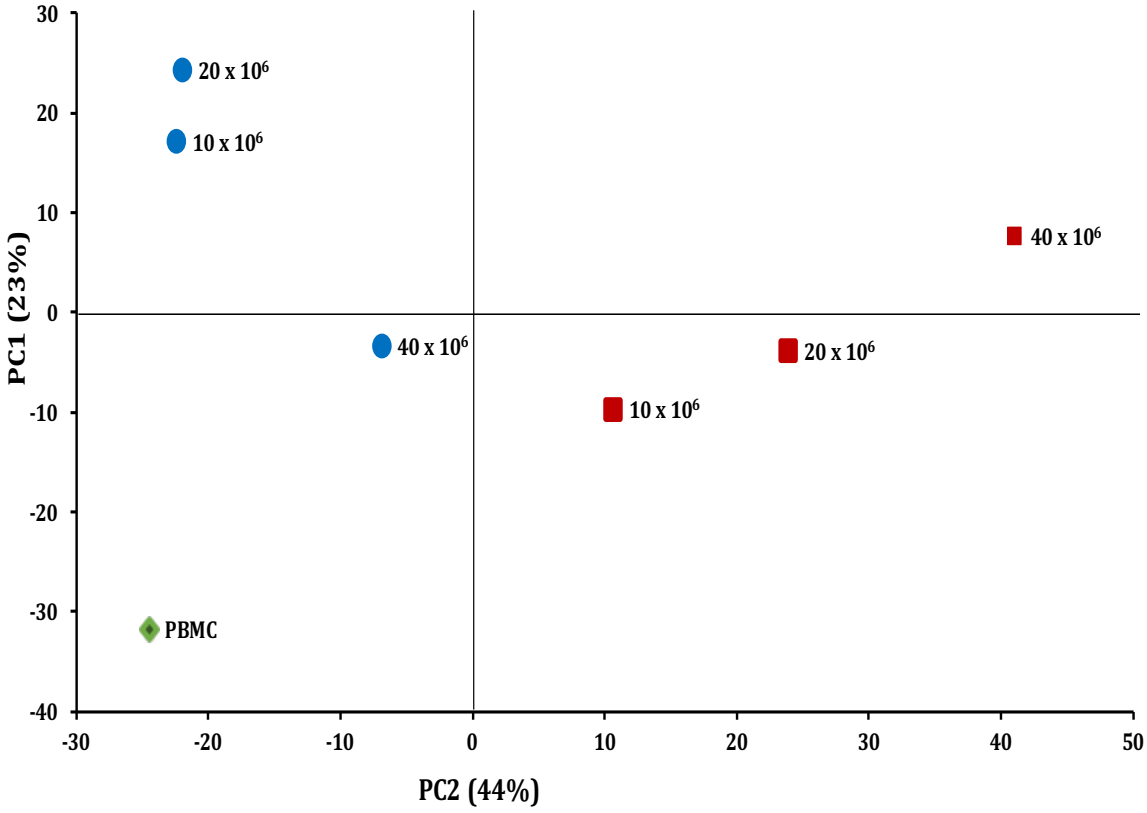

Figure 26 A: PCA of ratios of analytes from cells over media headspaces measured with SIFT-MS from K562 cell line (squares), Jurkat cell line (circles) and PBMC (diamonds). The numbers indicate cell concentration in 50 mL of medium. Each data point is the mean of 3 independent experiments.

Furthermore, I performed PCA of the full scan data of VOCs from leukaemia cell lines (Figure 26B). It is very clear that there is significant separation between the VOCs released by both Leukaemia cell lines (Figure 26B), which shows promising implementation of SIFT-MS in distinguishing different types of the disease.

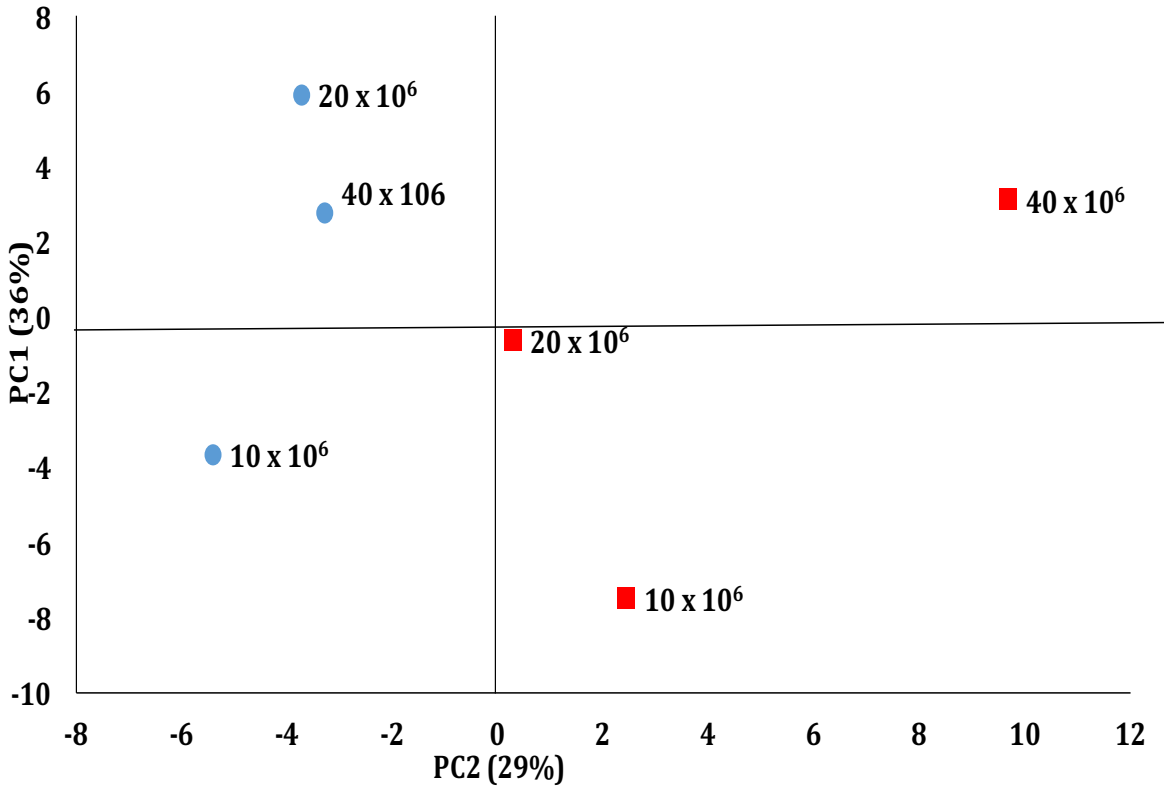

Figure 26 B: PCA of ratios of analytes from cells over media headspaces measured with SIFT-MS from K562 cell line (squares) and Jurkat cell line (circles). The numbers indicate cell concentration in 50 mL of medium. Each data point is the mean of 3 independent experiments.

During this project, bone marrow (BM) cells were acquired in order to study the release of VOCs from these cells. In these experiments, mononuclear BM cells were obtained in the first passage and seeded in 150 mL glass bottles in 50 mL of CM. However, before these experiments were done, I had to take into account that BM cells grew in DMEM while leukaemia cells grew in RPMI. In order to eliminate any possible confounding factors caused by different media on the release of VOCs,

leukaemia cells were incubated in DMEM as these cells are more resilient and therefore easier to grow in other cell culture media when compared to BM cells.

Preliminary experiments were carried out to assess cell survival in these new culture conditions. As can be seen in Table III, cell survival remained high for both cell lines incubated for 16 hours in 150 mL glass bottles in the same culture conditions as before except for changing RPMI medium to DMEM.

PCA of ratios of analytes from cells over media headspaces measured with SIFT-MS from K562 cell line, Jurkat cell line and bone marrow cells are shown in Figure 27. There is a remarkable separation among VOCs released by the Bone marrow and both leukaemia cell lines grown in DMEM. Figure 28 is the PCA of VOCs released by both cell lines grown in DMEM, a similar pattern of separation was observed among VOCs released by both leukaemia cell lines suggesting SIFT-MS could have a potential in the management of leukaemia.

The next step was to look at the analytes present in different concentration in the headspace of PBMC, leukaemia cells and BM cells. Out of 170 analytes, 2 were present in higher concentration in the headspace of BM cells when compared to the headspace of 10 x 10^6 leukaemia cells and PBMC. These were m/z 47 analyte and m/z 57 analytes using H_3O^+. The ppbv values for the former were 568 ± 115 and 1,085 ±186 for PBMC and bone marrow cells, respectively. They were 402 ± 83 ppbv and 272 ± 60 ppbv for K562 and Jurkat in RPMI, respectively, and 439 ± 215 ppbv and 529 ± 203 ppbv for K562 and Jurkat in DMEM, respectively. This analyte has been linked to ethanol or formic acid. [Michalcikova 2014]. Further work is needed to

better characterise not only the exact contribution of each compound but also whether other compounds could modify the values of m/z 47 analytes. On the other hand, the ppbv values for m/z 57 analytes were 809 ± 164 and 1,137 ± 176 for PBMC and bone marrow cells, respectively. They were 645 ± 223 ppbv and 755 ± 333 ppbv for K562 and Jurkat in RPMI, respectively, and 796 ± 126 ppbv, 684 ± 18 ppbv for K562 and Jurkat in DMEM, respectively. M/z 57 analyte has been linked to the presence of acrolein [Španěl 2012]. Acrolein, together with other aldehydes such as methacrolein, is a major product of lipid peroxidation [Onyango 2012] and might be involved in apoptotic effects on cancer cells [Onyango 2012]. Increasing the concentration of leukaemia cells up to 40 x 10^6 cells did not translate into an increase in the concentration of these 2 analytes (data not shown).

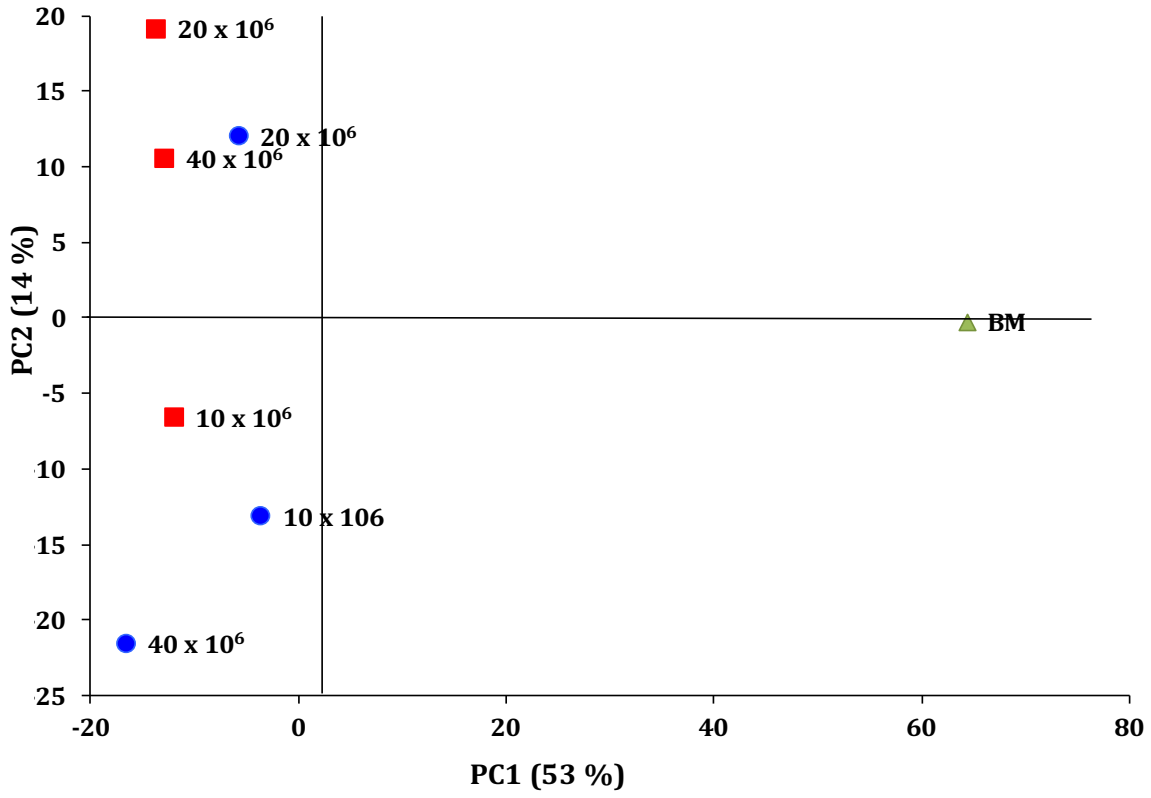

Figure 27: PCA of ratios of analytes from cells over media headspaces measured with SIFT-MS from K562 cell line (squares), Jurkat cell line (circles) and bone marrow cells (triangles). The numbers indicate cell concentration in 50 mL of medium. Each data point is the mean of 3 independent experiments.

Taken together, these data would indicate that SIFT-MS could be a potential technique to identify VOCs released by leukaemia cells which differ from those released by healthy BM cells. However, further work is required to fully characterise the metabolical pathways behind the release of VOCs by both leukaemia and BM cells, and to assess whether SIFT-MS might be able to separate individual types of leukaemia based on their VOCs' profile.

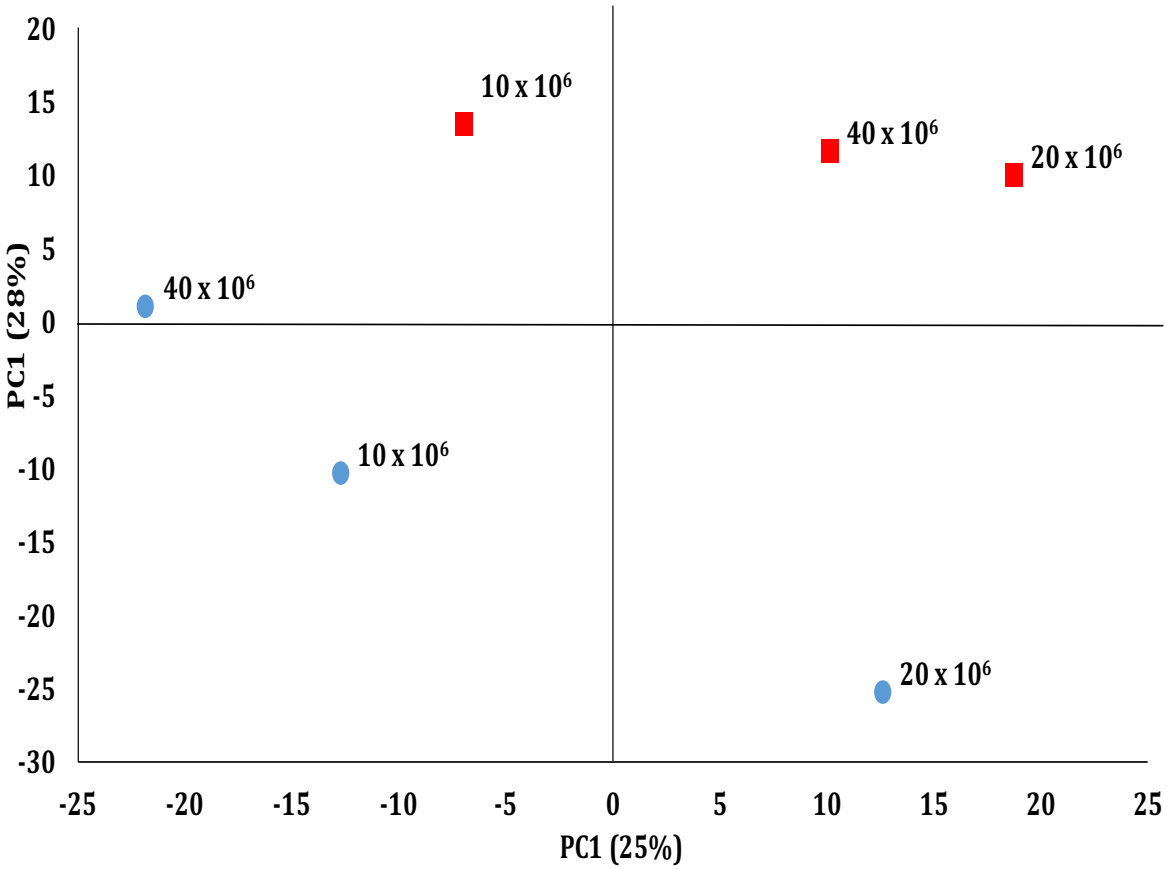

Figure 28: PCA of ratios of analytes from cells over media headspaces measured with SIFT-MS from K562 cell line (squares), Jurkat cell line (circles). The numbers indicate cell concentration in 50 mL of medium. Each data point is the mean of 3 independent experiments.

3.7: Conclusion

In this work, the feasibility of measuring both qualitatively and quantitatively VOCs released by PBMC, leukaemia cells and BM cells *in vitro* has been shown. The use of PCA along with SIFT-MS proved very important method as one could clearly notice the differences of the VOCs profile even among different leukaemia cells lines as well as from PBMCs and bone marrow. It is very much clear from the results shown in this study that PCA is the best way to analyse the SIFT-MS measurements. The data presented here indicate that the VOCs' profile of leukaemia cells might differ from the VOCs' profile of PBMC, and BM cells. The analysis of VOCs released by leukaemia cells and the use of PCA, could thus be useful in better understanding the metabolism of leukaemia cells. These differences in the VOCs release could be exploited towards a clinical application in the diagnosis of the disease and to assess tumour response to treatment. However, further work is needed to; 1. Better understand the metabolical pathways in blood cells leading to a specific VOCs profile. 2. Confirm that the study of VOCs released by leukaemia cells and, by extension, present in the breath of patients with leukaemia could have an application in the management of this disease.

Chapter 4

Quantification of Volatiles Released by Leukaemia Cells Following the Addition of Drugs by The Selected Ion Flow Tube Mass Spectrometry

4.1: Introduction

Volatile organic compounds represent a chemically diverse group of metabolites present in biological fluids with a boiling point less then 300 °C [Patti 2012]. At different stages of metabolism, VOC concentration tend to change, as these are intermediate products of metabolic pathways [Patti 2012]. Thus, their levels in the breath/headspace may provide a good understanding of the mechanisms involved in the cellular processes, disease diagnosis and monitoring, [Probert 2009]. Breath VOCs are normally collected from human breath. Since Pauling, reported around 250 different VOCs in breath in 1971, more than 3000 different VOCs have been reported in human breath [Phillips 1999]. These VOCs in breath range from parts per million by volume to parts per trillion by volume. However, information about the mechanism behind the production of these VOCs is limited, and, at present, it is not well understood for many of them [Hakim 2012].

Over the last few years, breath analysis for VOCs has gained growing significance in both the scientific and clinical communities. In terms of cancer diagnosis and therapeutic response, analysis of exhaled breath for detection and absolute quantification of VOCs has a promising potential. Thanks to the non-invasive nature of this technique and no or minimal sample preparation, breath analysis has great appeal for both clinicians and patients. Developments in the methodology for VOCs

analysis in clinical breath testing for specific cancers may potentially by-pass some of the invasive procedures for the detection and management of the disease. However, the clinical application of breath analysis remains limited. The C-urea breath testing for H. pylori bacterium, hydrogen test for small bowel bacteria overgrowth and breath test of nitric oxide in the management of asthma are just few routinely used clinical tests [Kharitonov 1994; Kawai 2008]. Thus, there is still major scientific interest in developing breath analysis for disease detection and management.

A lot of work carried out in recent years to identify breath biomarkers has been conducted by several groups studying different types of cancer i.e. leukemia, lung, prostate, breast and colon cancers, using different analytical techniques [Phillips 1994; Phillips 1999; Phillips 2003; Phillips 2007; Spaněl 2008; Shin 2009]. Some very promising results regarding VOCs being associated with cancer have been published [Liu 1998; Smith 2003; Deng 2004; Shin 2009]. Shin *et al*. (2009) reported release of acetaldehyde and hexanaldehyde from the head space of HL60 cells, in time dependent manner.

The most commonly used analytical technique for breath analysis is GC/MS. However due to its requirement of adsorption devices and long processing time along with quantifying problems of some important trace agents, it has not translated yet into clinical practice. Recently, other mass spectrometry techniques, i.e. proton transfer reaction mass spectrometry (PTR-MS) and SIFT-MS have attracted interest for the detection of VOCs for breath analysis [Smith 2005; Zhan 2013].

SIFT-MS offers quantification of several VOCs in exhaled breath thanks to its ability to

use three reagent ions, H_3O^+, NO^+, and O_2^+ [Smith 2005]. This technique allows the simultaneous quantification of several trace gasses in the sample without the need of sample preparation [Smith 2005]. In recent years, SIFT-MS has also been used in disease diagnosis and to assess therapeutic response [Amann 2005; Kumar 2013]. In this chapter, I have shown the capabilities of this technique in the management of leukemia.

Reciprocal translocation between chromosome 9 and 22 produces BCR-ABL gene that is the main cause of chronic myeloid Leukemia (CML). Imatinib is the first tyrosine kinase targeting BCR-ABL for the treatment of CML [Bumbea 2010]. Imatinib binds to ATP biding site of this BCR-ABL, inhibiting its kinase activity resulting in the start of the apoptotic process. Nilotinib is also one of the most important anti Leukemia, second-generation tyrosine kinase inhibitor used in the treatment of chronic myeloid Leukemia. Nilotinib not only inhibits the kinase activity of BCR-ABL but also inhibits c-KIT and platelet derived growth factor (PDGFR) [Weisberg 2006]. It is an effective drug in Imatinib resistant cases.

I have previously investigated VOCs in the headspace of normal leukemia cells (Jurkat, and K562) and PBMC along with bone marrow cells (Chapter 3). In the study, few compounds were detected to differ from the headspace of the leukemia cell lines when compared to the PBMC and/or healthy bone marrow cells. In the present study, I conducted experiments to assess any possible differences in the VOCs released by leukemia cells after their exposure to drugs, in the search of any possible biomarkers that could help in assessing tumor response to treatment.

4.2: Aims

1. To identify possible VOCs that could be used as biomarkers to monitor the tumour response of both leukaemia cell lines after their exposure to Imatinib or Nilotinib.
2. To assess whether changes in VOCs released by leukaemia cells correlate to drug concentration.

4.3: Material and Methods

4.3.1: Cell lines

The cell lines used in this study were K562 cell line, and Jurkat cell line. Both cell lines were cultured in suspension in 75 cm^2 cell culture flasks (Sarstedt, UK) and expanded in complete medium (CM) made up of RPMI 1640 with 10% Foetal Bovine Serum (FBS), 2 mM L-glutamine, Hepes buffer, and antibiotic/antimycotic at 37°C and 5% CO_2. Every 3-4 days, dead cells and debris were removed by spinning cells at 950 rpm for 3 minutes. After the supernatant was removed, the cell pellet was gently dislodged and cells were re-suspended in fresh media. Viable cells were counted using the trypan blue exclusion method.

4.3.2: Sample Preparation

Leukaemia cells were removed from the culture flasks as described above. After the supernatant was removed, the cell pellet was gently dislodged and cells were re-suspended in fresh RPMI 1640 medium supplemented with 10% Foetal Bovine

Serum (FBS), 1% L-Glutamine, 1% Hepes Buffer, and 1% Antibiotic/antimycotic. Viable cells were counted using the trypan blue exclusion method.

Cells were seeded in 150 ml glass bottles sealed with lids and septa in a final volume of 50 ml. Cells were incubated for 2 hours with the lid of each bottle slightly open to allow the air to exchange with the incubator environment (37 °C in 5% CO_2 atmosphere) to ensure they remained suitably oxygenated during this initial period. Following 2 hours' incubation, the drugs (Imatinib or Nilotinib) were added at a final concentration of 50 μM or 100 μM and cells were incubated for further 6 hours with the lids slightly open. A control case with cells without either drug was also formulated. Following these 6 hours incubation, the air space in each bottle was purged with dry cylinder air and the lids were tightly closed and sealed with parafilm. Cells were then incubated for a further 16 hours at 37 °C in order to allow the headspace to develop and equilibrate, as previously described [Sulé-Suso 2009]. For the duration of the SIFT-MS measurement, bottles were placed within a 37°C heated water bath to mimic in vivo conditions.

4.4: Selected ion Flow Tube Mass Spectrometry

Both the principle of the SIFT-MS technique [Smith 2005; Smith 2011; Španěl 2011], and the measurements of volatile biomarkers in the headspace of the cell cultures using a Profile 3 SIFT-MS instrument (Figure 1) (Trans Spectra Limited, UK) [Rutter 2013] have been previously described.

4.4.1: Data Processing (Water Correction)

Data processing for SIFT-MS has been previously described in chapter 2. For each acquired sample, a 6% water correction method was applied during MIM mode of SIFT-MS for the H_3O^+ precursor only. Each measurement was first brought up to 6% water level using the flow rate adjustment built in the SIFT-MS software.

4.4.2: Data Analysis

SIFT-MS data was transferred form SIFT-MS software to Microsoft Excel to the corrections and Principal Component Analysis was carried out using. Unscrambler software (Camo, Oslo, Norway) and visualised using Graph Pad Prism 6.

4.5: Results and Discussions

Survival of 10 x 10^6 cells incubated in the absence or presence of Imatinib or Nilotinib at three different doses (10 μM, 50 μM or 100 μM) is shown in Table VII. For Imatinib, cell survival ranges from 97.33 ± 1.15 % to 67.00 ± 8.19 %, and from 98.34 ± 0.81 % to 54.49 ± 14.49 % for Jurkat and K562, respectively. Cell survival is markedly lower for Nilotinib when compared to the same doses of Imatinib confirming that Nilotinib is more potent than Imatinib [Wei 2014]. Based upon these drug survival data, 10 μM, 50 μM and 100 μM doses of both drugs were used for this study. The survival with 500 μM of either dose was 0 for both cell lines.

Acetaldehyde has been shown as a possible VOC that could be linked to cancer [Sulé-Suso 2009; Schmidt 2015], although the results published in the literature have

sometimes been equivocal [Filipiak 2008]. Therefore, the release of acetaldehyde by cell cultures in the absence or presence of either drug was assessed.

As can be seen in Figures 29 and 30, the levels of acetaldehyde increased for K562 cells following the addition of Imatinib or Nilotinib. However, there were no clear differences in the levels of acetaldehyde for Jurkat cells following the addition of Imatinib or Nilotinib. For both cell lines, increasing the dose of Imatinib or Nilotinib to 100 μM did not translate into further increases in the levels of acetaldehyde. It is not yet clear as to why there is an increase in the acetaldehyde production by both the cells exposed to Nilotinib and not so clear when cells are exposed to Imatinib.

It could be hypothesised that this effect is due to a combination of several factors i. e., cells' death, cell in different phases of apoptosis and changes in some metabolical pathways amongst others. All these together might affect the activity of ALDH and/or the production of acetaldehyde. ALDH belongs to a family of cytosolic enzymes involved in various biological processes [Yoshida 1998; Duester 2000]. High ALDH activity has been identified in various tumor types, including breast, lung, and liver cancer [Croker 2008; Chu 2009].

Recent data has shown that ALDH is highly expressed in leukemic stem cells [Pearce 2005; Hess 2006] and has specific roles in stem cell function and chemotherapy resistance [Wang 2001; Chute 2006]. Further work is needed to clarify these issues.

Table VII. Cell survival of Jurkat and K562 cells exposed to Imatinib and Nilotinib

Leukemia cells survival with drug exposure (10 x 10^6 cells)		
Sample	**Imatinib (% ± SD)**	**Nilotinib (% ± SD)**
Jurkat		
Control	97.33 ± 1.15	99.0 ± 1
10 µM	95.33 ± 1.53	53.00 ± 23.67
50 µM	69.67 ± 7.09	39.00 ± 11.57
100 µM	67.00 ± 8.19	24.00 ± 6.35
K562		
Control	98.34 ± 0.81	97.13 ± 0.74
10 µM	96.99 ± 1.33	71.06 ± 11.11
50 µM	85.19 ± 2.52	48.57 ± 2.48
100 µM	54.49 ± 14.49	31.58 ± 15.43

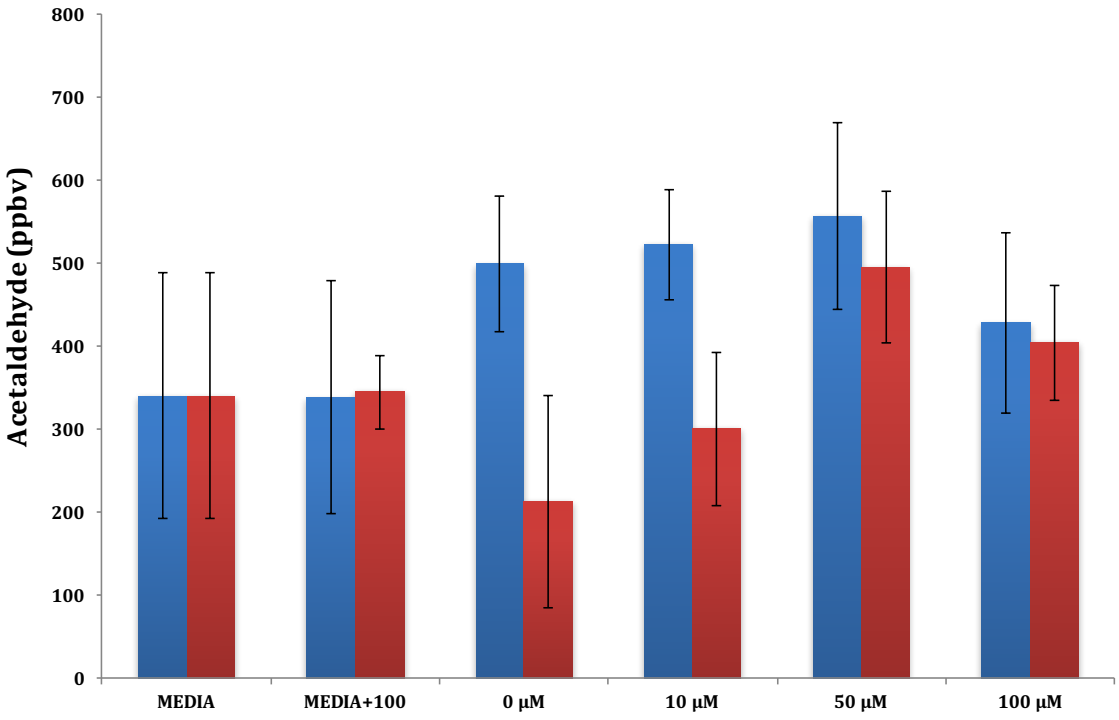

Figure 29 Average release of acetaldehyde in the headspace of media, media +100 µM of Imatinib, and Jurkat and K562 (Blue and Red respectively) cells incubated with 0 µM, 10 µM, 50 µM, and 100 µM of Imatinib (using H_3O^+ precursor ion).

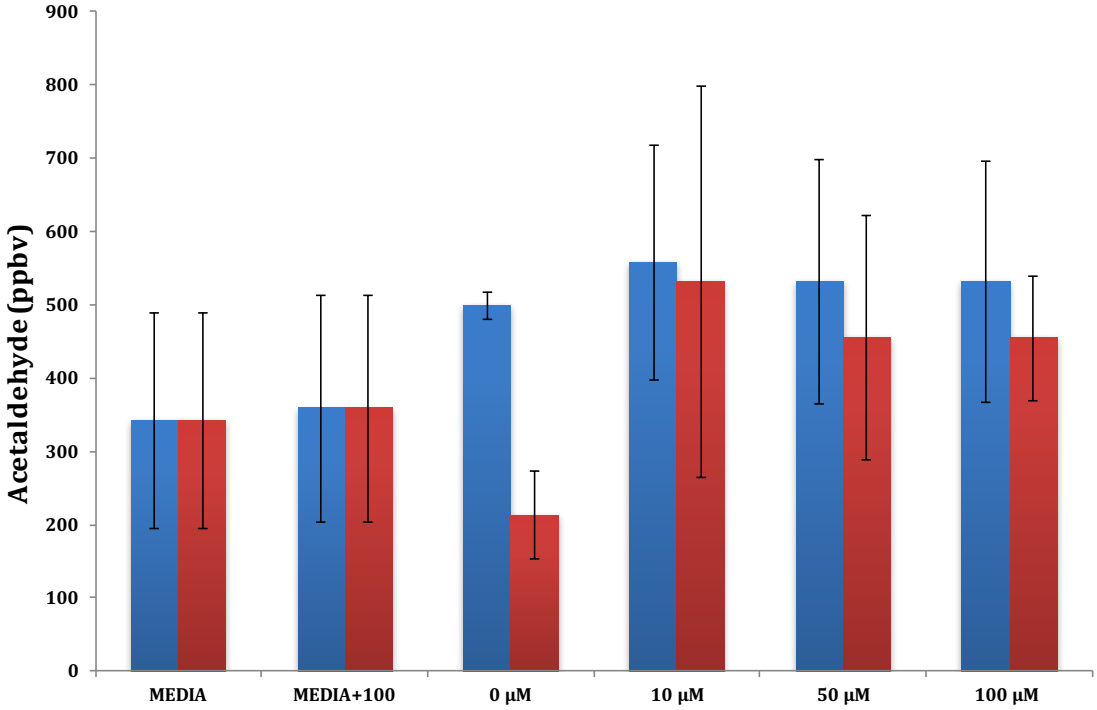

Figure 30: Average release of AA in the headspace of media, media+100 µM of Nilotinib, and Jurkat and K562 (Blue and Red respectively) cells incubated with 0 µM, 10 µM, 50 µM, and 100 µM of Nilotinib (using H_3O^+ precursor ion).

The next step was to look at the full scan data and carry out PCA in order to assess whether a separation between cells incubated in the presence or absence of Imatinib or Nilotinib could be identified. After the pre-processing and correcting the data, PCA is the first analysis method I used. PCA is widely used technique that extracts and displays the characteristics causing the variance in great term within the data set and loadings reveal how much is the contribution of each variable between the samples [Spooner 2009]. Figures 31 to 34 show the PCA for cells incubated with Imatinib and Nilotinib, respectively, and their corresponding loadings.

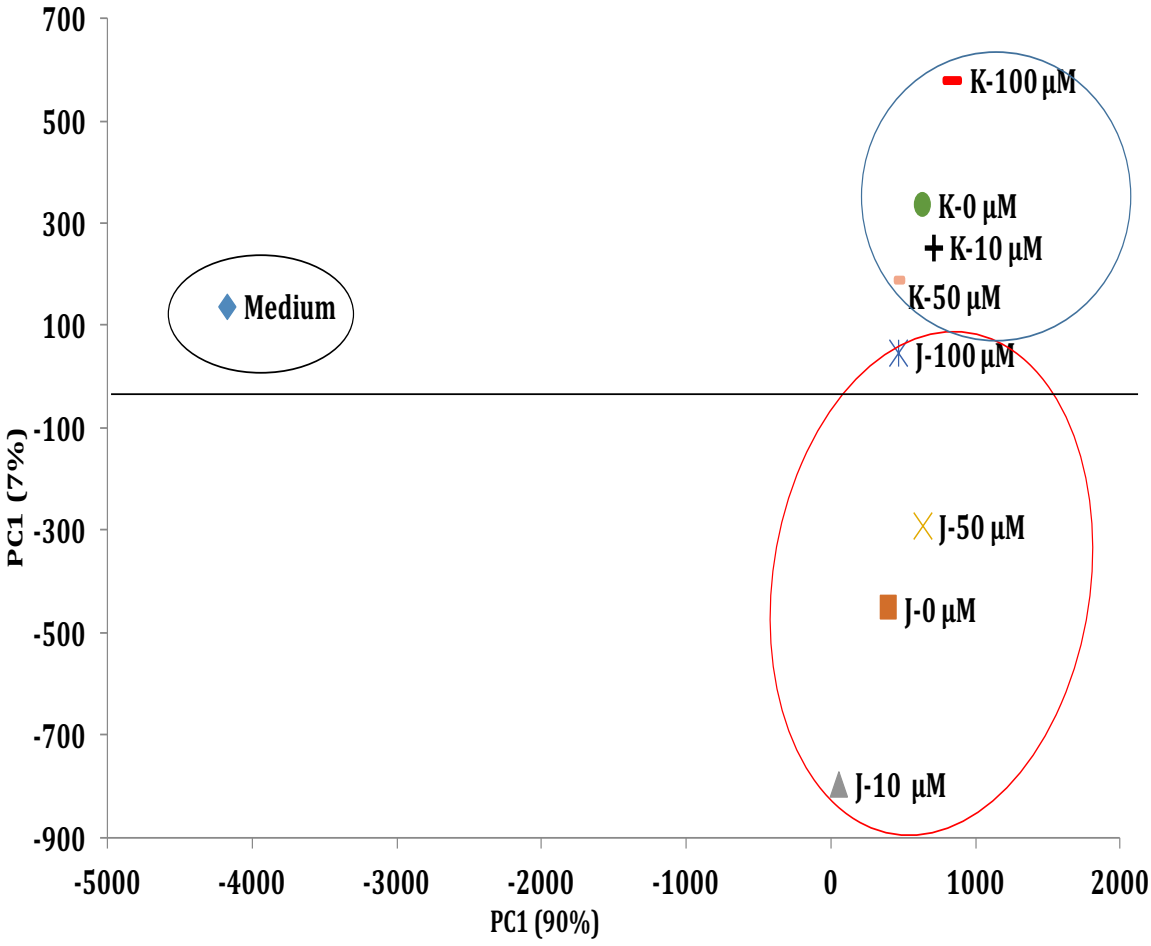

Figure 31: PCA of Full Scans of the headspace of control media (no cells) with 100 µM of Imatinib, and cells incubated with 0 µM, 10 µM, 50 µM, and 100 µM of Imatinib (using H_3O^+ reagent ion).

The PCA scores plots in Figures 31 and 33 show a clear difference between the signals from media with 100 µM of Imatinib or Nilotinib versus cells incubated in the absence or presence of either Imatinib or Nilotinib. Interestingly, there is also clear separation between both cell lines (Jurkat and K562) and, at the same time, PCA was able to indicate certain separation amongst cells incubated in different doses of either drug within the same cell line, especially when comparing control cells with cells incubated with the highest dose of Imatinib or Nilotinib. This would indicate that SIFT-MS might have a role in assessing tumor response to treatment and PCA could be used to explore it

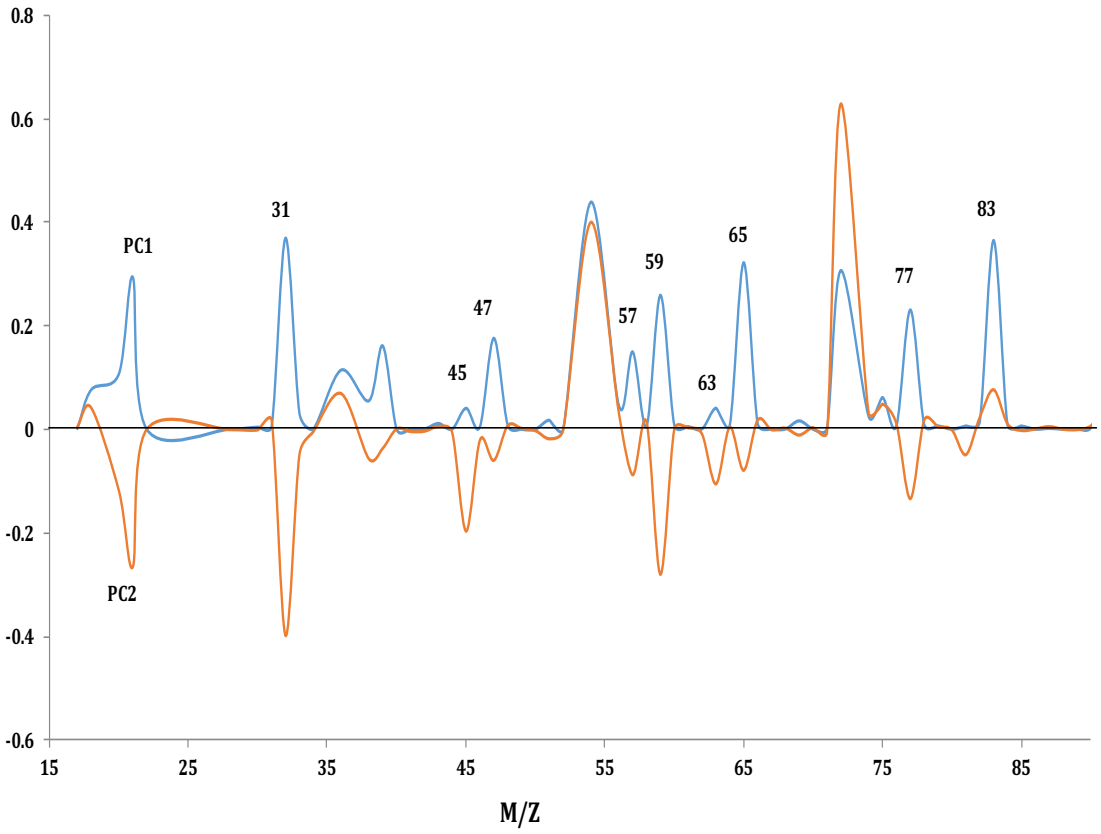

Figure 32: PCA loading of full scans from headspace of control media with no cells but with 100 µM of Imatinib and cells incubated with 0 µM, 10 µM, 50 µM, or 100 µM of Imatinib.

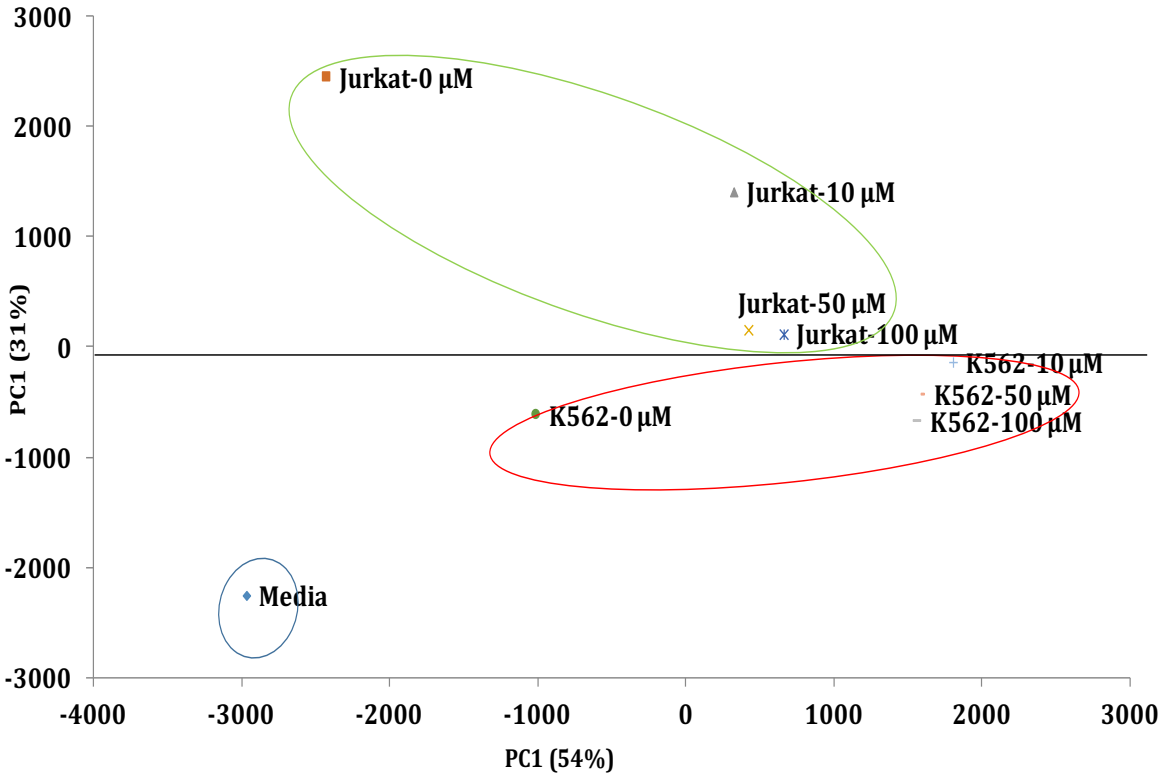

Figure 33: PCA of Full Scans of the headspace of control media (no cells) with 100 µM of Nilotinib, and cells incubated with 0 µM, 10 µM, 50 µM, and 100 µM of Nilotinib (using H_3O^+ reagent ion).

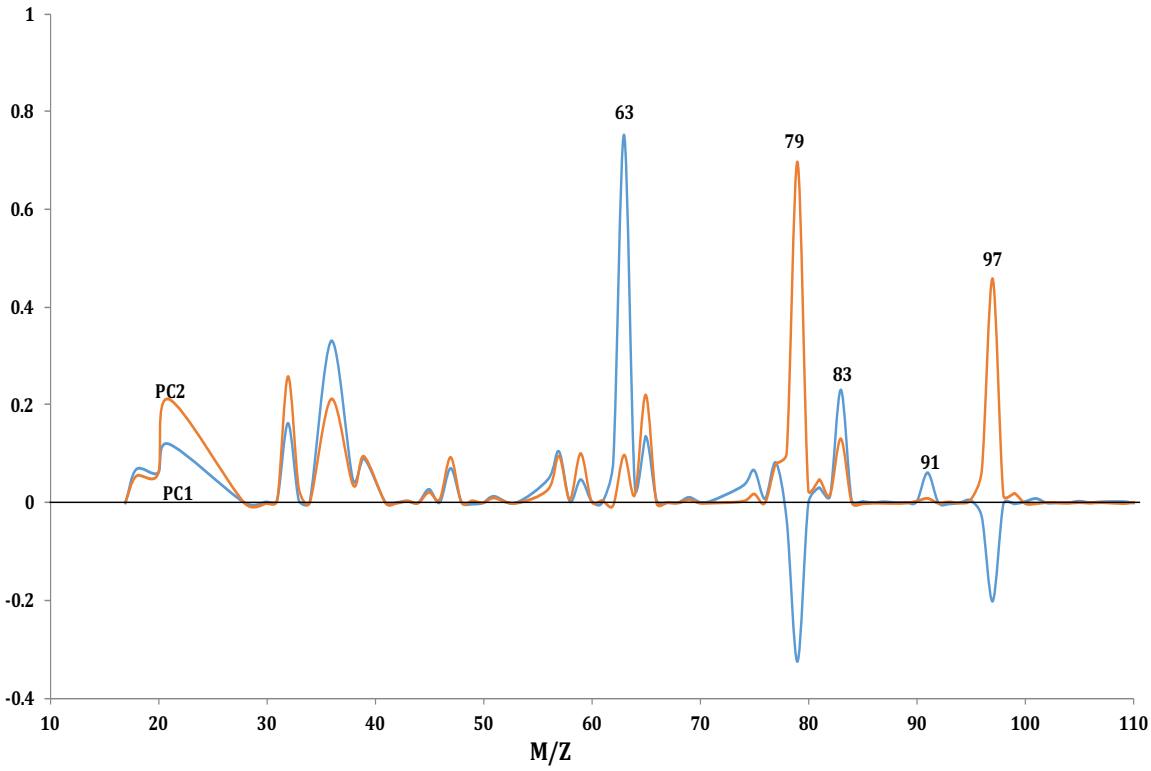

Figure 34: PCA loadings of Full Scans of the headspace of control media (no cells) with 100 µM of Nilotinib, and cells incubated with 0 µM, 10 µM, 50 µM, and 100 µM of Nilotinib (using H_3O^+ reagent ion).

The next step was to look for those analytes that could explain these differences. In the case of Imatinib, the loading plot (Figure 32) of PCA (Figure 31) showed differences as follows: m/z 31, associated with formaldehyde; m/z 45, associated with acetaldehyde; m/z 47, associated with formic acid and ethanol; m/z 57, associated with acrolein; m/z 59, associated with acetone and propanal; m/z 63, associated with dimethyl sulphide; m/z 77, associated with carbon disulphide and thioacetic acid; m/z 83, associated with 4-methyl-1, 3-pentadiene; m/z 65, not yet been assigned (all these associations have been obtained from the SIFT-MS library).

In the case of Nilotinib (Figure 34), the main differences reside in: m/z 63, associated with dimethyl sulphide; m/z 79, associated with benzene and dimethyl sulphoxide; m/z 83, associated with 4-methyl-1, 3-pentadiene; m/z 91, associated with phynylmethanol; and m/z 97, associated mostly with fluorobenzene and furancarboxaldehyde (all these associations have been obtained from the SIFT-MS library).

It is not clear from this preliminary work which would be the analyte or combination of analytes that could help in assessing leukaemia response to drugs. However, the data is very encouraging and should lead towards further work in which individual metabolical pathways can be enhanced or inhibited to better understand their role following the addition of drugs to leukaemia cells.

4.6: Conclusion

The VOCs exhaled by humans are a valuable source of information about the body's metabolism. The different body compartments produce a large variety of VOCs, a considerable part of which is found in the breath [De Lacy Costello 2014]. Mostly, these are metabolic products, so the exhaled breath may contain the footprints of cellular activities. Analysis of breath can reveal those pathologies that alter the metabolism induced by the drugs (Imatinib, Nilotinib). In the lungs, at the blood-air interface, the volatile metabolic compounds may be transferred from blood to air and released in breath. Collecting information contained in breath is attracting research interest and breath analysis is emerging as a major promising field of interest.

The interest in using exhaled gases as non-invasive markers in clinical diagnostics and therapeutic monitoring has steadily increased over the past ten years. Hence, substantial work has been done to understand the underlying source and metabolism of volatiles. The current study demonstrates that several VOCS might be useful in the monitoring of therapeutic response. However, further studies are needed to assess VOCs produced by cells from a particular cancer type, and to compare between *in vivo* and *in vitro* situations.

Furthermore, work is needed to assess whether each type of cancer could have a different VOCs profile, how varied they might be between cancers types and how they might change following the addition of drugs. A great deal of work still needs to be done *in vitro* before this technique is taken into a clinical set up.

Chapter 5

Development of a Methodology to Study Volatiles from Breath for Clinical Applications of SIFT-MS

5.1: Introduction

Research in medical science has advanced rapidly in recent years and has achieved higher survival rates for many chronic diseases, yet cancer remains the leading cause of the death in western world. Early detection of any type of cancer is a key issue in the management of the disease. It also applies to leukemia, as in most cases the disease goes un-noticed for a long time. Several techniques have been developed to detect cancer but these screening methods are mostly time consuming, invasive and costly. Yet, for leukemia, none of them has been proved to become a gold standard due to their limited reliability. Therefore, there is a need to develop non-invasive, reliable, fast and cheaper diagnostic techniques to detect leukemia at early stages, as it is widely accepted that survival is higher the earlier the disease is diagnosed.

Breath analysis to identify VOCs has received increasing attention from both the clinical and scientific points of view in the past two decades. There are research groups actively targeting biomarkers in exhaled breath for medical diagnoses or to monitor therapeutic strategies. Breath analysis techniques, can also be applied to *in-vitro* studies to analyze volatile organic chemical compounds produced during cellular metabolism and cell-to-cell interaction. Phillips 1999, stated there are 3481 different compounds in exhaled breath which have been observed at different concentrations ranging from ppbv to pptv, which also vary from person to person. Of

these, about 1753 compounds were observed showing positive alveolar gradient, i. e., their concentration was higher in exhaled breath than inhaled air [Phillips 1999]. Therefore, it could be hypothesised that some of these compounds could be linked to specific diseases, including leukaemia, and their changes in concentration in exhaled breath could be used for diagnosis and management of the disease.

Breath analysis has great potential in term of disease detection and its response to the treatment thanks to real time quantification of trace gases. The non-invasive nature and rapid sample analysis are the major advantages of the breath analysis techniques for both clinical and laboratory use [Kumar 2013].

To date, GCMS is a technique widely used in laboratories for the detection of VOCs in the exhaled breath. However, it requires breath absorption devices and particular column calibration for specific compounds which could be a time-consuming process. At the same time, it has limits when quantifying some trace gases present in exhaled breath [Kumar 2013]. Thus, other MS techniques such as PTR-MS and SIFT-MS have gained more interest in recent years due to their real time absolute quantification of trace gases at very low concentration.

All these techniques are still evolving in breath analysis due to the important challenges they have to face. VOCs in exhaled breath are produced from metabolical processes taking place in different organs in the body including the oral cavity and gut from, amongst other, bacteria present in these cavities. Age of the individual, gender, food and drink intake and smoking amongst other may result in different VOCs profiles identified in breath. Furthermore, many VOCs may come from the

environment rather than metabolical processes. Hence, human breath is a complex mixture of volatile organic and inorganic compounds. More important, some of them could become confounding factors when studying breath for disease management. It is therefore very important to understand the baseline physiology of the human breath prior to developing these techniques into clinical practice.

The next challenge is breath sampling. It has to be very well established how to collect breath samples, i. e., the environment (clean room), time of the day (early morning prior to eating or drinking anything), sample collection (directly into the instrument or using specially developed containers), number of exhaled breaths (one or several). Storage and transport of samples is one the biggest challenges due the possible loss of trace gases present in exhaled breath. Also, contamination of the sample by other VOCs could affect the analysis. It's not always possible to collect the breath directly from the patient, may be due to their condition or may be due to the mobility issues of the machine being used for the analysis. So, breath needs to be collected, stored, transported and analysed. This could take a lot of time to collect the breath and transport it to the place for analysis. Therefore, it is very important to establish a proper methodology with robust reproducibility and reliability so these techniques can be taken into the clinics.

At present, there are no gold standard methods for VOCs sampling and analysis. The American Thoracic Society proposed the first guidelines for breath sampling in 1999, aimed at monitoring NO in breath [Offline 1999]. Previously, polymer-sampling bags have been used to study the stability of selected breath species with the help of PTR-MS and GC-MS [Mochalski 2009; Mochalski 2013]. Tedlar bags (PTFE-

Polytetrafluoroethylene) are the most commonly used breath sampling container at present [O'Hara 2008]. Nalophan bags (PET-polyethylene terephthalate) are also being used by many researchers in the field. Other breath sampling methods include:

- Flex foil bags (PET/NY/AL/CPE-polyethylene terephthalate/nylon/aluminium foil/ chlorinated polyethylene).
- Glass bottles
- Thermal Desorption tubes (Different absorbents)
- Metal Canisters

In this chapter, three different sampling methods for breath analysis were used, i. e. exhaling directly into the SIFT-MS instrument, Nalophan bags, and glass bottles. In order to take this technique into a clinical application, the best sampling model needs to be well characterised. On this basis, the breath of 7 healthy control cases was studied. In this chapter, the best suitable sampling technique among the ones presently being used in our laboratory were explored. The VOC of interest chosen to assess the best sampling technique of breath was acetaldehyde. This compound has been chosen based on previous work in our laboratory [Sulé-Suso 2009] and the studies carried out in chapters 3 and 4.

5.2: Aims of the study

I. To establish the best methodology suitable for the acquisition of breath samples.

II. To identify changes in VOCs' concentration over a storage time ranging from 0 to 24 hours.

III. To identify the best suitable breath volume for a clinical application.

5.3: Materials and methods

5.3.1: Control Group

Healthy participants within a breath analysis study were included in this project. The study had received ethical approval form the Local Ethics Committee. This is an on-going study and the results of only 7 individuals have been included in this chapter. Table VIII summarises the study methodology.

5.3.2: Sampling Methods

The participants entering the study were requested not to eat or drink anything apart from water the morning before providing a breath sample. Participants were allowed to take any medication they had been prescribed. Participants were also requested not to brush their teeth on the morning of sampling. Samples were always obtained at 9.00 o'clock in the morning Prior to providing a breath sample, a cup of water was provided to rinse the mouth with. Breath samples (direct breath or collected in bags or bottles) were always obtained in the same room. Furthermore, 2 bags were also filled with room air using a 50 mL syringe, in order to provide a control air sample. The bags were then sealed with a lure lock syringe inserted into the sampling pipe and parafilmed.

Table VIII: Summary of the study methodology

Participants	Reagent Ions Used	Mode of Acquisition	Sampling Method	Time Points (hours)	Exhalations
Healthy Participants	H_3O^+, NO^+	MUI, FSM	Direct	0 (in triplicate)	1
			Bag	0 (in triplicate), 1, 3, 6, 24	3, 5
			Bottle	0 (in triplicate), 1, 3, 6, 24	3,5

Figure 35: SIFT-MS sampling 150ml bottle, with steel screw cap and penetrable rubber septum.

5.3.3: Sampling into Bottles

Participants were asked to fill 150 mL sterile glass bottles using a straw of 10 cm in length, 8 cm of which inserted into the bottles (Figure 35). Participants were requested to fill the bottles with 3 breaths (3 bottles) or 5 breaths (3 bottles). The bottles were then immediately tightly sealed with lids containing a septum, suitable for puncture by the SIFT-MS sampling needle. Bottles were then sealed with parafilm around the lid of the bottle until sampled. These sealed bottles were kept at room temperature prior to SIFT-MS experiments. However, they were brought to 37 °C by keeping them in a water bath immediately prior to running the SIFT-MS experiments.

5.3.4: Sampling into Nalophan Bags

Nalophan tube sheeting was cut into 30 cm length and a 3 cm poly-tubing length was introduced into one end, fixing it into place with a cable tie and sealed with parafilm (Figure 36). The far end was also sealed using a cable tie and parafilm over it.

Participants were asked to fill each bag with at least 3 breaths, exhaling normally. Each bag was then sealed with a lure lock syringe and wrapped in parafilm. Bags were stored at room temperature, under ambient conditions until sampling time. They were brought to 37 °C by keeping them in a temperature controlled box before running the SIFT-MS experiments.

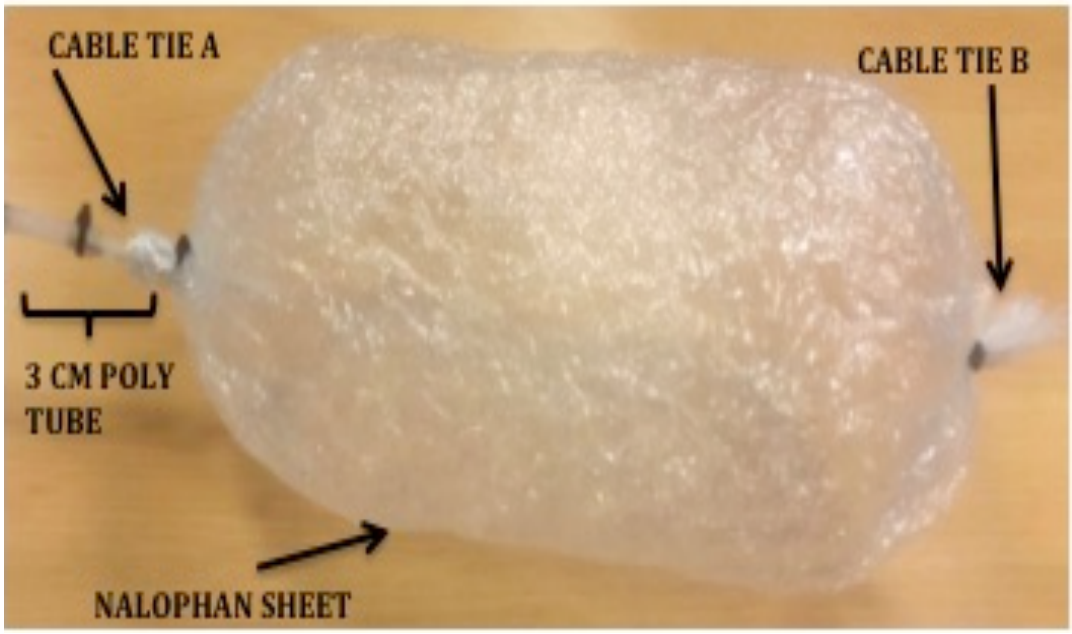

Figure 36: SIFT-MS sampling bag comprised of a Nalophan sheet, cable ties and poly tubing sampling orifice.

5.3.5: Direct Breath Sampling

A sterile sampling tube was attached to the sampling arm of the SIFT-MS by replacing the sampling needle. Participants were requested to exhale one long, continuous breath into the sampling tube attached to SIFT-MS sampling arm, in order to maximise the amount of exhaled breath for analysis (figure 37). Breath was acquired in triplicate for each precursor ion (H_3O^+ and NO^+). Direct breath sampling was acquired at the same time as bottle and bag samples were sampled.

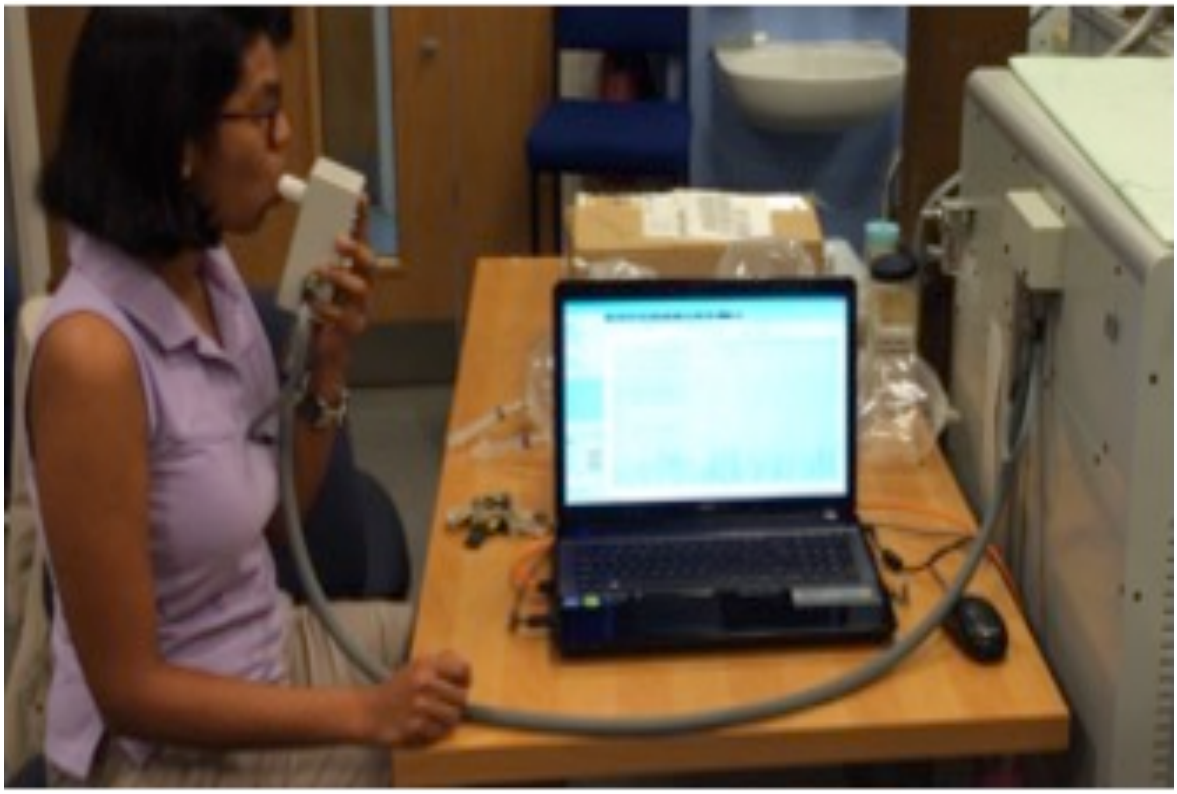

Figure 37: Direct Sampling into the Profile 3 SIFT-MS instrument

5.4: Selected Ion Flow Tube Mass Spectrometer Sampling

The profile 3 SIFT-MS (Figure 37) instrument was used to analyse the breath samples. Two reagent ions, H_3O^+ and NO^+ were used in this study. Both operational mode of SIFT-MS, MUI (to identify specific compounds) and FSM (to study full scan data) were also used. For bottle-sampled breath, the bottle environment pressure was equilibrated by using a bag of dry purged air attached to a puncturing needle, placed through the septum of the sampling bottles. For bags sampling, the needle in the SIFT-MS sampling arm was directly inserted into the bags by puncturing the bag. For direct sampling, a sterile sampling tube was attached to the sampling arm of the SIFT-MS by replacing the sampling needle. Air in bottle and bag samples was measured with SIFT-MS for 1 minute. Direct sampling breath was measured for as long as the participant was able to exhale in one single breath.

5.5: Data Processing (Water Correction)

Data processing for SIFT-MS has been previously described in chapter 2. For each acquired sample, a 6% water correction method was applied during MIM mode of SIFT-MS for the H_3O^+ precursor only. Each measurement was first brought up to 6% water level using the flow rate adjustment built in the SIFT-MS software.

5.6: Data Analysis

SIFT-MS data was transferred form SIFT-MS software to Microsoft Excel.

5.7: Results

5.7.1: Number of breath exhalation

As it has already been stated in the Introduction chapter, a single breath might not be a true representation of the physiology of the body. Therefore, the first 3 participants were asked to fill in glass bottles with either 3 or 5 exhalations. Breath was then measured and the results are shown in Figure 38. The bars show no major differences between the measurements of 3 or 5 exhalations. The results indicate that when collecting breath samples in bottles, 3 exhalations provide good data and no improvement is seen by increasing the number of exhalations.

5.7.2: Loss of Humidity Among Different Sampling Methods Over Time

There has been a great debate regarding loss of humidity during sampling and over the time period for sample storage [Offline 1999; Diskin 2003; Lourenço 2014]. In this

study, the results indicate that there is a clear loss of humidity over the time of storage depending upon the sampling approach (Figure 39).

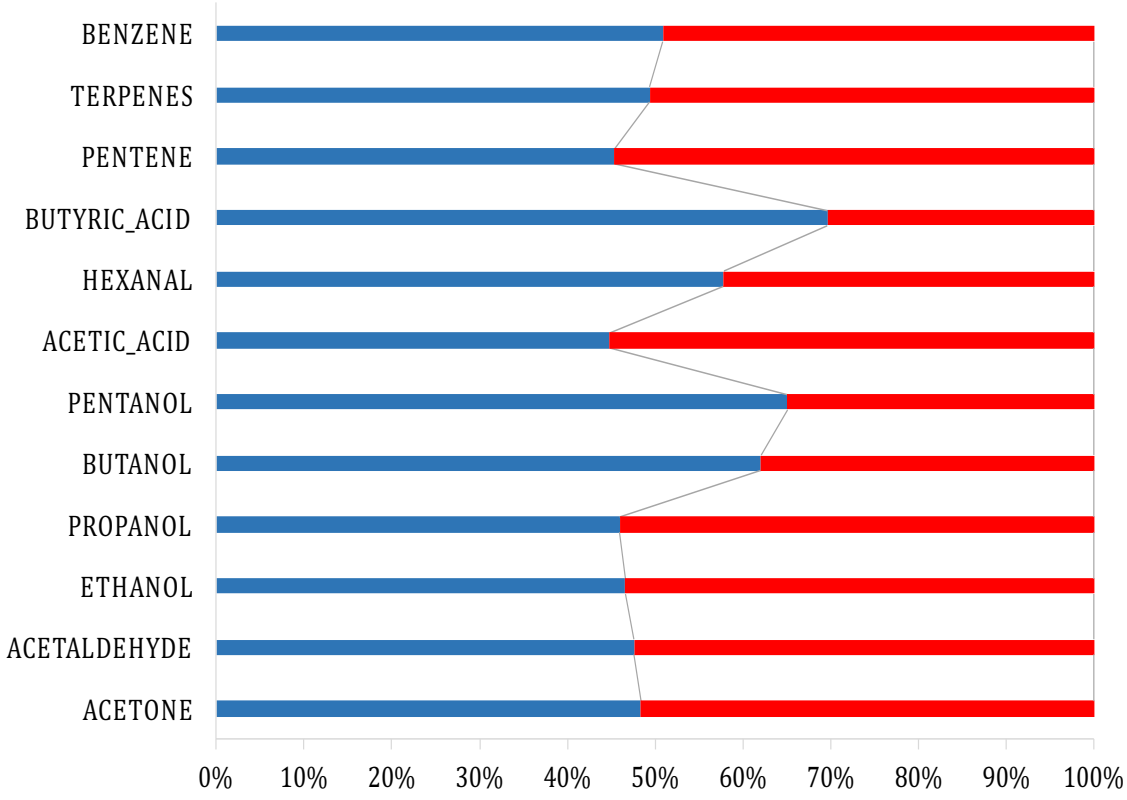

Figure 38: 3 Exhalation (blue) vs 5 Exhalation (red) for specific compounds measured with SIFT-MS (all data are mean of three independent controls).

The storage of breath samples in bags translates into a rapid loss of humidity over a period of 24 hours. This is noticeable even after one hour of storage. However, this is not the case for breath samples stored in bottles. Direct sampling confirmed the 6% humidity in physiological conditions.

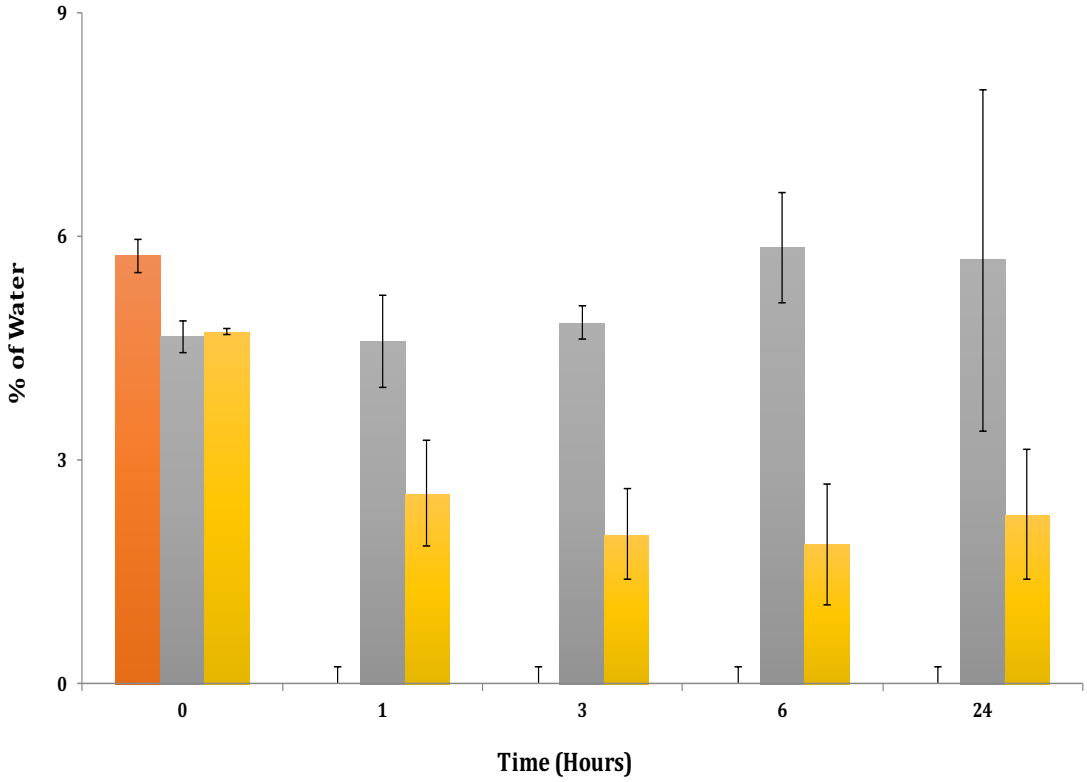

Figure 39: Loss of Humidity over the time from 0 to 24 hours among three methods of sampling, direct method (red), bottles (grey), and bags (yellow).

5.7.3: Identification of Best Sampling Technique for Breath Sampling

Representative data examples of breath samples obtained with the 3 techniques (direct, bag or bottle) at time point 0 are shown in Figures 40 and 41 using H_3O^+ or NO^+ precursors, respectively. The results indicate that the best methods to identify VOCs are collecting the breath in bottles or bags, especially for those VOCs that might be present in a very low concentration. An example is propanol where the concentration in breath was detected at lower levels in direct breath when compared to breath samples collected in either bags or bottles.

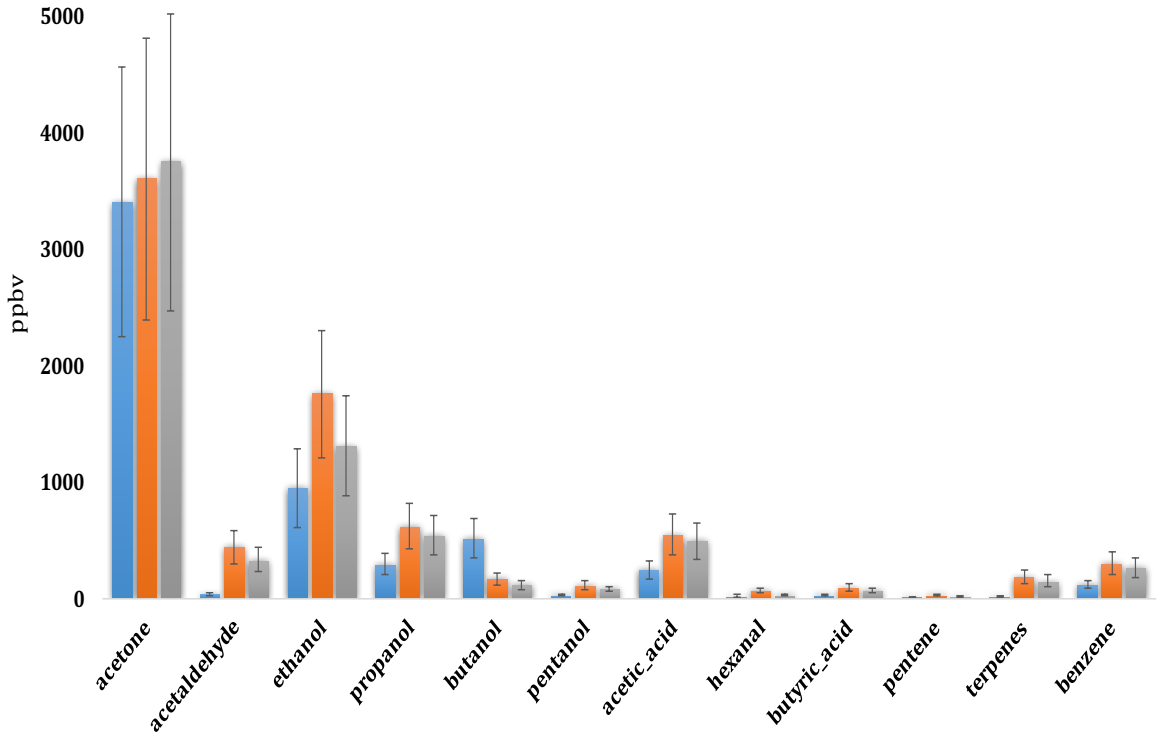

Figure 40: Representative examples of breath samples collected at 0 hours by all three methods direct breath (blue), bags (red), and bottles (grey) using the H_3O^+ precursor. (All compounds are mean of five independent controls).

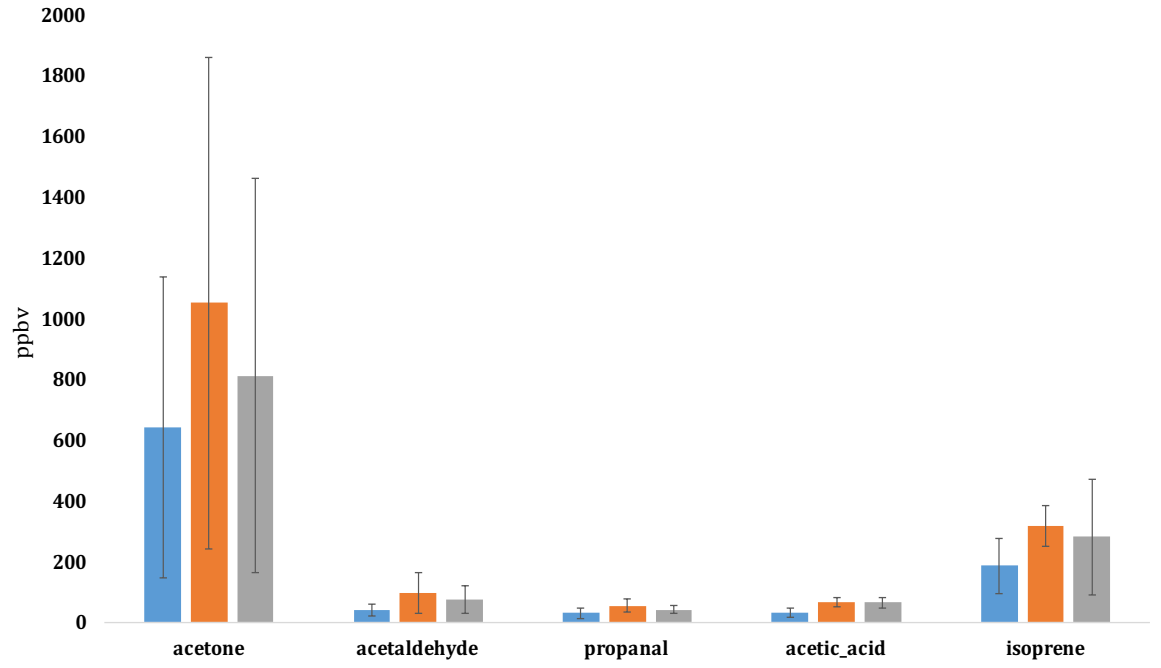

Figure 41: Representative examples of breath samples collected at 0 hours by all three methods direct breath (blue), bags (red), and bottles (grey) using the NO^+ precursor. (All compounds are mean of five independent controls).

5.7.4: Measurement of breath sample over time

The next step was to assess how storage of breath samples over time could affect the measurement of VOCs especially regarding diffusion and/or absorption of VOCs to the sample vessel. Figures 42 to 45 show representative examples of the concentration of analytes measured at 0, 6 and 24 hours.

The data obtained did not show a clear pattern of decrease or increase of VOCs concentration that could be applied to all participants for samples collected either in bags or in bottles. The concentration of some analytes decreased with storage time while in other cases it remained similar. The results would indicate that storage might affect the concentration of each analyte in different ways, therefore, it would be advisable to measure breath samples as soon as they have been collected.

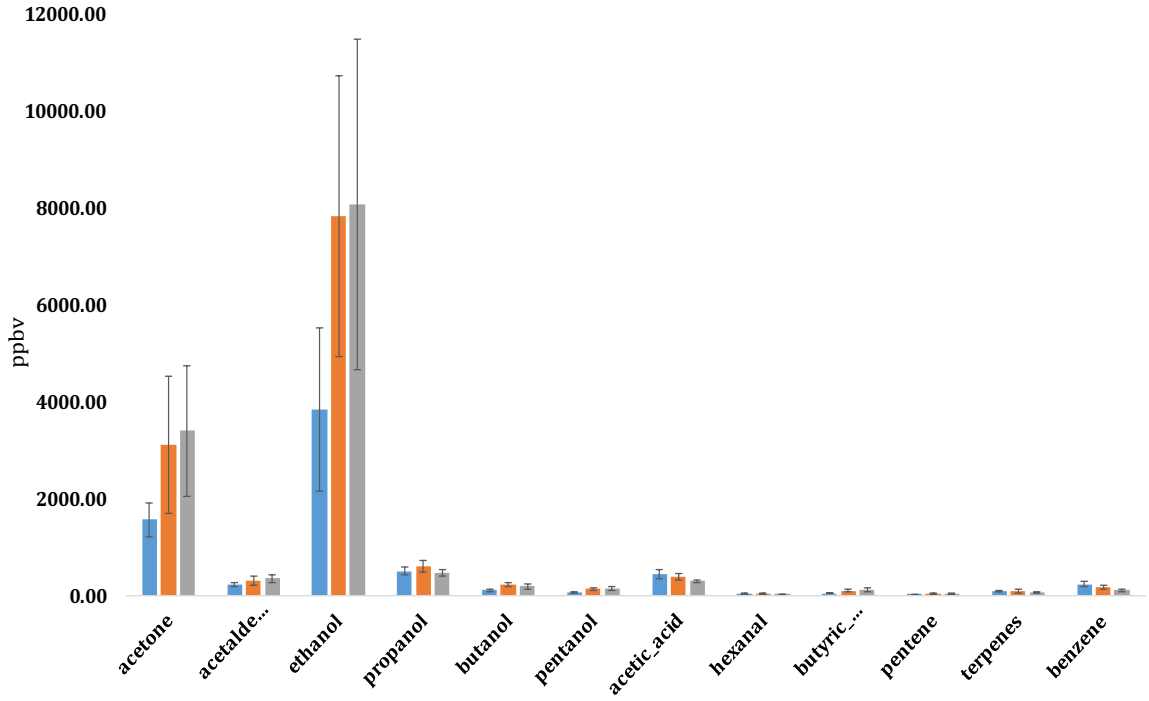

Figure 42: Representative examples of breath from participants collected in bags and measured at 0 (blue), 6 (brown) and 24 (grey) hours after collection using H_3O^+ precursor. (all compounds are mean of five independent controls).

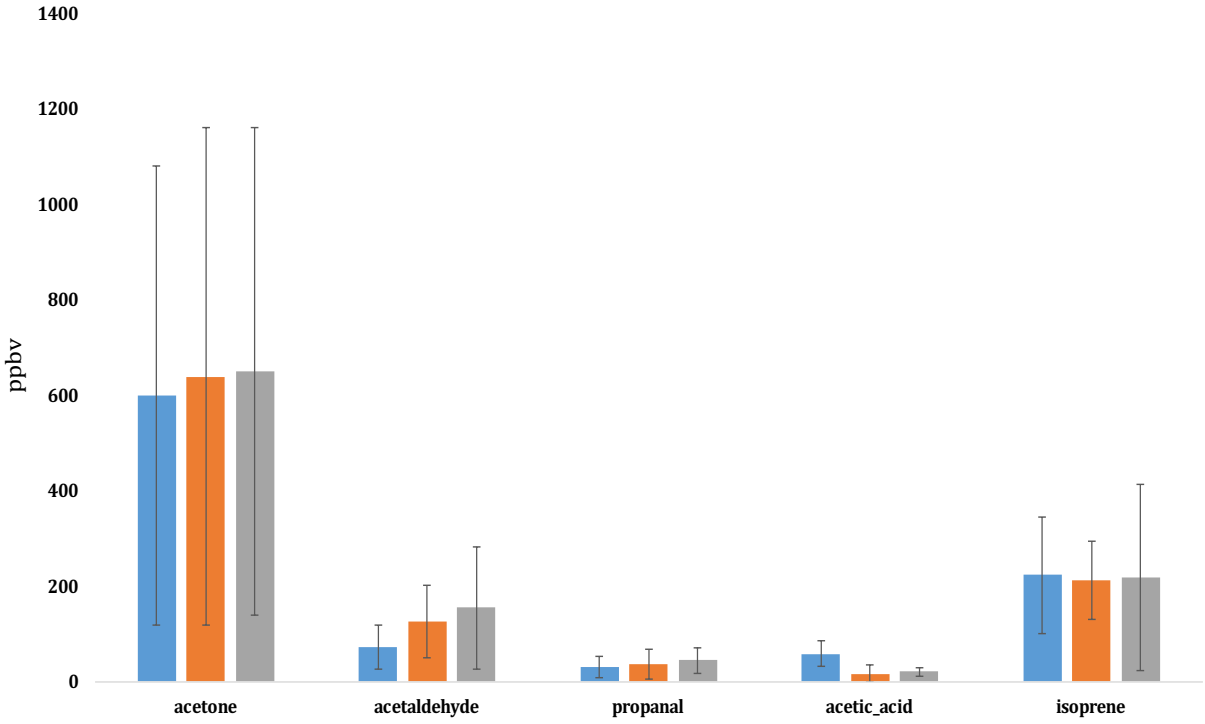

Figure 43: Representative examples of breath from participants collected in bags and measured at 0 (blue), 6 (brown) and 24 (grey) hours after collection using NO^+ precursor. (all compounds are mean of five independent controls).

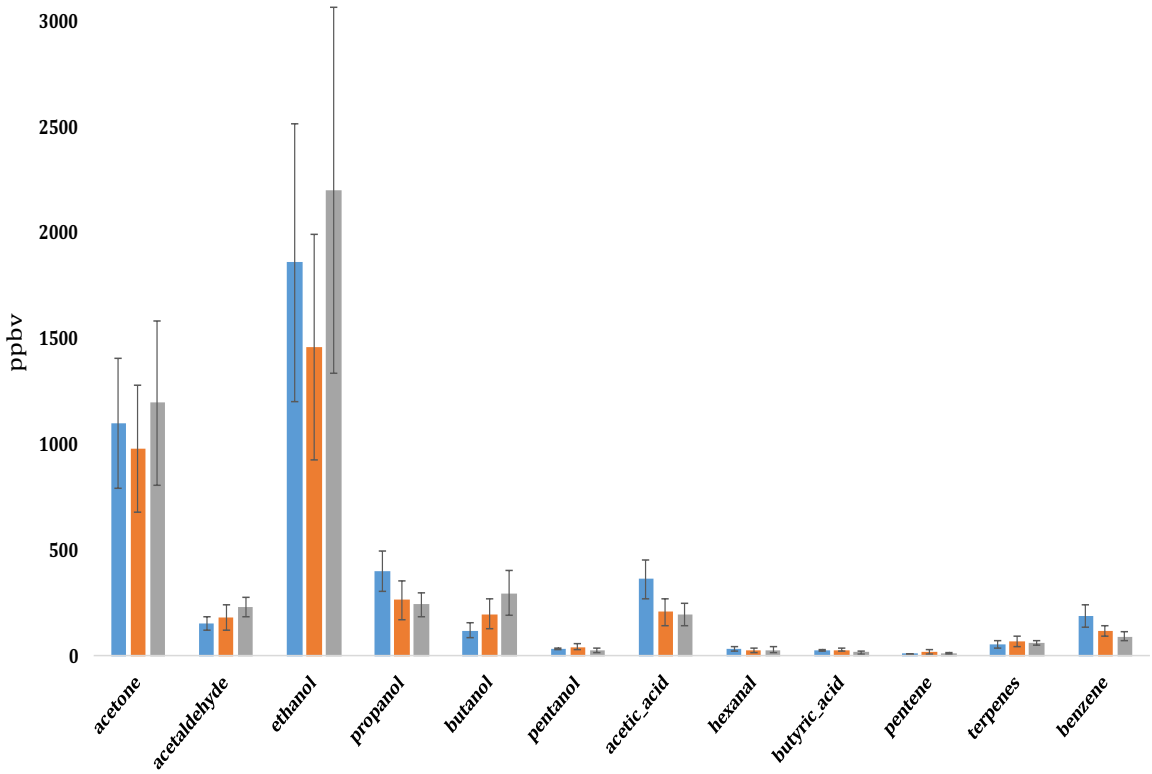

Figure 44: Representative examples of breath from participants collected in bottles and measured at 0 (blue), 6 (brown) and 24 (grey) hours after collection using H_3O^+ precursor. (all compounds are mean of five independent controls).

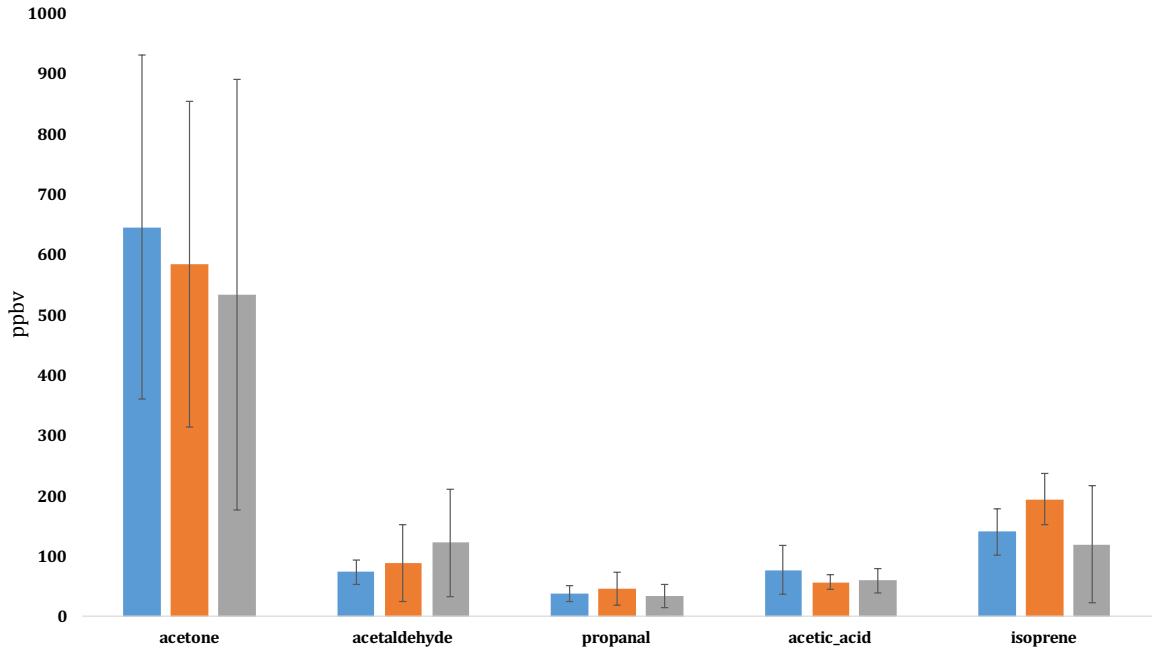

Figure 45: Representative examples of breath from participants collected in bottles and measured at 0 (blue), 6 (brown) and 24 (grey) hours after collection using NO^+ precursor. (all compounds are mean of five independent controls).

However, this might not be the case for full scan data. Figures 46 to 49 show the full scans for breath collected in bags using H_3O^+ precursor for the breath of the same participants' breath data presented in Figures 42 and 44. Figures 50 to 52 show the full scans for breath collected in bottles. The results indicate there is a bigger variation between the full scan profiles of breath measured at different time points including the absence of some analytes at 6 and 24 hours. Furthermore, the differences at these time points seem to be higher in the case of breath stored in bags when compared to the breath stored in bottles. Similar data was obtained when using NO^+ as precursor. The data presented here further strengthens the case to analyse breath samples a soon as they have been collected. Further work is needed to better understand the reasons behind these changes in VOCs concentration at different time points.

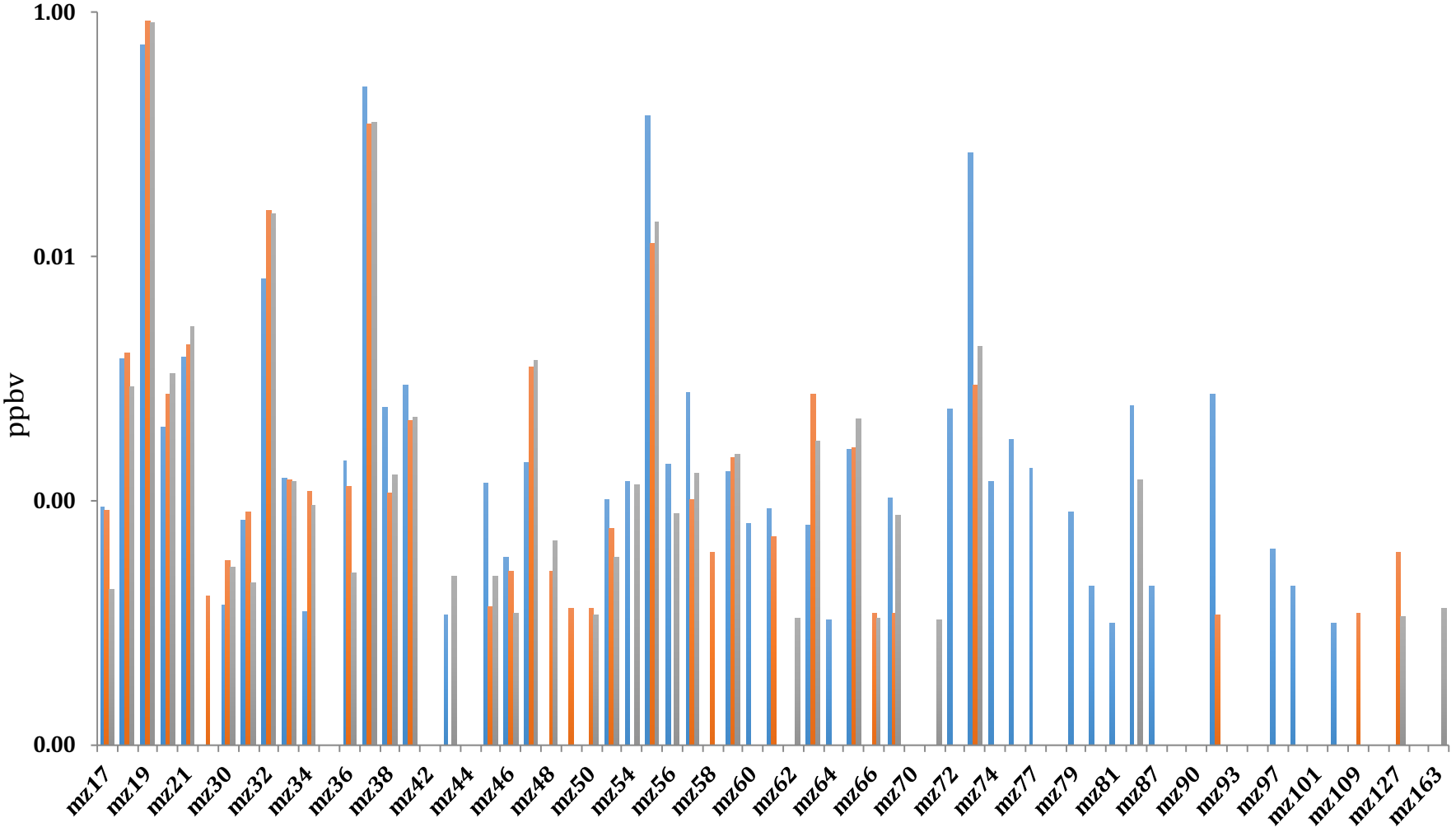

Figure 46: Full scan mode data of control 1 collected in bags and measured at 0 (blue), 6 (red), and 24 (grey) hours of collectio using H_3O^+ precursor.

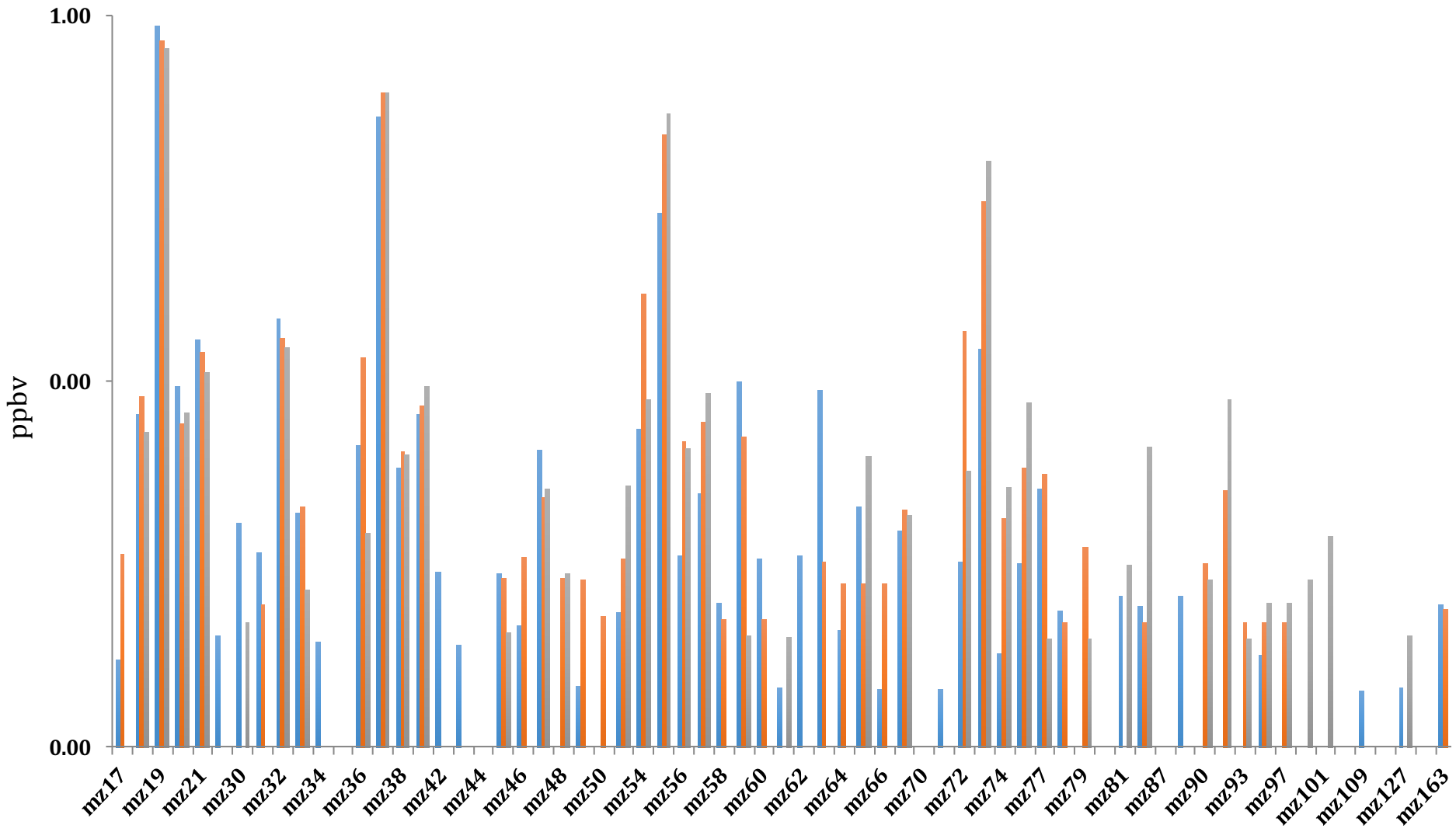

Figure 47: Full scan mode data of control 2 collected in bags and measured at 0 (blue), 6 (red), and 24 (grey) hours of collection usi
H_3O^+ precursor.

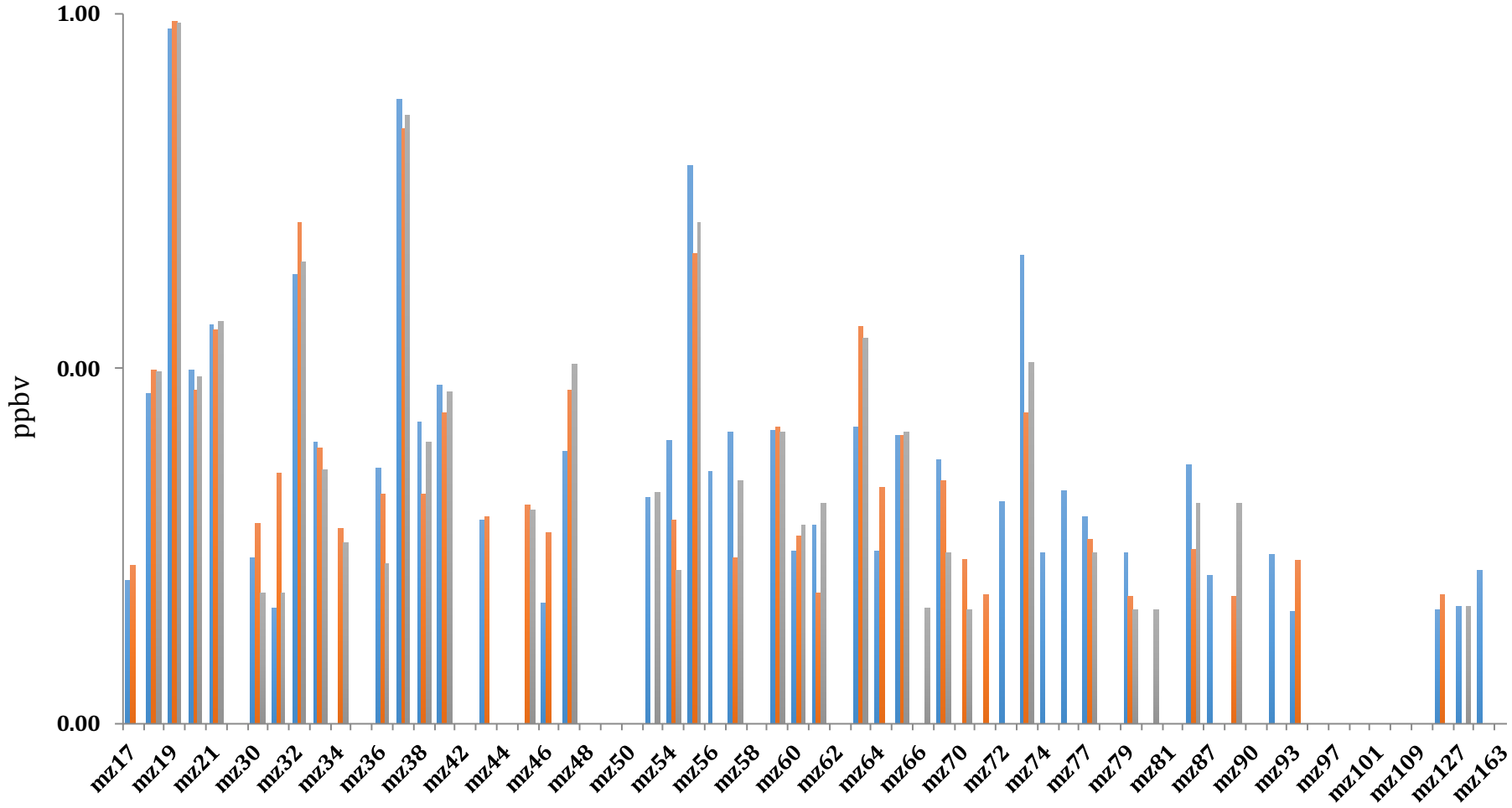

Figure 48: Full scan mode data of control 3 collected in bags and measured at 0 (blue), 6 (red), and 24 (grey) hours of collection us
H_3O^+ precursor.

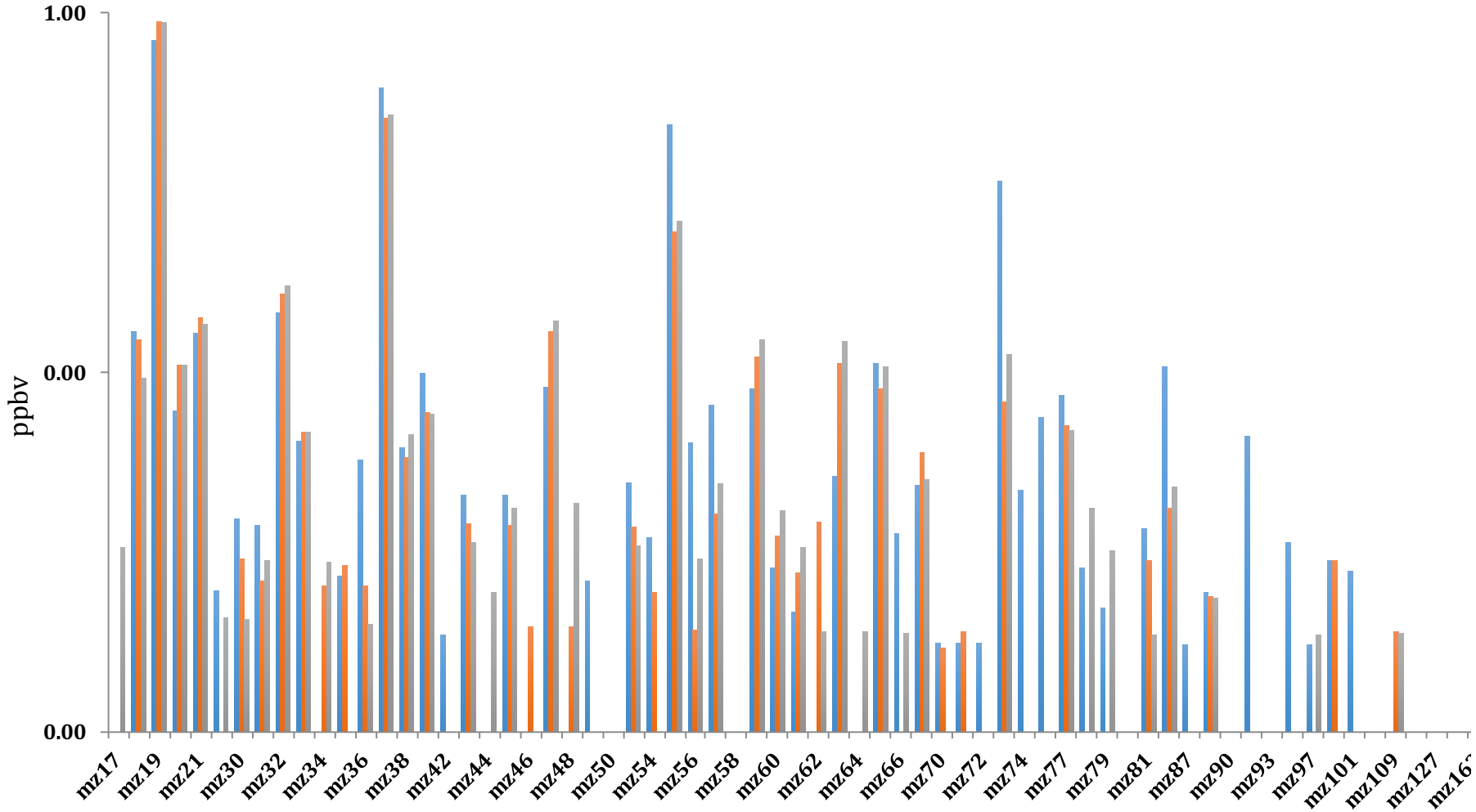

Figure 49: Full scan mode data of control 4 collected in bags and measured at 0 (blue), 6 (red), and 24 (grey) hours of collection u
H_3O^+ precursor.

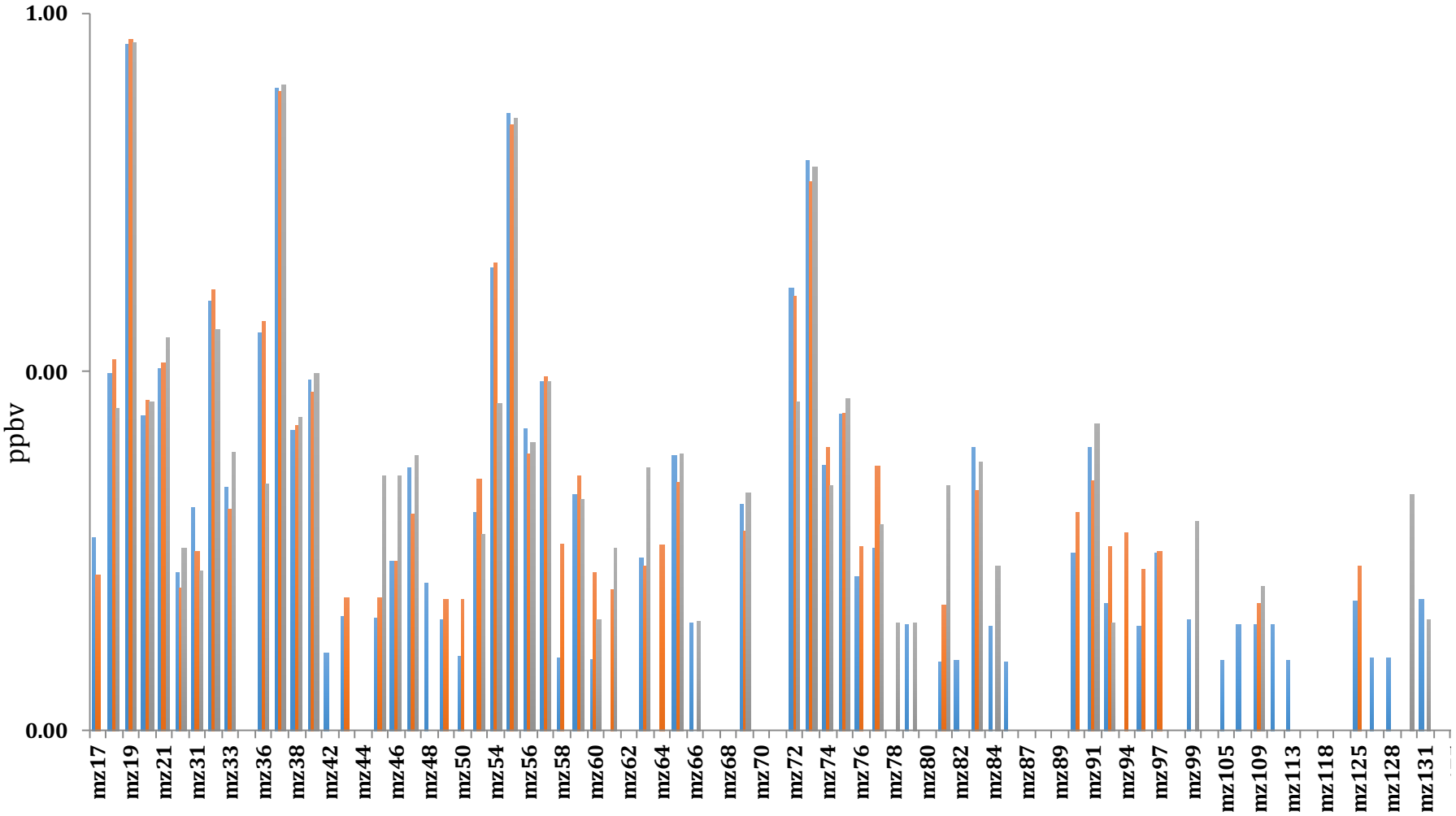

Figure 50: Full scan mode data of control 1 collected in bottles and measured at 0 (blue), 6 (red), and 24 (grey) hours of collectic using H_3O^+ precursor.

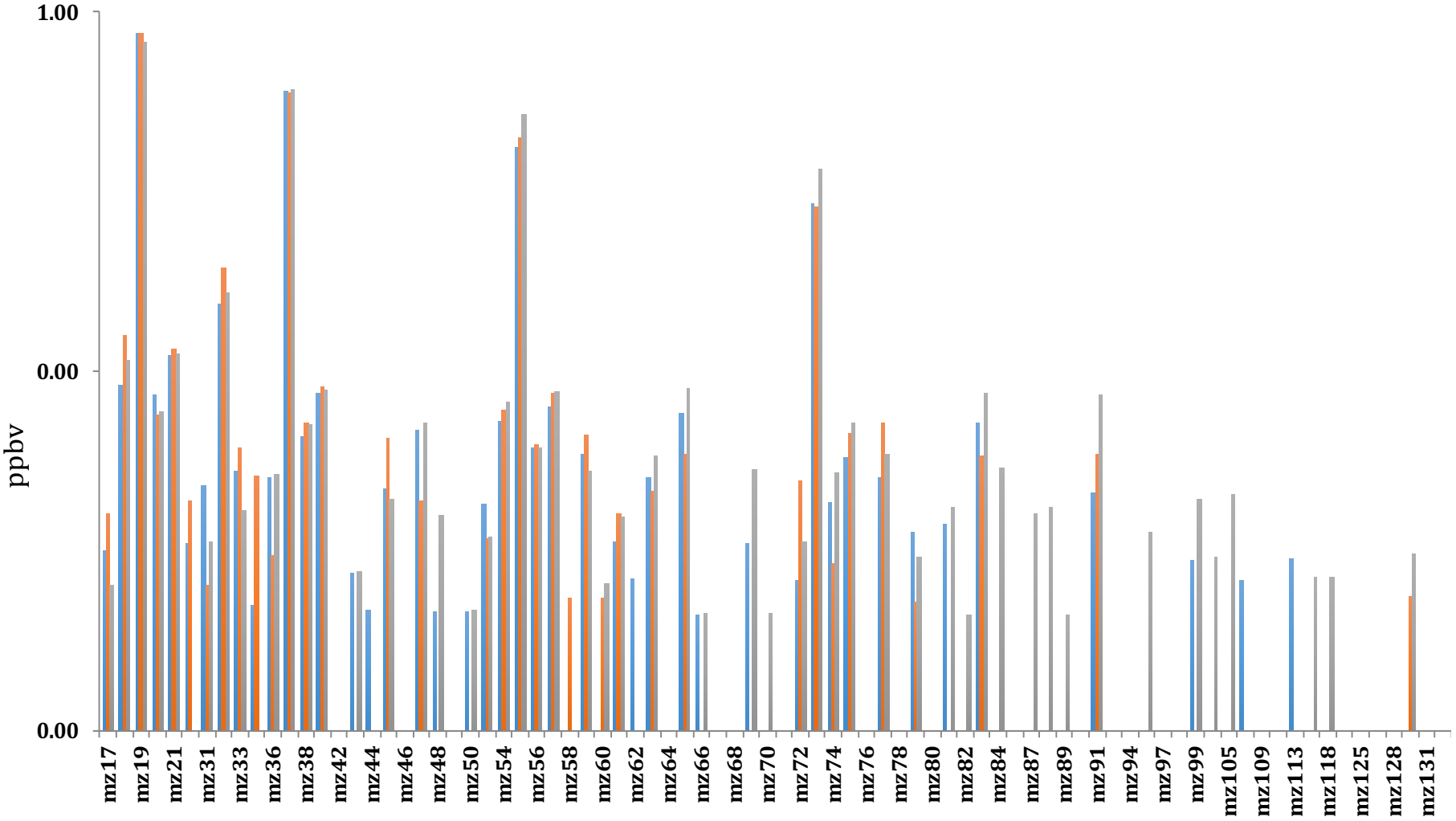

Figure 51: Full scan mode data of control 2 collected in bottles and measured at 0 (blue), 6 (red), and 24 (grey) hours of collection usir H_3O^+ precursor.

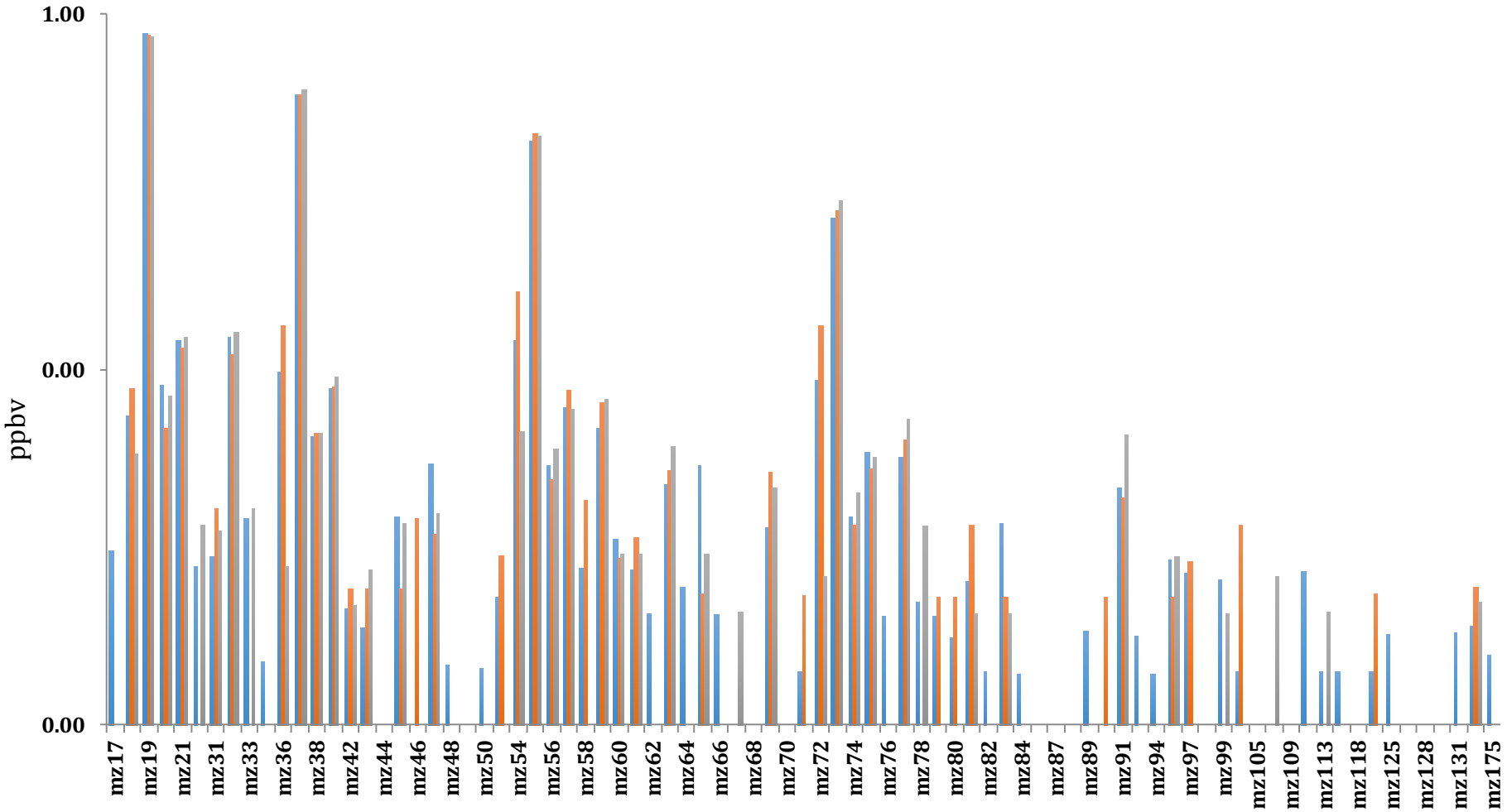

Figure 52 Full scan mode data of control 3 collected in bottles and measured at 0 (blue), 6 (red), and 24 (grey) hours of collection usin H_3O^+ precursor.

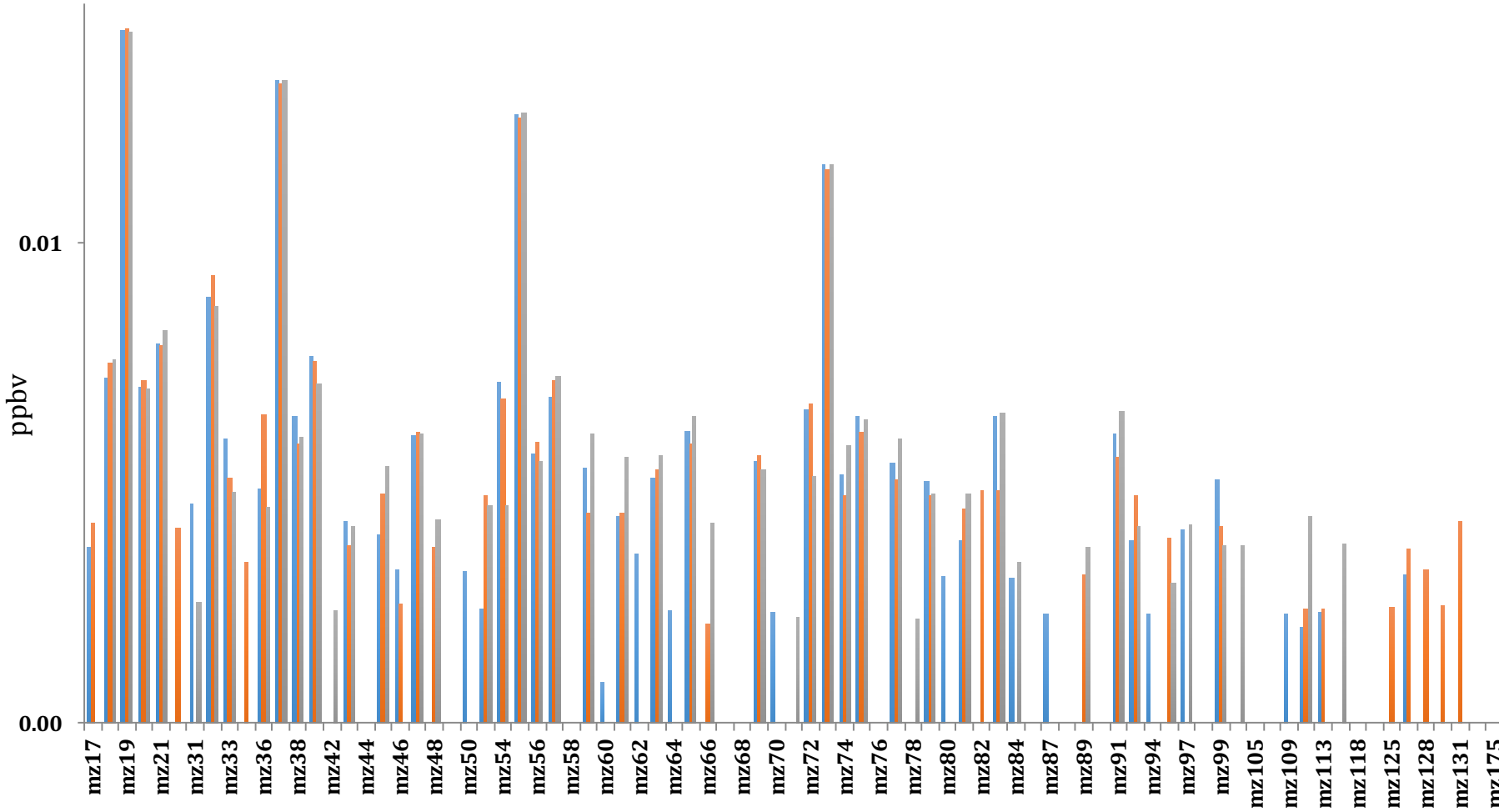

Figure 53: Full scan mode data of control 4 collected in bottles and measured at 0 (blue), 6 (red), and 24 (grey) hours of collection usir H_3O^+ precursor.

5.8: Discussions

Breath samples are performed for single or multiple breaths, but the composition of single breath may not necessarily be representative of the alveolar gas due to the fact that breath samples might considerably vary from one to other even for the same individual [Herbig 2008; O'Hara 2008; Filipiak 2012]. Multiple breaths are preferable to reduce this risk and to acquire reproducible breath samples. As an example, a highly soluble compound such as acetone that is produced in the airways rather than in alveoli and therefore its levels might not fully correlate with levels of acetone in blood [Anderson 2007], might be difficult to measure in a highly reproducible way. This would indicate that more than 1 exhalation might be required to obtain good reproducible data. In fact, it has been described that the smaller the sample, the greater the losses of analytes are [Harreveld 2003]. The data presented here, show that the levels of analytes identified are lower when measured in direct breath in comparison to breath collected in bottles or bags, would support this.

Another issue in breath analysis is the humidity of the sample and how this changes in time. Studies using Nalophan bags have proved that the sample decays during storage between 4-40 hours after the sampling [Harreveld 2003]. At least 10% difference in dry and wet conditions was reported while using Tedlar bags as samplers [Groves 1996]. Water vapour may diffuse through most of the materials that make the bags used in breath analysis although the loss rate will depend upon the material of the bag [Gilchrist 2012]. In this study, there was a loss of humidity even within one hour from the acquisition of the breath sample using bags. However, bottles were able to maintain a stable water vapour pressure even up to 24 hours. The levels of humidity have a great impact on the volatile species present in the

sample, as high levels of humidity, and therefore condensation, in the exhaled breath cause significant decrease in vapour concentrations for those compounds that are highly soluble in water [Mochalski 2013]. Water vapour can also be affected by temperature. As the temperature of the breath sample falls down below the body temperature (37 °C), water vapour may condense on the walls of the sampler, which could result in a decrease of the concentration of the more water soluble volatile compounds. So, keeping the sample at 37 °C is very important to avoid the risk of losing water-soluble volatile organic compounds.

It has been reported that VOCs might remain stable during the first 12 hours following sample acquisition [Harreveld 2003]. However, while no major differences were seen when studying few compounds, this did not apply when carrying out a full scan of the breath samples. This would indicate that stability over time might vary for different VOCs, especially those present in smaller concentrations.

From the work presented here and the work published, it is obvious that further studies are required to better understand the pathophysiology of VOCs present in breath. These studies need to take into account not only the metabolical pathways but also confounding factors such as age of the individual, gender and food and drink intake, smoking and environmental exposure. Other aspects of sampling which are of great debate among the scientific community are body posture of the subject during sampling, hyperventilation, control of the flow or volume of the breath during collection, sampling via nose or mouth, number of breaths exhaled, respiratory rate, and heart beat [Gilchrist 2012].

5.9: Conclusion

Direct sampling is the most convenient method of sampling, which could avoid loss of the many important VOCs by diffusion and/or absorption. Since it is not very easy to obtain direct breath in some occasions due to reasons such as age of the patient, inability to exhale for a period of time long enough, or the non-portability of the instrument, appropriate storage of exhaled breath and transportation are very important issues to be considered. There were no major differences observed, during multi ion mode. However, this did not apply when carrying out a full scan of the breath samples. This would indicate that stability over time might vary for different VOCs, especially those present in smaller concentrations. All these aspects of breath analysis need to be taken into consideration if the technique is to be applied in clinical practice.

Chapter 6

Synchrotron Based FTIR (S-FTIR) Spectroscopy Identifies Sensitive and Resistant Leukaemia Cells to Chemotherapy Drugs

Part of this chapter Published in Analyst: Effects of nilotinib on leukaemia cells using vibrational microspectroscopy and cell cloning
M. R. Siddique, A. V. Rutter, K. Wehbe, G. Cinque, G. Bellisola and J. Sulé-Suso

6.1: Introduction

Several studies have determined the problems and complexities along with the risks involved in the diagnosis and management of leukaemia. Currently there are several parameters to assess leukaemia, such as blood count, immunophenotyping, and presence of blast in peripheral blood and bone marrow biopsy.

Imatinib Mesylate is a tyrosine kinase inhibitor and first line treatment for Chronic Myeloid Leukaemia (CML) [Thota 2014; Gambacorti-Passerini 2015]. In a study trial, Imatinib achieved an 83% response rate in patients with newly diagnosed CML [Erba 2011]. However previous studies have shown CML in advanced phases might be resistant to Imatinib. The main mechanisms of resistance to Imatinib in patients with CML are mutations in the Bcr-Abl tyrosine kinase domain that obviate binding to the drug target, amplification of the BCR-ABL gene or clonal evolution [Nikolas 2006]. Nilotinib, a second-generation tyrosine kinase inhibitor, has been developed to override the resistance phenomenon [Burke 2003; Weisberg 2005]. It is a new ABL kinase inhibitor that has higher potency than Imatinib, especially in Imatinib resistant cells. Nilotinib can be used against many Imatinib resistant mutants of Bcr-Abl reducing the incidence of resistant mutants [Welsberg 2005]. Nilotinib has shown

greater efficacy than Imatinib in patients with newly diagnosed Philadelphia chromosome[10] (Ph) (appendix 3) positive CML in chronic phase after a minimum follow-up of 12 months [Kantarjian 2011]. These results support Nilotinib as a first-line treatment option for patients with newly diagnosed disease [Kantarjian 2011], but Weisberg E et al. (2005) has also reported some mutants, which also displayed significant resistance to Nilotinib [Weisberg 2005]. The choice of chemotherapy agents and combinations in the treatment of leukaemia is based on multicentre studies. However, within each individual type of leukaemia, cells do not exhibit the same sensitivity to the delivered drug and, as such, it is not clear yet how the best drug or combination of drugs can be identified for each individual patient. Companion diagnostics are a key part of personalized medicine and will likely continue to rapidly increase in number and application to disease areas [Agarwal 2015, Olsen. 2013], as I discussed in introduction chapter, despite of the promising results, there are also complications associated with companion diagnostic assays i.e. developing a successful companion diagnostic with its complementary drug is complex, disintegrated and apprehensive with several challenges. Therefore, it is obvious that further developments are needed for a better and faster identification of leukaemia cells' sensitivity to drugs. This would lead to improved leukaemia patient tailored treatment.

Over the last few years, there has been an increasing interest in Fourier Transform Infrared (FTIR) microspectroscopy as a tool to study cell sensitivity to drugs [Krishna

[10] A piece of chromosome 9 and a piece of chromosome 22 break off and trade places. The BCR-ABL gene is formed on chromosome 22 where the piece of chromosome 9 attaches. The changed chromosome 22 is called the Philadelphia chromosome, abbreviated as Ph.

2006; Bellisola 2012; Rutter 2013]. Vibrational spectroscopy has been used to study leukaemia cells' sensitivity/resistance to drugs *in vitro* [Le Gal 1993; Liu 2001; Gaigneaux 2002; Gault 2003; Liu 2003; Krishna 2006; Moritz 2010; Machana 2012; Ceylan 2012; Travo 2012; Baran 2013; Bellisola 2013;; Yandim 2016;] and to assess tumour response in patients with leukaemia [Ramesh 2002; Sahu 2006; González-Solís, 2014]. The ability of FTIR coupled with PCA to distinguish BCR/ABL positive cells from normal or BCR/ABL negative cells has already been reported. Bellisola 2015, stated that FTIR spectroscopy can distinguish between BCR/ABL positive and BCR/ABL negative cells. Babrah 2008 reported that it is possible to classify cells of different lineage via its spectral signature [Babrah 2008]. All these studies have proven that vibrational spectroscopy using either FTIR or Raman microspectroscopy could not only distinguish between the sensitivity and resistance of given cell line to the particular drug [Krishna 2006] but also able to identify changes in leukaemia cells prior to and after the addition of drugs that could relate to leukaemia cell sensitivity/resistance to drugs. Furthermore, the possibility of studying the effects of drugs on cancer cells at sub-cellular level using synchrotron based FTIR (S-FTIR) microspectroscopy could help to better characterize spectral biomarkers of cancer cells sensitivity to drugs. However, cell morphology can introduce spectral deformations as well [Diem 2012] such as those associated with Mie scattering and dispersive artefact caused mostly by the cell nucleus [Bassan 2010; Rutter 2014]. Although several algorithms have been developed to correct for Mie scattering and the dispersive artefact none of them is widely used. Therefore, this poses an important problem when studying cells following the addition of chemotherapy drugs since spectral biochemical changes have to be identified separately from the morphologically induced spectral changes. The ideal alternative I followed in this

work was to obtain S-FTIR spectra of sensitive and resistant cells to Imatinib and Nilotinib prior to adding the drug so neither biochemical nor morphological changes caused by the drug itself interfered with their S-FTIR spectra. This could provide more robust data leading towards a better characterization of possible spectral biomarkers of cell sensitivity to chemotherapy. This should help in the future to figure out for each individual patient whether he/she would respond to a given treatment.

6.2: Aims

1. To better characterize spectral biomarkers of cell sensitivity to chemotherapy for leukaemia following the addition of the drug.
2. To be able to identify sensitivity/resistance of leukaemia cells to a given drug prior to the addition of the drug.

6.3: Materials and Methods

6.3.1: Cell line

The K562 (kind gift of Dr G. Bellisola), a CML cell line was used in this study. Cells were cultured and maintained in suspension in RPMI 1640 with 10% FBS 1% L-Glutamine (200nM), 1% Hepes buffer (1M) and 1% Antibiotic/Antimycotic (100x) and incubated at 37°C and 5% CO_2. Culture medium was changed every 3-4 days.

6.3.2: Cell survival

Parental K562 cells were incubated in 24 well plates at 10^5 cells/well in the absence and presence of Imatinib or Nilotinib (0 μM, 50 μM or 100 μM) for 5 days.

6.3.3: Cell cloning

The K562 cell line was cultured under standard conditions as mentioned in Chapter 2. Cells were collected before reaching confluence and counted with the trypan blue exclusion method after centrifuging at 950 rpm for 3 minutes. Cells were seeded in flat-bottomed 96 well plates at a concentration of 0.5 cells/well and topped up to 200 μL of fresh complete medium. In order to get a reasonable number of clones, 5 x 96 well plates were seeded. After the addition of the medium, plates were wrapped with foil to avoid dehydration and incubated at 37°C and 5% CO_2. Clones were inspected regularly so those wells with more than 1 clone could be discarded (see Chapter 2). Medium was changed after one-week culture by spinning the plates at 1200 rpm for 7 minutes. Following this, 100 μL of medium were removed and 100 μL of fresh complete medium was added. Plates were further incubated at 37°C and 5% CO_2 for one week to allow the clones to develop.

6.4: Addition of Drugs to Clones

Imatinib and Nilotinib were used in this study at two different concentrations, 50 μM and 100 μM. These two doses were chosen based on preliminary studies showing that clonal cells survived with 10 μM of either drug and there was little cell survival with 500 μM of either drug.

Following 2 weeks' culture, clones were collected and seeded proportionally in 3 wells in 96 flat-bottomed plates. Cells were allowed to grow for 24 hours at 37 °C and 5% CO_2. Following this incubation period, Imatinib or Nilotinib were added as follows. Plates were spun at 1200 rpm for 7 minutes. Following this, 100 µL of medium were removed and 100 µL of fresh media with different final concentrations of Imatinib or Nilotinib were added (0 µM, 50 µM or100 µM). Clones were allowed to grow for 5 days at 37 °C and 5% CO_2 in order to assess clone survival. Wells with control cells (0 µM Imatinib or Nilotinib) started to become fully confluent after 5 days culture. Therefore, it was decided to collect cells at day 5 after the addition of the drugs.

Synchrotron beam time at Diamond Light Source, Oxford, UK and Synchrotron Soleil, France, is limited in its allocation, so only few clones were selected for analysis. Clones in which cells in control wells were completely confluent were discarded as this could modify their metabolical and proliferative properties. The clones were selected by visually observing the wells under the microscope and classed as sensitive, where there were no cells or very low number of live cells in the well (- -); resistant, where the well is at least semi-confluent (+ +); and semi-resistant/semi-sensitive where the well is half full (+ -). Resistant, sensitive and semi-resistant/semi-sensitive clones to different doses of Imatinib or Nilotinib were selected (table IX)

6.5: Clone Selection

Table IX: Representative example of K562 Clones following 5 days incubation with Imatinib or Nilotinib at different doses. 2 plus signs indicate semi-confluent wells; one plus sign indicates wells with cells occupying less than half the surface of the well; plus/minus sign indicates the presence of very few cells; minus sign indicates absence of cells.

Clones	Control	50 µM	100 µM
1	++	+/-	+/-
2	++	+	+
3	++	+	+/-
4	++	+	+
5	++	+	+
6	++	+	+/-
7	++	+	+
8	++	+	-
9	++	++	+
10	++	+	+/-
11	++	+	+/-
12	++	+	+
13	+-	+/-	+/-
14	++	-	-
15	++	+	+

6.6: Sample Preparation

UV graded CaF_2 slides (26 x 22 x 0.5 mm) (Crystan Ltd, UK) were chosen as they are polished slides suitable for both FTIR and Raman microspectroscopy [Grills 2015].

Following the incubation with either drug, clones were selected as described in section 6.5 (Table XI), collected and spun in eppendorfs at 950 rpm for 5 minutes. Cells were then cytospun onto CaF_2 slides for 1 minute at 550 rpm, through a cytofunnel and filter card (Shandon, UK). Once cells had been deposited on CaF_2 slides in single monolayer, samples were placed in a Petri dish and fixed using 4% Paraformaldehyde (PFA) in 0.9% NaCl for 20 minutes as previously described [Pijanka 2009], followed by 3 washes with 0.9% NaCl and 3 washes with distilled water and then air-dried at room temperature.

6.7: S-FTIR microspectroscopy

Synchrotron sources, Diamond Light Source, Oxford, UK, and Soleil Synchrotron Paris, France, were used to obtain the data because of the limitations of the beamtime at each centre. In both beamlines, spectra were collected at 4 cm^{-1} resolution with 128 co-added spectra. Measurements were taken in transmission mode, using 15×15 μm aperture with a 36x objective. The measurements were taken by centring the aperture at the nucleus of the cells. Background spectra of the substrate were taken after every 15 cells' measurement. Images of the studied cells with FTIR microspectroscopy were taken so they could be easily identified when further studied with Raman Spectroscopy.

For each individual sample, a minimum of 50 spectra for 50 individual cells were collected. However, in those cases were cells were sensitive to either drug, the number of cells could be lower than 50. In these cases, as many cells as possible were analysed. Images of the cell population were obtained throughout and cells labelled so each cell was analysed only once.

6.7.1: S-FTIR Spectra Pre-Processing and Analysis

All S-FTIR spectra were imported into Matlab 7.5 (Mathworks, Natick, USA) to apply Extended Multiplicative Signal Correction (EMSC) in order to correct for Mie scattering effects using an algorithm created by Dr Achim Kohler [Kohler 2008]. S-FTIR Spectra were processed using The Unscrambler Software (Version X, Camo, Oslo, Norway) for normalisation (Standard Normal Variate (SNV)) and smoothing (Savitzky-Golay).

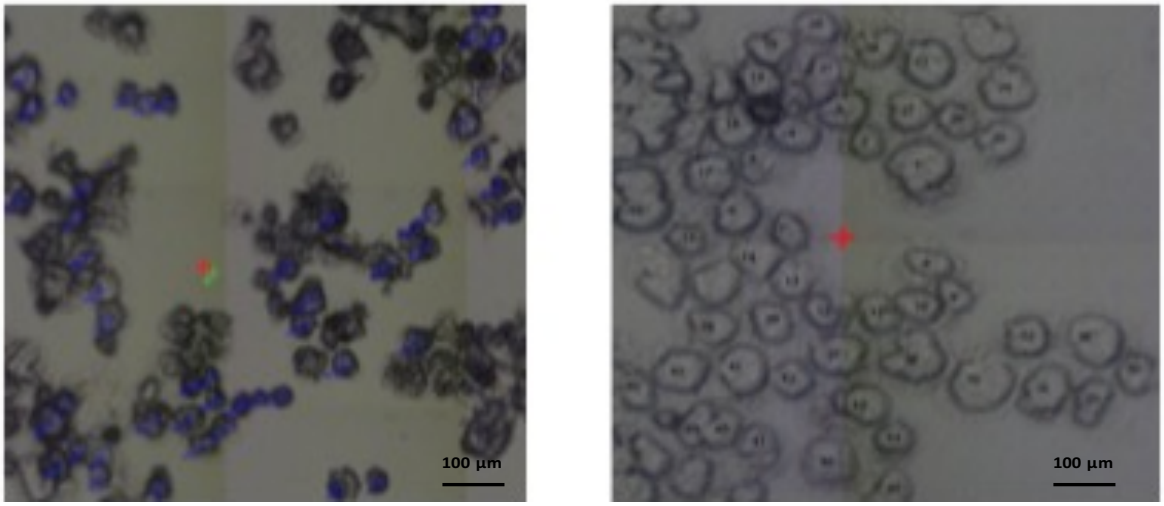

Figure 54: Image of cytospun cells, depicting the number labelled cells from which FTIR measurement had been taken in order to only analyse each cell once.

Following EMSC application, spectra were imported into Unscrambler (VERSION X, Camo, Oslo, Norway), then cropped to the area to be analysed (2700 cm^{-1} to 3100 cm^{-}

^{1} for the lipid region and 1000 cm^{-1} to 1800 cm^{-1} for the fingerprint area) and normalized using standard normal variate (SNV). This removes the effect of sample thickness and any baseline offset that may have occurred.

6.7.2: Analysis

Principal Components Analysis (PCA) is an unsupervised analysis method that allows to reduce big numbers of variables into a few principle components. This allows to understand where possible differences in data sets might lie. PCA was performed using The Unscrambler Software (VERSION X, Camo, Oslo, Norway). Loading plots were also produced using the same software.

6.8: Results

Table X: Survival for K562 in the presence and absence of Imatinib or Nilotinib.

K562	Imatinib Survival (%± SD)	Nilotinib Survival (%± SD)
0 µM	98.34 ± 0.81	97.13 ± 0.74
50 µM	85.19 ± 2.52	48.57 ± 2.48
100 µM	54.49 ± 14.49	31.58 ± 15.43

S-FTIR spectroscopy is a technique that investigates biological systems at molecular level enabling the study of the structural composition of macromolecules such as

lipids, proteins, and nucleic acids (DNA, RNA) [Ramesh 2002; Toyran 2005; Dogan 2007]. Hence, in this study, this technique was used to assess the resistance and sensitivity of leukaemia cells to Imatinib or Nilotinib and identify possible spectral biomarkers.

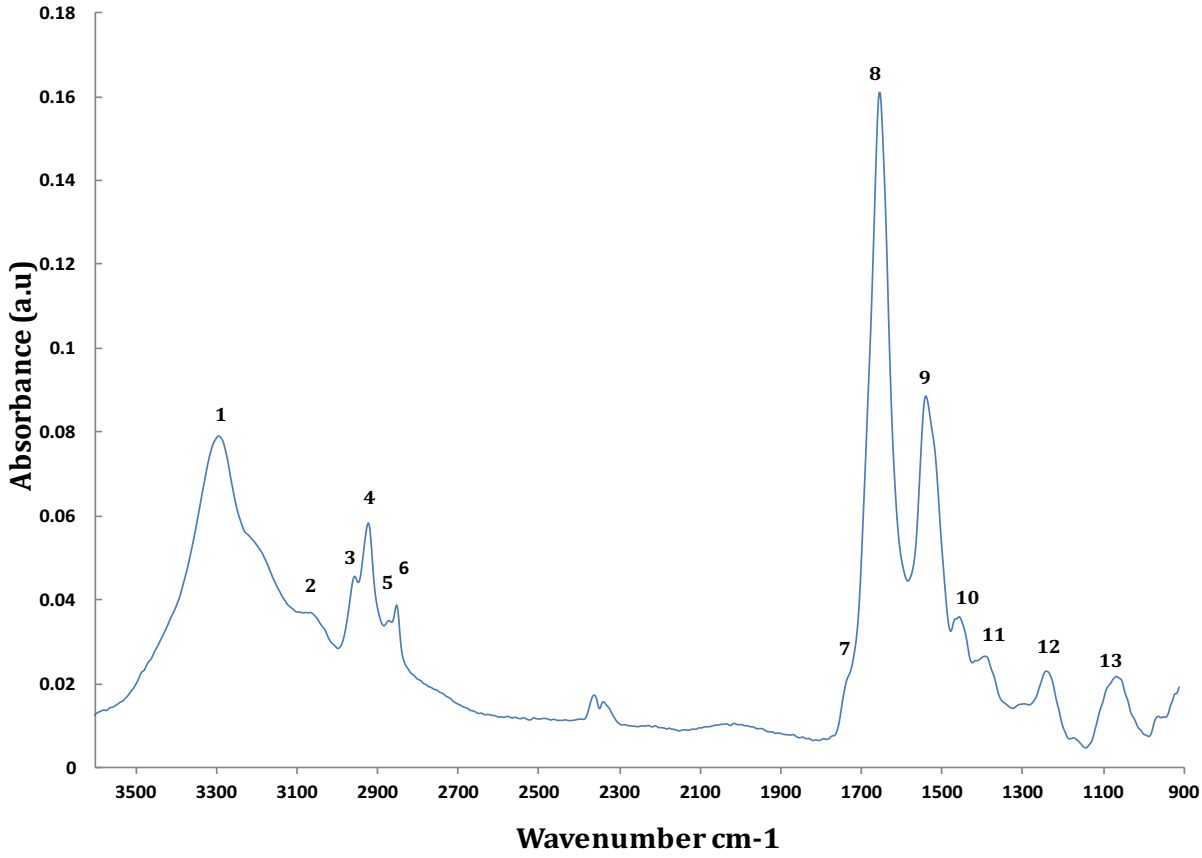

Figure 55: Representative example of an FTIR spectrum of a K562 cell in the 900-3600 cm^{-1} region.

Figure 55 shows the average FTIR spectra of the control K562 cells in the 900-3600 cm^{-1} spectral region. Major bands assigned in Figure 55 are presented in Table XI. An S-FTIR spectrum of K562 cells contains several bands due to the contribution of different functional macromolecules. The spectra for the following regions, 2800-3600 cm^{-1} for protein and lipids, and 1000-1800 cm^{-1} for the fingerprint area were analysed.

Table XI: List of peaks assigned to K562 cells' spectra in the absence of drugs.

Peaks	Approximate Frequency cm^{-1}	Assignments
1	3290-3300	Amide A: Mainly N-H stretching of proteins with little O-H stretching of polysaccharides [Lyng 2015].
2	3075	Amide B: C-N stretching of Protein and N-H stretching of proteins [Movasaghi 2008]
3	2960	CH_3 asymmetric stretching: lipids, protein side chains and some carbohydrates [Lyng 2015].
4	2925	CH_2 asymmetric stretching: lipids, and little proteins and carbohydrates [Movasaghi 2008; Lyng 2015].
5	2870	CH_3 symmetric stretching: protein side chains, lipids and some carbohydrates and nucleic acid [Baran 2013].
6	2850	CH_2 symmetric stretching: mainly lipids, little proteins, nucleic acids, and carbohydrates [Movasaghi 2008; Lyng 2015].
7	1740	Ester C=O Stretching: triglycerides and cholesterol esters [Movasaghi 2008].
8	1600-1700	Amide I: C=O Stretching: proteins [Movasaghi 2008; Lyng 2015].
9	1520-1550	Amide II: N-H bending and C-N stretch: proteins [Movasaghi 2008; Lyng 2015].
10	1465	CH_2 bending: lipids, with little proteins, CH_3 symmetric bending: methyl group of proteins [Baran 2013].
11	1250-1400	COO- symmetric stretch: lipids with little proteins, CH_3 symmetric bending: methyl group of proteins [Movasaghi 2008].
12	1240	PO_2-asymmetric stretch: mainly nucleic acid with little from phospholipids [Lyng 2015].
13	1080	PO_2- symmetric stretch: nucleic acid and phospholipids [Lyng 2015].

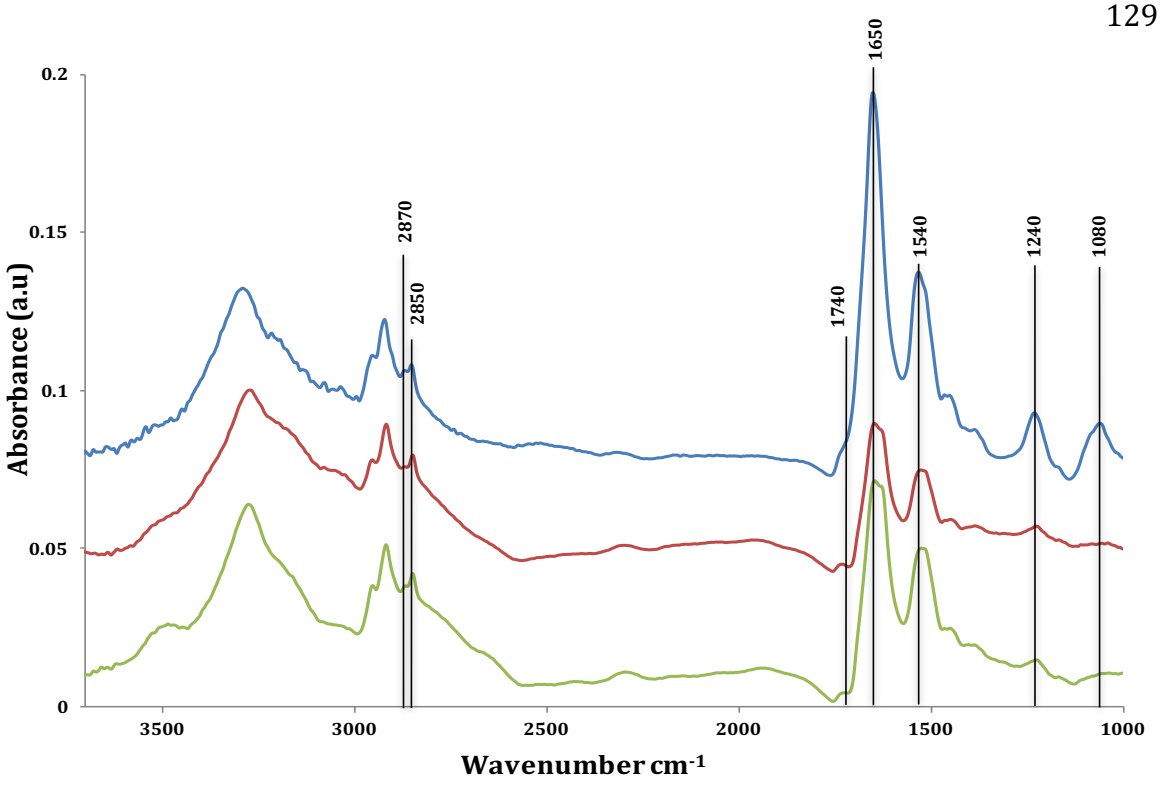

Figure 56: Mean spectra of resistant clone 10 cells in the absence of Imatinib (top spectrum), in the presence of 50 µM of Imatinib (middle spectrum) and 100 µM of Imatinib (bottom spectrum). Each spectrum is the mean of 50 individual spectra from 50 individual cells. Spectra are offset for clarity

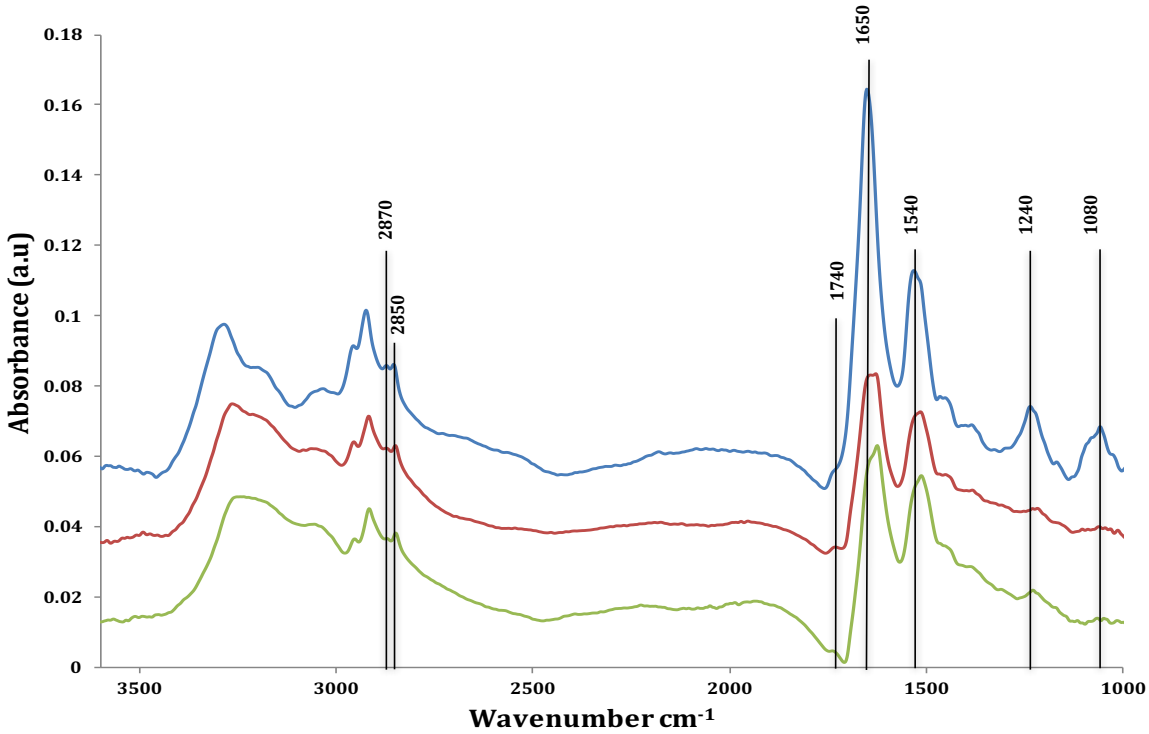

Figure 57: Mean spectra of semi-resistant clone 3 cells in the absence of Imatinib (top spectrum), in the presence of 50 µM of Imatinib (middle spectrum) and 100 µM of Imatinib (bottom spectrum) Each spectrum is the mean of 50 individual spectra from 50 individual cells except bottom spectrum which is the mean of 20 individual spectra from 20 individual cells. Spectra are offset for clarity.

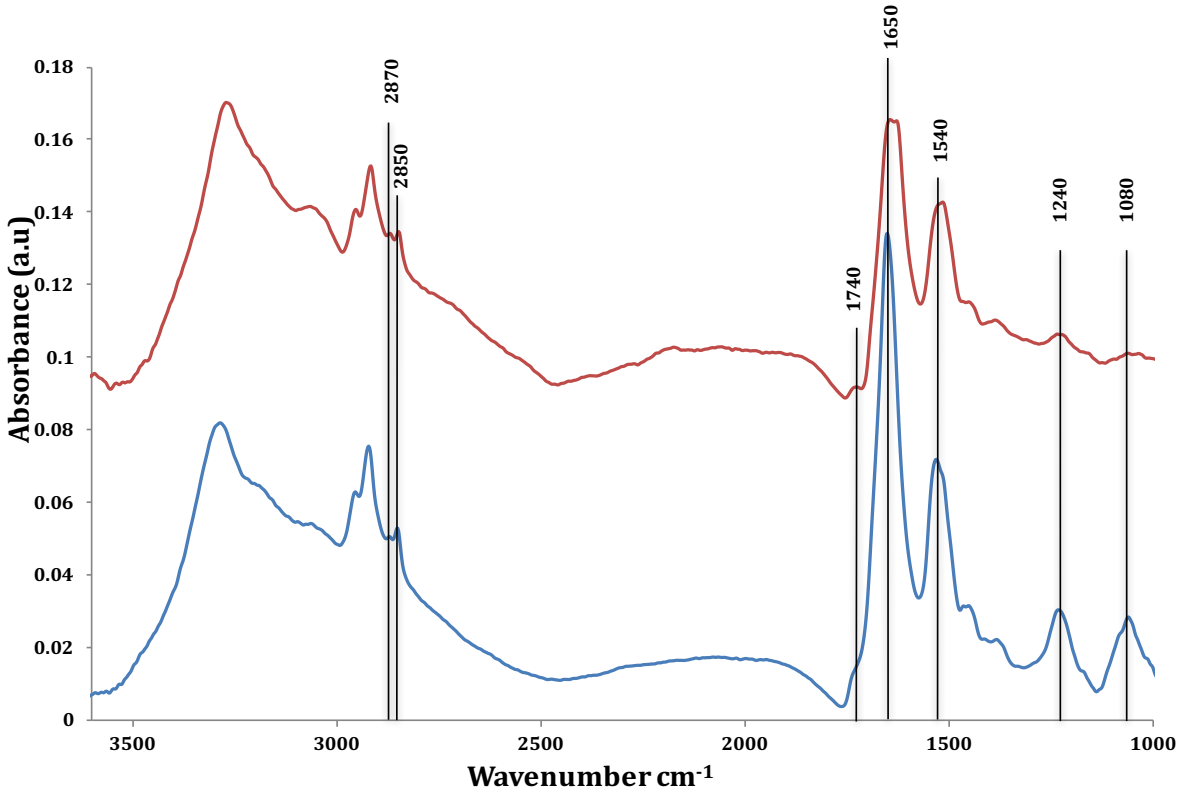

Figure 58: Mean spectra of sensitive clone 7 cells to 100 µM Imatinib in the absence of Imatinib (bottom spectrum), in the presence of 50 µM of Imatinib (top spectrum). Bottom spectrum is the mean of 50 individual spectra from 50 individual cells and top spectrum is the mean of 12 individual spectra from 12 individual cells. Spectra are offset for clarity.

As previously reported, various degrees of sensitivity and resistance to a given drug can be identified in cells following cell cloning [Rutter 2014]. Based on their therapeutic response, I classed these clones as sensitive, semi-sensitive/semi-resistant and resistant clones. Figures 56 to 58 show representative mean spectra of three individual K562 clones with varying degree of sensitivity to Imatinib incubated with different doses of the drug. Figure 56 shows the spectra of clone 10, which proved resistant to both doses of Imatinib (50 µM and 100 µM). Figure 57 shows the spectra of clone 3, semi-sensitive/semi-resistant, i. e., resistant to 50 µM Imatinib but only 20 cells could be identified in the presence of 100 µM Imatinib. Figure 58 is the mean spectra of clone 7, which was sensitive to Imatinib at 100 µM (no cells were

identified) and only 12 cells were recovered following incubation with 50 μM Imatinib.

It is obvious from Figures 57 to 58 that Imatinib induces changes in the spectra of cells sensitive and semi-sensitive/semi-resistant to Imatinib. More important, changes can also be seen in the spectra of resistant cells incubated with 100 μM and even with 50 μM of Imatinib (Figure 56).

The main changes following the addition of Imatinib are a decrease in the intensity of the bands at 1080 cm^{-1} and 1240 cm^{-1}, a decrease in the intensity of the peak at 1740 cm^{-1}, changes in the shape of amide I and II bands and an increase in the intensity of the peak at 2850 cm^{-1} when compared to the peak at 2870 cm^{-1}.

The peak 1740 cm^{-1} band is mainly assigned to the C=O ester stretching vibration of triglycerides and cholesterol esters [Movasaghi 2008]. The peak at 1740 cm^{-1} appears as a shoulder in the spectra of cells incubated in the absence of Imatinib while it becomes a small peak when cells have been incubated with either 50 μM or 100 μM of Imatinib (Figures 56, 57, and 58). The band at 1650 cm^{-1} corresponds to the Amide I. Cells incubated in the absence of Imatinib present a sharp Amide I band. However, following the incubation with Imatinib at either 50 μM or 100 μM, this band becomes broader and intensity increases around 1630 cm^{-1} (Figures 56, 57, and 58). Similarly, the Amide II band at 1540 cm^{-1} also becomes broader following the addition of Imatinib at either 50 μM or 100 μM with increasing intensity at around 1520 cm^{-1} (Figures 56, 57, and 58). Any change in these two bands is an indication of the changes in the proteomes of cells as these two bands are known to be sensitive to

protein conformation and are used to determine the secondary structure of proteins [Dogan 2007]. On the other hand, the nucleic acid related bands at 1240 cm^{-1} and 1080 cm^{-1} attributed to PO_2 asymmetric and symmetric stretch [Ramesh 2002; Lyng 2015] show loss of intensity in the spectra of cells exposed to Imatinib.

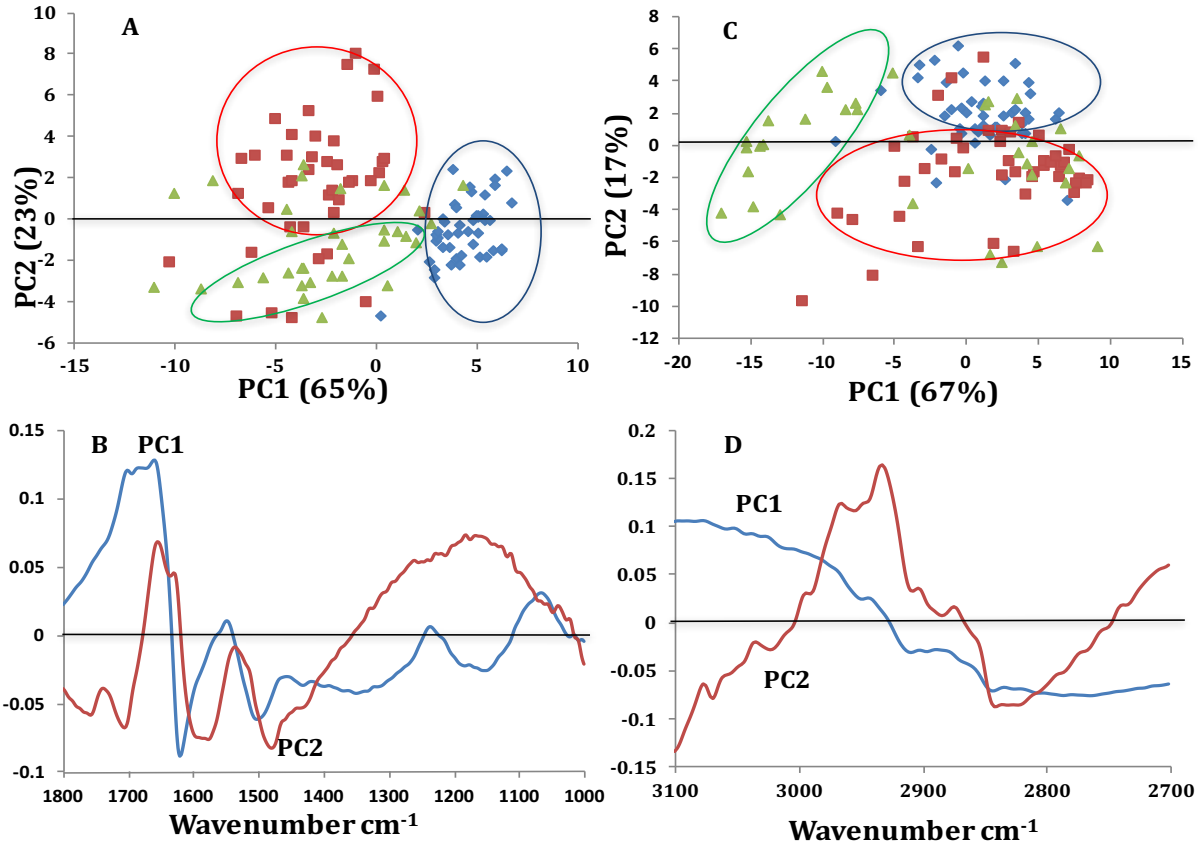

Figure 59: PCA of clone 10 (resistant to both 50 µM and 100 µM of Imatinib) for cells incubated with 0 µM Imatinib (diamonds), 50 µM Imatinib (squares), and 100 µM Imatinib (triangles) for fingerprint (A) and lipid (C) regions and loading plots, respectively (B and D).

PCA was carried out in order to identify any possible differences between cells incubated in the absence or the presence of Imatinib. As can be seen in Figure 59, PCA could separate between cells incubated in the absence of Imatinib and in the presence of Imatinib in the fingerprint region for resistant clone 10.

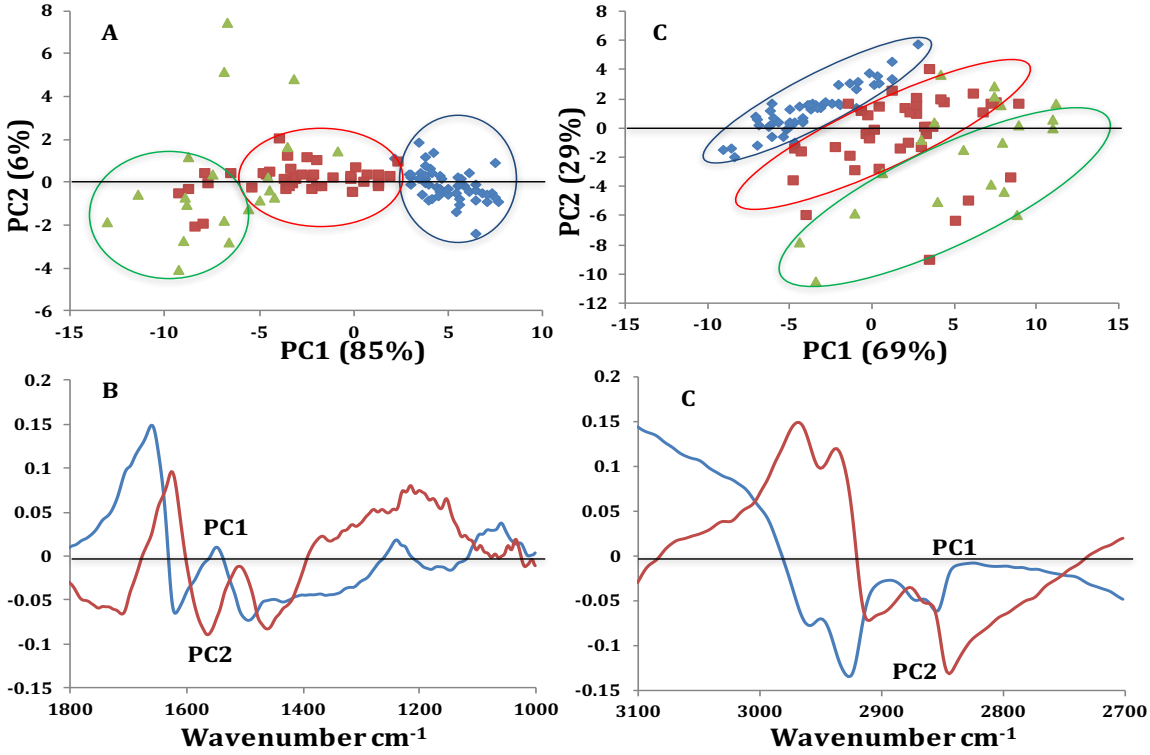

Figure 60: PCA of clone 3 (semi-resistant to both 50 µM and 100 µM of Imatinib) for cells incubated with 0 µM Imatinib (diamonds), 50 µM Imatinib (squares), and 100 µM Imatinib (triangles) for fingerprint (A) and lipid (C) regions and loading plots, respectively (B and D).

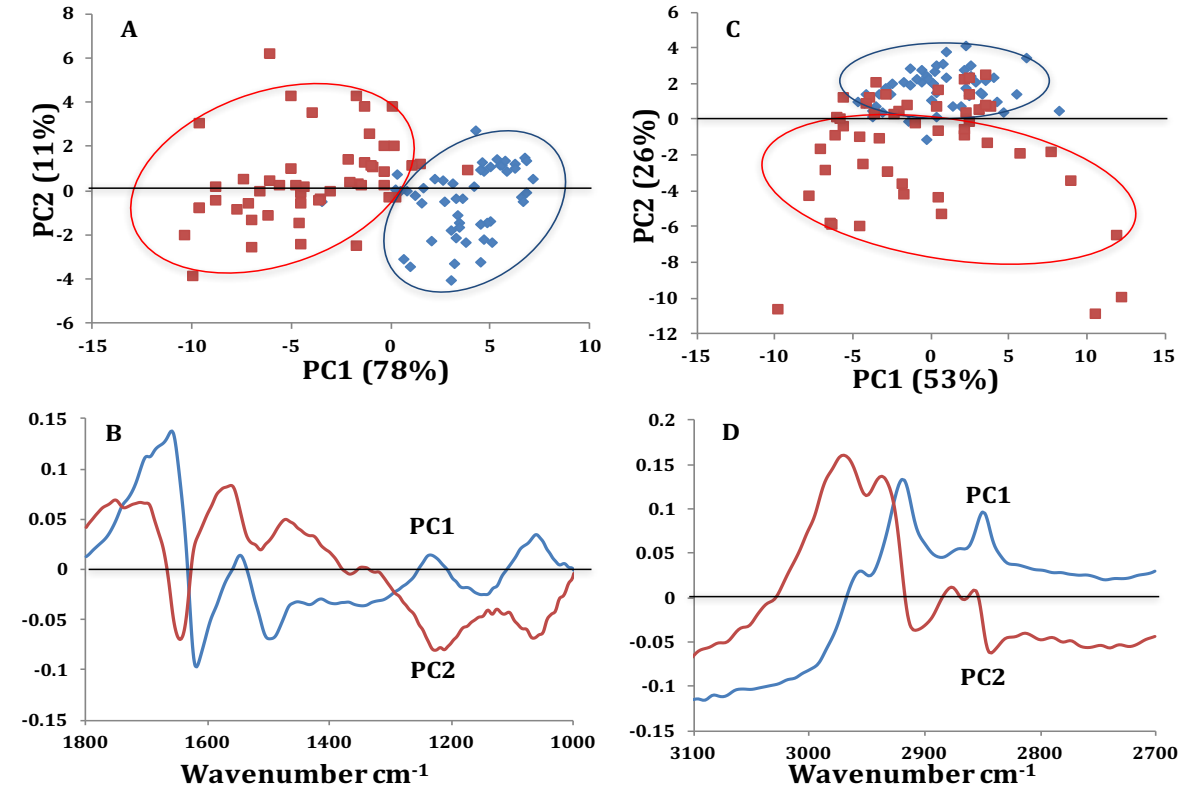

Figure 61: PCA of clone 7 (sensitive to 100 µM of Imatinib) for cells incubated with 0 µM Imatinib (diamonds) and 50 µM Imatinib (squares), for fingerprint (A) and lipid (C) regions and loading plots, respectively (B and D).

There is trend to separate between cells incubated with either 50 µM or 100 µM of Imatinib for clone 10. However, there were no clear differences between cells incubated in the absence or presence of Imatinib for the lipid region (Figure 59 C).

In the case of clone 3 (semi-resistant/semi-sensitive), there was clear separation between cells incubated in the absence of Imatinib and those incubated in the presence of Imatinib for both the fingerprint and the lipid regions (Figure 60). Furthermore, there was a higher separation between cells incubated in the absence of Imatinib and those incubated with 100 µM Imatinib (Figure 60) for both regions (Fingerprint and lipids). Again, for clone 7, a separation was seen between cells incubated in the absence of Imatinib and those incubated with 50 µM Imatinib. However, the difference was less for the lipid region (figure 61).

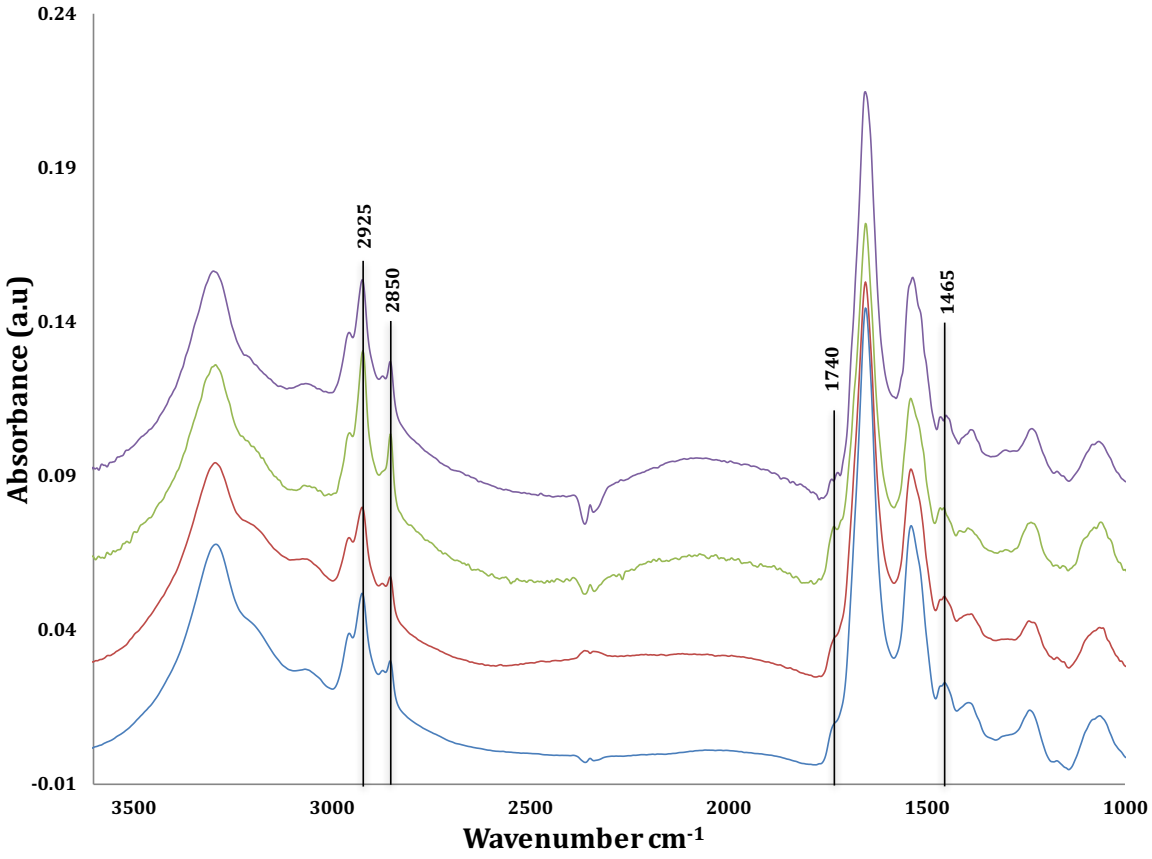

Figure 62: Mean spectra of resistant clones 4 and 10 (resistant to both 50 µM and 100 µM of Imatinib) for cells incubated with 0 µM Imatinib (Blue and red) and of sensitive clones 12 and 13 (sensitive to both 50 µM and 100 µM of Imatinib) for cells incubated with 0 µM Imatinib (Green and purple). Spectra are offset for clarity.

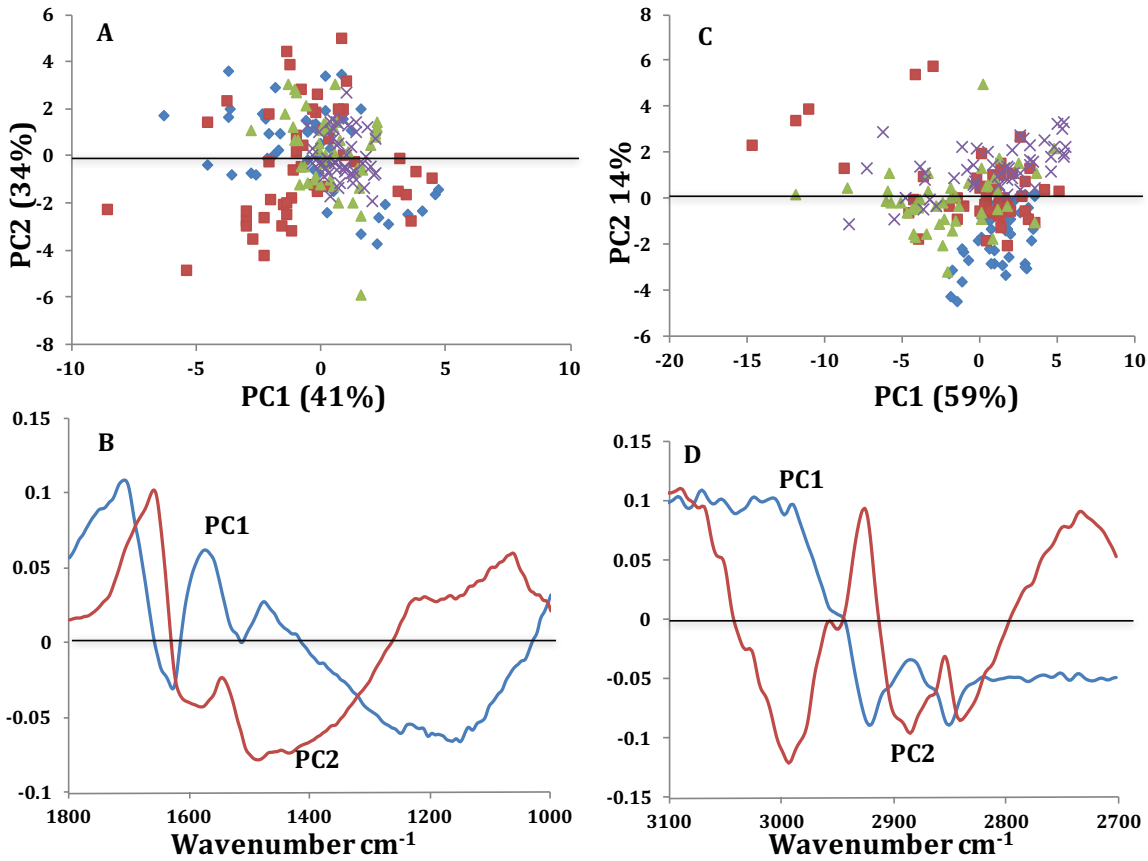

Figure 63: PCA of resistant clones 4 and 10 (resistant to both 50 µM and 100 µM of Imatinib) for cells incubated with 0 µM Imatinib (diamonds and squares, respectively) and of sensitive clones 12 and 13 (sensitive to both 50 µM and 100 µM of Imatinib) for cells incubated with 0 µM Imatinib (crosses and triangles, respectively) for fingerprint (A) and lipid (C) regions and loading plots, respectively (B and D).

Figure 62 shows the comparison between resistant clones 4, 10 and sensitive clones 12, 13. It is obvious there are no major differences among resistant and sensitive clones spectra, but slight changes in bands related to CH_2 symmetric stretching and bending of lipids with little contribution of protein and carbohydrates, increase in the intensities of 2925 cm^{-1} and 1740 cm^{-1} in sensitive clone spectra as compared to resistant clone spectra. Hence increases in 2850 cm^{-1} along with 2925 cm^{-1} indicates significant increased lipid and protein contents in sensitive clone cells.

PCA score plots (figure 63) show that there was no clear separation between resistant and sensitive clones to Imatinib incubated in the absence of the drug. Furthermore, these would have indicated that even being different clones, PC was not able to separate them for this fact. This would indicate that cloning K562 leads to obtaining cell clones that might not differ much between themselves based on IR spectral data. Further work is required to assess whether this is the case in other leukaemia cell lines. On the other hand, the results presented here indicate that the changes in the spectra of cells incubated in the presence of imatinib are probably due to sensitive cells to imatinib that were still alive or entering apoptosis when they were collected and cytospun to prepare the samples for S-FTIR microspectroscopy.

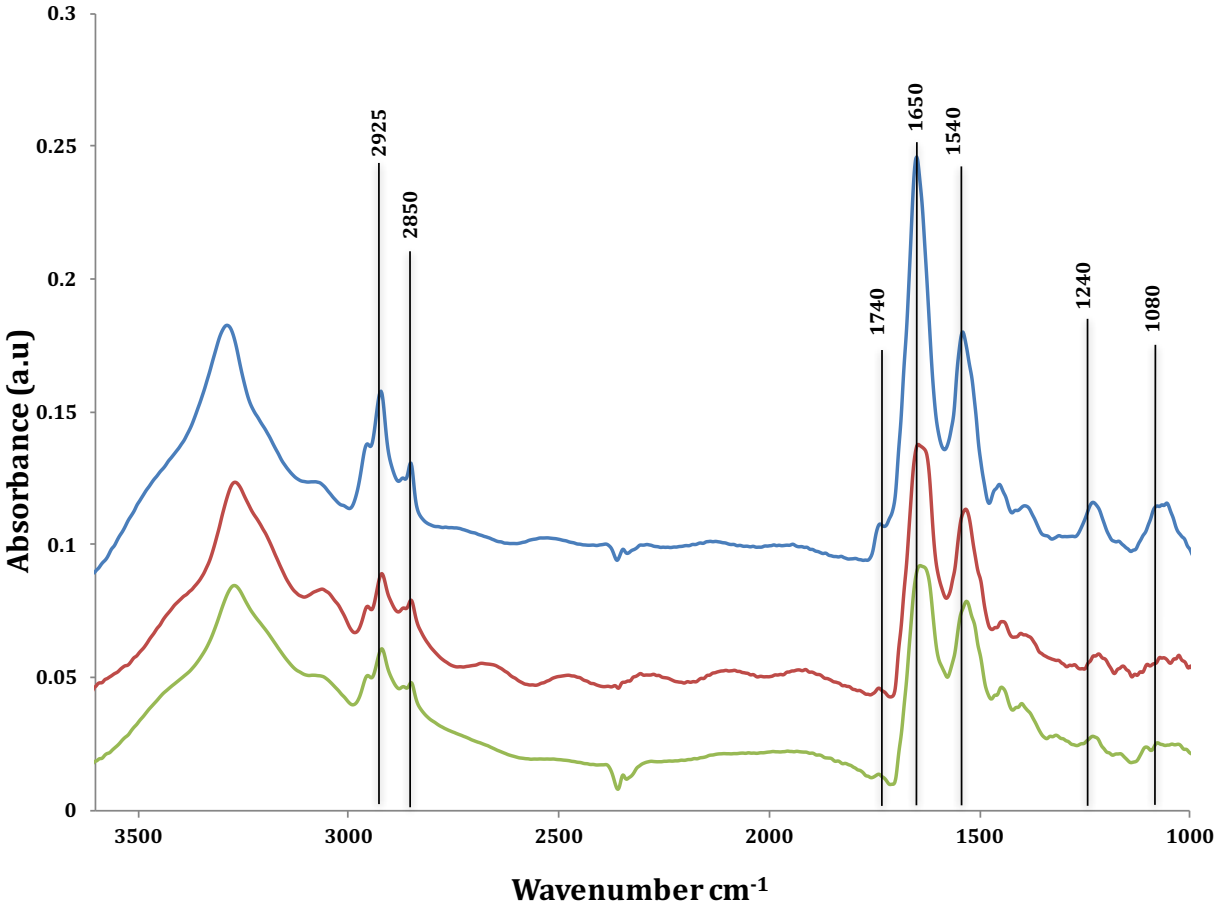

Figure 64: Mean spectra of clone 4 (resistant) cells in the absence of Nilotinib (top spectrum), in the presence of 50 µM Nilotinib (middle spectrum) and 100 µM Nilotinib (bottom spectrum). Each spectrum is the mean of 50 individual spectra from 50 individual cells. Spectra are offset for clarity

Further experiments were carried out with Nilotinib, another drug used in the management of leukaemia. Figures 64 and 65 show the mean spectra for a resistant clone to both 50 μM and 100 μM of Nilotinib and a sensitive clone to 100 μM of Nilotinib. Due to time constraints during our beamtime at Diamond Light Source, only these 2 clones were studied. During the same beamtime, these clones were studied with Raman spectroscopy (Chapter 7).

The incubation of resistant clone 4 (figure 64) in the presence of Nilotinib caused spectral changes, mainly in the amide bands and in the peaks at 1080 cm^{-1}, 1240 cm^{-1}, 1740 cm^{-1}, 2850 cm^{-1}, and 2925 cm^{-1}. The addition of the drug caused a broadening of both the Amide I and II as it was seen in the case of cells incubated with Imatinib. Furthermore, there was a decrease in the intensity of the peaks at 1080 cm^{-1}, 1240 cm^{-1} and 1740 cm^{-1} in cells incubated with either 50 μM or 100 μM Nilotinib, Again, this is in accordance with the data obtained for cells incubated with Imatinib. Therefore, although cells were able to survive at higher doses of Nilotinib, it caused changes in cells' chemical makeup (Figure 65). Similar data was seen for the semi-sensitive/semi-resistant clone 7.

PCA of resistant clone (clone 4) did show separation between the cells incubated with 0 μM**,** 50 μM or 100 μM of Nilotinib for both fingerprint and lipid regions of the spectra (figure 66). In the case of sensitive clone 7 (figure 67), there was a clear separation between control cells incubated in the absence of Nilotinib and those incubated with 50 μM of Nilotinib. The results clearly indicated that S-FTIR microspectroscopy can definitely separate between cells incubated in the presence or absence of Nilotinib.

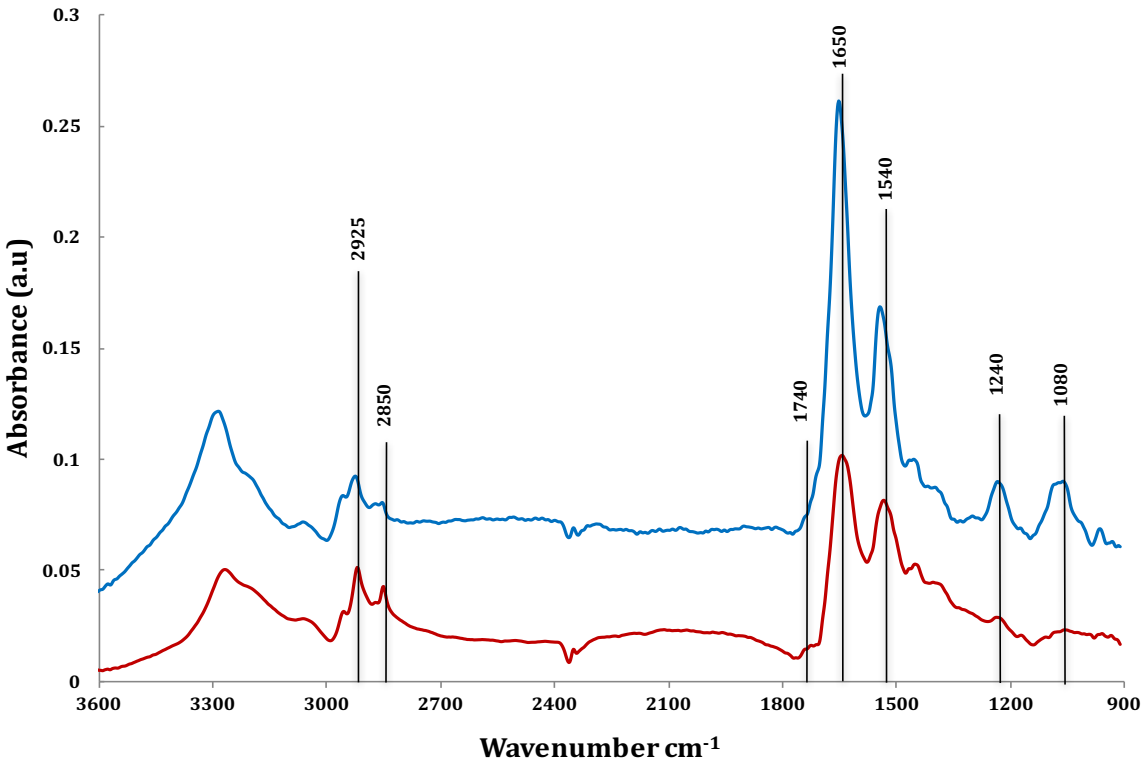

Figure 65: Mean spectra of clone 7 (semi-sensitive/semi-resistant) cells in the absence of Nilotinib (top spectrum) and in the presence of 50 µM of Nilotinib (bottom spectrum). Spectra are offset for clarity.

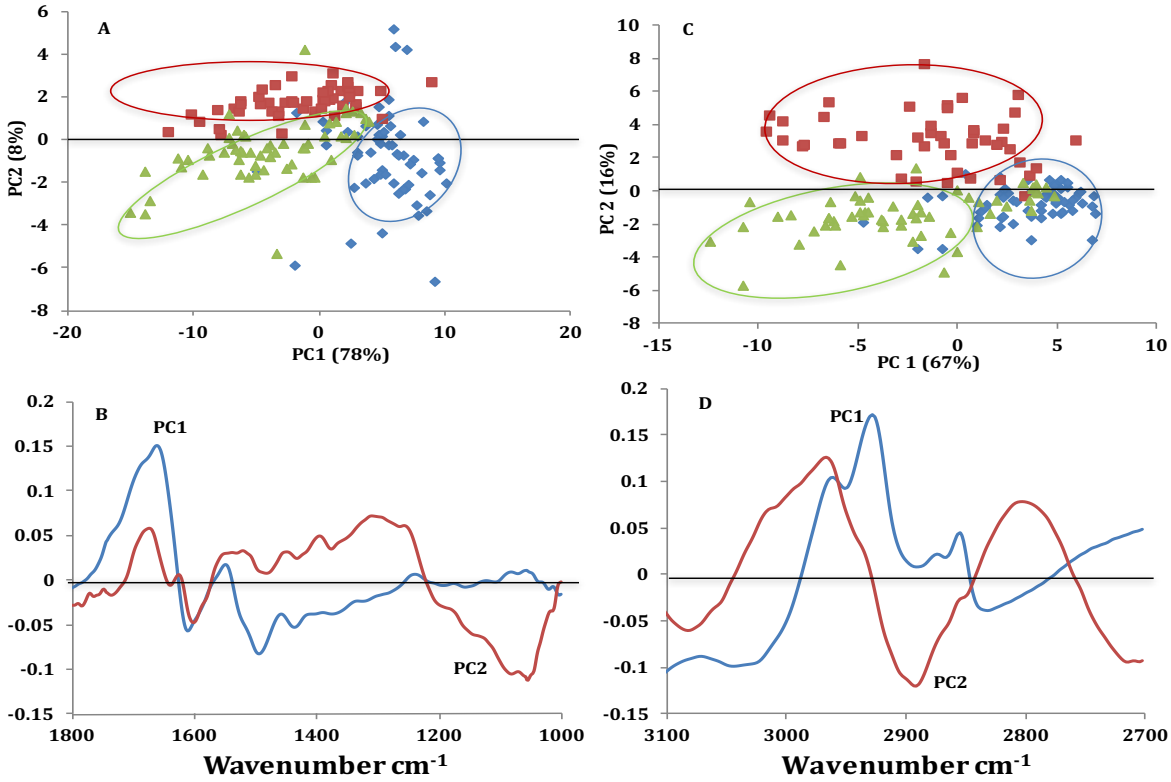

Figure 66: PCA of clone 4 (resistant to both 50 and 100 µM of Nilotinib) for cells incubated with 0 µM Nilotinib (diamonds), 50 µM Nilotinib (squares), and 100 µM Nilotinib (triangles) for fingerprint (A) and lipid (C) regions and loading plots, respectively (B and D).

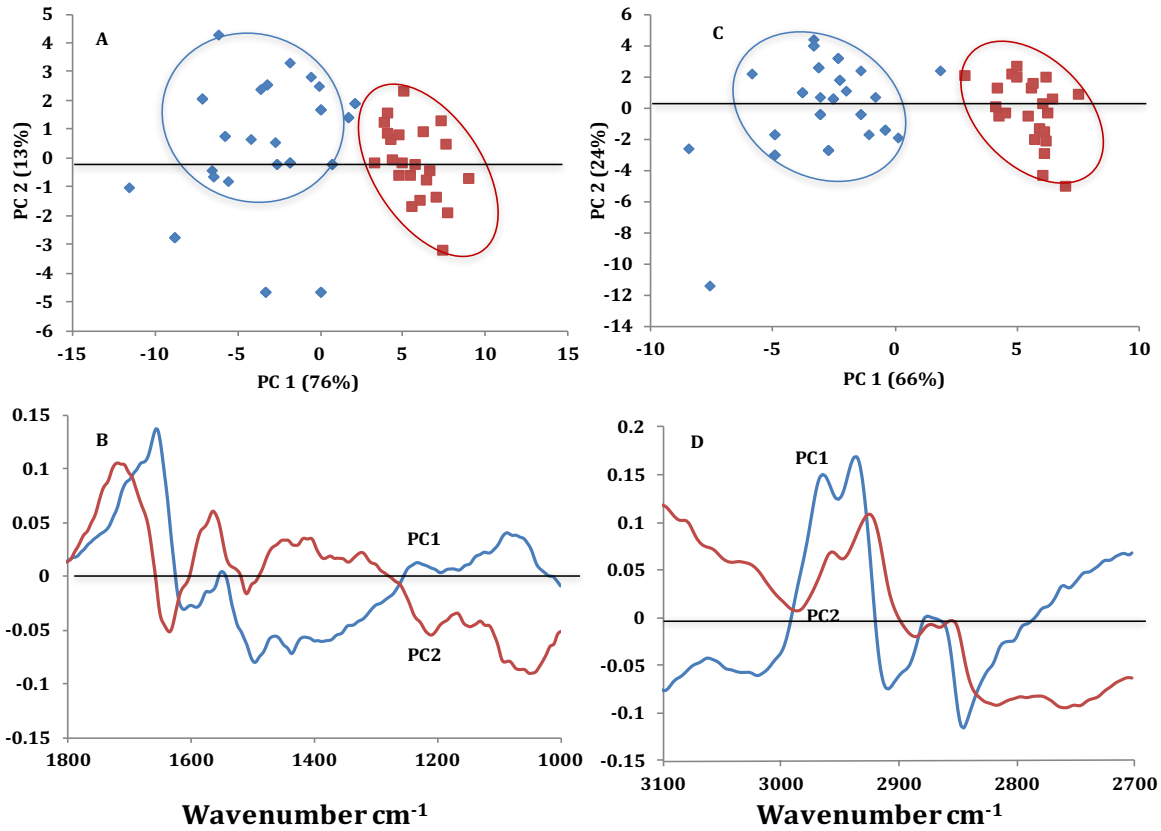

Figure 67: PCA of clone 7 (Sensitive to both 50 µM and 100 µM of Nilotinib) for cells incubated with 0 µM Nilotinib (diamonds), 50 µM Nilotinib (squares), for fingerprint (A) and lipid (C) regions and loading plots, respectively (B and D).

The results obtained showed that this technique can identify cells sensitive and/or resistant cells to drugs which could be used in clinics for the management of the leukaemia and help clinicians to tailor treatment to each individual patient.

Figure 68 shows comparison spectra of resistant clones versus sensitive clones. Although, there are not many remarkable differences between resistant and sensitive clone spectra, yet some band changes can be seen such as increase in the intensities of bands at 2925 cm^{-1}, 2850 cm^{-1} and 1740 cm^{-1} for resistant clones as compared to sensitive clones. There were also changes in shape of the peaks at 1400, 1240 and 1080 cm^{-1}. A lower peak at 1400 cm^{-1} is seen in the spectra of sensitive clone.

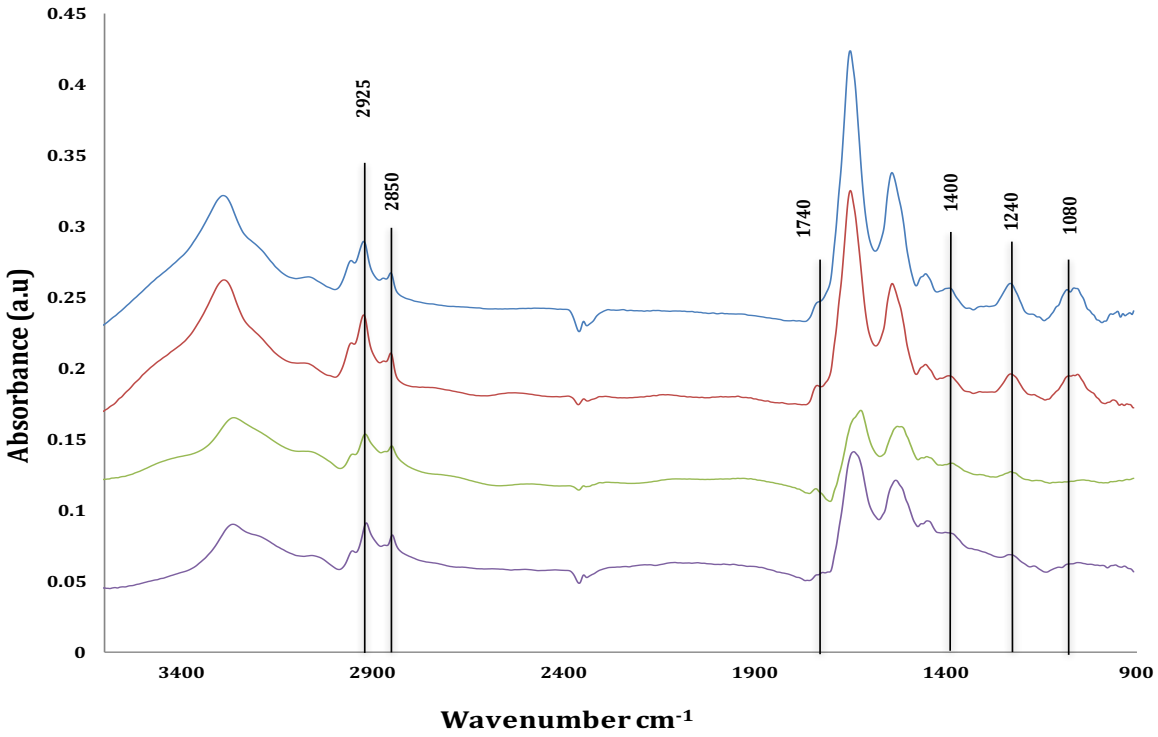

Figure 68: Mean spectra of resistant clones (resistant to both 50 µM and 100 µM of Nilotinib) for cells incubated with 0 µM Nilotinib (top spectrums blue and red) and of sensitive clones (sensitive to both 50 µM and 100 µM of Nilotinib) for cells incubated with 0 µM Nilotinib (bottom spectrums, green and purple).

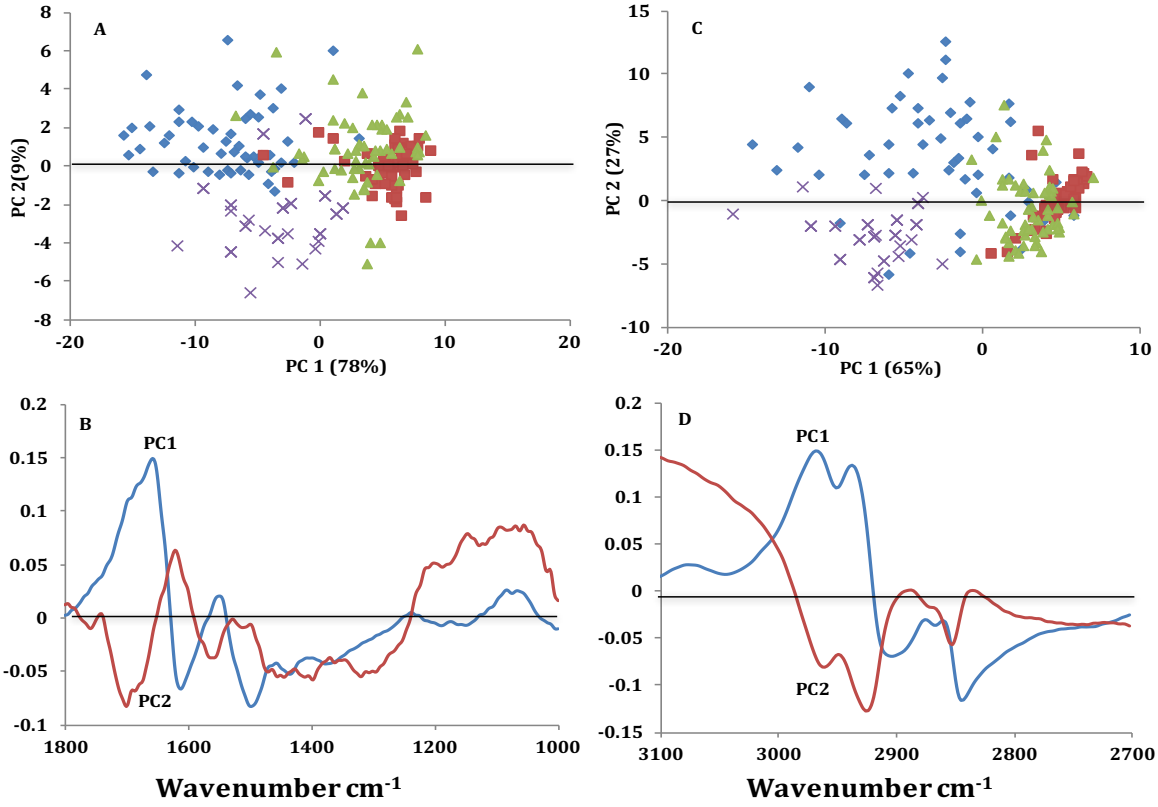

Figure 69: PCA of resistant clones 4 and 2 (resistant to both 50 µM and 100 µM of Nilotinib) for cells incubated with 0 µM Nilotinib (Triangle and Squares) and of sensitive clone 1 and 7 (sensitive to 50 µM of Nilotinib) for cells incubated with 0 µM Nilotinib (crosses and diamonds) for fingerprint (A), and lipid (C) regions, and loading plots (B and D), respectively)

An increase in the intensities for resistant clone could be due to the fact that resistant clone to Nilotinib have higher lipid and protein in their cellular matrix.

The PCA results of Nilotinib resistant clones versus Nilotinib sensitive clones incubated in the absence of Nilotinib showed clear separation between resistant and sensitive clones in both fingerprint and lipid regions (Figure 69). PC1 versus PC2 loading (Figure 69 B and D) for both fingerprint and lipid regions also showed a clear separation. These results could indicate that S-FTIR microspectroscopy can identify sensitive clones to a drug. However, it has to be acknowledged that the differences could just be due to the fact these are different clones. Further work is therefore needed to assess to what extent S-FTIR microspectroscopy can identify sensitive cells to drugs.

6.9: Discussion

Tyrosine kinase inhibitor Imatinib mesylate, in a randomized study, achieved a complete cytogenetic response rate of 84% in patients with newly diagnosed CML after 42-month follow up [Guilhot 2004]. However, it has been reported that in advanced phase of CML, response to Imatinib mesylate may be short lived [Druker 2001]. Mutations in the BCR-ABL gene, clonal evolution and amplification of BCR-ABL gene hindering the binding of the drug to the target site are the main causes behind clinical resistance to Imatinib mesylate [Gorre 2001; Hochhaus 2002]. An alternative BCR-ABL kinase inhibitor Nilotinib was developed and is already in clinical use. Nilotinib has shown promising results in patients with Imatinib mesylate resistance. It is more potent than Imatinib mesylate in suppressing BCR-ABL tyrosine kinase activity and cell growth of BCR-ABL transformed cells. Nilotinib is also capable of

suppressing Imatinib mesylate resistant cells and mutant forms of BCR-ABL [La Rosee 2002; Weisberg 2005]. It has been suggested that Imatinib and Nilotinib both have different binding properties to the BCR-ABL kinase domain [Weisberg 2005]. Therefore, specific resistance profiles for different kinase inhibitors can be expected to emerge in treated patients. On this basis, it might be important to know these resistant profiles upfront which would guide clinicians in decision making for the management-of leukemia.

One of the major problems in the management of leukaemia is the nonhomogeneous characteristic of the cancer cells. For any cancer, some cells will be sensitive to the drug and some will present resistance to the drug with all the variations between these two possibilities. There are several techniques such as gene expression profiling [Chang 2003; Robert 2004], in vitro clonogenic and proliferation assays, cell metabolic activity assays, molecular assays, in vivo tumor growth and survival assays, and in vivo imaging assays amongst other [Blumenthal 2007; Cree 2009] that are used to assess cell sensitivity to drugs. However, tumour cell sensitivity or resistance prior to treatment is not being checked in clinics at present.

Many studies have shown S-FTIR microspectroscopy as a powerful and potential tool to screen cancer cells to chemotherapy drugs and to study tumour progression. It has been evaluated as a possible technique for cancer diagnosis and/or for the detection of chemical abnormalities in cells and body fluids [Neviliappa 2002; Wong 2002]. This study has been focused on the biochemical information available in infrared spectra to assess possible spectral changes in cells incubated in the presence or absence of drugs [Krishna 2006].

My studies have shown that there are changes in the spectra of cell clones following the addition of Imatinib or Nilotinib (Figures 56, 57, 58, 64 and 65). The decrease in lipids' absorption, can be attributed to the presence of apoptotic cells following the addition of the drugs. The main changes are an increase in the peak at 1740 cm^{-1} and a decrease in the intensity in the region from 1000 cm^{-1} to 1300 cm^{-1} and changes in the amide I and II peaks for cells incubated in either Imatinib or Nilotinib. An increase in the intensity of the peak at 1740 cm^{-1} has been associated with spectral markers of oxidative stress [Vileno 2010]. Furthermore, the increased intensity in this peak has been reported as appearing in dying cells [Holman 2000]. Apoptotic cells are known to have a series of changes in phospholipid composition and structure [Hengartner 2000; Ramesh 2002], which induces changes in lipid absorption in the IR spectra. In fact, it has been reported in *in vitro* studies for leukemia cell lines that an increase in lipid absorption is present following incubation with cytotoxic drugs [Zelig 2009]. Furthermore, apoptosis is also associated with increased oxidative damage [Holman 2000]. In our study cells, the peak at 1740 cm^{-1} presents as a small shoulder in cells incubated in the absence of Imatinib. However, once cells are incubated with the drug, the peak becomes clearer even in resistant cells incubated with the drug. Similar data are seen for sensitive cells incubated with Nilotinib. From previous published data and the data obtained in this work, it could be hypothesized that this peak could be a marker of cell death and/or help to identify in which stage(s) of apoptosis cells might be present following the addition of a drug. However, further studies are needed to confirm this.

The bands at 1080 cm^{-1} and 1240 cm^{-1} are associated with nucleic acids. The 1240 cm^{-1} band is due to asymmetric phosphate stretching and 1080 cm^{-1} is due to symmetric phosphate stretching of the nucleic acids [Wang 1997; Chiriboga 1998]. The changes in the intensities of the bands at this region indicate changes in nuclear morphology and architecture [Ramesh 2002]. It has already been reported that multi drug resistance is linked with nuclear morphological changes [Dufer 1995; Mannechez 2005]. Furthermore, changes in some of these bands were found in apoptotic cells [Pocaly 2008]. The results of this study showing decrease in the intensity of these bands indicate that the incubation of cells in the presence of either Imatinib or Nilotinib causes alterations in nuclear composition that can be translated into changes in the cells' S-FTIR spectra.

The third main change observed in the study cells in the presence of drugs was a broadening of the amide I and II peaks, mainly in sensitive cells. However, slight changes in these peaks could also be seen in resistant cells. It has been described that such changes might imply conformational changes in tissue proteins or the expression of a new set of proteins [Jackson 1998]. As an example, the presence of a toxic external agent such as drugs can initiate a stress response causing expression of new proteins in the cell to protect itself. That could explain in part why the proteome of the sensitive and resistant cells differs between them [Pocaly 2008].

There are numerous chemotherapy drugs and combinations of drugs used in the management of cancer. However, it is not unusual for cancer cells to develop

resistance to these drugs. A better understanding of these processes would help clinicians to tailor treatment to each individual patient. The results presented here not only confirm previously reported data but also further indicate, using cell cloning, that S-FTIR microspectroscopy could help to better identify resistant/sensitive cells to drugs. However, it is important to identify the biological processes leading to specific spectral changes and cross-validate these data with already established techniques.

Conclusion

The results of this study have revealed that the addition of Imatinib or Nilotinib to K562 cell clones induces changes in cell biology and cellular structure which translates into changes in the S-FTIR spectra of cells. These data further highlight the potential of S-FTIR microspectroscopy as a technique to assess cell sensitivity to drugs which could have a clinical application in the management of leukemia. However, further work is required to confirm this.

Chapter 7

Application of Raman Spectroscopy in the Management of Leukaemia

Part of this chapter Published in Analyst: Effects of nilotinib on leukaemia cells using vibrational microspectroscopy and cell cloning
M. R. Siddique, A. V. Rutter, K. Wehbe, G. Cinque, G. Bellisola and J. Sulé-Suso

7.1: Introduction

Raman spectroscopy is a well-established analytical method, which can provide valuable information about biological samples [De Gelder 2007; Movasaghi 2007]. It is viewed as a complementary technique to IR spectroscopy but shows remarkable advantages for many applications, especially biological [Byrne 2011]. The basics of Raman spectroscopy are inelastic scattering of photons by molecular bond vibrations. When a small portion of the incident photons is scattered by interaction with the bonds, it results in a shift toward lower frequencies. The energy difference between the incident and scattered photons corresponds to the vibrational energy of the specific molecular bond studied. Raman Spectroscopy has the ability to obtain rich biochemical information from single cells without staining or labelling the cells. Changes in cellular biochemistry as indicators of cell behaviour can be detected using Raman microspectroscopy. Raman scattering can be used in the UV, visible, or near infrared regions of the spectrum [Singh 2015]. A Raman spectrum taken from cells or tissues is a molecular fingerprint of the studied sample, which reveals detailed information on molecular constituents such as proteins (amino acids and conformational structures), nucleic acids (DNA and RNA) and lipids (cholesterol and CH_2 groups) [Pully 2011; Matthews 2011; Palonpon 2013; Pascut 2013]. This technique is not only fast but also has potential as novel, non-invasive and non-destructive diagnostic tool

for cancer detection [Huang 2003; Crow 2004; Min 2005] and identification of malignancy at various stages [Mahadevan-Jansen 1998; Clare 2006; Chen 2016]. Due to recent developments in Raman instrumentation that includes high quality lasers, CCD cameras and optical elements, mapping whole single cells can be done within minutes. Single cell analysis has great importance for biomedical, cell biology, and pharmacology research amongst other.

A Raman spectrum provides information on molecular interactions within a cell that enables the study of metabolic changes involved in specific cell–drug interactions. Guo et al. (2009) reported Raman spectroscopy studies on the interaction of malignant hepatocytes with the antitumor drug doxorubicin, and their study established that doxorubicin affected the secondary structure and the environment of the proteins of the cells. H. Yao et al. (2009) studied the effects of the anticancer drug 5- fluorouracil on gastric carcinoma cells. Reduction in the intensity of vibrational bands generated by cellular lipids, proteins and nucleic acids as a result of apoptosis were observed [Yao 2009; Fu 2014]. Also, many groups have reported that it can successfully differentiate dead cells from live cells [Uzunbajakava 2003; Notingher 2007]. More important, Draux et al. (2009), were able to obtain not only Raman spectra of live cells but also to monitor the effects of sub toxic doses of a chemotherapy drug on single living cancer cells [Draux 2011].

However, there is an issue that has not been fully dealt in Raman spectroscopy of cells. All animal cells either freshly isolated or established cell lines are usually maintained in incubators with atmospheric oxygen levels, that is 21% and 5% CO_2. However, *in vivo* conditions of cells are very different as levels of oxygen vary from 12% in arterial blood to

3-5% in tissues [Caldwell 2001]. Immune cell development and activation happens in primary, secondary or tertiary lymphoid organs with different infrastructure and oxygen supply [Caldwell 2001]. Since immune cells migrate between blood and various tissues during their development, they could be exposed to various levels of oxygen from high (normoxia) to very low (hypoxia) levels [Westermann 1999]. The oxygen level in peripheral blood is much lower than in air, and the smaller the arteries, the lower the oxygen level is. In *in vitro* conditions, growing cells are usually maintained in air supplemented with 5% CO_2, which is several folds higher than *in vivo* conditions [de Souza 2007]. Therefore, most of the knowledge to date about white cell behaviour *in vitro* is taken from the experiments on the T cells at much higher oxygen level than *in vivo* [de Souza 2007]. It has been reported that the mean oxygen level experienced by T cells ranges from 1- 10% [Caldwell 2001; Atkuri 2007]. Several groups have reported that incubator oxygen levels can affect the cells in several ways such as modulating their metabolism, changes in gene expression [Haddad 2004; Chi 2006] and function of primary cells [Carswell 2000; Caldwell 2001; Atkuri 2005].

There are recent advances in cell culture techniques including the use of improved media avoiding the addition of animal derived serum that might cause artefacts [Larbi 2010]. Yet, one very important and critical parameter being neglected over the decades is the level of oxygen to which cells are being exposed *in vitro*. Therefore, it is very important to understand cell culture systems that more closely relate to *in vivo* conditions, thus making the findings more relevant to understand truly physiological processes. Incubators equipped with atmospheric oxygen level of 21% clearly raises the questions of whether current cell culture conditions are appropriate for the cell functions to closely relate to *in vivo* situations. Already several groups have studied the effects of different incubators

environment upon cell proliferation [Krieger 1996], cytolysis [Caldwell 2001], and cytokine [Derevianko 1996; Caldwell 2001] and antibody production. However, the outcomes of these studies vary considerably, with no clear understanding on how and to what extent the behaviour of cells cultured at atmospheric oxygen mimics *in vivo* behaviour. To address this issue, clonal populations of leukaemia cell line K562 were obtained, and cultured in incubators at which the gas phase is set at atmospheric oxygen level of 21% or at lower oxygen levels of 10%. The influence of these oxygen conditions on the effects of drugs on cells was also assessed.

The choice of the most effective chemotherapy drug for an individual patient and monitoring the efficacy of ongoing chemotherapy are important steps in the management of cancer. Thereby, an objective method able to assess tumour cell sensitivity/resistance to a given drug prior to giving the drug would be most welcomed. Early biochemical changes can be identified using Raman spectroscopy [Lyng 2007; Fu 2014]. In this work, Raman spectroscopy has been used to investigate changes in cells' biochemistry prior to and after the addition of a drug and at different oxygen concentrations (10% and 21%). Control cells (cultured in the absence of a drug) were used to assess effects of oxygen concentration on cells' biochemistry.

To the best of my knowledge, no cancer studies using Raman spectroscopy have so far been done on the effect of different oxygen concentration on cells and their response to drugs.

7.2: Aims

I. To identify biochemical changes in cells grown in different oxygen concentrations, and its impact on the effects of drugs on cells using Raman microspectroscopy.

II. To better characterize spectral biomarkers of cell sensitivity/resistance to drugs for leukaemia, using Raman microspectroscopy

7.3: Materials and Methods

7.3.1: Cell line

K562 cell line, a chronic myelogenous Leukaemia (CML) cell line was used in this study. Cells were cultured and maintained in suspension in RPMI 1640 with 10% Foetal Bovine Serum (FBS), 1% L-Glutamine (200 nM), 1% Hepes buffer (1 M) and 1% Antibiotic/Antimycotic (100x) and incubated at 37°C and 5% CO_2. Medium was changed every 3-4 days.

7.3.2: Cell survival

Parental K562 cells were incubated in 24 well plates at 10^5 cells/well in the absence and presence of Nilotinib (10, 50 and 100 μM) for 5 days at both oxygen concentrations 10% and 21%. Cell survival was assessed using the Trypan blue exclusion method.

7.3.3: Cell cloning

As it has already been stated in section 2.1.2, *in-vitro* cell culture work is mostly conducted with mixed cell populations. In a mixed population, a mixture of sensitive and resistant

cells to a given drug will be present. In order to maintain a higher level of homogeneity across a cellular population, clonal culture methods were established (see Materials and Methods chapter 2).

The K562 cell line was cultured under standard conditions as mentioned in chapter 2. Before reaching confluence, cells were collected, spun at 950 rpm for 3 minutes and counted with the trypan blue exclusion method. The detailed protocol for cell cloning has already been discussed in Materials and Methods. Once the clones were selected, they were divided into six wells in two separate 96 well plates. One plate was incubated at standard conditions (21% O_2, 37 °C and 5% CO_2), while the second one was incubated at 10% O_2, 37 °C and 5% CO_2 for 24 hours for clones to adapt to the new culture conditions.

7.3.4: Application of Drugs to clones

Nilotinib was used in this study at two different concentrations, 50 μM and 100 μM. These two doses were chosen based on preliminary studies on clonal populations as described in Materials and Methods. Following 24 hours of incubation at 21% O_2 or 10% O_2, 37 °C and 5% CO_2, Nilotinib was added as follows. Plates were spun at 1200 rpm for 7 minutes. Following this, 100 μL of media were removed and 100 μL of fresh media with different final concentrations of Nilotinib was added (0 μM, 50 μM, or 100 μM). Following the addition of the drug, cells were allowed to grow for 5 days at 21% O_2 and 10% O_2, 37 °C or 5% CO_2. Five days were chosen based on preliminary studies on clonal populations as described in Materials and Methods.

7.3.5: Clone Selection

Clones were selected for analysis as follows. Clones in which cells in control wells were completely confluent were discarded as this could modify their metabolical and proliferative properties. Clones were selected by visually observing the wells under the microscope and classed as sensitive where there were no cells or very low number of live cells in the well; as described in previous chapter 6 section 6.5 and table XI, resistant clones where cells were semi-confluent even at high concentration of the drug and semi-resistant/semi-sensitive where the well was half full. Clones were selected based on their quality and choosing examples of sensitive clones (few live cells incubated with 50 μM Nilotinib but no cells incubated with 100 μM Nilotinib), resistant clones (good number of cells at both 50 μM and 100 μM incubation) and semi-resistant/semi-sensitive clones (few live cells at 100 nM incubation and good number of cells at 50 μM incubation). Each individually selected clone included cells incubated in the presence or absence of Nilotinib in either 21% or 10% O_2 concentration.

7.3.6: Sample Preparation

UV graded CaF_2 slides (26 x 22 x 0.5 mm) (Crystan Ltd, UK) windows were selected as substrate due to their suitability for Raman and S-FTIR spectroscopies. Following incubation in the presence or absence of the drug, selected clones were collected and spun in Eppendorfs at 950 rpm for 3 minutes. Supernatant was discarded and the cell pellet was dislodged and re-suspended in 0.9% NaCl. Cell suspension was then cytospun onto CaF_2 slides for 1 minute at 550 rpm through a cytofunnel and a filter card (Shandon, UK). Once cells have been deposited on CaF_2 slides in a single monolayer, slides were placed in a Petri dish and fixed using 4% Paraformaldehyde (PFA) in 0.9% NaCl for 20 minutes as

previously described [Pijanka 2009], followed by 3 washes with 0.9% NaCl and 3 washes with distilled water and then air-dried at room temperature.

7.3.7: Raman Spectroscopy

Raman spectra were obtained by a Senterra Micro Raman laser class 1 (Bruker) spectroscope at Diamond Light Source, equipped with a 532-nm Laser. An Olympus microscope objective with 100x magnification was used to focus the incident laser light on the individual cells and backscattered Raman light was collected with a CCD thermoelectrically cooled detector in the range of 40-4450 cm^{-1}, with the help of Opus (Bruker) software using Neon emission lamp for Raman as source. Spectra were collected at 9-18 cm^{-1} resolutions with 2 co-added spectra with integration time of 10 second with 50 μm pinhole type aperture by using spot size of 2F μm. The measurements were taken by pointing the laser at the nucleus of the cell. Five spectra of each cell were recorded. The laser was pointed at the nucleus especially as the drug I was using, interrupts the DNA synthesis and replication Spectra obtained from the nucleus of the cell would better describe the possible effect of the drug on the cells. Background spectra of the substrate were taken at the start of measurement. Spectra of at least 50 cells where possible were collected from each sample.

7.3.8: Data Processing

The spectrum was processed using Opus (Bruker). The data was cropped between 400-1800 cm^{-1} and baseline corrected. Following baseline correction, data was normalized using SNV using The Unscrambler Software (VERSION X, Camo, Oslo, Norway).

PCA is generally known as a technique for presenting the variation in a multivariate data set. It is used as an effective approach to visualize and to mine information from data set with a large number of variables such as those contained in Raman spectra. PCA was performed using The Unscrambler Software (VERSION X, Camo, Oslo, Norway). Loading plots were also produced using the same software.

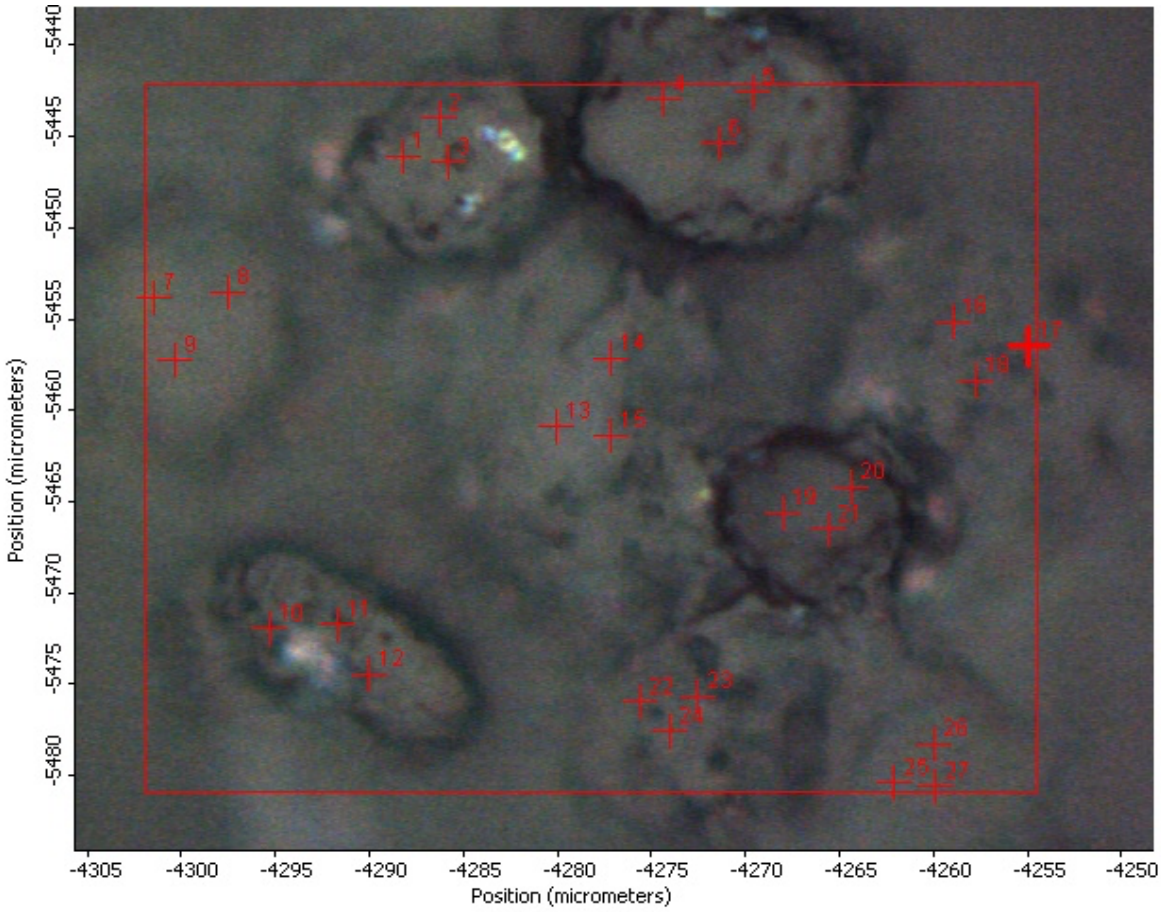

Figure 70: Image of cytospun cells, depicting the labelled cells that Raman measurement had been taken from.

7.4: Results and Discussion

Raman spectra of the study cells were obtained from 3 different areas within the cell and averaged. Figure 70 shows a representative example of few cells with the areas from where

the spectra were obtained and figure 71 shows a representative example of a Raman spectrum of a single K562 cell.

Based on previous studies summarized in Table XII, Figure 71 shows the peaks present in K562 cell spectra and among them, observed peaks primarily show twisting doublet at 620 and 640 cm^{-1} belonging to tyrosine/phenylalanine, while a doublet for the tyrosine ring breathing was observed at 829 and 852 cm^{-1} [Poon 2012]. The phenylalanine symmetric breathing mode peak was observed at 1003 cm^{-1} [Poon 2012]. Major intense peaks are 1657 cm^{-1} (Protein, Amide I), 1613 cm^{-1} (Tyrosine, Tryptophan, Protein C=C), 1550 cm^{-1} (Guanine, Tryptophan), 1448 cm^{-1} (protein, C-H2 deformation), and 1335 cm^{-1} (C-H3 deformation of protein and lipids, nucleic acid) amongst other [Kneipp 2003; Short 2005; Chan 2006; Akyuz 2011; Byrne 2011; Poon 2012; Lyng 2015]. Previously it has been claimed that Nilotinib and Imatinib exhibit strong Raman peaks in the regions of 1300, 1370 and 1600 cm^{-1} [Fu 2014], in my studies I did not observe any peaks at these regions in the spectra of the clones exposed to Nilotinib.

Preliminary work was carried out to assess any possible differences between control cells (incubated with 0 μM Nilotinib) incubated at 21 or 10% oxygen. Figures 72 and 73 show the mean spectra of 50 individual cells from a resistant clone to Nilotinib and a sensitive clone to 100 μM to Nilotinib, respectively. The spectra of the resistant control cells did not show major differences in the spectra regardless whether they had been incubated with 21% or 10 % oxygen. However slight changes in the intensities could be observed in the spectra in Figure 72. These changes are slight increase in the intensities of 1243 cm^{-1} belonging to protein of Amide III and DNA backbone breathings, 1031 cm^{-1} for C-N stretch of proteins and phenylalanine, 1003

cm^{-1} belonging to protein, and ring breathing mode of phenylalanine, and a slight decrease at 1092 cm^{-1} attributed to DNA/RNA O-P-O symmetric stretch, and 929 cm^{-1} belonging to proteins and lipids for the mean spectra of cells incubated at 10% oxygen as compared to the mean spectra of cells incubated at 21% oxygen.

However, for the sensitive clone to 100 μM (figure 73) there were significant differences between the Raman spectra of cells incubated in 21% or 10% O_2. The major changes were shown at characteristic nucleic acid bands.

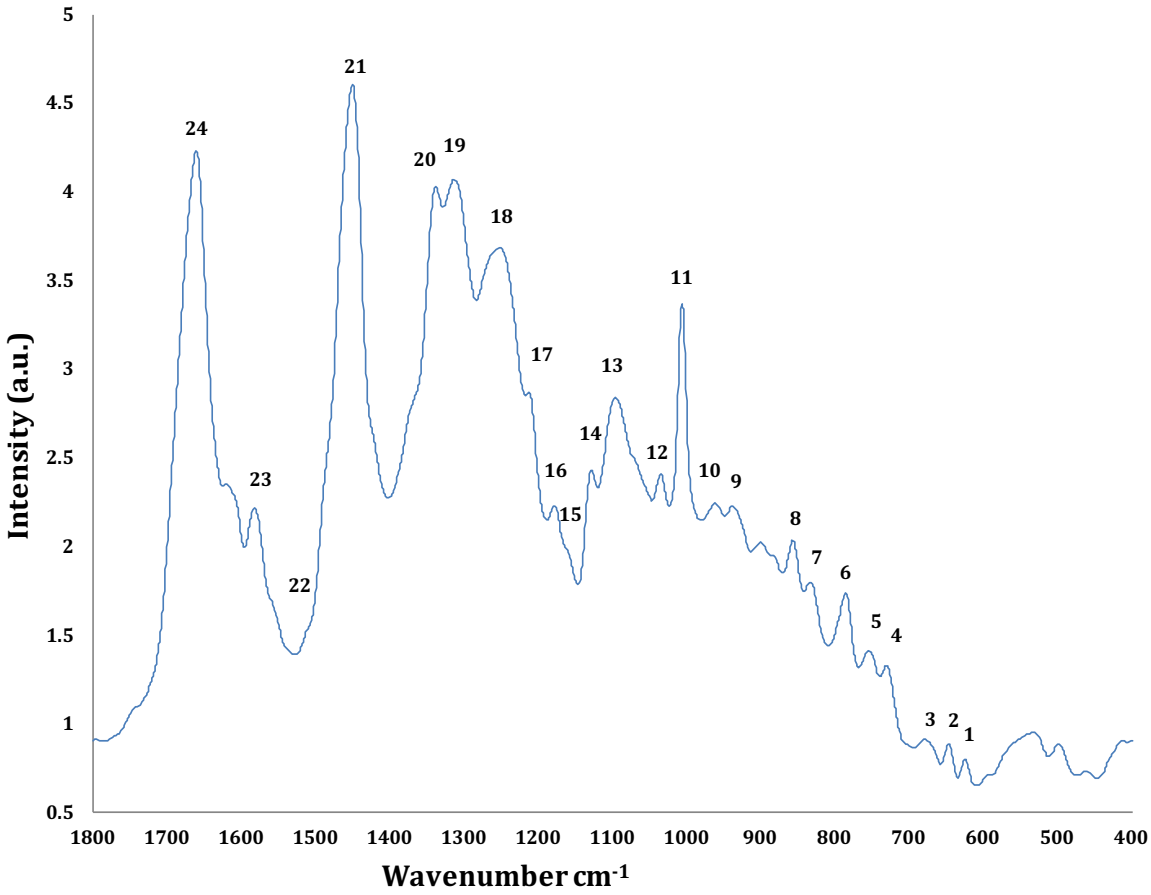

Figure 71: Representative example of a Raman spectrum of a K562 cell

Table XII: List of frequencies in a Raman Spectrum [Kneipp 2003; Short 2005; Chan 2006; Akyuz 2011; Byrne 2011; Poon 2012]

NO	Raman frequency units (cm-1)	Assignment
1	620	Protein C-C twist
2	640	Protein C-S stretching and C-C twist of tyrosine
3	668	Guanine, Thymine, Tyrosine,
4	728	Adenine, Lipid
5	748	Tryptophan, Thymine
6	782	Cytosine, Uracil, Thymine,
7	828	O-P-O asymmetric stretch, Tyrosine
8	852	Tyrosine, Lipid
9	929	Protein, Lipids
10	952	Protein, Lipids
11	1003	Protein: ring breathing Phenylalanine
12	1031	Phenylalanine, Protein C-N stretch
13	1092	DNA/ RNA: O-P-O symmetric stretch
14	1125	Protein C-N stretch
15	1157	Protein C-C, C-N stretching
16	1174	Tyrosine, Phenylalanine, Protein C-H bend
17	1209	Adenine, Thymine, Protein Amide III
18	1243	Adenine, Thymine, Protein Amide III
19	1306	Protein Amide III, lipid, Nucleic acids
20	1335	C-H3 deformation (Protein, Lipid), Nucleic Acid
21	1448	Protein C-H2 deformation
22	1553	Protein: C=C stretching, Tryptophan
23	1575	DNA/RNA: ring mode (Guanine, Adenine)
24	1616	Tyrosine, Tryptophan, Protein C=C
25	1660	Protein Amide I

These include an increase in the prominent bands at 668, 728, 728, 782, 1092, 1243, 1335, and 1575 cm^{-1} [Kneipp 2003; Akyuz 2011; Byrne 2011; Poon 2012] along with the appearance of distinct shoulders at 1366 cm^{-1} and 1486 cm^{-1} also attributed to the nucleic acid, and significant decrease at the peak 1448 cm^{-1} belonging to protein deformation, in the spectra of the cells incubated at 21% O_2 (Figure 73). This increase in nucleic acid bands may be the result of increased proliferation of the leukaemia cells at 21% O_2 [Byrne 2011]. This would indicate increased DNA concentration in sensitive cells incubated in 21% O_2. While it could be hypothesised that the growth in different O_2 concentrations could lead to different spectra between resistant and sensitive clones to Nilotinib, it has to be recognised these are 2 different clones.

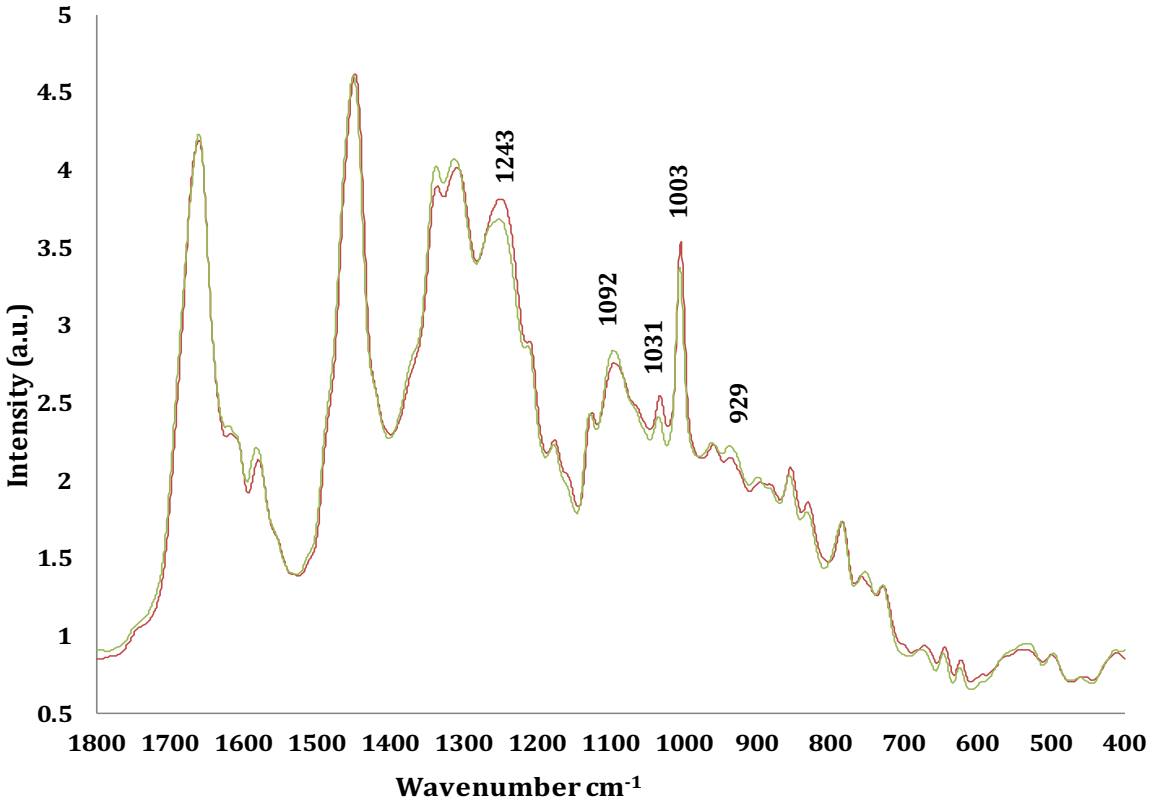

Figure 72: Mean spectra of 50 cells of a resistant clone control cells incubated with 0 µM Nilotinib and incubated at 10% (red) and 21% (green) oxygen. Spectra are offset for clarity.

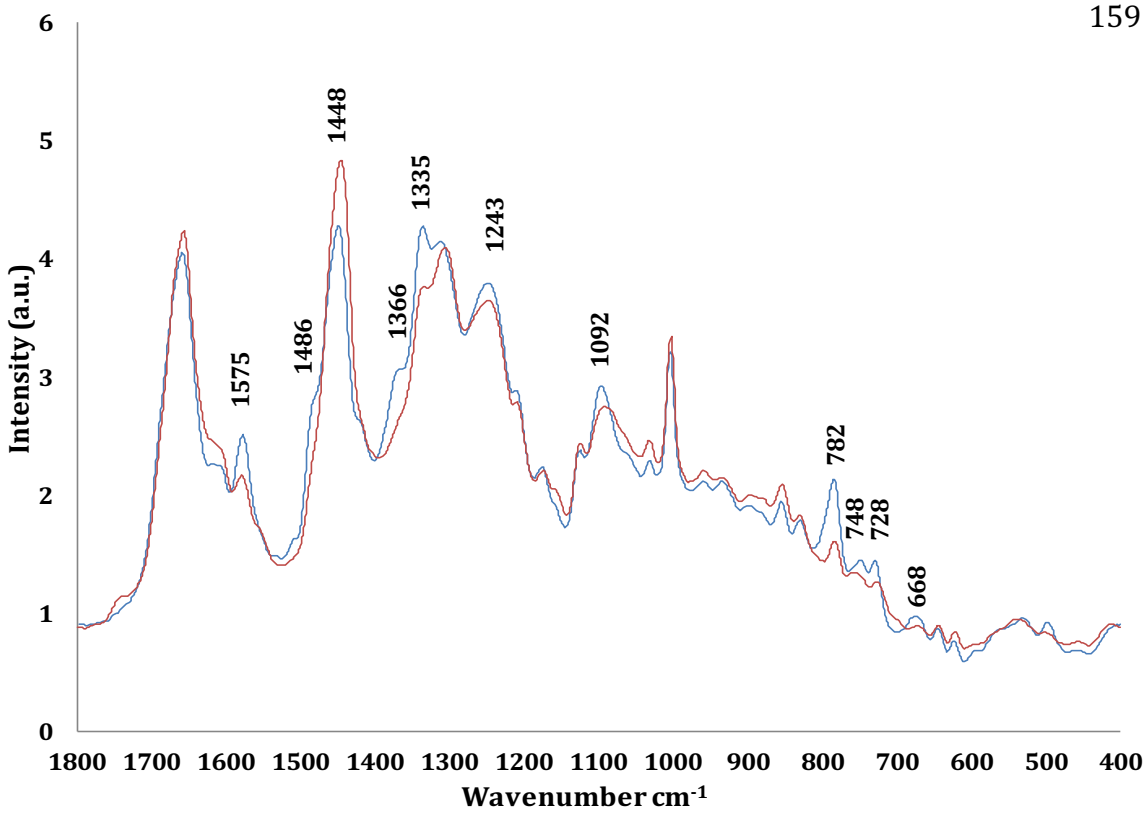

Figure 73: Mean spectra of 50 cells of a sensitive clone to 100 µM of Nilotinib control cells incubated with 0 µM Nilotinib and at 10% (Red) and 21% (Blue) oxygen. Spectra are offset for clarity.

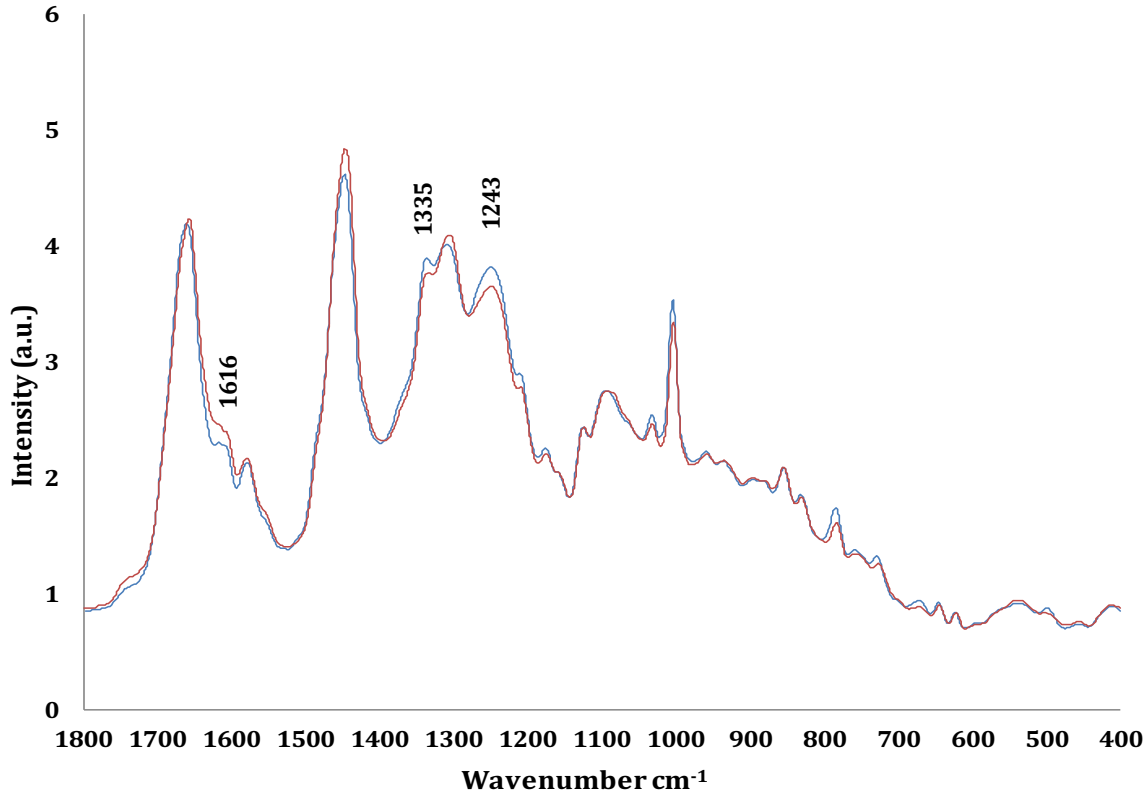

Figure74: Mean spectra of 50 cells of control from sensitive clone cells (red) vs mean spectra of resistant clone cells (blue) incubated at 10% O_2. Spectra are offset for clarity Spectra are offset for clarity.

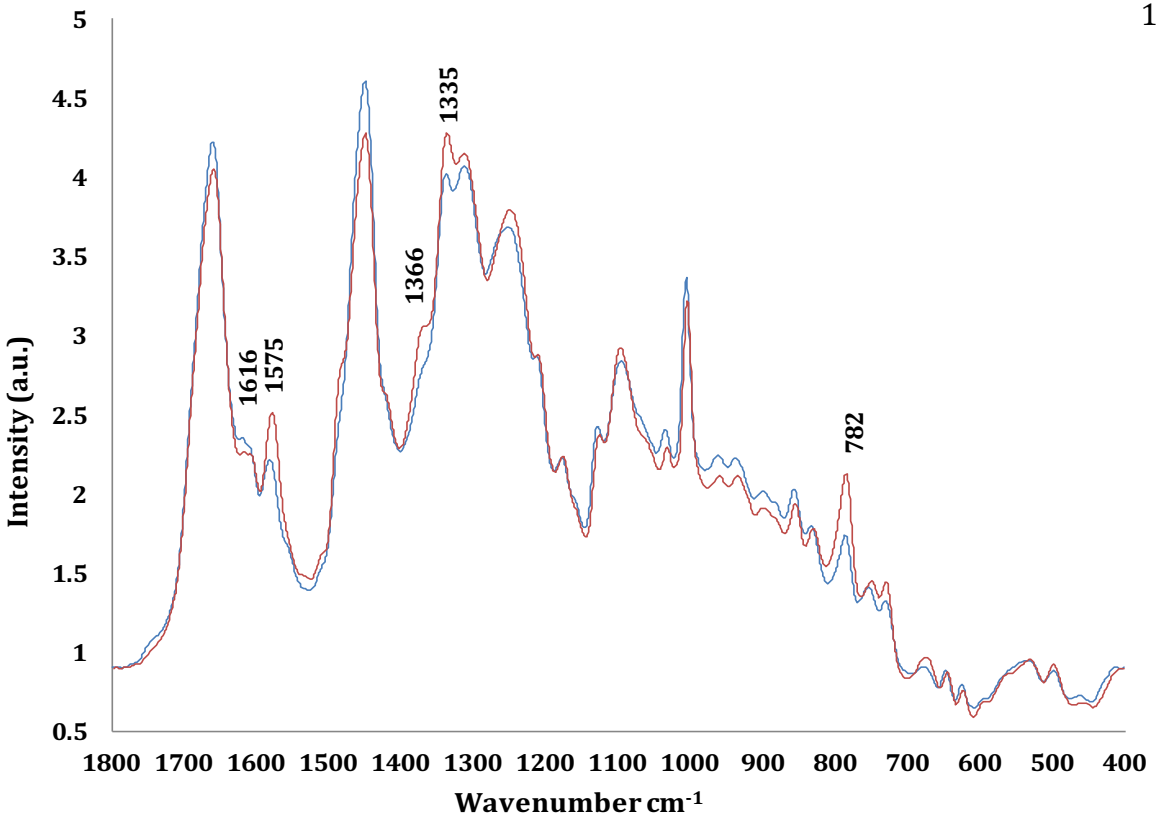

Figure 75: Mean spectra of 50 cells of control sensitive clone cells (Blue) vs mean spectra of resistant clone cells (Red) incubated at 21% O_2. Spectra are offset for clarity.

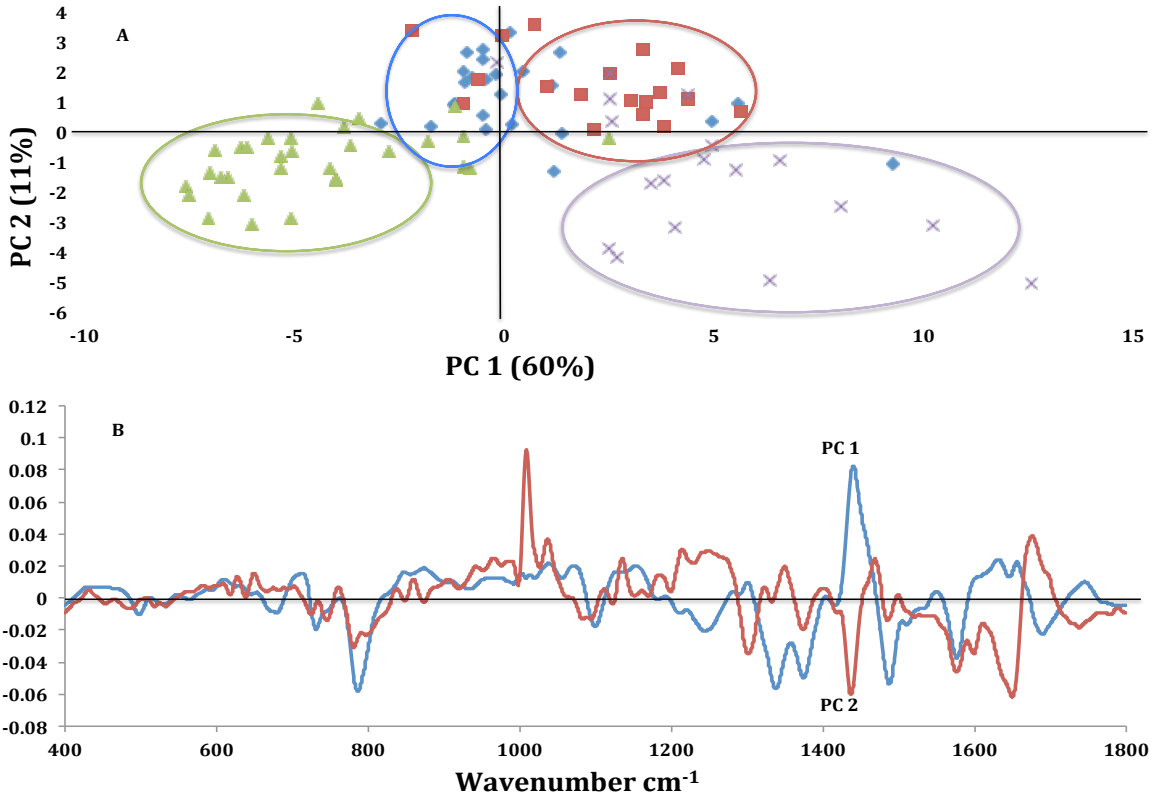

Figure 76: PCA and Loading of a resistant clone control cells incubated with 0 µM Nilotinib at 21% O_2 (diamonds) and 10% O_2 (squares), and of a sensitive clone to 100 µM Nilotinib control cells incubated with 0 µM Nilotinib at 21% O_2 (triangles) and 10% O_2 (crosses).

Therefore, the data presented here indicates that oxygen concentration in culture conditions could definitely affect the Raman spectra of some leukaemia cell clones.

Figures 74 and 75 are representative examples of the comparison between resistant clone cells versus sensitive clone cells incubated at both O_2 levels (10% and 21%). Interestingly, there were no any major variations between the spectra of cells incubated at 10% O_2 but only a slight decrease in the protein concentrations but an increase in DNA content in resistant clone shown by a decrease in the intensity of 1616 cm^{-1} peak, and an increase in the peaks at 1243 cm^{-1} and 1335 cm^{-1} (Figure 74). However, when comparing spectra of both clones' cells incubated at 21% O_2 (Figure 75), there are major changes in the intensities and frequencies of the peaks. These data suggest that oxygen levels do make a difference in the biology of cells which can be measured with Raman microspectroscopy. As it can be seen in Figure 75, there is a decrease in the intensity of the peaks attributed to nucleic acid (e.g. 1575 cm^{-1}, 1366 cm^{-1}, 1335 cm^{-1}, and 782 cm^{-1}), while there is an increase in 1616 cm^{-1} for the resistant clone, Further work is needed to better understand how culture conditions mimic *in vivo* conditions.

The spectral data was analysed with PCA. As can be seen in figure 76, there was a small separation between cells incubated with 21% O_2 and 10% O_2 for the resistant clone as it would be expected from the spectra presented in figure 72, which did not show major differences. However, for the sensitive clone, there was a clear separation between cells incubated in 21% O_2 and 10% O_2. Furthermore, there was a trend in the PCA to separate between clones incubated in 21% O_2 and 10% O_2. These data stresses the importance of taking into account that changing cell culture conditions to those that best mimic the real physiological situation could also translate into changes in their Raman spectra. It also

stresses the need to understand in drug related studies that even within a cell line, there will be different clonal cells which could present different spectral characteristics not related to the effects of a given drug.

PC1 verses PC2 loading plots for both groups shown in Figure 76 highlight the peaks that are important in the separation. It is clear from the loadings that the main differences reside at DNA signals and protein concentrations, confirming the data observed in the spectra (Figure 72 and 73).

Loading curves indicate which variables account for the differences among the groups. PC1 versus PC2 loading plots for both groups shown in figure 76B highlights the peaks that are important in the separation. The main differences are at DNA signal (e.g. 725, 783, 853, 1090, 1306, and 1335 cm^{-1}) (Chan 2006; Short 2005; Akyuz 2011], as appeared in the spectra.

So, it could be concluded that DNA could be the main difference between normal K562 cells and the cells exposed to the Nilotinib for both groups. As we have observed that there is a remarkable decrease in the DNA content of the cells exposed to the Nilotinib.

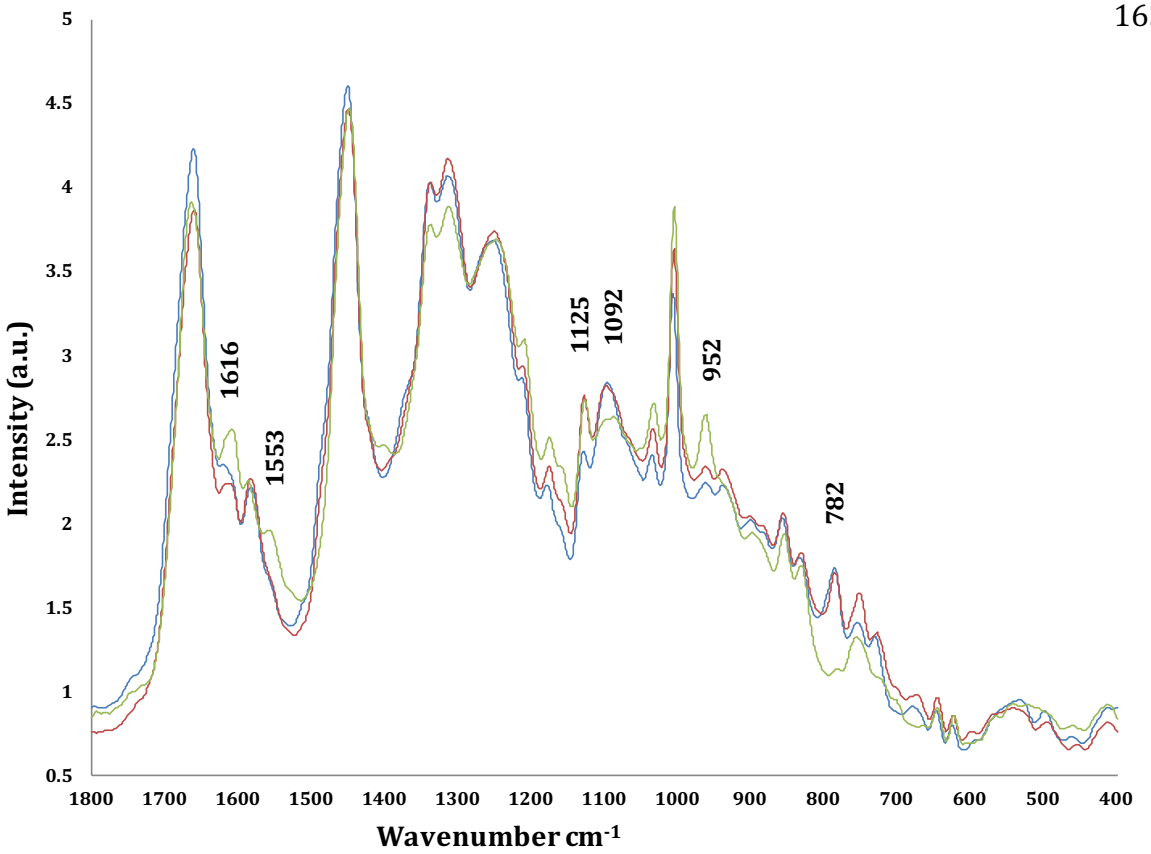

Figure 77: Mean spectra of resistant clone incubated at 21% O_2 with Nilotinib 0 µM (blue), 50 µM (red), and 100 µM (green). Spectra are offset for clarity.

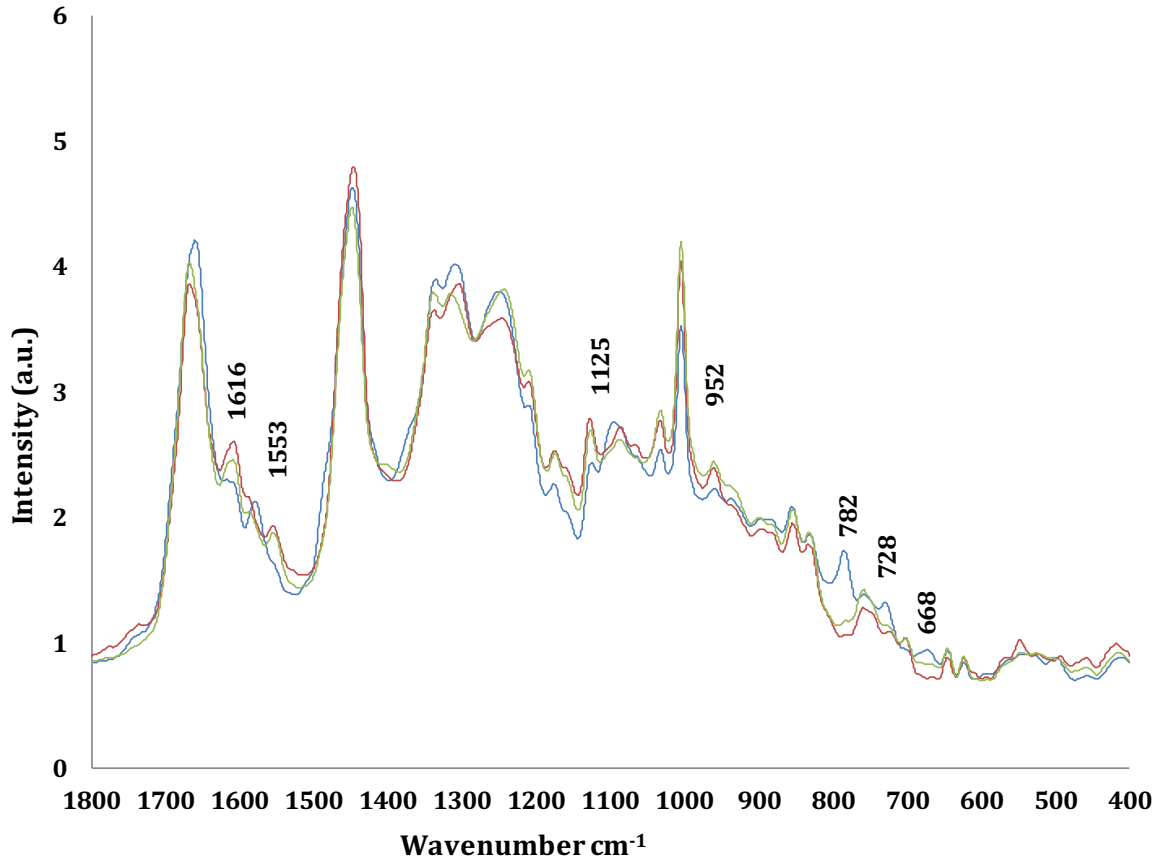

Figure 78: Mean spectra of resistant clone incubated at 10% O_2 with Nilotinib 0 µM (blue), 50 µM (red), and 100 µM (green). Spectra are offset for clarity.

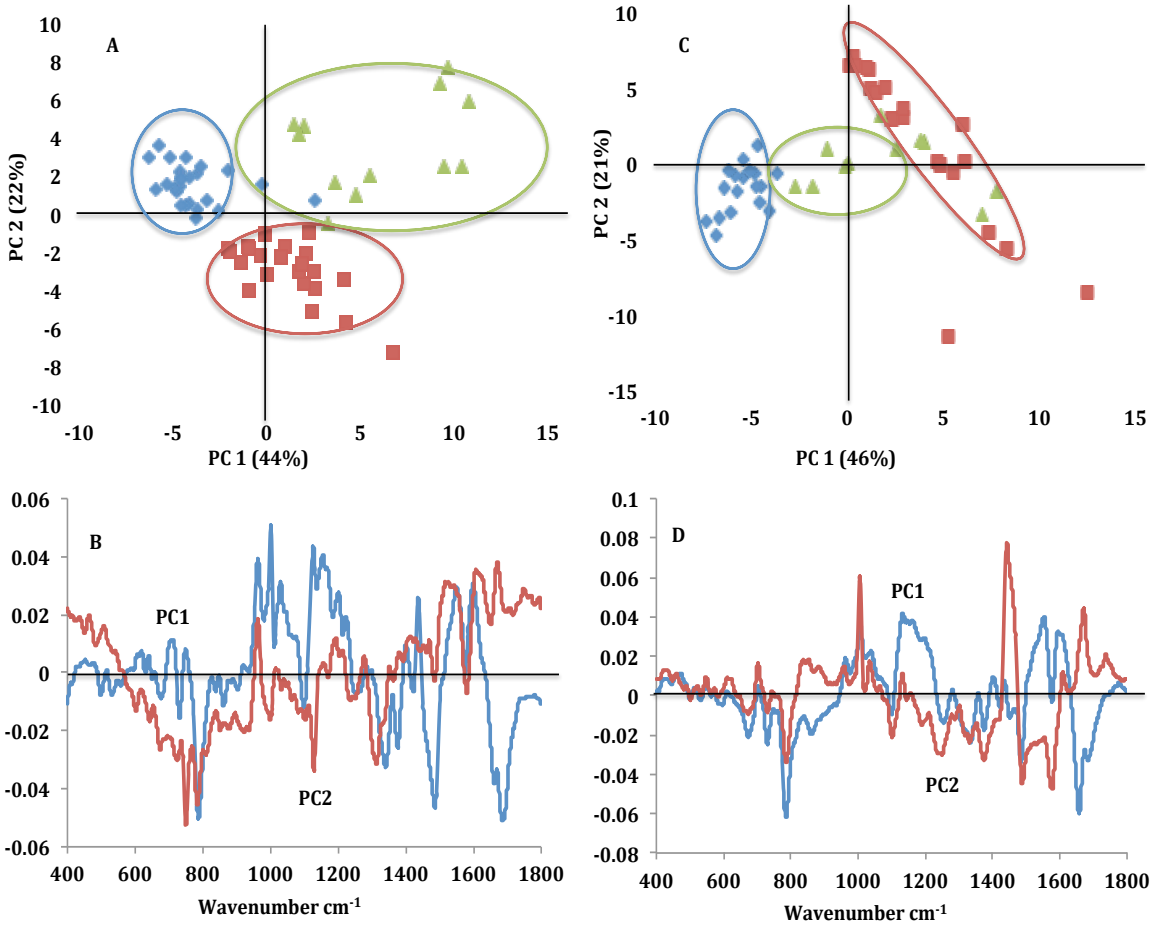

Figure 79: PCA and loading of a resistant clone cells incubated at 21% O_2 (A and B) and cells incubated at 10% O_2 (C and D) with 0 µM (diamonds), 50 µM (squares) and 100 µM (triangles) doses of Nilotinib.

The next step was to obtain Raman spectra of clone cells in the presence and absence of Nilotinib but incubated at either 21% or 10% O_2. Figures 77, 78, 79, and 81, show the Raman spectra of a resistant and a sensitive clone to 100 µM Nilotinib in the presence and absence of Nilotinib and in 2 different O_2 concentrations. This study focused on distinct peaks that exhibit the major differences between the spectra of the cells incubated at different doses of Nilotinib at both concentration of oxygen, 10% and 21%.

Generally, most features of the Raman spectra from controls and cells incubated in the

presence of Nilotinib for both clones are very similar, but there are some spectral changes in cells incubated with the drug. The data show that the biochemical changes in the spectra are both dose and oxygen concentration dependent.

In cells incubated in 21% O_2, drug exposure translated into an increase in the intensity of peaks 1616 cm^{-1}, 1553 cm^{-1}, 1125 cm^{-1}, and 952 cm^{-1} for the resistant clone, and of peak 1125 cm^{-1} and 748 cm^{-1} for the sensitive clone (figure 80) at 100 μM Nilotinib. On the other hand, there was a decrease in the intensity of peaks 782 cm^{-1} and 1092 cm^{-1} for the resistant clone and of peaks 1575 cm^{-1}, 1335 cm^{-1} and 782 cm^{-1} for the sensitive clone.

In the case of cells incubated in the presence of 10% O_2, there was an increase in intensity of the peaks at 1616 cm^{-1}, 1550 cm^{-1}, 1125 cm^{-1}, and 952 cm^{-1} for the resistant clone (figure 78) and of peak 1335 cm^{-1} for the sensitive clone (figure 81). On the other hand, there was a remarkable decrease in the intensity of peak 782 cm^{-1}, 728 cm^{-1}, and 668 cm^{-1} for the resistant clone and for peak 1448 cm^{-1}, 1306 cm^{-1}, 728 cm^{-1}, and 668 cm^{-1} for the sensitive clone. Taken together, these results indicated that the O_2 concentration will affect the Raman spectra of cells in the presence or absence of Nilotinib. On the other hand, O_2 concentration does not seem to affect the effects on certain peaks caused by Nilotinib. For the resistant clone, the peaks at 1550 cm^{-1} and 1616 cm^{-1} increase in the presence of Nilotinib and the peak at 782 cm^{-1} decreases in the presence of Nilotinib regardless of O_2 concentration. For the sensitive clone, there was no clear pattern with different changes occurring at different O_2 concentrations.

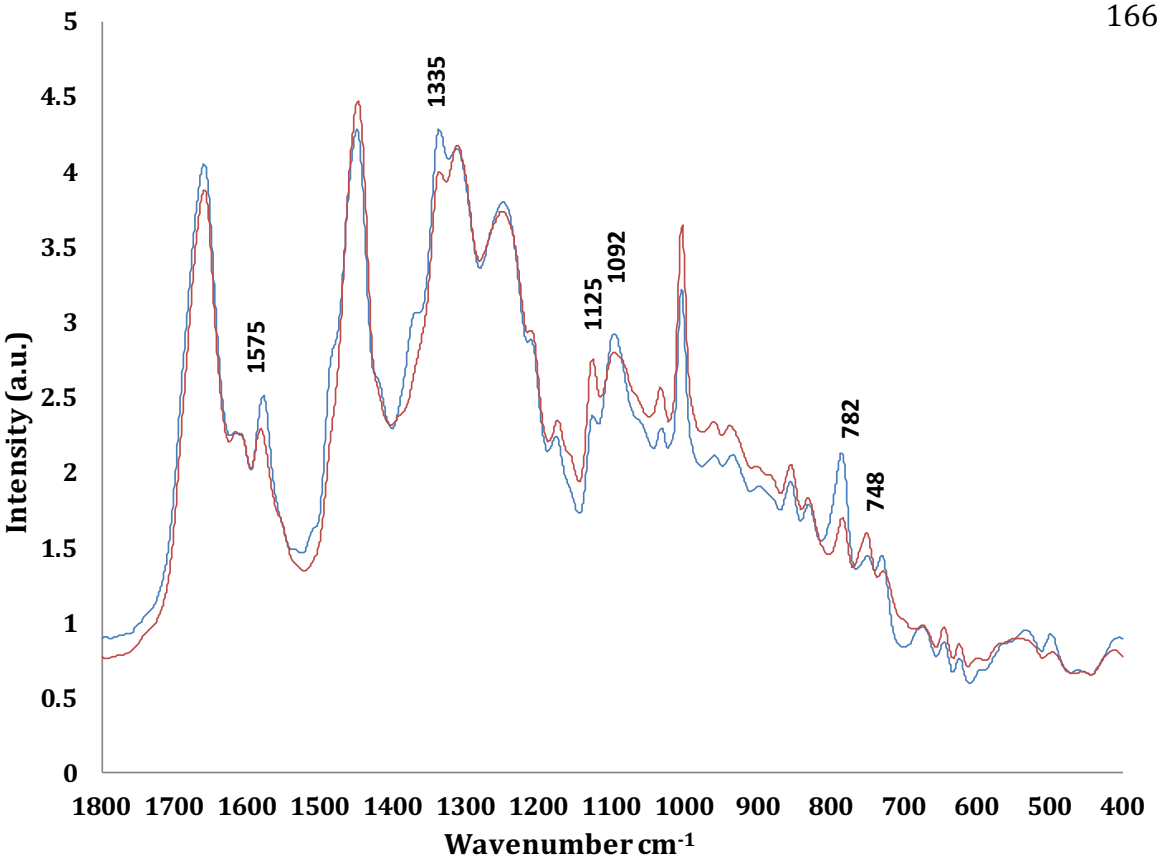

Figure 80: Mean spectra of a clone sensitive to 100 µM Nilotinib incubated at 21% O_2 with Nilotinib 0 µM (blue) and 50 µM (red). Spectra are offset for clarity.

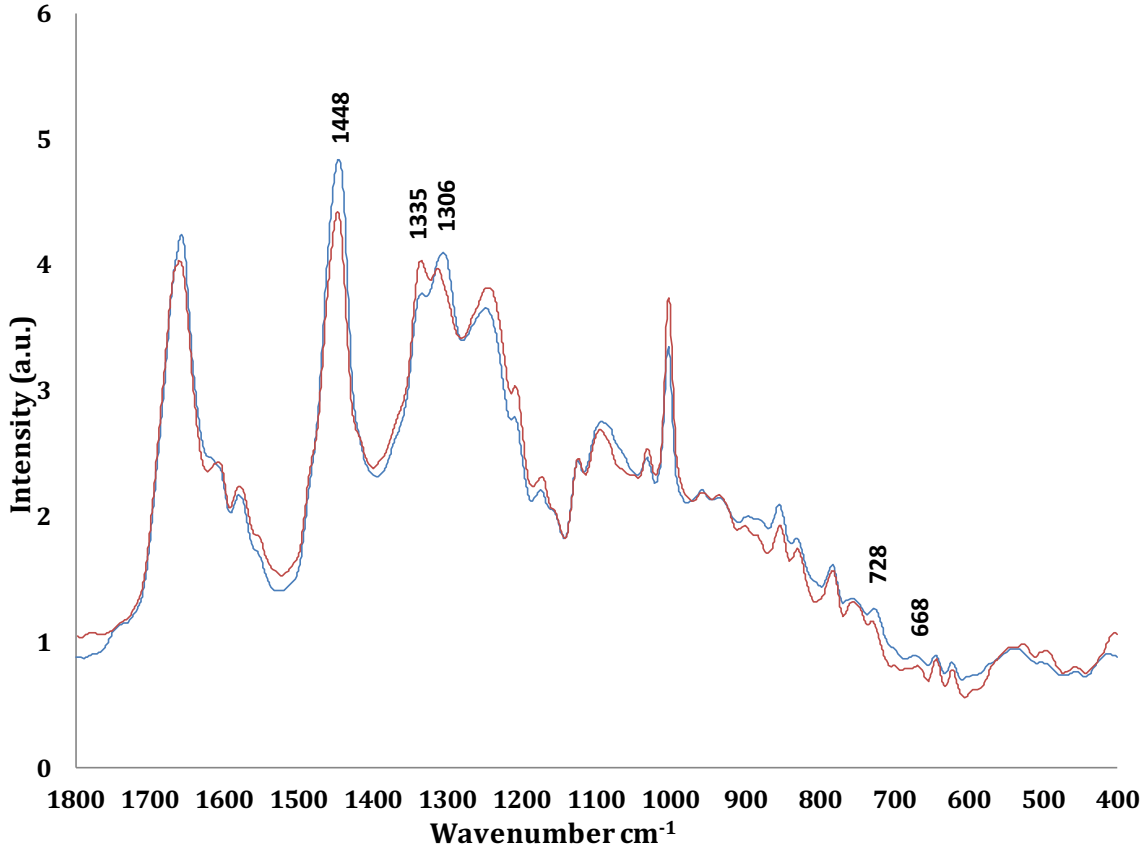

Figure 81: Mean spectra of a clone sensitive to 100 µM Nilotinib incubated at 10% O_2 with Nilotinib 0 µM (blue) and 50 µM (red). Spectra are offset for clarity.

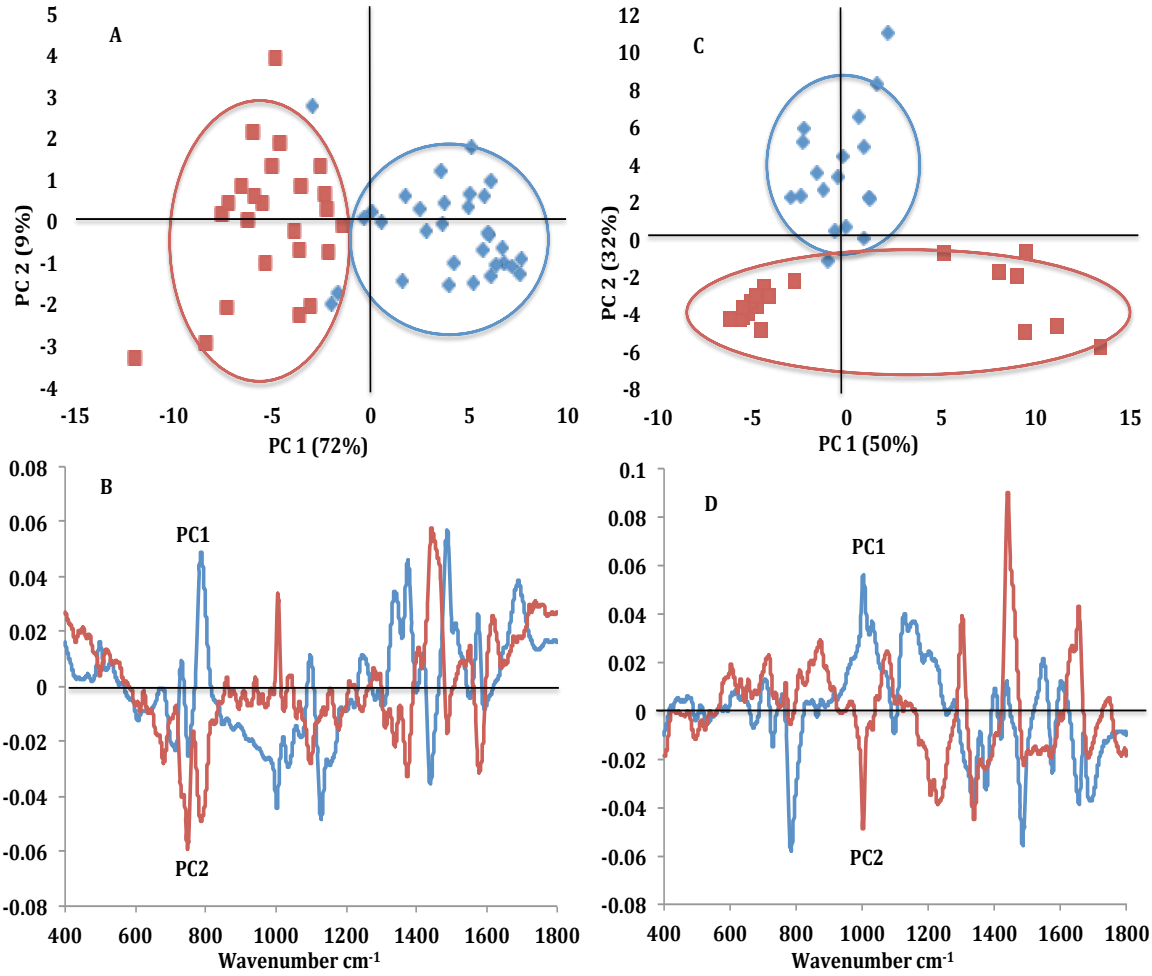

Figure 82: PCA and Loading of a clone sensitive to 100 µM Nilotinib incubated at 21% O_2 (A and B) and cells incubated at 10% O_2 (C and D) with 0 µM (diamonds) and 50 µM (squares) of Nilotinib.

It is immediately clear that there is significant heterogeneity in the Raman spectra within each dose of drug exposure, reflecting the variability in cellular response due to the nature of biochemical reactions inside the cell or drug sensitivity [Niepel 2009].

In general, the major changes in the Raman spectra for both clones at both oxygen concentrations can be attributed to a decrease of DNA signal (e.g. 668, 728, 782, 1092, 1306, 1335 and 1575 cm^{-1}) [Short 2005; Chan 2006; Akyuz 2011]. Interestingly a decrease of DNA signal at band 668 cm^{-1} appears in both clones but only in the spectra of the

second group (10% O_2). There is a decrease for 782 cm-^{1} peak with the addition of the drug in the sensitive clone incubated in 10% O_2 but not when incubated in 21% O_2. There is an increase of lipid intensity (e.g. 952 cm-^{1}), in the resistant clone incubated at both O_2 concentrations but not in the sensitive clone.

Lyng et al. (2007) reported that increased nucleic acid and protein bands are a result of the increased proliferation of the cancerous cells [Lyng 2007]. Thus, it could be hypothesised that decrease in the intensity of DNA specific peaks and increase in intensity of protein specific peaks in the spectrum of both groups suggests late phases of apoptosis or may be dead cells, as nuclear fragments are expelled from the cell leaving an empty shell of cell membrane and cytoplasm [Lavie 1999]. However, an increase in the intensity of DNA specific bands can also be associated with chromatin condensation and nuclear fragmentation during the apoptosis process [George 1996; Johnson 2000; Sokolovskaya 2001]. An increase in DNA density due to chromatin condensation would lead to an increase in the DNA peak intensities in the Raman spectra. The increase of intensity in the lipid related peak at 952 cm^{-1} could be attributed to the presence of intracellular vesicles. This observation is consistent with the formation of lipid vesicles at the cell surface [Ferraro-Peyret 2002] that is known to occur during early stages of apoptosis of leukemic T-lymphocytes cells when exposed to anticancer drugs (e.g. doxorubicin) [Gamen 2000; Dartsch 2002]. Zoladek A et al. (2010) reported spectral changes in lipid and DNA bands consistent with the appearance of lipid vesicles at early stages of apoptosis and DNA condensation. Changes in DNA and protein associated peaks of the cells exposed to drug have also been observed by other groups [Owen 2006; Buckmaster 2009; Yao 2009].

PCA was carried out to assess possible differences between cells incubated in the presence or absence of Nilotinib and different O_2 concentrations. The grouping of the samples into three clusters according to cells incubated in either of the 3 doses of Nilotinib indicates that differences between the Raman spectra can be revealed easily by PCA (Figures 79, and 82). The loadings curves reveal the scores plot of the second principal component (PC2) versus the first principal component (PC1) and which variables account for the differences among the groups. PC1 verses PC2 loading plots for both groups shown in figure 80B, 80D, 83B, and 83D, highlight the peaks that are important in the separation. So, it could be concluded that DNA could be one of the main differences between K562 cells exposed to different doses of Nilotinib for both groups.

7.4: Conclusion

Overall, the differences I observed in both groups incubated in different oxygen levels pose a key challenge to investigators using these types of assays. Somehow, it has been assumed in some cases that results obtained when cells are cultured at atmospheric oxygen levels might mimic *in vivo* behaviour. This theory appears reasonably secure, as a lot of the data obtained through conventional culture systems is compatible with *in vivo* findings. But with the advanced knowledge of signalling pathways and other molecular mechanisms of cells' development and function, it is necessary to use culture systems that more closely approximate *in vivo* conditions. Conventional *in vitro* cell culture is performed at ambient oxygen concentration. Lukashev 2006, reported that under changing oxygen concentrations, the HIF-1α pathway shows considerably different effects on the post-translational modification of proteins and it can also influence a broad range of pathways by acting at the transcriptional level [Lukashev 2006]. The exact oxygen level *in vivo* is unknown yet, although recent improvements in technology, have allowed its measurement

ex vivo [Zhdanov 2008]. Although it was reported that the extracellular environment of cells rapidly equilibrated to the ambient oxygen level [Newby 2005], it would be appropriate to take oxygen level into account for *in vitro* work.

Raman spectroscopy is shown to be a powerful technique for the investigation of drug-induced alterations in cells. The most effective application of Raman spectroscopy in the field of oncology could be in the area of therapeutic management. Due to the complexity of tumours, histopathology is not able to predict tumour/ cancer's therapeutic response or recurrence and the associated biochemical processes *in-vivo*. It can be hypothesized, that Raman spectroscopy could provide information on the mechanical and biochemical structure of cells and be able to identify changes in cells due to different levels of oxygen and the effects of drugs at different oxygen concentrations. I propose that careful, *in vitro* studies as close as possible to the *in vivo* environment will be necessary to determine the efficacy of the Raman approach for drug response assessment. Data from Raman spectroscopy along with PCA has improved the reliability and the accuracy of Raman spectra interpretation and classification. Importantly, this proposed approach provides a useful tool to assess cell behaviour in different physiological conditions.

The results obtained in this work show there are changes in DNA concentration in the spectra of cells exposed to Nilotinib such as a decrease in the peak at 782 cm^{-1} and as one of the main mechanism for the induction of cell apoptosis. Decreased DNA content would suggest cells to be in the late apoptosis stage. Nuclear condensation occurs in early stages of the apoptosis process as chromatin compacts (pyknosis) being a hallmark process of apoptosis. However, this process is short-termed as during fragmentation DNA is cleaved into very short fragments that cause reduction in the intensity of DNA peaks [Yaho 2009].

It has been shown in this study that there are remarkable differences in the biochemical composition of cells incubated at different oxygen concentrations. Further studies are needed to confirm these difference and changes in the spectra that could be linked to mechanisms behind these changes.

The future of Raman microspectroscopy in treatment response assessment is exciting. With recent and promising technological developments, cancer patients might one day benefit from the capability of this technology to predict tumour response to drugs.

Chapter 8

Discussion and Future Work

Early detection of leukaemia is critical for a successful treatment and in the reduction of morbidity and mortality. In the last few years, significant technological developments have taken place that could be exploited for the detection and management of the disease. However, the real challenge is to enhance these technologies further to enable the early detection of the cancer and monitor its progression and therapeutic response. Several studies have determined the problems and complexities along with the risk level involved in the diagnosis and management of leukaemia for each individual patient. Due to the complexities of disease diagnosis, high costs, its prognosis and management, there is a great prerequisite for the development of new ways and approaches which would be safe, non invasive, low-cost and could detect cancer at early stages. This would lead to better patient management and improve survival. The aim of this thesis was to use 3 techniques, (SIFT-MS, S-FTIR Spectroscopy, and Raman Spectroscopy) to address some of the practical issues associated with their potential clinical application, which should lead towards better management of leukaemia.

The first experimental chapter (Chapter 3) is focused on the use of SIFT-MS to quantify the VOCs released by leukaemia cells compared to PBMC and bone marrow cells. As a novel technique, SIFT-MS offers non-destructive and real-time analysis of VOCs released through breath. SIFT-MS, used in this work, detects accurately and in real time several compounds simultaneously down to concentrations of parts-per-billion by volume (ppbv). More importantly, it obviates

sample preparation, thus speeding the process to obtain data when compared to other instruments where sample processing is a crucial step. SIFT-MS could be used to identify VOCs profiles that could differentiate leukaemia cells from healthy cells.

One possible VOC identified for cancer diagnosis is acetaldehyde. It has been shown to be released by lung cancer cells both in 2D and 3D cell culture conditions and its concentration to correlate with cancer cell number [Smith 2003; Sulé-Suso 2009]. In the study presented here, the levels of acetaldehyde released by both leukaemia cell lines and PBMC were similar to the acetaldehyde released by culture medium. However, it is important to understand the metabolical pathways of the different VOCs and whether and how modifying them could lead to improving the management of cancer. As an example, the inhibition of ALDH with disulfiram translated into an increase of the levels of acetaldehyde in the headspace of Jurkat and K562 cells but not in the headspace of PBMC (Chapter 3). This shows that modifying VOCs metabolism could lead to a differential in the concentration of VOCs which could have clinical application.

Another important point is to understand the origin of the cancer cells and whether VOCs could be used to better identify the different steps of cancer progression. On this basis, the VOCs of bone marrow cells were also studied. The results showed that the VOCs profile of leukaemia cells and bone marrow cells could be easily separated.

The work presented in Chapter 3 sets up the basis to further develop SIFT-MS as a potential technique in the diagnosis of leukaemia. The data obtained is now part of a

manuscript in preparation. However, it is obvious that further work is needed to assess the potential of SIFT-MS in the management of leukaemia, and more important, to better understand the metabolical pathways behind the release of VOCs by both leukaemia cells and blood cells.

Chapter 3 also set up the basis for Chapter 4. In the former, work was carried out to develop the experimental set up for VOCs analysis. This was then used to study the effects of drugs on leukaemia cells as described in Chapter 4.

The first aim of the study in Chapter 4 was to find out whether VOCs' analysis could have a role to assess the therapeutic response of leukaemia to drugs. For this purpose, Jurkat and K562 leukaemia cells were exposed to either Imatinib or Nilotinib and the release of VOCs was measured using SIFT-MS prior to and after the addition of the drugs. As in the previous chapter, the levels of acetaldehyde were measured both in cells cultured in the absence or in the presence of either drug. The results indicated that the release of VOCs from different cell lines varies following the addition of drugs. In fact, the levels of acetaldehyde released by K562 cell line increased following the addition of either Imatinib or Nilotinib while the levels of acetaldehyde remained similar for the Jurkat cell line. Therefore, it is obvious that the application of breath analysis in the management of cancer should not limit itself to studying one or a few VOCs, but rather a whole profile of VOCs. SIFT-MS has the possibility of analysing several VOCs at the same time using the full scan mode. Therefore, the VOCs profile of leukaemia cells prior to and after the addition of either imatinib or Nilotinib were studied in order to assess whether they could be used as biomarkers for therapeutic response of leukaemia. PCA of full scan data

was able to separate both cell lines but more importantly, it showed a difference between control cells and cells exposed to drugs at different drug concentrations. These data show promise as a tool to assess tumour response to treatment in a non-invasive way.

It is, however, important to recognise that while the *in vitro* studies can help to assess the potential of a new technique in clinical practice and are a necessary step in this process, the results obtained in a clinical set up might not be so straightforward. Several aspects need to be taken into account, one of them being sample collection. The way samples are collected and stored could affect the final results and its potential clinical application.

The work in Chapter 5 was carried out with this in mind so a better understanding of sample collection for SIFT-MS analysis could be achieved. This chapter complements the previous findings towards the translation of this novel technique (SIFT-MS) into clinics. At the same time, the data presented in this chapter is the first step towards *in vivo* breath analysis. The chapter was aimed at establishing a suitable methodology for the acquisition of breath samples from leukaemia patients. This study was also aimed at assessing the loss of VOCs during sample storage over time.

In this chapter three different sampling methods direct, Nalophan bags and Glass bottles were studied. We found that establishing a suitable sampling method was a real challenge with each sampling method having its own advantages and disadvantages.

The presence of humidity in the samples is crucial as it will affect the concentration of VOCs measured. Higher levels of humidity in the exhaled breath cause significant decrease in concentration for those VOCs that are highly soluble in water [Mochalski 2013]. The work presented in this chapter indicated that loss of humidity takes place even within one hour of breath acquisition in case of bags. However, the humidity of breath collected in bottles did not change markedly up to 24 hours storage. On the other hand, it has to be taken into account that depending upon the material of the bag, water vapours may diffuse in different proportions [Gilchrist 2012]. Background contamination and diffusion are the main problems of bags. Another factor that affects VOCs' concentration is temperature. As the temperature of the breath sample falls down below the body temperature (37 °C), water vapour may condense on the walls of the sample container, which could result in lower concentration of the more water soluble VOCS. Therefore, keeping the sample at 37 °C is an important step to avoid the risk of losing water-soluble VOCs.

One way to avoid this issue is through direct sampling. While this is the most convenient method to obtain breath samples, it also has its problems. Some patients, specially the elderly, might find difficult to breathe directly into the instrument due to the flow resistance inherent to the instrument. Also, not every patient will be able or exhale for a prolonged period of time.

The data presented in this chapter indicated that collecting breath in either bottles of bags allowed for a better identification of VOCs, especially those present in very low concentrations. Furthermore, this allows the storage and transport of breath samples,

an important point when carrying out studies involving different centres some of which might not be able to have the SIFT-MS instrument.

If bottles or bags are to be used in breath analysis, the next step is to assess how many exhalations are needed to get a reproducible sample. A single exhalation may not necessarily be representative of the alveolar air [Herbig 2008; O'Hara 2008; Filipiak 2012]. Multiple breaths are therefore preferable to reduce this risk. The work presented in this chapter indicated that there are no major differences in the VOCs measured between 3 or 5 exhalations.

There are other aspects of sampling which are of great debate among the scientific community and should be taken into account when running large multicentre studies. These include body posture of the subject during sampling, hyperventilation, control of the flow or volume of the breath during collection, sampling via nose or mouth, number of breaths exhaled, respiratory rate, and heart beat amongst other [Gilchrist 2012]. Furthermore, different body compartments produce a large variety of VOCs, a considerable part of which is found in the breath. Therefore, different diseases in patients could affect the VOCs released in breath. This is important when studying VOCs from patients with cancer as other metabolical processes and diseases could produce confounding factors. All these factors will need to be taken into account if this technique is to be taken into clinical practice.

Future work will need to refine the sampling methods, including finding some other material that could hold the VOCs for long periods during storage minimising the loss of trace gases. Storage temperature of the sample is also

another major point to be considered, as reducing the temperature of the samples below -80°C, for example, would slow down the loss of VOCs. Further work is needed to assess whether this could potentially decrease the overall loss of VOCs from the samples but how it might affect the measurement of VOCs by SIFT-MS when returning the sample to 37 °C.

In Chapter 6, S-FTIR microspectroscopy as a tool to study the spectral changes induced by drugs on clonal populations of leukaemia was used. The aim of the chapter was to characterize spectral biomarkers of leukaemia cells sensitivity/resistance to drugs. Whole cancer populations are composed of a combination of different cells sensitive and resistant to drugs and all the variation between them. Most studies aimed at characterising spectral markers of sensitivity/resistance to drugs have used whole cancer cell populations. This might make it more difficult to fully characterise these markers. This problem was approached in this chapter by obtaining cell clones and identifying those clones sensitive to a drug, those clones resistant to the same drug and those clones that were resistant to lower doses of the drug but sensitive to higher doses of the same drug.

Another problem on the study of the effects of drugs on cells using FTIR microspectroscopy is the fact that drugs cause not only biochemical changes but also morphological changes. Therefore, spectral biochemical changes have to be identified separately from the morphologically induced spectral changes. The ideal alternative in this work was to obtain S-FTIR spectra of sensitive and resistant cells to Imatinib or Nilotinib prior to adding the drug so neither biochemical nor morphological changes caused by the drug itself interfere with their S-FTIR spectra.

The data presented in Chapter 6 showed clear FTIR spectral changes in sensitive cells exposed to a drug when compared to the same clonal cells in the absence of the drug. More important, those clones resistant to the higher concentration of the drug also presented the same spectral changes albeit to a lower level. This is an important finding as it shows that the spectra of sensitive cells are obtained from those cells that have suffered damage by the drug but they were still alive (repairing the damage or not) when they were collected for S-FTIR analysis. More important, the data indicates that even in resistant clones, some cells will have suffered this damage and probably trying to repair it when they were collected for S-FTIR analysis.

The second aim of this chapter was to assess whether S-FTIR microspectroscopy can identify resistant and sensitive cells prior to drug exposure. In the present study, no major spectral differences between resistant and sensitive clones prior to the addition of the drug were seen. PCA might have shown some separation but it has to be taken into account that these were different clones. Therefore, it is not possible to say how much a difference is due to the fact that these are different clones and/or to some of them being sensitive to a drug while others are resistant. Further work is needed to better understand where exactly these differences lie.

The results of the present study have revealed that s-FTIR microspectroscopy has great potential to be used as an analytical method to assess tumor cell response to treatment. There are different mechanisms that cause resistance in cancer cells. Therefore, comprehensive studies should be carried out to better understand the onset and progression of cancer resistance to drugs. This work was carried out using a synchrotron, the next step is to carry out this work using benchtop spectrometers.

In Chapter 7 Raman Spectroscopy was used to assess the sensitivity and resistance of leukaemia cells to drugs and the consequences of culture conditions on the effects of drugs on leukaemia cells. Raman spectroscopy is a complementary technique to IR spectroscopy. As it was the case in the previous chapter, Raman spectroscopy could also identify changes in leukaemia cells cultured in the presence or absence of drugs.

The oxygenation levels of cancer cells can play a role in the resistance of these cells to drugs. In the case of leukaemia, cells circulate in both arterial and venous blood where the levels of oxygen vary. Furthermore, in advance stages, leukaemia cells might migrate to lymph nodes where, again, the levels of oxygen vary. Conventional cell culture *in-vitro* is performed at ambient oxygen concentration, Lukashev (2006), reported that changing oxygen concentrations can influence a broad range of pathways acting at the transcriptional level [Lukashev 2006]. Exact oxygen levels in *in vivo* conditions is unknown yet, only recent improvements have allowed its measurement *ex vivo* [Zhdanov 2008]. To assess this, leukaemia cells were incubated in 21% or 10% O_2. PCA provided certain degree of separation between clones incubated in 21% O_2 or 10% O_2. Furthermore, for sensitive clones, PCA was able to separate between cells incubated in 21% O_2 or 10% O_2. The separation was not so clear for resistant clones.

These data stress the importance of taking into account not only cell culture conditions but also the fact that leukaemia cells obtained from different compartments could produce different spectral results. It also stresses the need to understand those factors that even in a cloned cell line, could affect the spectral characteristics linked to drugs. Further work is needed to extend this knowledge.

8.1: Future work

This thesis has set up the basis to further develop SIFT-MS and vibrational spectroscopy into their potential applications in the management of leukaemia, i. e., improving diagnosis and assessing tumour response to treatment. The next step in SIFT-MS research would be to obtain the breath of patients with leukaemia and compare to age and sex matched controls (ethical approval will obviously be needed). Also, to obtain the breath of patients with leukaemia prior to and after treatment to assess whether it could identify tumour response to treatment in a fast-non-invasive way. This would help to clarify if this technique can make it into the clinics.

Vibrational spectroscopy has been used here to assess the effects of drugs on cloned leukaemia cells. The next step would be to obtain blood from patients with leukaemia and assess, following the addition of the drug, leukaemia cell sensitivity/resistance to a given drug or combination of drugs. These data could be obtained within few days and could be used to better tailor treatment to each individual patient. Further work is, however, needed to see whether this also applies to different drugs.

Reference:

- Adult Acute Myeloid Leukaemia Treatment, Sep 2015. [http://www.cancer.gov/types/leukemia/patient/adult-aml-treatment-pdq].
- Akyuz, S., Ozel, A.E., Balci, K., Akyuz, T., Çoker, A., Arisan, E.D., Palavan-Unsal, N. and Ozalpan, A., 2011. Raman micro-spectroscopic analysis of cultured HCT116 colon cancer cells in the presence of roscovitine. *Spectrochimica Acta Part A: Molecular and Biomolecular Spectroscopy*, *78*(5), pp.1540-1547.
- Agarwal, A., Ressler, D. and Snyder, G., 2015. The current and future state of companion diagnostics. *Pharmgenomics Pers Med*, *8*, pp.99-110.
- Amann, A. and Smith, D. eds., 2005. *Breath Analysis for Clinical Diagnosis and Therapeutic Monitoring:(With CD-ROM)*. World Scientific.
- Anderson, J.C. and Hlastala, M.P., 2007. Breath tests and airway gas exchange. *Pulmonary pharmacology & therapeutics*, *20*(2), pp.112-117.
- Atkuri, K.R., Herzenberg, L.A. and Herzenberg, L.A., 2005. Culturing at atmospheric oxygen levels impacts lymphocyte function. *Proceedings of the National Academy of Sciences of the United States of America*, *102*(10), pp.3756-3759.
- Atkuri, K.R., Herzenberg, L.A., Niemi, A.K., Cowan, T. and Herzenberg, L.A., 2007. Importance of culturing primary lymphocytes at physiological oxygen levels. *Proceedings of the National Academy of Sciences*, *104*(11), pp.4547-4552.
- Babrah, J., McCarthy, K., Lush, R.J., Rye, A.D., Bessant, C. and Stone, N., 2009. Fourier transform infrared spectroscopic studies of T-cell lymphoma, B-cell lymphoid and myeloid leukaemia cell lines. *Analyst*, *134*(4), pp.763-768.
- Bajtarevic, A., Ager, C., Pienz, M., Klieber, M., Schwarz, K., Ligor, M., Ligor, T., Filipiak, W., Denz, H., Fiegl, M. and Hilbe, W., 2009. Noninvasive detection of lung cancer by analysis of exhaled breath. *BMC cancer*, *9*(1), p.348.
- Baran, Y., Ceylan, C. and Camgoz, A., 2013. The roles of macromolecules in imatinib resistance of chronic myeloid leukemia cells by Fourier transform infrared spectroscopy. *Biomedicine & Pharmacotherapy*, *67*(3), pp.221-227.

- Bassan, P., Kohler, A., Martens, H., Lee, J., Byrne, H.J., Dumas, P., Gazi, E., Brown, M., Clarke, N. and Gardner, P., 2010. Resonant Mie scattering (RMieS) correction of infrared spectra from highly scattering biological samples. *Analyst*, *135*(2), pp.268-277.
- Bell, R.G. and Smith, H.W., 1949. CLINICAL TRIALS OF ANTABUSE. *Canadian Medical Association Journal*, *60*(3), p.286.
- Bellisola, G., Della Peruta, M., Vezzalini, M., Moratti, E., Vaccari, L., Birarda, G., Piccinini, M., Cinque, G. and Sorio, C., 2010. Tracking infrared signatures of drugs in cancer cells by Fourier transform microspectroscopy. *Analyst*, *135*(12), pp.3077-3086.
- Bellisola, G. and Sorio, C., 2012. Infrared spectroscopy and microscopy in cancer research and diagnosis. *Am J Cancer Res*, *2*(1), pp.1-21.
- Bellisola, G., Cinque, G., Vezzalini, M., Moratti, E., Silvestri, G., Redaelli, S., Passerini, C.G., Wehbe, K. and Sorio, C., 2013. Rapid recognition of drug-resistance/sensitivity in leukemic cells by Fourier transform infrared microspectroscopy and unsupervised hierarchical cluster analysis. *Analyst*, *138*(14), pp.3934-3945.
- Bellisola, G., Vittori, M.B., Cinque, G., Dumas, P., Fiorini, Z., Laudanna, C., Mirenda, M., Sandt, C., Silvestri, G., Tomasello, L. and Vezzalini, M., 2015. Unsupervised explorative data analysis of normal human leukocytes and BCR/ABL positive leukemic cells mid-infrared spectra. *Analyst*, *140*(13), pp.4407-4422.
- Benedetti, E., Vergamini, P. and Spremolla, G., 1988. FT-IR analysis of single human normal and leukemic lymphocytes. *Microchimica Acta*, *94*(1-6), pp.139-141.
- Bhayat, F., Das-Gupta, E., Smith, C., McKeever, T. and Hubbard, R., 2009. The incidence of and mortality from leukaemias in the UK: a general population-based study. *BMC cancer*, *9*(1), p.252.
- Blumenthal, R.D. and Goldenberg, D.M., 2007. Methods and goals for the use of in vitro and in vivo chemosensitivity testing. *Molecular biotechnology*, *35*(2), pp.185-197.
- Bone marrow biopsy online at [http://www.nlm.nih.gov/MEDLINEPLUS/ency/article/003934.htm].

- Buckmaster, R., Asphahani, F., Thein, M., Xu, J. and Zhang, M., 2009. Detection of drug-induced cellular changes using confocal Raman spectroscopy on patterned single-cell biosensors. *Analyst*, *134*(7), pp.1440-1446.
- Bumbea, H., Vladareanu, A.M., Voican, I., Cisleanu, D., Barsan, L. and Onisai, M., 2010. Chronic myeloid leukemia therapy in the era of tyrosine kinase inhibitors-the first molecular targeted treatment. *Journal of medicine and life*, *3*(2), p.162.
- Burke, J.R., Pattoli, M.A., Gregor, K.R., Brassil, P.J., MacMaster, J.F., McIntyre, K.W., Yang, X., Iotzova, V.S., Clarke, W., Strnad, J. and Qiu, Y., 2003. BMS-345541 is a highly selective inhibitor of IκB kinase that binds at an allosteric site of the enzyme and blocks NF-κB-dependent transcription in mice. *Journal of Biological Chemistry*, *278*(3), pp.1450-1456.
- Byrne, H.J., Ostrowska, K.M., Nawaz, H., Dorney, J., Meade, A.D., Bonnier, F. and Lyng, F.M., 2014. Vibrational spectroscopy: disease diagnostics and beyond. In *Optical Spectroscopy and Computational Methods in Biology and Medicine* (pp. 355-399). Springer Netherlands.
- Byrne, H., Sockalingum, G. and Stone, N., 2011. Raman microscopy: complement or competitor. RSC Analytical Spectroscopy; Pp. 105-142.
- Cakmak, G., Zorlu, F., Severcan, M. and Severcan, F., 2011. Screening of protective effect of amifostine on radiation-induced structural and functional variations in rat liver microsomal membranes by FT-IR spectroscopy. *Analytical chemistry*, *83*(7), pp.2438-2444.
- Caldwell, C.C., Kojima, H., Lukashev, D., Armstrong, J., Farber, M., Apasov, S.G. and Sitkovsky, M.V., 2001. Differential effects of physiologically relevant hypoxic conditions on T lymphocyte development and effector functions. *The Journal of Immunology*, *167*(11), pp.6140-6149.
- Campana, D. and Behm, F.G., 2000. Immunophenotyping of leukemia. *Journal of immunological methods*, *243*(1), pp.59-75.
- Cancer Stats childhood cancer Great Britain & UK. 2010. http://publications.cancerresearchuk.org/downloads/product/CS_CS_CHILDHOOD.pdf
- Cancer Research UK: UK Leukaemia Statistics. Cancer Stats, 2011 [http://www.cancerresearchuk.org/cancerinfo/cancerstats/types/leukaemia

/incidence/].

- Cancer research UK: Worldwide Cancer, 2014 [http://publications.cancerresearchuk.org/downloads/Product/CS_KF_WORLDWIDE.pdf].
- Cancer research UK: Cancer mortality for common cancer, 2014 [http://www.cancerresearchuk.org/health-professional/cancer-statistics/mortality/common-cancers-compared#heading-Three].
- Cancer Research UK: UK Leukaemia Statistics. Cancer Stats. 2011 [http://www.cancerresearchuk.org/cancerinfo/cancerstats/types/leukaemia/incidence/].
- Carswell, K.S., Weiss, J.W. and Papoutsakis, E.T., 2000. Low oxygen tension enhances the stimulation and proliferation of human T lymphocytes in the presence of IL-2. *Cytotherapy*, *2*(1), pp.25-37.
- Ceylan, C., Camgoz, A. and Baran, Y., 2012. Macromolecular changes in nilotinib resistant K562 cells; an in vitro study by Fourier transform infrared spectroscopy. *Technology in cancer research & treatment*, *11*(4), pp.333-344.
- Chan, J.W., Taylor, D.S., Zwerdling, T., Lane, S.M., Ihara, K. and Huser, T., 2006. Micro-Raman spectroscopy detects individual neoplastic and normal hematopoietic cells. *Biophysical journal*, *90*(2), pp.648-656.
- Chang, J.C., Wooten, E.C., Tsimelzon, A., Hilsenbeck, S.G., Gutierrez, M.C., Elledge, R., Mohsin, S., Osborne, C.K., Chamness, G.C., Allred, D.C. and O'Connell, P., 2003. Gene expression profiling for the prediction of therapeutic response to docetaxel in patients with breast cancer. *The Lancet*, *362*(9381), pp.362-369.
- Chen, G., Lin, X., Lin, D., Ge, X., Feng, S., Pan, J., Lin, J., Huang, Z., Huang, X. and Chen, R., 2016. Identification of different tumor states in nasopharyngeal cancer using surface-enhanced Raman spectroscopy combined with Lasso-PLS-DA algorithm. *RSC Advances*, *6*(10), pp.7760-7764.
- Chen, X., Xu, F., Wang, Y., Pan, Y., Lu, D., Wang, P., Ying, K., Chen, E. and Zhang, W., 2007. A study of the volatile organic compounds exhaled by lung cancer cells in vitro for breath diagnosis. *Cancer*, *110*(4), pp.835-844.
- Chi, J.T., Wang, Z., Nuyten, D.S., Rodriguez, E.H., Schaner, M.E., Salim, A., Wang, Y., Kristensen, G.B., Helland, A., Børresen-Dale, A.L. and Giaccia, A., 2006. van

de, Brown PO. *Gene expression programs in response to hypoxia: cell type specificity and prognostic significance in human cancers. PLoS Med*, *3*, p.e47.

- Chippendale, T.W., Hu, B., El Haj, A.J. and Smith, D., 2012. A study of enzymatic activity in cell cultures via the analysis of volatile biomarkers. *Analyst*, *137*(20), pp.4677-4685.
- Chippendale, T.W., 2012. *Volatile biomarkers emitted by cell cultures: headspace analysis using selected ion flow tube mass spectrometry, SIFT-MS* (Doctoral dissertation, PhD thesis, Keele University, 91-92).
- Chiriboga, L., Xie, P., Vigorita, V., Zarou, D., Zakim, D. and Diem, M., 1998. Infrared spectroscopy of human tissue. II. A comparative study of spectra of biopsies of cervical squamous epithelium and of exfoliated cervical cells. *Biospectroscopy*, *4*(1), pp.55-59.
- Chu, P., Clanton, D.J., Snipas, T.S., Lee, J., Mitchell, E., Nguyen, M.L., Hare, E. and Peach, R.J., 2009. Characterization of a subpopulation of colon cancer cells with stem cell-like properties. *International journal of cancer*, *124*(6), pp.1312-1321.
- Chute, J.P., Muramoto, G.G., Whitesides, J., Colvin, M., Safi, R., Chao, N.J. and McDonnell, D.P., 2006. Inhibition of aldehyde dehydrogenase and retinoid signaling induces the expansion of human hematopoietic stem cells. *Proceedings of the National Academy of Sciences*, *103*(31), pp.11707-11712.
- Clare, S.E., Neubauer, H., Schuetz, C., Kurek, R., Solomayer, E., Wallwiener, D., Dye, D.F., Zaleski, J.M., Goulet Jr, R.J. and Fehm, T., 2006. Raman spectroscopy to distinguish progression stages in breast cancer. *Journal of Clinical Oncology*, *24*(18_suppl), pp.10619-10619.
- Corradi, M., Poli, D., Banda, I., Bonini, S., Mozzoni, P., Pinelli, S., Alinovi, R., Andreoli, R., Ampollini, L., Casalini, A. and Carbognani, P., 2015. Exhaled breath analysis in suspected cases of non-small-cell lung cancer: a cross-sectional study. *Journal of breath research*, *9*(2), p.027101.
- Cree, I.A., 2009. Chemosensitivity and chemoresistance testing in ovarian cancer. *Current Opinion in Obstetrics and Gynecology*, *21*(1), pp.39-43.

- Crow, P., Uff, J.S., Farmer, J.A., Wright, M.P. and Stone, N., 2004. The use of Raman spectroscopy to identify and characterize transitional cell carcinoma in vitro. *BJU international*, *93*(9), pp.1232-1236.
- Croker, A.K., Goodale, D., Chu, J., Postenka, C., Hedley, B.D., Hess, D.A. and Allan, A.L., 2009. High aldehyde dehydrogenase and expression of cancer stem cell markers selects for breast cancer cells with enhanced malignant and metastatic ability. *Journal of cellular and molecular medicine*, *13*(8b), pp.2236-2252.
- Dartsch, D.C., Schaefer, A., Boldt, S., Kolch, W. and Marquardt, H., 2002. Comparison of anthracycline-induced death of human leukemia cells: programmed cell death versus necrosis. *Apoptosis*, *7*(6), pp.537-548.
- Davis, A.S., Viera, A.J. and Mead, M.D., 2014. Leukemia: an overview for primary care. *Am Fam Physician*, *89*(9), pp.731-738.
- De Gelder, J., De Gussem, K., Vandenabeele, P. and Moens, L., 2007. Reference database of Raman spectra of biological molecules. *Journal of Raman Spectroscopy*, *38*(9), pp.1133-1147.
- de Lacy Costello, B., Amann, A., Al-Kateb, H., Flynn, C., Filipiak, W., Khalid, T., Osborne, D. and Ratcliffe, N.M., 2014. A review of the volatiles from the healthy human body. *Journal of breath research*, *8*(1), p.014001.
- De Souza, N., 2007. Too much of a good thing. *Nature methods*, *4*(5), pp.386-387.
- Derevianko, A., D'amico, R. and Simms, H., 1996. Polymorphonuclear leucocyte (PMN)-derived inflammatory cytokines—regulation by oxygen tension and extracellular matrix. *Clinical & Experimental Immunology*, *106*(3), pp.560-567.
- Deng, C., Li, N. and Zhang, X., 2004. Development of headspace solid-phase microextraction with on-fiber derivatization for determination of hexanal and heptanal in human blood. *Journal of Chromatography B*, *813*(1), pp.47-52.
- Diem, M., Miljković, M., Bird, B., Chernenko, T., Schubert, J., Marcsisin, E., Mazur, A., Kingston, E., Zuser, E., Papamarkakis, K. and Laver, N., 2012. Applications of infrared and Raman microspectroscopy of cells and tissue in medical diagnostics: Present status and future promises. *Journal of Spectroscopy*, *27*(5-6), pp.463-496.

- Dimopoulos, M., Terpos, E., Comenzo, R.L., Tosi, P., Beksac, M., Sezer, O., Siegel, D., Lokhorst, H., Kumar, S., Rajkumar, S.V. and Niesvizky, R., 2009. International myeloma working group consensus statement and guidelines regarding the current role of imaging techniques in the diagnosis and monitoring of multiple Myeloma. *Leukemia*, *23*(9), pp.1545-1556.
- Di Natale, C., Macagnano, A., Martinelli, E., Paolesse, R., D'Arcangelo, G., Roscioni, C., Finazzi-Agrò, A. and D'Amico, A., 2003. Lung cancer identification by the analysis of breath by means of an array of non-selective gas sensors. *Biosensors and Bioelectronics*, *18*(10), pp.1209-1218.
- Diskin, A.M., Španěl, P. and Smith, D., 2003. Time variation of ammonia, acetone, isoprene and ethanol in breath: a quantitative SIFT-MS study over 30 days. *Physiological measurement*, *24*(1), p.107.
- Dogan, A., Ergen, K., Budak, F. and Severcan, F., 2007. Evaluation of disseminated candidiasis on an experimental animal model: a Fourier transform infrared study. *Applied spectroscopy*, *61*(2), pp.199-203.
- Döhner, H., Stilgenbauer, S., Benner, A., Leupolt, E., Kröber, A., Bullinger, L., Döhner, K., Bentz, M. and Lichter, P., 2000. Genomic aberrations and survival in chronic lymphocytic leukemia. *New England Journal of Medicine*, *343*(26), pp.1910-1916.
- Downes, A. and Elfick, A., 2010. Raman spectroscopy and related techniques in biomedicine. *Sensors*, *10*(3), pp.1871-1889.
- Draux, F., Jeannesson, P., Beljebbar, A., Tfayli, A., Fourre, N., Manfait, M., Sulé-Suso, J. and Sockalingum, G.D., 2009. Raman spectral imaging of single living cancer cells: a preliminary study. *Analyst*, *134*(3), pp.542-548.
- Draux, F., Gobinet, C., Sulé-Suso, J., Manfait, M., Jeannesson, P. and Sockalingum, G.D., 2011. Raman imaging of single living cells: probing effects of non-cytotoxic doses of an anti-cancer drug. *Analyst*, *136*(13), pp.2718-2725.
- Druker, B.J., Sawyers, C.L., Kantarjian, H., Resta, D.J., Reese, S.F., Ford, J.M., Capdeville, R. and Talpaz, M., 2001. Activity of a specific inhibitor of the BCR-ABL tyrosine kinase in the blast crisis of chronic myeloid leukemia and acute lymphoblastic leukemia with the Philadelphia chromosome. *New England Journal of Medicine*, *344*(14), pp.1038-1042.

- Druker, B.J., 2003, January. Imatinib alone and in combination for chronic myeloid leukemia. In *Seminars in hematology* (Vol. 40, No. 1, pp. 50-58). WB Saunders.
- Dubois, J. and Shaw, R.A., 2004. Peer Reviewed: IR Spectroscopy in Clinical and Diagnostic Applications. Anal. Chem. 76, 360A–367A.
- Dumas, P., Sockalingum, G.D. and Sule-Suso, J., 2007. Adding synchrotron radiation to infrared microspectroscopy: what's new in biomedical applications?. *Trends in biotechnology*, *25*(1), pp.40-44.
- Duester, G., 2000. Families of retinoid dehydrogenases regulating vitamin A function. *European Journal of Biochemistry*, *267*(14), pp.4315-4324.
- Dufer, J., Millot-Broguo, C., Hamed, Z.O., Lialtaud-Roger, F., Joly, P., Desplaces, A. and Jardillier, J.C., 1995. Nuclear DNA content and chromatin texture in multidrug-resistant human leukemic cell lines. *International journal of cancer*, *60*(1), pp.108-114.
- Ellis, D.I. and Goodacre, R., 2006. Metabolic fingerprinting in disease diagnosis: biomedical applications of infrared and Raman spectroscopy. *Analyst*, *131*(8), pp.875-885.
- Erba, H.P., 2011. Improving frontline treatment for chronic myeloid leukemia: emerging evidence for use of nilotinib and dasatinib. *Ann Arbor*, *1001*, p.48109.
- Fayed L. 2006. Diagnosing Leukemia How is Leukemia diagnosed? Fro http://cancer.about.com/od/leukemia/a/diagnoseleukemi.htm.
- Filipiak, W., Sponring, A., Mikoviny, T., Ager, C., Schubert, J., Miekisch, W., Amann, A. and Troppmair, J., 2008. Release of volatile organic compounds (VOCs) from the lung cancer cell line CALU-1 in vitro. *Cancer cell international*, *8*(1), p.17.
- Filipiak, W., Sponring, A., Filipiak, A., Ager, C., Schubert, J., Miekisch, W., Amann, A. and Troppmair, J., 2010. TD-GC-MS analysis of volatile metabolites of human lung cancer and normal cells in vitro. *Cancer Epidemiology and Prevention Biomarkers*, *19*(1), pp.182-195.
- Filipiak, W., Filipiak, A., Ager, C., Wiesenhofer, H. and Amann, A., 2012. Optimization of sampling parameters for collection and preconcentration of alveolar air by needle traps. *Journal of breath research*, *6*(2), p.027107.

- Ferraro-Peyret, C., Quemeneur, L., Flacher, M., Revillard, J.P. and Genestier, L., 2002. Caspase-independent phosphatidylserine exposure during apoptosis of primary T lymphocytes. *The Journal of Immunology*, *169*(9), pp.4805-4810.
- Friesen, C., Fulda, S. and Debatin, K.M., 1999. Cytotoxic drugs and the CD95 pathway. *Leukemia*, *13*, pp.1854-1858.
- FTIR gas analysis: An online primer. Online at: http://www.gascell.com/htmls/primer.htm
- Fu, D., Zhou, J., Zhu, W.S., Manley, P.W., Wang, Y.K., Hood, T., Wylie, A. and Xie, X.S., 2014. Imaging the intracellular distribution of tyrosine kinase inhibitors in living cells with quantitative hyperspectral stimulated Raman scattering. *Nature chemistry*, *6*(7), pp.614-622.
- Fuchs, P., Loeseken, C., Schubert, J.K. and Miekisch, W., 2010. Breath gas aldehydes as biomarkers of lung cancer. *International Journal of Cancer*, *126*(11), pp.2663-2670.
- Gaigneaux, A., Ruysschaert, J.M. and Goormaghtigh, E., 2002. Infrared spectroscopy as a tool for discrimination between sensitive and multiresistant K562 cells. *European journal of biochemistry*, *269*(7), pp.1968-1973.
- Gambacorti-Passerini, C., Kantarjian, H.M., Kim, D.W., Khoury, H.J., Turkina, A.G., Brümmendorf, T.H., Matczak, E., Bardy-Bouxin, N., Shapiro, M., Turnbull, K. and Leip, E., 2015. Long-term efficacy and safety of bosutinib in patients with advanced leukemia following resistance/intolerance to imatinib and other tyrosine kinase inhibitors. *American journal of hematology*, *90*(9), pp.755-768.
- Gambacorti-Passerini, C. and Piazza, R., 2015. How I treat newly diagnosed chronic myeloid leukemia in 2015. *American journal of hematology*, *90*(2), pp.156-161.
- Gamen, S., Anel, A., Pérez-Galán, P., Lasierra, P., Johnson, D., Piñeiro, A. and Naval, J., 2000. Doxorubicin treatment activates a Z-VAD-sensitive caspase, which causes ΔΨm loss, caspase-9 activity, and apoptosis in Jurkat cells. *Experimental cell research*, *258*(1), pp.223-235.
- Garaycoechea, J.I., Crossan, G.P., Langevin, F., Daly, M., Arends, M.J. and Patel, K.J., 2012. Genotoxic consequences of endogenous aldehydes on mouse haematopoietic stem cell function. *Nature*, *489*(7417), pp.571-575.

- Gault, N. and Lefaix, J.L., 2003. Infrared microspectroscopic characteristics of radiation-induced apoptosis in human lymphocytes. *Radiation research*, *160*(2), pp.238-250.
- George, E.N., Eriksson, J.E., Marianne, W.E.I.S. and ORRENIUS, S., 1996. Chromatin condensation during apoptosis requires ATP. *Biochemical Journal*, *318*(3), pp.749-752.
- Gerber, J.M., Smith, B.D., Ngwang, B., Zhang, H., Vala, M.S., Morsberger, L., Galkin, S., Collector, M.I., Perkins, B., Levis, M.J. and Griffin, C.A., 2012. A clinically relevant population of leukemic CD34+ CD38-cells in acute myeloid leukemia. *Blood*, pp.blood-2011.
- Gilchrist, F.J., Razavi, C., Webb, A.K., Jones, A.M., Španěl, P., Smith, D. and Lenney, W., 2012. An investigation of suitable bag materials for the collection and storage of breath samples containing hydrogen cyanide. *Journal of breath research*, *6*(3), p.036004.
- Godet, C., Elsendoorn, A. and Roblot, F., 2012. Benefit of CT scanning for assessing pulmonary disease in the immunodepressed patient. *Diagnostic and interventional imaging*, *93*(6), pp.425-430.
- Golemovic, M., Verstovsek, S., Giles, F., Cortes, J., Manshouri, T., Manley, P.W., Mestan, J., Dugan, M., Alland, L., Griffin, J.D. and Arlinghaus, R.B., 2005. AMN107, a novel aminopyrimidine inhibitor of Bcr-Abl, has in vitro activity against imatinib-resistant chronic myeloid leukemia. *Clinical Cancer Research*, *11*(13), pp.4941-4947.
- Gorre, M.E., Mohammed, M., Ellwood, K., Hsu, N., Paquette, R., Rao, P.N. and Sawyers, C.L., 2001. Clinical resistance to STI-571 cancer therapy caused by BCR-ABL gene mutation or amplification. *Science*, *293*(5531), pp.876-880.
- Gremel, G., Grannas, K., Sutton, L.A., Pontén, F. and Zieba, A., 2013. In situ protein detection for companion diagnostics. Front Oncol; 3: 271.
- Grills, D.C., Farrington, J.A., Layne, B.H., Preses, J.M., Bernstein, H.J. and Wishart, J.F., 2015. Development of nanosecond time-resolved infrared detection at the LEAF pulse radiolysis facility. *Review of Scientific Instruments*, *86*(4), p.044102.
- Groves, W.A. and Zellers, E.T., 1996. Investigation of organic vapor losses to condensed water vapor in Tedlar® bags used for exhaled-breath sampling. *American Industrial Hygiene Association*, *57*(3), pp.257-263.

- Guilhot, F., 2004. Sustained durability of responses plus high rates of cytogenetic responses result in long-term benefit for newly diagnosed chronic-phase chronic myeloid leukemia (CML-CP) treated with imatinib (IM) therapy: update from the IRIS Study. *Blood*, *104*(11), pp.21-21.
- Guo, J., Cai, W., Du, B., Qian, M. and Sun, Z., 2009. Raman spectroscopic investigation on the interaction of malignanthepatocytes with doxorubicin. *Biophysical chemistry*, *140*(1), pp.57-61.
- Haddad, H., Windgassen, D., Ramsborg, C.G., Paredes, C.J. and Papoutsakis, E.T., 2004. Molecular understanding of oxygen-tension and patient-variability effects on ex vivo expanded T cells. *Biotechnology and bioengineering*, *87*(4), pp.437-450.
- Hakim, M., Broza, Y.Y., Barash, O., Peled, N., Phillips, M., Amann, A. and Haick, H., 2012. Volatile organic compounds of lung cancer and possible biochemical pathways. *Chemical reviews*, *112*(11), pp.5949-5966.
- Harreveld, A.P.T.V., 2003. Odor concentration decay and stability in gas sampling bags. *Journal of the Air & Waste Management Association*, *53*(1), pp.51-60.
- Hengartner, M.O., 2000. The biochemistry of apoptosis. *Nature*, *407*(6805), pp.770-776.
- Herbig, J., Titzmann, T., Beauchamp, J., Kohl, I. and Hansel, A., 2008. Buffered end-tidal (BET) sampling—a novel method for real-time breath-gas analysis. *Journal of breath research*, *2*(3), p.037008.
- Hess, D.A., Wirthlin, L., Craft, T.P., Herrbrich, P.E., Hohm, S.A., Lahey, R., Eades, W.C., Creer, M.H. and Nolta, J.A., 2006. Selection based on CD133 and high aldehyde dehydrogenase activity isolates long-term reconstituting human hematopoietic stem cells. *Blood*, *107*(5), pp.2162-2169.
- Hochhaus, A., Kreil, S., Corbin, A.S., La Rosee, P., Müller, M.C., Lahaye, T., Hanfstein, B., Schoch, C., Cross, N.C.P., Berger, U. and Gschaidmeier, H., 2002. Molecular and chromosomal mechanisms of resistance to imatinib (STI571) therapy. *Leukemia*, *16*(11), p.2190.
- Holman, H.Y.N., Martin, M.C., Blakely, E.A., Bjornstad, K. and McKinney, W.R., 2000. IR spectroscopic characteristics of cell cycle and cell death probed by

synchrotron radiation based Fourier transform IR spectromicroscopy. *Biopolymers*, *57*(6), pp.329-335.

- Huang, Z., McWilliams, A., Lui, H., McLean, D.I., Lam, S. and Zeng, H., 2003. Near-infrared Raman spectroscopy for optical diagnosis of lung cancer. *International journal of cancer*, *107*(6), pp.1047-1052.
- Imatinib (Glivec®). [online]. http://www.nhs.uk/ipgmedia/National/Macmillan%20Cancer%20Support/assets/ImatinibMCS3pages.pdf
- Incident of childhood leukaemia. [http://www.euro.who.int/__data/assets/pdf_file/0005/97016/4.1.-Incidence-of-childhood-leukaemia-EDITED_layouted.pdf].
- Jackson, M., Kim, K., Tetteh, J., Mansfield, J.R., Dolenko, B., Somorjai, R.L., Orr, F.W., Watson, P.H. and Mantsch, H.H., 1998, April. Cancer diagnosis by infrared spectroscopy: methodological aspects. In *BiOS'98 International Biomedical Optics Symposium* (pp. 24-34). International Society for Optics and Photonics.
- Jackson, M., Ramjiawan, B., Hewko, M. and Mantsch, H.H., 1998. Infrared microscopic functional group mapping and spectral clustering analysis of hypercholesterolemic rabbit liver. *Cellular and molecular biology (Noisy-le-Grand, France)*, *44*(1), pp.89-98.
- Jackson, M., Mansfield, J.R., Dolenko, B., Somorjai, R.L., Mantsch, H.H. and Watson, P.H., 1998. Classification of breast tumors by grade and steroid receptor status using pattern recognition analysis of infrared spectra. *Cancer detection and prevention*, *23*(3), pp.245-253.
- Johnson, V.L., Ko, S.C., Holmstrom, T.H., Eriksson, J.E. and Chow, S.C., 2000. Effector caspases are dispensable for the early nuclear morphological changes during chemical-induced apoptosis. *J Cell Sci*, *113*(17), pp.2941-2953.
- Jones, A.W., 1995. Measuring and reporting the concentration of acetaldehyde in human breath. *Alcohol and alcoholism*, *30*(3), pp.271-285.
- Kantarjian, H.M., Hochhaus, A., Saglio, G., De Souza, C., Flinn, I.W., Stenke, L., Goh, Y.T., Rosti, G., Nakamae, H., Gallagher, N.J. and Hoenekopp, A., 2011. Nilotinib versus imatinib for the treatment of patients with newly diagnosed chronic phase, Philadelphia chromosome-positive, chronic myeloid leukaemia:

24-month minimum follow-up of the phase 3 randomised ENESTnd trial. *The lancet oncology*, *12*(9), pp.841-851.

- Kawai, T., Kawakami, K., Kataoka, M., Itoi, T., Takei, K., Moriyasu, F., Takagi, Y., Aoki, T., Serizawa, H., Rimbard, E. and Noguchi, N., 2007. A study of the relationship between Helicobacter pylori microbial susceptibility, 13C-urea breath test values. *Hepato-gastroenterology*, *55*(82-83), pp.786-790.
- Kawamoto, H. and Minato, N., 2004. Myeloid cells. *The international journal of biochemistry & cell biology*, *36*(8), pp.1374-1379.
- Kay, A.G., Dale, T.P., Akram, K.M., Mohan, P., Hampson, K., Maffulli, N., Spiteri, M.A., El Haj, A.J. and Forsyth, N.R., 2015. BMP2 repression and optimized culture conditions promote human bone marrow-derived mesenchymal stem cell isolation. *Regenerative medicine*, *10*(2), pp.109-125.
- Keung, W.M. and Vallee, B.L., 1993. Daidzin: a potent, selective inhibitor of human mitochondrial aldehyde dehydrogenase. *Proceedings of the National Academy of Sciences*, *90*(4), pp.1247-1251.
- Kharitonov, S.A., Yates, D., Robbins, R.A., Barnes, P.J., Logan-Sinclair, R. and Shinebourne, E.A., 1994. Increased nitric oxide in exhaled air of asthmatic patients. *The Lancet*, *343*(8890), pp.133-135.
- Kim, H.H., Joo, H., Kim, T.H., Kim, E.Y., Park, S.J., Park, J.K. and Kim, H.J., 2009. The mitochondrial Warburg effect: a cancer enigma. *Interdisciplinary Bio Central*, *1*(2), pp.7-1.
- Kim, S.K., Kim, H., Lee, D.H., Kim, T.S., Kim, T., Chung, C., Koh, G.Y., Kim, H. and Lim, D.S., 2013. Reversing the intractable nature of pancreatic cancer by selectively targeting ALDH-high, therapy-resistant cancer cells. *PloS one*, *8*(10), p.e78130.
- Kimball JW. 1999. “Chronic Myelogenous Leukemia (CML)”. http://www.ultranet.com/~jkimball/BiologyPages/C/CML.html
- Kocjan, G., Chandra, A., Cross, P., Denton, K., Giles, T., Herbert, A., Smith, P., Remedios, D. and Wilson, P., 2009. BSCC Code of Practice–fine needle aspiration cytology. *Cytopathology*, *20*(5), pp.283-296.
- Krafft, C. and Sergo, V., 2006. Biomedical applications of Raman and infrared spectroscopy to diagnose tissues. *Journal of Spectroscopy*, *20*(5-6), pp.195-218.

- Krieger, J.A., Landsiedel, J.C. and Lawrence, D.A., 1996. Differential in vitro effects of physiological and atmospheric oxygen tension on normal human peripheral blood mononuclear cell proliferation, cytokine and immunoglobulin production. *International journal of immunopharmacology*, *18*(10), pp.545-552.
- Krishna, C.M., Kegelaer, G., Adt, I., Rubin, S., Kartha, V.B., Manfait, M. and Sockalingum, G.D., 2006. Combined Fourier transform infrared and Raman spectroscopic approach for identification of multidrug resistance phenotype in cancer cell lines. *Biopolymers*, *82*(5), pp.462-470.
- Kneipp, J., Schut, T.B., Kliffen, M., Menke-Pluijmers, M. and Puppels, G., 2003. Characterization of breast duct epithelia: a Raman spectroscopic study. *Vibrational spectroscopy*, *32*(1), pp.67-74.
- Kumar, S., Huang, J., Abbassi-Ghadi, N., Španěl, P., Smith, D. and Hanna, G.B., 2013. Selected ion flow tube mass spectrometry analysis of exhaled breath for volatile organic compound profiling of esophago-gastric cancer. *Analytical chemistry*, *85*(12), pp.6121-6128.
- Kushch, I., Schwarz, K., Schwentner, L., Baumann, B., Dzien, A., Schmid, A., Unterkofler, K., Gastl, G., Španěl, P., Smith, D. and Amann, A., 2008. Compounds enhanced in a mass spectrometric profile of smokers' exhaled breath versus non-smokers as determined in a pilot study using PTR-MS. *Journal of breath research*, *2*(2), p.026002.
- La Rosée, P., Corbin, A.S., Stoffregen, E.P., Deininger, M.W. and Druker, B.J., 2002. Activity of the Bcr-Abl kinase inhibitor PD180970 against clinically relevant Bcr-Abl isoforms that cause resistance to imatinib mesylate (Gleevec, STI571). *Cancer research*, *62*(24), pp.7149-7153.
- Lachenmeier, D.W., Kanteres, F. and Rehm, J., 2009. Carcinogenicity of acetaldehyde in alcoholic beverages: risk assessment outside ethanol metabolism. *Addiction*, *104*(4), pp.533-550.
- Larbi, A., Cabreiro, F., Zelba, H., Marthandan, S., Combet, E., Friguet, B., Petropoulos, I., Barnett, Y. and Pawelec, G., 2010. Reduced oxygen tension results in reduced human T cell proliferation and increased intracellular oxidative damage and susceptibility to apoptosis upon activation. *Free Radical Biology and Medicine*, *48*(1), pp.26-34.

- Lavie, Y., Fiucci, G., Czarny, M. and Liscovitch, M., 1999. Changes in membrane microdomains and caveolae constituents in multidrug-resistant cancer cells. *Lipids*, *34*, pp.S57-S63.
- Le Gal, J.M., Morjani, H. and Manfait, M., 1993. Ultrastructural appraisal of the multidrug resistance in K562 and LR73 cell lines from Fourier transform infrared spectroscopy. *Cancer research*, *53*(16), pp.3681-3686.
- Leukemia Types, Causes, Symptoms, Treatment, Prevention. Online at [http://www.lloydhealthcare.org/leukemia-types-causes-symptoms-treatment-prevention/#].
- Lexicon of some useful terms online at [http://nrumiano.free.fr/PagesU/Elexique.html].
- Ligor, T., Ligor, M., Amann, A., Ager, C., Bachler, M., Dzien, A. and Buszewski, B., 2008. The analysis of healthy volunteers' exhaled breath by the use of solid-phase microextraction and GC-MS. *Journal of breath research*, *2*(4), p.046006.
- Lin, J., Haffner, M.C., Zhang, Y., Lee, B.H., Brennen, W.N., Britton, J., Kachhap, S.K., Shim, J.S., Liu, J.O., Nelson, W.G. and Yegnasubramanian, S., 2011. Disulfiram is a DNA demethylating agent and inhibits prostate cancer cell growth. *The Prostate*, *71*(4), pp.333-343.
- Lindinger, W., Hansel, A. and Jordan, A., 1998. On-line monitoring of volatile organic compounds at pptv levels by means of proton-transfer-reaction mass spectrometry (PTR-MS) medical applications, food control and environmental research. *International Journal of Mass Spectrometry and Ion Processes*, *173*(3), pp.191-241.
- Liu, C.Y., Wang, C.H., Chen, T.C., Lin, H.C., Yu, C.T. and Kuo, H.P., 1998. Increased level of exhaled nitric oxide and up-regulation of inducible nitric oxide synthase in patients with primary lung cancer. *British journal of cancer*, *78*(4), p.534.
- Liu, K.Z. and Mantsch, H.H., 2001. Apoptosis-induced structural changes in leukemia cells identified by IR spectroscopy. *Journal of Molecular Structure*, *565*, pp.299-304.
- Liu, M.J., Wang, Z., Wu, R.C., Sun, S.Q. and Wu, Q.Y., 2003. Monitoring all-trans-retinoic acid-induced differentiation of human acute promyelocytic leukemia

NB4 cells by Fourier-transform infrared spectroscopy. *Leukemia*, *17*(8), pp.1670-1670.

- Lourenço, C. and Turner, C., 2014. Breath analysis in disease diagnosis: methodological considerations and applications. *Metabolites*, *4*(2), pp.465-498.
- Lukashev, D., Klebanov, B., Kojima, H., Grinberg, A., Ohta, A., Berenfeld, L., Wenger, R.H., Ohta, A. and Sitkovsky, M., 2006. Cutting edge: hypoxia-inducible factor 1α and its activation-inducible short isoform I. 1 negatively regulate functions of CD4+ and CD8+ T lymphocytes. *The Journal of Immunology*, *177*(8), pp.4962-4965.
- Lyman, D.J. and Murray–Wijelath, J., 1999. Vascular graft healing: I. FTIR analysis of an implant model for studying the healing of a vascular graft. *Journal of Biomedical Materials Research Part A*, *48*(2), pp.172-186.
- Lyng, F.M., Faoláin, E.Ó., Conroy, J., Meade, A.D., Knief, P., Duffy, B., Hunter, M.B., Byrne, J.M., Kelehan, P. and Byrne, H.J., 2007. Vibrational spectroscopy for cervical cancer pathology, from biochemical analysis to diagnostic tool. *Experimental and molecular pathology*, *82*(2), pp.121-129.
- Lyng, F.M., Ramos, I.R., Ibrahim, O. and Byrne, H.J., 2015. Vibrational Microspectroscopy for Cancer Screening. *Applied Sciences*, *5*(1), pp.23-35.
- Maeda, K., Alessio, R.C. and Hawley, R.C., 1993. Recent advances in diagnosis of leukemia. *Japanese journal of clinical oncology*, *23*(2), pp.79-84.
- Machana, S., Weerapreeyakul, N., Barusrux, S., Thumanu, K. and Tanthanuch, W., 2012. FTIR microspectroscopy discriminates anticancer action on human leukemic cells by extracts of Pinus kesiya; Cratoxylum formosum ssp. pruniflorum and melphalan. *Talanta*, *93*, pp.371-382.
- Mahadevan-Jansen, A., Mitchell, M.F., Ramanujamf, N., Malpica, A., Thomsen, S., Utzinger, U. and Richards-Kortumt, R., 1998. Near-Infrared Raman Spectroscopy for In Vitro Detection of Cervical Precancers. *Photochemistry and photobiology*, *68*(1), pp.123-132.
- Marcato, P., Dean, C.A., Giacomantonio, C.A. and Lee, P.W., 2011. Aldehyde dehydrogenase: its role as a cancer stem cell marker comes down to the specific isoform. *Cell cycle*, *10*(9), pp.1378-1384.
- Mannechez, A., Reungpatthanaphong, P., de Certaines, J.D., Leray, G. and Le Moyec, L., 2005. Proton NMR visible mobile lipid signals in sensitive and

multidrug-resistant K562 cells are modulated by rafts. *Cancer cell international*, *5*(1), p.2.

- Manoharan, R., Baraga, J.J., Rava, R.P., Dasari, R.R., Fitzmaurice, M. and Feld, M.S., 1993. Biochemical analysis and mapping of atherosclerotic human artery using FT-IR microspectroscopy. *Atherosclerosis*, *103*(2), pp.181-193.
- Masters, J.R. and Stacey, G.N., 2007. Changing medium and passaging cell lines. *Nature protocols*, *2*(9), pp.2276-2284.
- Matthews, Q., Jirasek, A., Lum, J.J. and Brolo, A.G., 2011. Biochemical signatures of in vitro radiation response in human lung, breast and prostate tumour cells observed with Raman spectroscopy. *Physics in medicine and biology*, *56*(21), p.6839-6855.
- Mazzone, P.J., 2008. Analysis of volatile organic compounds in the exhaled breath for the diagnosis of lung cancer. *Journal of Thoracic Oncology*, *3*(7), pp.774-780.
- Melin, A.M., Perromat, A. and Déléris, G., 2000. Pharmacologic application of Fourier transform IR spectroscopy: in vivo toxicity of carbon tetrachloride on rat liver. *Biopolymers*, *57*(3), pp.160-168.
- Michalčíková, R.B. and Španěl, P., 2014. A selected ion flow tube study of the ion molecule association reactions of protonated (MH+), nitrosonated (MNO+) and dehydroxidated (M− OH)+ carboxylic acids (M) with H 2 O. *International Journal of Mass Spectrometry*, *368*, pp.15-22.
- Miller, L.M. and Dumas, P., 2006. Chemical imaging of biological tissue with synchrotron infrared light. *Biochimica et Biophysica Acta (BBA)-Biomembranes*, *1758*(7), pp.846-857.
- Min, Y.K., Yamamoto, T., Kohda, E., Ito, T. and Hamaguchi, H.O., 2005. 1064 nm near-infrared multichannel Raman spectroscopy of fresh human lung tissues. *Journal of Raman Spectroscopy*, *36*(1), pp.73-76.
- Mochalski, P., Wzorek, B., Śliwka, I. and Amann, A., 2009. Suitability of different polymer bags for storage of volatile sulphur compounds relevant to breath analysis. *Journal of Chromatography B*, *877*(3), pp.189-196.
- Mochalski, P., King, J., Unterkofler, K. and Amann, A., 2013. Stability of selected volatile breath constituents in Tedlar, Kynar and Flexfilm sampling bags. *Analyst*, *138*(5), pp.1405-1418.

- Moore, M.W., Babu, D. and Cotter, P.D., 2012. Challenges in the codevelopment of companion diagnostics. *Personalized Medicine*, *9*(5), pp.485-496.
- Moritz, T.J., Taylor, D.S., Krol, D.M., Fritch, J. and Chan, J.W., 2010. Detection of doxorubicin-induced apoptosis of leukemic T-lymphocytes by laser tweezers Raman spectroscopy. *Biomedical optics express*, *1*(4), pp.1138-1147.
- Moreb, J.S., Ucar, D., Han, S., Amory, J.K., Goldstein, A.S., Ostmark, B. and Chang, L.J., 2012. The enzymatic activity of human aldehyde dehydrogenases 1A2 and 2 (ALDH1A2 and ALDH2) is detected by Aldefluor, inhibited by diethylaminobenzaldehyde and has significant effects on cell proliferation and drug resistance. *Chemico-biological interactions*, *195*(1), pp.52-60.
- Movasaghi, Z., Rehman, S. and Rehman, I.U., 2007. Raman spectroscopy of biological tissues. *Applied Spectroscopy Reviews*, *42*(5), pp.493-541.
- Movasaghi, Z., Rehman, S. and ur Rehman, D.I., 2008. Fourier transform infrared (FTIR) spectroscopy of biological tissues. *Applied Spectroscopy Reviews*, *43*(2), pp.134-179.
- Navaneethan, U., Parsi, M.A., Gutierrez, N.G., Bhatt, A., Venkatesh, P.G., Lourdusamy, D., Grove, D., Hammel, J.P., Jang, S., Sanaka, M.R. and Stevens, T., 2014. Volatile organic compounds in bile can diagnose malignant biliary strictures in the setting of pancreatic cancer: a preliminary observation. *Gastrointestinal endoscopy*, *80*(6), pp.1038-1045.
- Nechushtan, H., Hamamreh, Y., Nidal, S., Gotfried, M., Baron, A., Shalev, Y.I., Nisman, B., Peretz, T. and Peylan-Ramu, N., 2015. A phase IIb trial assessing the addition of disulfiram to chemotherapy for the treatment of metastatic non-small cell lung cancer. *The oncologist*, *20*(4), pp.366-367.
- Neviliappan, S., Kan, L.F., Walter, T.T.L., Arulkumaran, S. and Wong, P.T.T., 2002. Infrared spectral features of exfoliated cervical cells, cervical adenocarcinoma tissue, and an adenocarcinoma cell line (SiSo). *Gynecologic oncology*, *85*(1), pp.170-174.
- Newby, D., Marks, L. and Lyall, F., 2005. Dissolved oxygen concentration in culture medium: assumptions and pitfalls. *Placenta*, *26*(4), pp.353-357.
- Newson DL. 2011. Acute Myeloid Leukaemia. From [http://www.patient.co.uk/health/Leukaemia-Acute-Myeloid.htm].

- Niepel, M., Spencer, S.L. and Sorger, P.K., 2009. Non-genetic cell-to-cell variability and the consequences for pharmacology. *Current opinion in chemical biology*, *13*(5), pp.556-561.
- von Bubnoff, N., Manley, P.W., Mestan, J., Sanger, J., Peschel, C. and Duyster, J., 2006. Bcr-Abl resistance screening predicts a limited spectrum of point mutations to be associated with clinical resistance to the Abl kinase inhibitor nilotinib (AMN107). *Blood*, *108*(4), pp.1328-1333.
- Normal production of blood cells online at [https://ghr.nlm.nih.gov/art/large/bone-anatomy-blood-cells.jpeg].
- Notingher, I., 2007. Raman spectroscopy cell-based biosensors. *Sensors*, *7*(8), pp.1343-1358.
- Notter, R.H. ed., 2000. *Lung surfactants: basic science and clinical applications*. CRC Press.
- Ochs, M., Nyengaard, J.R., Jung, A., Knudsen, L., Voigt, M., Wahlers, T., Richter, J. and Gundersen, H.J.G., 2004. The number of alveoli in the human lung. *American journal of respiratory and critical care medicine*, *169*(1), pp.120-124.
- O'hara, M.E., O'Hehir, S., Green, S. and Mayhew, C.A., 2008. Development of a protocol to measure volatile organic compounds in human breath: a comparison of rebreathing and on-line single exhalations using proton transfer reaction mass spectrometry. *Physiological Measurement*, *29*(3), p.309.
- Offline, N.O., 1999. Recommendations for standardized procedures for the online and offline measurement of exhaled lower respiratory nitric oxide and nasal nitric oxide in adults and children—1999. *Am. J. Respir. Crit. Care Med*, *160*, pp.2104-2117.
- Olsen, D. and Jørgensen, J.T., 2014. Companion diagnostics for targeted cancer drugs–clinical and regulatory aspects. *Drug-Diagnostics Co-Development in Oncology*, p.8.
- Onyango, A.N., 2012. Small reactive carbonyl compounds as tissue lipid oxidation products; and the mechanisms of their formation thereby. *Chemistry and physics of lipids*, *165*(7), pp.777-786.

- Owen, C.A., Selvakumaran, J., Notingher, I., Jell, G., Hench, L.L. and Stevens, M.M., 2006. In vitro toxicology evaluation of pharmaceuticals using Raman micro-spectroscopy. *Journal of cellular biochemistry*, *99*(1), pp.178-186.
- Pietarinen, P.O., Pemovska, T., Kontro, M., Yadav, B., Mpindi, J.P., Andersson, E.I., Majumder, M.M., Kuusanmäki, H., Koskenvesa, P., Kallioniemi, O. and Wennerberg, K., 2015. Novel drug candidates for blast phase chronic myeloid leukemia from high-throughput drug sensitivity and resistance testing. *Blood cancer journal*, *5*(5), p.e309.
- Palonpon, A.F., Sodeoka, M. and Fujita, K., 2013. Molecular imaging of live cells by Raman microscopy. *Current opinion in chemical biology*, *17*(4), pp.708-715.
- Pascut, F.C., Kalra, S., George, V., Welch, N., Denning, C. and Notingher, I., 2013. Non-invasive label-free monitoring the cardiac differentiation of human embryonic stem cells in-vitro by Raman spectroscopy. *Biochimica et Biophysica Acta (BBA)-General Subjects*, *1830*(6), pp.3517-3524.
- Patti, G.J., Yanes, O. and Siuzdak, G., 2012. Innovation: Metabolomics: the apogee of the omics trilogy. *Nature reviews Molecular cell biology*, *13*(4), pp.263-269.
- Pearce, D.J., Taussig, D., Simpson, C., Allen, K., Rohatiner, A.Z., Lister, T.A. and Bonnet, D., 2005. Characterization of cells with a high aldehyde dehydrogenase activity from cord blood and acute myeloid leukemia samples. *Stem cells*, *23*(6), pp.752-760.
- Peggs, K. and Mackinnon, S., 2003. Imatinib mesylate-the new gold standard for treatment of chronic myeloid leukemia. *New England Journal of Medicine*, *348*(11), pp.1048-1048.
- Phillips, M., Greenberg, J. and Sabas, M., 1994. Alveolar gradient of pentane in normal human breath. *Free radical research*, *20*(5), pp.333-337.
- Phillips, M., Herrera, J., Krishnan, S., Zain, M., Greenberg, J. and Cataneo, R.N., 1999. Variation in volatile organic compounds in the breath of normal humans. *Journal of Chromatography B: Biomedical Sciences and Applications*, *729*(1), pp.75-88.
- Phillips, M., Gleeson, K., Hughes, J. M. B., Greenberg, J., Cataneo, R. N., Baker, L., & McVay, W. P. (1999). Volatile organic compounds in breath as markers of lung cancer: a cross-sectional study. *The Lancet*, *353*(9168), 1930-1933.

- Phillips, M., Cataneo, R.N., Cummin, A.R., Gagliardi, A.J., Gleeson, K., Greenberg, J., Maxfield, R.A. and Rom, W.N., 2003. Detection of lung cancer with volatile markers in the breath. *Chest Journal*, *123*(6), pp.2115-2123.
- Phillips, M., Altorki, N., Austin, J.H., Cameron, R.B., Cataneo, R.N., Greenberg, J., Kloss, R., Maxfield, R.A., Munawar, M.I., Pass, H.I. and Rashid, A., 2007. Prediction of lung cancer using volatile biomarkers in breath1. *Cancer biomarkers*, *3*(2), pp.95-109.
- Pijanka, J.K., Kohler, A., Yang, Y., Dumas, P., Chio-Srichan, S., Manfait, M., Sockalingum, G.D. and Sulé-Suso, J., 2009. Spectroscopic signatures of single, isolated cancer cell nuclei using synchrotron infrared microscopy. *Analyst*, *134*(6), pp.1176-1181.
- Pocaly, M., Lagarde, V., Etienne, G., Dupouy, M., Lapaillerie, D., Claverol, S., Vilain, S., Bonneu, M., Turcq, B., Mahon, F.X. and Pasquet, J.M., 2008. Proteomic analysis of an imatinib-resistant K562 cell line highlights opposing roles of heat shock cognate 70 and heat shock 70 proteins in resistance. *Proteomics*, *8*(12), pp.2394-2406.
- Poli, D., Goldoni, M., Corradi, M., Acampa, O., Carbognani, P., Internullo, E., Casalini, A. and Mutti, A., 2010. Determination of aldehydes in exhaled breath of patients with lung cancer by means of on-fiber-derivatisation SPME–GC/MS. *Journal of Chromatography B*, *878*(27), pp.2643-2651.
- Poon, K.W., Lyng, F.M., Knief, P., Howe, O., Meade, A.D., Curtin, J.F., Byrne, H.J. and Vaughan, J., 2012. Quantitative reagent-free detection of fibrinogen levels in human blood plasma using Raman spectroscopy. *Analyst*, *137*(8), pp.1807-1814.
- Probert, C.S., Khalid, T., Ahmed, I., Johnson, E., Smith, S. and Ratcliffe, N.M., 2009. Volatile organic compounds as diagnostic biomarkers in gastrointestinal and liver diseases. *Journal of Gastrointestinal and Liver Disease*, *18*(3), pp.337-343.
- Pui, C.H., Robison, L.L. and Look, A.T., 2008. Acute lymphoblastic leukaemia. *The Lancet*, *371*(9617), pp.1030-1043.
- Pully, V.V., Lenferink, A.T.M. and Otto, C., 2011. Time-lapse Raman imaging of single live lymphocytes. *Journal of Raman spectroscopy*, *42*(2), pp.167-173.

- Quesenberry, P.J. and Colvin, G.A., 2001. Hematopoietic stem cells, progenitor cells, and cytokines. *Williams Hematology*, *338*, pp.153-174.
- Quintás-Cardama, A. and Cortes, J.E., 2006, July. Chronic myeloid leukemia: diagnosis and treatment. In *Mayo Clinic Proceedings* (Vol. 81, No. 7, pp. 973-988). Elsevier.
- Ramesh, J., Kapelushnik, J., Mordehai, J., Moser, A., Huleihel, M., Erukhimovitch, V., Levi, C. and Mordechai, S., 2002. Novel methodology for the follow-up of acute lymphoblastic leukemia using FTIR microspectroscopy. *Journal of biochemical and biophysical methods*, *51*(3), pp.251-261.
- Ran, D., Schubert, M., Pietsch, L., Taubert, I., Wuchter, P., Eckstein, V., Bruckner, T., Zoeller, M. and Ho, A.D., 2009. Aldehyde dehydrogenase activity among primary leukemia cells is associated with stem cell features and correlates with adverse clinical outcomes. *Experimental hematology*, *37*(12), pp.1423-1434.
- Robert, J., Vekris, A., Pourquier, P. and Bonnet, J., 2004. Predicting drug response based on gene expression. *Critical reviews in oncology/hematology*, *51*(3), pp.205-227.
- Rutter, A.V., Chippendale, T.W., Yang, Y., Španěl, P., Smith, D. and Sulé-Suso, J., 2013. Quantification by SIFT-MS of acetaldehyde released by lung cells in a 3D model. *Analyst*, *138*(1), pp.91-95.
- Rutter, A.V., Siddique, M.R., Filik, J., Sandt, C., Dumas, P., Cinque, G., Sockalingum, G.D., Yang, Y. and Sulé-Suso, J., 2014. Study of gemcitabine-sensitive/resistant cancer cells by cell cloning and synchrotron FTIR microspectroscopy. *Cytometry Part A*, *85*(8), pp.688-697.
- Sapoval, B., Filoche, M. and Weibel, E.R., 2002. Smaller is better—but not too small: a physical scale for the design of the mammalian pulmonary acinus. *Proceedings of the National Academy of Sciences*, *99*(16), pp.10411-10416.
- Schindler, T., Bornmann, W., Pellicena, P., Miller, W.T., Clarkson, B. and Kuriyan, J., 2000. Structural mechanism for STI-571 inhibition of abelson tyrosine kinase. *Science*, *289*(5486), pp.1938-1942.

- Schmidt, K. and Podmore, I., 2015. Current challenges in volatile organic compounds analysis as potential biomarkers of cancer. *Journal of biomarkers*, *2015*.
- Schneider, U., Schwenk, H.U. and Bornkamm, G., 1977. Characterization of EBV-genome negative "null" and "T" cell lines derived from children with acute lymphoblastic leukemia and leukemic transformed non-Hodgkin lymphoma. *International journal of cancer*, *19*(5), pp.621-626.
- Scientific discussion online at http://www.ema.europa.eu/docs/en_GB/document_library/EPAR_-_Scientific_Discussion/human/000798/WC500034398.pdf.
- Seitz, H.K. and Stickel, F., 2007. Molecular mechanisms of alcohol-mediated carcinogenesis. *Nature Reviews Cancer*, *7*(8), pp.599-612.
- Shin, H.W., Umber, B.J., Meinardi, S., Leu, S.Y., Zaldivar, F., Blake, D.R. and Cooper, D.M., 2009. Acetaldehyde and hexanaldehyde from cultured white cells. *Journal of translational medicine*, *7*(1), p.31.
- Short, K.W., Carpenter, S., Freyer, J.P. and Mourant, J.R., 2005. Raman spectroscopy detects biochemical changes due to proliferation in mammalian cell cultures. *Biophysical journal*, *88*(6), pp.4274-4288.
- Singh, S.P., Ibrahim, O., Byrne, H.J., Mikkonen, J.W., Koistinen, A.P., Kullaa, A.M. and Lyng, F.M., 2015. Recent advances in optical diagnosis of oral cancers: Review and future perspectives. *Head & neck*.
- Smith, D., Wang, T., Sulé-Suso, J., Španěl, P. and Haj, A.E., 2003. Quantification of acetaldehyde released by lung cancer cells in vitro using selected ion flow tube mass spectrometry. *Rapid communications in mass spectrometry*, *17*(8), pp.845-850.
- Smith, D. and Španěl, P., 2005. Selected ion flow tube mass spectrometry (SIFT-MS) for on-line trace gas analysis. *Mass Spectrometry Reviews*, *24*(5), pp.661-700.
- Smith, D. and Španěl, P., 2011. Ambient analysis of trace compounds in gaseous media by SIFT-MS. *Analyst*, *136*(10), pp.2009-2032.
- Sokolovskaya, A.A., Zabotina, T.N., Blokhin, D.Y., Kadagidze, Z.G. and Baryshnikov, A.Y., comparative analysis of apoptosis induced by various anticancer drugs in jurkat cells. *Experimental Oncology*, *23*, pp.46-50

- Španěl, P., Ji, Y. and Smith, D., 1997. SIFT studies of the reactions of H3O+, NO+ and O2+ with a series of aldehydes and ketones. *International journal of mass spectrometry and ion processes*, *165*, pp.25-37.
- Španěl, P. and Smith, D., 2001. Quantitative selected ion flow tube mass spectrometry: the influence of ionic diffusion and mass discrimination. *Journal of the American Society for Mass Spectrometry*, *12*(7), pp.863-872.
- Španěl, P. and Smith, D., 2008. Quantification of trace levels of the potential cancer biomarkers formaldehyde, acetaldehyde and propanol in breath by SIFT-MS. *Journal of breath research*, *2*(4), p.046003.
- Španěl, P. and Smith, D., 2011. Progress in SIFT-MS: Breath analysis and other applications. *Mass spectrometry reviews*, *30*(2), pp.236-267.
- Sponring, A., Filipiak, W., Mikoviny, T., Ager, C., Schubert, J., Miekisch, W., Amann, A. and Troppmair, J., 2009. Release of volatile organic compounds from the lung cancer cell line NCI-H2087 in vitro. *Anticancer research*, *29*(1), pp.419-426.
- Spooner, A.D., Bessant, C., Turner, C., Knobloch, H. and Chambers, M., 2009. Evaluation of a combination of SIFT-MS and multivariate data analysis for the diagnosis of Mycobacterium bovis in wild badgers. *Analyst*, *134*(9), pp.1922-1927.
- Sulé-Suso, J., Pysanenko, A., Španěl, P. and Smith, D., 2009. Quantification of acetaldehyde and carbon dioxide in the headspace of malignant and non-malignant lung cells in vitro by SIFT-MS. *Analyst*, *134*(12), pp.2419-2425.
- Swain, R.J. and Stevens, M.M., 2007. Raman microspectroscopy for non-invasive biochemical analysis of single cells.
- Takahashi, H., French, S.W. and Wong, P.T., 1991. Alterations in Hepatic Lipids and Proteins by Chronic Ethanol Intake: A High-Pressure Fourier Transform Infrared Spectroscopic Study on Alcoholic Liver Disease in the Rat. *Alcoholism: Clinical and Experimental Research*, *15*(2), pp.219-223.
- Treatment of leukaemia. April 2013. [http://www.cancervic.org.au/about cancer/cancer_types/leukaemia/treatment_for_leukaemia.html].
- Toyran, N., Zorlu, F. and Severcan, F., 2005. Effect of stereotactic radiosurgery on lipids and proteins of normal and hypoperfused rat brain homogenates: a

Fourier transform infrared spectroscopy study. *International journal of radiation biology*, *81*(12), pp.911-918.

- Travo, A., Desplat, V., Barron, E., Poychicot-Coustau, E., Guillon, J., Déléris, G. and Forfar, I., 2012. Basis of a FTIR spectroscopy methodology for automated evaluation of Akt kinase inhibitor on leukemic cell lines used as model. *Analytical and bioanalytical chemistry*, *404*(6-7), pp.1733-1743.
- Ulanowska, A., Ligor, M., Amann, A. and Buszewski, B., 2008. Determination of volatile organic compounds in exhaled breath by ion mobility spectrometry. *Chemia Analityczna*, *53*(6), pp.953-965.
- Uzunbajakava, N., Lenferink, A., Kraan, Y., Volokhina, E., Vrensen, G., Greve, J. and Otto, C., 2003. Nonresonant confocal Raman imaging of DNA and protein distribution in apoptotic cells. *Biophysical journal*, *84*(6), pp.3968-3981.
- Vileno, B., Jeney, S., Sienkiewicz, A., Marcoux, P.R., Miller, L.M. and Forro, L., 2010. Evidence of lipid peroxidation and protein phosphorylation in cells upon oxidative stress photo-generated by fullerols. *Biophysical chemistry*, *152*(1), pp.164-169.
- Voortman, G., Gerrits, J., Altavilla, M., Henning, M., Bergeijk, L.V. and Hessels, J., 2002. Quantitative determination of faecal fatty acids and triglycerides by Fourier transform infrared analysis with a sodium chloride transmission flow cell. *Clinical chemistry and laboratory medicine*, *40*(8), pp.795-798.
- Wang, F., Zhai, S., Liu, X., Li, L., Wu, S., Dou, Q.P. and Yan, B., 2011. A novel dithiocarbamate analogue with potentially decreased ALDH inhibition has copper-dependent proteasome-inhibitory and apoptosis-inducing activity in human breast cancer cells. *Cancer letters*, *300*(1), pp.87-95.
- Wang, J.J., Chi, C.W., Lin, S.Y. and Chern, Y.T., 1996. Conformational changes in gastric carcinoma cell membrane protein correlated to cell viability after treatment with adamantyl maleimide. *Anticancer research*, *17*(5A), pp.3473-3477.
- Wang, J.S., Fang, Q., Sun, D.J., Chen, J., Zhou, X.L., Lin, G.W., Lu, H.Z. and Fei, J., 2001. Genetic modification of hematopoietic progenitor cells for combined resistance to 4-hydroperoxycyclophosphamide, vincristine, and daunorubicin. *Acta pharmacologica Sinica*, *22*(10), pp.949-955.

- Wehinger, A., Schmid, A., Mechtcheriakov, S., Ledochowski, M., Grabmer, C., Gastl, G.A. and Amann, A., 2007. Lung cancer detection by proton transfer reaction mass-spectrometric analysis of human breath gas. *International Journal of Mass Spectrometry*, *265*(1), pp.49-59.
- Wei, J., Freytag, M., Schober, Y., Nockher, W.A., Mautner, V.F., Friedrich, R.E., Manley, P.W., Kluwe, L. and Kurtz, A., 2014. Nilotinib is more potent than imatinib for treating plexiform neurofibroma in vitro and in vivo. *PloS one*, *9*(10), p.e107760.
- Weisberg, E., Manley, P.W., Breitenstein, W., Brüggen, J., Cowan-Jacob, S.W., Ray, A., Huntly, B., Fabbro, D., Fendrich, G., Hall-Meyers, E. and Kung, A.L., 2005. Characterization of AMN107, a selective inhibitor of native and mutant Bcr-Abl. *Cancer cell*, *7*(2), pp.129-141.
- Weisberg, E., Manley, P., Mestan, J., Cowan-Jacob, S., Ray, A. and Griffin, J.D., 2006. AMN107 (nilotinib): a novel and selective inhibitor of BCR-ABL. *British Journal of Cancer*, *94*(12), pp.1765-1769.
- Westermann, J. and Bode, U., 1999. Distribution of activated T cells migrating through the body: a matter of life and death. *Immunology today*, *20*(7), pp.302-306.
- Wong, P.T., Senterman, M.K., Jackli, P., Wong, R.K., Salib, S., Campbell, C.E., Feigel, R., Faught, W. and Fung Kee Fung, M., 2002. Detailed account of confounding factors in interpretation of FTIR spectra of exfoliated cervical cells. *Biopolymers*, *67*(6), pp.376-386.
- Yandim, M.K., Ceylan, C., Elmas, E. and Baran, Y., 2016. A molecular and biophysical comparison of macromolecular changes in imatinib-sensitive and imatinib-resistant K562 cells exposed to ponatinib. *Tumor Biology*, *37*(2), pp.2365-2378.
- Yao, H., Tao, Z., Ai, M., Peng, L., Wang, G., He, B. and Li, Y.Q., 2009. Raman spectroscopic analysis of apoptosis of single human gastric cancer cells. *Vibrational Spectroscopy*, *50*(2), pp.193-197.
- Yoshida, A., Rzhetsky, A., Hsu, L.C. and Chang, C., 1998. Human aldehyde dehydrogenase gene family. *European Journal of Biochemistry*, *251*(3), pp.549-557.

- Zaharieva, M.M., Amudov, G., Konstantinov, S.M. and Guenova, M.L., 2013. Modern Therapy of Chronic Myeloid Leukemia. *Edited by Margarita Guenova and Gueorgui Balatzenko*, p.227.
- Zelig, U., Kapelushnik, J., Moreh, R., Mordechai, S. and Nathan, I., 2009. Diagnosis of cell death by means of infrared spectroscopy. *Biophysical journal*, *97*(7), pp.2107-2114.
- Zemaitis, M.A. and Greene, F.E., 1976. Impairment of hepatic microsomal and plasma esterases of the rat by disulfiram and diethyldithiocarbamate. *Biochemical pharmacology*, *25*(4), pp.453-459.
- Zhan, X., Duan, J. and Duan, Y., 2013. Recent developments of proton-transfer reaction mass spectrometry (PTR-MS) and its applications in medical research. *Mass spectrometry reviews*, *32*(2), pp.143-165.
- Zhang, L., Wang, L., Liu, X., Zheng, D., Liu, S. and Liu, C., 2014. ALDH expression characterizes G1-phase proliferating beta cells during pregnancy. *PloS one*, *9*(5), p.e96204.
- Zhdanov, A.V., Ward, M.W., Prehn, J.H. and Papkovsky, D.B., 2008. Dynamics of intracellular oxygen in PC12 Cells upon stimulation of neurotransmission. *Journal of Biological Chemistry*, *283*(9), pp.5650-5661.
- Zoladek, A., Pascut, F.C., Patel, P. and Notingher, I., 2011. Non-invasive time-course imaging of apoptotic cells by confocal Raman micro-spectroscopy. *Journal of Raman Spectroscopy*, *42*(3), pp.251-258.

Appendix 1

Stages of Leukaemia

Leukaemia starts in the bone marrow and often has spread to other organs by the time it is detected, so traditional staging is not being done. Staging is the process used to find out how far the cancer has spread. It is important to know the stage of the disease in order to plan the best treatment. Instead, cytologic classification systems to identify the type and subtype of leukaemia are used.

Chronic Lymphocytic Leukemia:

The following stages are used for chronic lymphocytic leukemia:

1. Stage 0
2. Stage I
3. Stage II
4. Stage III
5. Stage IV

Stage 0

In stage 0 chronic lymphocytic leukemia, there are too many lymphocytes in the blood, but there are no other signs or symptoms of leukemia. Stage 0 chronic lymphocytic leukemia is indolent (slow-growing).

Stage I

In stage I chronic lymphocytic leukemia, there are too many lymphocytes in the blood and the lymph nodes are larger than normal.

Stage II

In stage II chronic lymphocytic leukemia, there are too many lymphocytes in the blood, the liver or spleen are larger than normal, and the lymph nodes may be larger than normal.

Stage III

In stage III chronic lymphocytic leukemia, there are too many lymphocytes in the blood and there are too few red blood cells. The lymph nodes, liver, or spleen may be larger than normal.

Stage IV

In stage IV chronic lymphocytic leukemia, there are too many lymphocytes in the blood and too few platelets. The lymph nodes, liver, or spleen may be larger than normal and there may be too few red blood cells.

Chronic Myelogenous Leukemia

CML instead of stages have 3 phases. The number of blast cells in the blood and bone marrow and the severity of signs or symptoms determine the phase of the disease.

The phases are:

1. Chronic phase

2. Accelerated phase
3. Blastic phase

Chronic phase

In chronic phase CML, fewer than 10% of the cells in the blood and bone marrow are blast cells.

Accelerated phase

In accelerated phase CML, 10% to 19% of the cells in the blood and bone marrow are blast cells.

Blastic phase

In blastic phase CML, 20% or more of the cells in the blood or bone marrow are blast cells. When tiredness, fever, and an enlarged spleen occur during the blastic phase, it is called blast crisis.

Acute Lymphocytic Leukemia:

There is no standard staging system for adult ALL.

The disease is described as untreated, in remission, or recurrent.

Acute Myelogenous Leukemia

There is no standard staging system for adult AML.

The disease is described as untreated, in remission, or recurrent.

Hairy Cell Leukemia

There is no standard staging system for hairy cell leukemia.

Groups are used in place of stages for hairy cell leukemia. The disease is grouped as;

1. Untreated
2. Progressive
3. Refractory.

Untreated Hairy Cell Leukemia

The hairy cell leukemia is newly diagnosed and has not been treated except to relieve signs or symptoms such as weight loss and infections. In untreated hairy cell leukemia, some or all of the following conditions occur:

- Hairy (leukemia) cells are found in the blood and bone marrow.
- The number of red blood cells, white blood cells, or platelets may be lower than normal.
- The spleen may be larger than normal.

Progressive Hairy Cell Leukemia

In progressive hairy cell leukemia, the leukemia has been treated with either chemotherapy or splenectomy (removal of the spleen) and one or both of the following conditions occur:

- There is an increase in the number of hairy cells in the blood or bone marrow.
- The number of red blood cells, white blood cells, or platelets in the blood is

lower than normal.

Childhood Acute Lymphocytic Leukemia

In childhood ALL, risk groups are used to plan treatment.

There are two risk groups

1. Standard (low) risk: Includes children aged 1 to younger than 10 years who have a white blood cell count of less than 50,000/μL at diagnosis.
2. High risk: Includes children 10 years and older and/or children who have a white blood cell count of 50,000/μL or more at diagnosis.

Childhood Acute Myelogenous Leukemia

There is no standard staging system for childhood AML, childhood chronic myelogenous leukemia (CML), juvenile myelomonocytic leukemia (JMML), or myelodysplastic syndromes (MDS).

Instead of stages, treatment of childhood AML, childhood CML, JMML, and MDS is based on one or more of the following:

1. The type of disease or the subtype of AML.
2. Whether leukemia has spread outside the blood and bone marrow.
3. Whether the disease is newly diagnosed, in remission, or recurrent.

Newly Diagnosed Childhood AML

Newly diagnosed childhood AML has not been treated except to relieve signs and symptoms such as fever, bleeding, or pain, and one of the following is true:

1. More than 20% of the cells in the bone marrow are blasts (leukemia cells).*or*
2. Less than 20% of the cells in the bone marrow are blasts and there is a specific change in the chromosome.

Appendix 2: Typical Operating Conditions of the SIFT-MS

Parameter	Symbol	Typical value	Unit
Flow tube (reaction) length	l	50	mm
End correction factor	ε	20	mm
Flow tube diameter	d_t	10	mm
Injection orifice diameter	O_2	1.0-2.0	mm
Ion sampling orifice diameter	O_3	0.3	mm
Reaction time	t	5×10^{-4}	s
Bulk velocity	υ_g	10^4	$cm.s^{-1}$
Precursor ion velocity	υ_i	1.5×10^4	$cm.s^{-1}$
Carrier gas flow rate	ϕ_C	11.0 820	$Torr.l.s^{-1}$ ml/min
Sample flow rate	$\phi_{A,M}$	0.32 24	$Torr.l.s^{-1}$ ml/min
Helium number density	[He]	3×10^{16}	cm^{-3}
Flow tube pressure	P_g	1.0	Torr
Ion source pressure		0.5	Torr
Precursor ion filter pressure		10^{-4}	Torr
Downstream mass spectrometer pressure		10^{-4}	Torr
Gas temperature	T_g	300	K

Appendix 3 Schematic mechanism of Philadelphia chromosome production.